UNIVERSITY OF CRETE

DEPARTMENT OF MATERIALS SCIENCE AND TECHNOLOGY

PhD Thesis

SYNTHESIS OF MULTIRESPONSIVE COPOLYMERS FOR THE DEVELOPMENT OF "SMART" ORGANIC-INORGANIC HYBRIDS

DEMETRA S. ACHILLEOS

Supervisor: Associate Professor Maria Vamvakaki

Foundation for Research and Technology

Institute of Electronic Structure and Lasers

Polymer Group

ΠΑΝΕΠΙΣΤΗΜΙΟ ΚΡΗΤΗΣ

ΤΜΗΜΑ ΕΠΙΣΤΗΜΗΣ ΚΑΙ ΤΕΧΝΟΛΟΓΙΑΣ ΥΛΙΚΩΝ

ΔΙΔΑΚΤΟΡΙΚΗ ΔΙΑΤΡΙΒΗ

ΣΥΝΘΕΣΗ ΣΥΜΠΟΛΥΜΕΡΩΝ ΑΠΟΚΡΙΝΟΜΕΝΩΝ ΣΕ ΠΟΛΛΑΠΛΑ ΕΡΕΘΙΣΜΑΤΑ ΓΙΑ ΤΗΝ ΑΝΑΠΤΥΞΗ «ΕΞΥΠΝΩΝ» ΟΡΓΑΝΙΚΩΝ/ΑΝΟΡΓΑΝΩΝ ΥΒΡΙΔΙΩΝ

ΔΗΜΗΤΡΑ ΑΧΙΛΛΕΩΣ

ΕΠΙΒΛΕΠΟΥΣΑ: ΑΝΑΠΛΗΡΩΤΡΙΑ ΚΑΘΗΓΗΤΡΙΑ ΜΑΡΙΑ ΒΑΜΒΑΚΑΚΗ

ΙΔΡΥΜΑ ΤΕΧΝΟΛΟΓΙΑΣ ΚΑΙ ΕΡΕΥΝΑΣ

ΙΝΣΤΙΤΟΥΤΟ ΗΛΕΚΤΡΟΝΙΚΗΣ ΔΟΜΗΣ ΚΑΙ ΛΕΙΖΕΡ

ΟΜΑΔΑ ΠΟΛΥΜΕΡΩΝ

I would like to dedicate this Doctoral dissertation to my family. There is no doubt in my mind that without their continued support I could not have completed this process.

προσπάθησα να επαναφέρω στη μνήμη μου αυτά που περάσαμε μαζί όλα αυτά τα χρόνια και συνειδητοποίησα ότι ένα ευχαριστώ δεν είναι αρκετό για να ανταμείψει τη προσφορά τους.

Αυτή η διδακτορική διατριβή, είναι αφιερωμένη στην οικογένεια μου, η οποία είναι το στήριγμα μου και στην οποία οφείλω ότι έχω καταφέρει μέχρι τώρα στη ζωή μου. Είναι απίστευτα σημαντικό να έχεις δίπλα σου ανθρώπους με αρχές που να υποστηρίζουν όχι απλά οικονομικά αλλά και ουσιαστικά τις επιλογές και τα όνειρα σου, και είναι πάντα κοντά σου ανά πάσα στιγμή για να σε στηρίξουν με κάθε τρόπο.

Table of contents

ABSTRACT

The aim of this work is the synthesis and the investigation of the responsive behavior of a range of spiropyran (SP)-based materials including random copolymers, spherical polymer brushes and hollow nanoparticles. The ability of these materials to respond to a variety of applied external stimuli such as light, pH, temperature and solvent polarity renders them excellent candidates for various applications.

Multiresponsive SP-based random copolymers which vary in the content of the SP moieties, were synthesized by the random copolymerization of 2-(dimethylamino)ethyl methacrylate (DMAEMA) or methyl methacrylate (MMA) with the in-house synthesized SP monomer 1',3',3'-trimethyl-6-methacryloyloxy-spiro(2H-1-benzopyran-2,2'-indoline) by ATRP in solution. The PDMAEMA-co-PSP copolymers exhibited "reverse photochromism" and "negative solvatochromism" upon increasing the polarity of the solvent, in contrast to the PMMA-co-PSP analogue. Moreover, the PDMAEMA-co-PSP copolymers exhibited a reversible pH-responsive character in aqueous media with an acid-induced the SP-to-merocyanine (MC) isomerization and the formation of $[MC\text{-}OH]^+$ and $[SP\text{-}NH]^+$ species. The lower critical solution temperature (LCST) of the copolymers increased with their content in hydrophilic MC moieties, while the recovery of the hydrophobic SP species decreased the LCST. Finally, the copolymers exhibited a first-order photoinduced bleaching of the chromophore units in water and acetonitrile, with a slower decoloration rate in the aqueous medium due to the effective stabilization of the bipolar MC form. A PDMAEMA-co-(1´-(2-methacryloxyethyl)-3´,3´-dimethyl-6-nitrospiro-(2H-1-benzopyran-2,2´-indoline)) (PSPMA) random copolymer which exhibited "normal photochromism", that is the SP-to-MC isomerization upon stimulation with UV light was also synthesized using the in-house synthesized monomer SPMA. The stimulation of the PDMAEMA-co-PSPMA copolymer with UV light in water resulted in the generation of three switterionic moieties from the same parent SP molecule; namely the non-planar X isomer and two different planar MC species, MC_1 and MC_2 which differ in polarity. The photo-isomers followed a biexponential thermal bleaching mechanism originated from localized barriers inherent in the polymer matrix which establish a non-homogeneous microenvironment around the chromophores. Moreover, the copolymer exhibited an intra- and inter-chain fluorescence resonance energy transfer (FRET) upon the photo-induced generation of

both X and MC species which are FRET donor-acceptor pairs, respectively, from the SP isomers. The photo-regulated energy transfer was favored by the close proximity of the bipolar isomers promoted by the association of the random copolymers in water and the spectral overlap of the emission and absorption bands of X and MC isomers, respectively. The FRET process is interrupted by the thermal MC-to-SP isomerization which is retarded by the polar microenvironment and enabled before relaxation of the acceptors the read-out process.

In the second part of this work, SiO$_2$-g-(PDMAEMA-co-PSPMA) spherical brushes were synthesized from the surface of silica particles via copper-mediated ATRP in bulk. Stimulation of the hybrids with UV light resulted in the isomerization of the SP units to two different bipolar species; the cisoid non-planar X and the planar MC isomers which followed a biexponential thermal relaxation process to reform the SP isomers due to variations in the microenvironment polarity and the free volume in the polymer brush layer. The generation of two different bipolar species, X and MC, in aqueous media from the same parent SP molecule upon UV irradiation of the hybrids provided the unique property to the system of exhibiting FRET between X and MC residues. In this case, the proximity of the donor-acceptor pairs was promoted by the steric crowding within the polymer brush layer. The energy transfer was switched "off" upon the thermal fading of the MC species which exhibited adequate kinetic rates and enabled the monitoring of the process. This property of the nanohybrids can be successfully applied for the detection of biological substances such as proteins and aminoacids. In particular, the presence of bovine serum albumin (BSA) in the aqueous dispersion of the hybrids was proved to enhance significantly the FRET efficiency of the system, due to the accelerated MC formation catalyzed by the protein, while L-histidine did not affect the FRET efficiency of the hybrids however it retarded the MC bleaching by interaction with the MC dipoles.

Finally, the light-driven supramolecular engineering of fluorescent nanocapsules (NCPs) utilizing the appropriate phototrigger to stimulate the SiO$_2$-g-(PDMAEMA-co-PSPMA) spherical brushes, was also studied. The fabrication of the nanospheres was based on the formation of π-π H-type interactions between the MC photoisomers being in close proximity within the sterically crowded environment of the polymer brushes by applying UV irradiation which enabled the SP-to-MC isomerization of the photosensitive species. HF etching of the inorganic core resulted in the formation of dual-responsive polymeric vesicles whose wall's robustness is

provided by the MC-MC cross-link points. The disruption of the NCPs could be achieved remotely and progressively by applying a harmless trigger such as visible light irradiation. The hydrophilic nature of the DMAEMA comonomer not only provided dispersability of the vesicles in the environmentally benign aqueous media but also enabled the controlled alteration of the NCPs size stimulated by variations in the solution pH. The inherent ability of the NCPs to fluoresce in water opens new possibilities for the development of addressable nanoscale capsules for biomedical applications.

KEYWORDS

ΠΕΡΙΛΗΨΗ

Στα πλαίσια της εργασία αυτής συντέθηκαν πολυμερικές αλυσίδες, υβριδικά υλικά και νανοκάψουλες (ΝΚ) που βασίζονται σε μόρια σπιροπυρανίου (ΣΠ). Τα υλικά συντέθηκαν με τη μέθοδο ριζικού πολυμερισμού μεταφοράς ατόμου στην παρουσία ή απουσία διαλύτη από μόρια εκκινητή στο διάλυμα ή αγκυροβολημένα σε επιφάνειες. Η απόκριση των υλικών αυτών σε μεταβολές της πολικότητας του διαλύτη, του pH, και στην επίδραση ηλεκτρομαγνητικής ακτινοβολίας καθώς επίσης και η ιδιότητα τους να φθορίζουν μελετήθηκαν εκτενώς.

Συμπολυμερή που βασίζονται σε μόρια ΣΠ και είναι αποκρίσιμα σε πολλά ερεθίσματα συντέθηκαν με τυχαίο συμπολυμερισμό του 2-(dimethylamino)ethyl methacrylate (DMAEMA) και του 1',3',3'-trimethyl-6-methacryloyloxy-spiro(2*H*-1-benzopyran-2,2'-indoline). Τα πολυμερή εμφανίζουν «ανάστροφο φωτοχρωμισμό» και «αρνητικό διαλυτοχρωμισμό» όταν η πολικότητα του μέσου αυξάνεται. Αποκρίνονται επίσης αντιστρεπτά σε αλλαγές του pH, ενώ η ευαισθησία τους σε μεταβολές της θερμοκρασίας εξαρτάται από την περιεκτικότητα τους σε μεροκυανίνη (ΜΕ) και τον φωτοεπαγώμενο επανασχηματισμό του ΣΠ. Ένα τυχαίο συμπολυμερές που εμφανίζει «κανονικό φωτοχρωμισμό» και βασίζεται στο μονομερές 1´-(2-methacryloxyethyl)-3´,3´-dimethyl-6-nitrospiro-(2*H*-1-benzopyran-2,2´-indoline) (SPMA), επίσης συντέθηκε. Μετά από ακτινοβόληση με υπεριώδες φως, το ΣΠ ισομερίστηκε σε ένα μόριο Χ και δύο ισομερή ΜΕ. Αυτό είχε σαν αποτέλεσμα τη συντονιζόμενη μεταφορά ενέργειας Förster (ΣΜΕF) μεταξύ των μορίων Χ και ΜΕ, τα οποία αποτελούν ζεύγη δότη και δέκτη, αντίστοιχα, και τα οποία βρίσκονται στην ίδια ή σε διαφορετικές πολυμερικές αλυσίδες. Το φαινόμενο προάγεται από την συσσωμάτωση των πολυμερικών αλυσίδων στο νερό και την εγγύτητα των χρωμοφόρων.

Στην εργασία αυτή, συντέθηκαν επίσης πολυμερικές ψήκτρες στην επιφάνεια νανοσωματιδίων σίλικας με τυχαία κατανομή μορίων DMAEMA και SPMA. Όταν τα υβρίδια ακτινοβολήθηκαν με υπεριώδες φως, το ΣΠ ισομερίστηκε σε μόρια Χ και ΜΕ. Κατά συνέπεια, τα υβρίδια εμφανίζουν ΣΜΕF μεταξύ χρωμοφόρων που βρίσκονται στο ίδιο σωματίδιο. Το φαινόμενο ευνοείται από την εγγύτητα των μορίων στις πολυμερικές ψήκτρες και μπορεί να εφαρμοστεί για την ανίχνευση πρωτεϊνών και αμινοξέων.

Τέλος, χρησιμοποιήθηκε μια πρωτοποριακή μέθοδος για τον αντιστρεπτό σχηματισμό ΝΚ που προάγεται από φώς και βασίζεται στην ανάπτυξη π-π αλληλεπιδράσεων μεταξύ ΣΠ που βρίσκονται σε πολυμερικές ψήκτρες. Η ιδιότητα των ΝΚ αυτών να φθορίζουν, να αποκρίνονται σε αλλαγές του pH στο νερό, και να καταστρέφονται μετά από ακτινοβόληση με ορατό φώς, δημιουργεί νέες προοπτικές για την ανάπτυξη ΝΚ με βιοϊατρικές εφαρμογές.

ΛΕΞΕΙΣ ΚΛΕΙΔΙΑ

Σπιροπυράνια, τυχαία συμπολυμερή, οργανικά-ανόργανα υβρίδια, νανοκάψουλες, ριζικός πολυμερισμός μεταφοράς ατόμου, ανάστροφος και κανονικός φωτοχρωμισμός, αρνητικός διαλυτοχρωμισμός, συντονιζόμενη μεταφορά ενέργειας Förster.

Abbreviations

2VP 2-vinylpyridine

AA acrylic acid

AaH sodium 6-acrylamido hexanoate

AMBA sodium 3-acrylamido- 3-methylbutanoate

AMPS sodium 2-acrylamido-2-methylpropanesulfonate

DEAEMA 2-(diethylamino)ethyl methacrylate

DMAEMA 2-(dimethylamino)ethyl methacrylate

DMAPS 3-[*N*-(2-methacryloyethyl)-*N,N*-dimethylammonio] propanesulfonate

DMVBA *N,N*-dimethylvinylbenzylamine

DMVBAPS 3-(*N,N*-dimethylvinylbenzylammonio)-propanesulfonate

MAA methacrylic acid

MAEDAPS 3-[2-(*N*-methylacrylamido)-ethyldimethylammonio] propanesulfonate

MEMA 2-(*N*-morpholino)ethyl methacrylate

METAC 2-(methacryloyloxy)ethyl]trimethylammonium chloride

NaSS sodium 4-styrenesulfonate

PEO poly(ethylene oxide)

PNIPAM poly(*N*-isopropylacrylamide)

PnPA poly(*N*-n-propylacrylamide)

PPO poly(propylene oxide)

4-VBA sodium 4-vinylbenzoic

PMPC 2-methacryloyloxyethyl phosphorylcholine

ATRP Atom Transfer Radical Polymerization

DMNA 5-(2'- (dimethylamino)ethoxy)-2-nitrobenzyl acrylate

NBDAE (4-(2-acryloyloxyethylamino)-7-nitro-2,1,3-benzoxadiazole

RhBEA Rhodamine B

FRET Fluorescence resonance energy transfer

B18C6Am 4-acrylamidobenzo-18-crown-6

CHAPTER 1

Introduction

1 Introduction

1.1 Stimuli Responsive Polymers

"Smart" or "stimuli responsive" polymeric materials is an area of substantial interest. These polymers can undergo relatively large and abrupt, physical and/or chemical changes in response to external changes in the environmental conditions. Chemical stimuli such as pH, ionic factors and chemical agents can affect the interactions between the polymer chains or between polymer chains and the solvent. Physical stimuli such as temperature, magnetic and electric fields, mechanical stress and light irradiation can alter the molecular interactions and can induce conformational changes.[1] This response to external stimuli that causes changes in the physicochemical properties of the polymers can also impact a significant number of the material properties such as surface wetting, metal binding, adhesion, dispersion, lubrication, permeability and optical response.[2] This inductive responsiveness to external stimuli render them promising materials for various applications such as in drug delivery systems, biotechnology, catalysis, sensors, separations and others.[3-9]

1.1.1 pH-responsive polymers

pH-sensitive polymers consist of ionizable groups that can either accept or donate protons in response to changes in the solution pH. The polymers containing such ionizable units can form polyelectrolytes or polyzwitterions in an aqueous solution. Polyelectrolytes contain either anionically or cationically charged species as side groups or along the polymeric backbone. Polyzwitterions have both anionic and cationic charged groups and depending on the location of the charges they are characterized as polybetaines or polyampholytes. Polybetaines have both charges on the same monomer repeat unit, while polyampholytes possess the charges on different monomer units.[10] By varying the pH, the net charge of the polyampholyte polymeric chain can change. Around the isoelectric point, which is the pH value where the net charge of the chain is zero, the polymeric chain will exhibit a polyampholyte behavior. At lower or higher pH values an asymmetric charge exists along the polymeric chain and the polymer exhibits polyelectrolyte behavior.[11] It is worthwhile to mention that pH-responsive polymers are also sensitive to

salt concentration. In the absence of added salt the ionized polymer chains are stabilized due to the electrostatic repulsive forces and the high osmotic pressure. The addition of salt progressively screens the charges on the polymer chains and leads to the shrinkage of the macromolecule.   Some typical ionizable and zwitterionic monomers used for the preparation of pH-responsive polymers are illustrated in Figure 1.1.

Ionic/IonizableMonomers
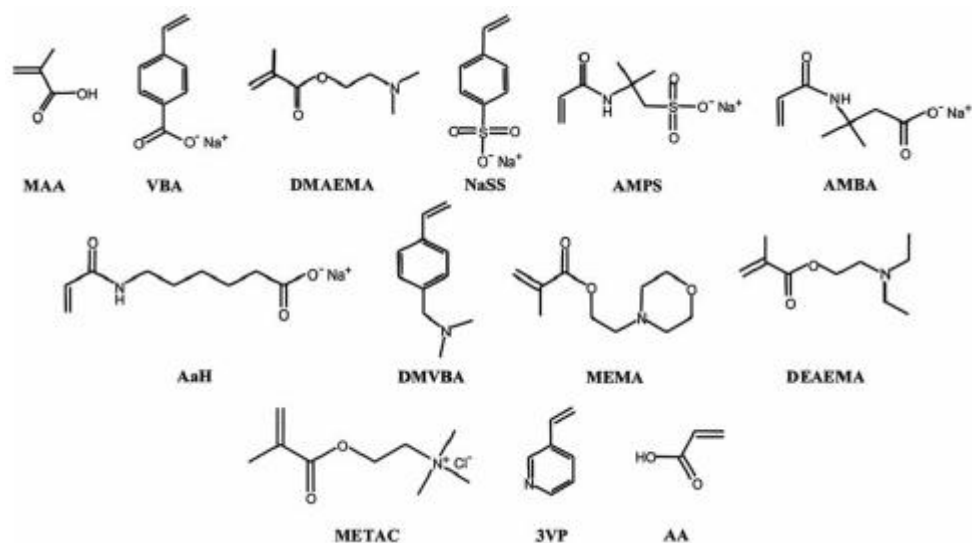
Zwitterionic Monomers
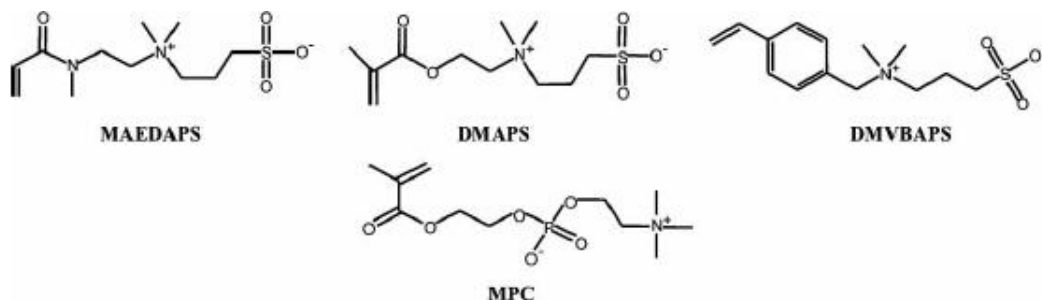
Figure 1.1. Typical ionizable and zwitterionic monomers used for the preparation of pH-responsive polymers.

Several studies have been reported on the synthesis of ionizable block copolymers,[12] zwitterionic diblock copolymers[13-17] and ABS triblock terpolymers[18-19] by "living" anionic and group transfer polymerizations (GTP). These polymers exhibit very

interesting solution properties. More specifically, amphiphilic diblock copolymers comprising an ionizable hydrophilic block and a permanent hydrophobic block are amphiphilic water-soluble copolymers that self-assemble in an aqueous medium forming micellar nanostructures of various shapes (spheres, cylinders, vesicles, etc.). On the other hand, zwitterionic diblock copolymers and ABC triblock terpolymers precipitate around their isoelectric point which is determined by the segment ratio of the two blocks, while at low and high pH values diblock copolymers and triblock terpolymer assemblies are formed. The aggregation around the isoelectric point can be explained by the annihilation of the electrostatic repulsive forces at zero net charge of the polymeric chains and thus the domination of the hydrophobic interactions.[20] Such materials find interesting applications as surfactants, dispersants in nanoreactors, in the development of sensors and in biomedical applications.

1.1.1.1 Polyacids

Polymers bearing carboxylic acid groups with pK_α's of around 5-6, are the most representative weak polyacids. Poly(acrylic acid) (PAA)[20] and poly(methacrylic acid) (PMAA)[21] have been extensively reported as pH-responsive polyacids. The carboxylic pendant groups accept protons at low pH, while these protons are released at high pH values. Consequently, at high pH, the polymer acts as a polyelectrolyte with electrostatic repulsive forces between the monomer repeat units.[20] At this pH the polymer chain takes up water, and hence exists in a swollen (dissolved) state. On the contrary, at low pH the polymer chains will be uncharged and thus in an unswollen (insoluble) state. PMAA exhibits an abrupt phase transition compared to the phase transition of PAA. This happens because the α-methyl groups of MAA induce strong hydrophobic interactions that favor aggregation and thus PMAA adopts a more compact conformation at low pH values before a critical charge density is attained. This compact conformation of PMAA in the uncharged state is referred to as the "hypercoiled" conformation.[22] Increase of the hydrophobic character of the monomer repeat units along the polymer chain leads to more compact conformations at low pH values. Such behavior found for poly(2-ethyl acrylic acid) (PEAA) and poly(2-propyl acrylic acid) (PPAA) (Figure 1.2a and b). Another class of acidic pH-sensitive polymers is that containing sulfonamide groups

(Figure 1.2c). These polymers are polyacids with pK_α values varying between pH 3 and 11, which result from the different substituents at the sulfonamide group acting as electron withdrawing or donating groups.[23-24]

a   b   c
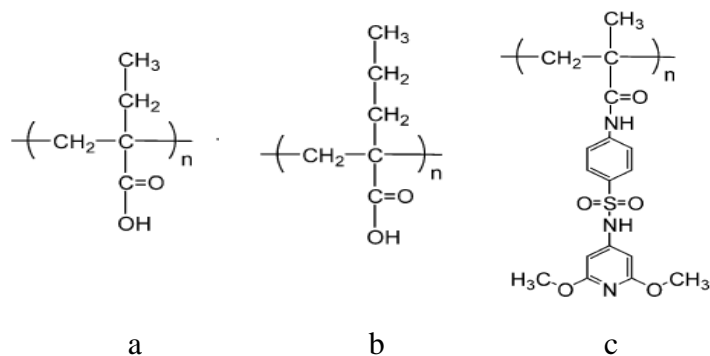
Figure 1.2. pH-responsive polyacids PEAA (a), PPAA (b), and polymers containing sulfonamide groups (c).

1.1.1.2   Polybases

One of the most significant categories of polybases is that of the polyamine polymers. 2-(dimethylamino)ethyl methacrylate (PDMAEMA) is a well known pH-sensitive polymer. Due to its tertiary amine groups it behaves as a weak polybase with a pK_α of about 8.0.[25] Below pH 8.0 PDMAEMA is a cationic polyelectrolyte due to the protonation of the tertiary amine groups and is soluble over a wide range of temperatures. 2-(diethylamino)ethyl methacrylate (PDEAEMA) has a similar structure to PDMAEMA with the difference that PDEAEMA has two ethyl groups attached on the nitrogen atom of the amine group instead of the two methyl groups for PDMAEMA which induce stronger hydrophobic interactions at pH higher than 7.0 and consequently the polymer adopts a "hypercoiled" conformation.[26] Poly(vinyl imidazole) (PVI) is another pH-responsive polybase due to the imidazole group.[27] Furthermore, another important class of polybases are the polymers of 2- and 4-vinyl pyridines.

1.1.1.3   Acid-degradable polymers

Another significant class of pH-sensitive materials is that of degradable pH-responsive polymers. Two well-known systems with such properties are the poly(ortho esters) and the poly(β-amino)esters (Figure 1.3).
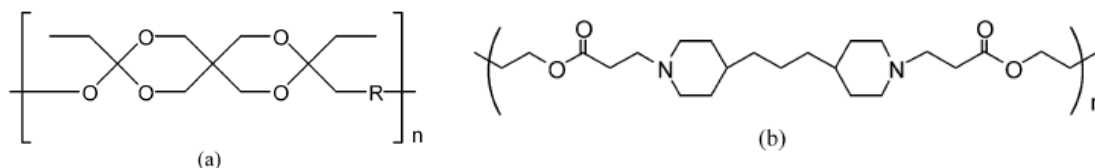
Figure 1.3. pH-responsive degradable polymers: Poly(ortho ester)s (a) and poly(β-amino ester)s (b).

Poly(ortho ester)s are very stable at physiological pH but they exhibit fast degradation under mildly acidic conditions.[28] These polymers find applications as drug delivery systems targeted to weak acidic environments[29] or as hydrogel matrices for pulsatile insulin delivery.[30] Poly(β-amino ester)s also represent a very important class of degradable polymers. Due to the amine groups that these polymers contain in their structure they become protonated at low pH values and they readily dissolve around pH 6.5. The particular characteristic of these polymers is that they degrade faster at pH 5.1 than 7.4 which is an unusual property for polymeric systems.[31] Studies have shown that microspheres composed of this polymer exhibit a rapid release of encapsulated material within the range of endosomal pH.[32]

1.1.2 *Temperature responsive polymers*

Temperature-responsive polymers are a significant class of stimuli-responsive materials since they have been proposed for potential applications in a wide range of fields. Their phase transition (Figure 1.4), and hence "smart" behavior, arises from the entropic gain as water molecules associated with the polymer chain are released into the bulk aqueous phase as the temperature passes a critical value. The temperature at which this occurs (Lower Critical Solution Temperature or LCST) corresponds to the region in the phase diagram at which the enthalpic contribution of water hydrogen-bonded to the polymer chain becomes less important than the entropic gain of the system as a whole and thus is largely dependent on the hydrogen-bonding capabilities of the constituent monomer units.[33]
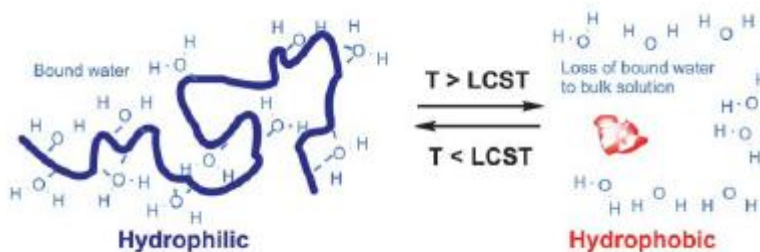
Figure 1.4. Conformational changes of a polymeric chain
above and below the LCST

Consequently, when the temperature of the solution is increased above the LCST or decreased below the Upper Critical Solution Temperature (UCST) the polymer chains undergo a coil-to-globule transition (volume transition) since the segments become hydrophobic in nature. Intramolecular collapse occurs before the intermolecular aggregation and the collapse of the polymer chains increases the scattering of light from the solution. Consequently, the LCST or UCST is also called cloud point and results in phase separation between the collapsed polymer molecules and the expelled water molecules.[34] The intermolecular forces which govern the above processes are hydrogen bonding and hydrophobic interactions. The balance between these interactions determines the phase behavior of the polymer.

Temperature-responsive polymers can be classified into those exhibiting an LCST and a UCST behavior.

1.1.2.1 Polymers exhibiting LCST

A well-known category of temperature-responsive polymers exhibiting a LCST behavior arises from the polymerization of N-alkyl acrylamide monomers such as those shown in Figure 1.5.[2] Poly(*N*-acryloylpiperidine) (PNAPi), poly(*N*-n-propylacrylamide) (PnPA), poly(*N*-isopropylacrylamide) (PNIPAM), and poly(*N*-acryloylpyrrolidine) (PAPy) display LCSTs at 5 $^{\circ}$C, 22 $^{\circ}$C, 32 $^{\circ}$C, and 55 $^{\circ}$C, respectively. Among them PNIPAM has attracted considerable attention because it exhibits an LCST very close to the temperature of the human body which renders it a very promising material for biological applications.[2] Poly(*N*-acryloyl-*N'*-alkylpiperazine) was recently reported as another novel

temperature and pH-responsive polymer. Poly(*N*-acryloyl-*N'*-propylpiperazine) exhibited a LCST at ~37 °C, while the introduction of methyl or ethyl groups at the N atom instead of propyl groups resulted in the loss of the LCST behavior due to the substantial increase of the hydrophilicity of the polymer.[35]

| N-acryloylpiperidine | N-n-propylacrylamide | N-isopropylacrylamide | N-acryloylpyrrolidine |
| a | b | c | d |

R= -CH₃, -CH₂CH₃
-CH₂CH₂CH₃

N-acryloyl-N'-alkylpiperazine

e
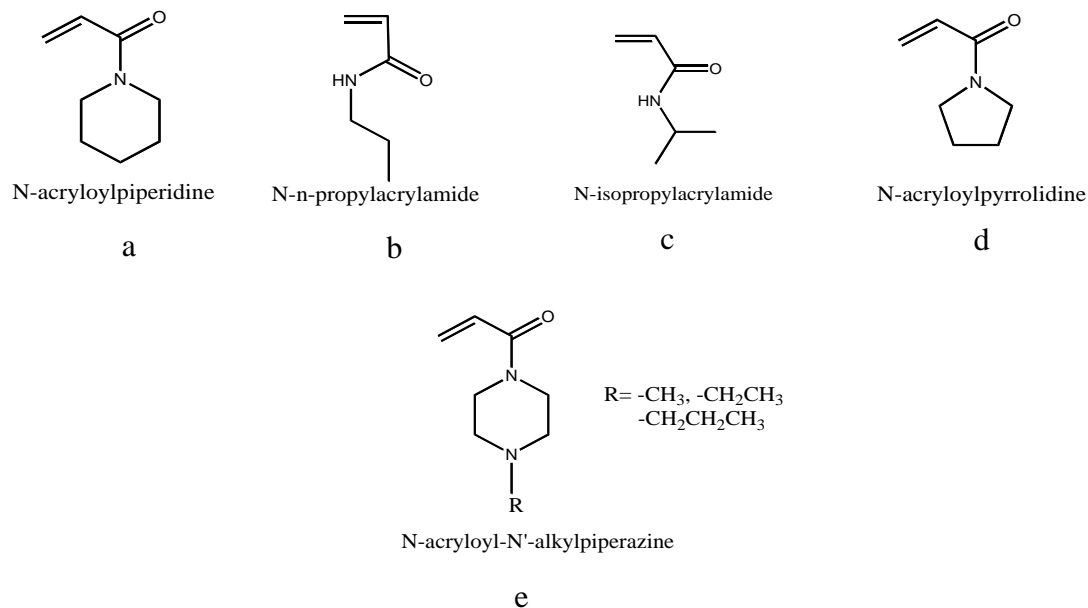
Figure 1.5. N-alkyl acrylamide monomers employed for the preparation of temperature-responsive polymers.

However, an LCST behavior for methyl- and ethyl-piperazine is observed upon their copolymerization with hydrophobic methacrylamide which results in an increase in the hydrophobicity of the material and thus a decrease in its LCST.[36] Except for the *N*-alkyl acrylamide-based polymers, poly(N-vinylcaprolactam) (PVCL), PDMAEMA and PDEAEMA are temperature-responsive polymers that have been studied extensively (Figure 1.6).

N-vinyl caprolactam   2-(dimethylamino)ethyl methacrylate
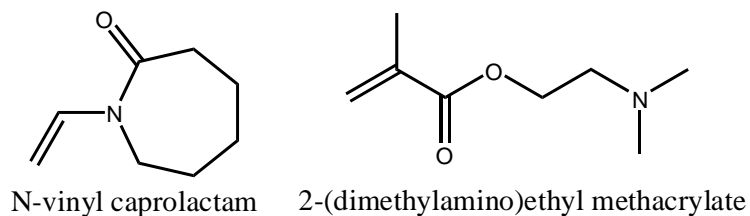
Figure 1.6. Chemical structures of PVCL and PDMAEMA.

PVCL is hydrophilic and water soluble at room temperature but when the solution temperature is increased to 25-30 ^{o}C it becomes hydrophobic and insoluble.[37-38] PDMAEMA also displays a temperature response. PDMAEMA exhibits a temperature-dependent solubility in aqueous solution and has an LCST in the range of 32-53 ^{o}C depending on the polymer molecular weight, the solution pH, and the salt concentration.[39-40] Poly(ethylene oxide)s are also temperature-sensitive polymers. PEO is insoluble in water at temperature above 85 ^{o}C while PPO itself is hydrophobic at room temperature. A large variety of PEO and PPO block copolymers known as Pluronics, Poloxamers and Tetronics are commercially available and exhibit phase transitions ranging from 20 ^{o}C to 85 ^{o}C.[41]

1.1.2.2 *Polymers exhibiting UCST*

A well-known type of temperature-responsive polymers are those exhibiting a UCST behavior. Such polymers are soluble in aqueous media at high temperatures while they become insoluble in water below a critical temperature value. The most common polymers exhibiting a UCST behavior are polymeric betaines. Polybetaines are macromolecules containing an identical number of anionic and cationic species on the same monomer unit. Depending on the type of the ionic groups, polymeric betaines are divided into various subclasses, the most common ones being polycarboxybetaines, polysulfobetaines and polyphosphobetaines. In these types, the repeat units bear simultaneously a quaternized ammonium group and a carboxylate, sulfonate or phosphate group, respectively. The chemical structure of the polycarboxybetaines usually comprises: quaternary polypyrrolidinium-compounds containing linear and branched alkylcarboxy groups, quaternary esters or amides of (meth)acrylic acid, in which the quaternary nitrogen is substituted by an alkoxy group of different chain length and polyzwitterions derived from polymeric heterocyclic or aromatic vinyl compounds (Figure 1.7a).

9
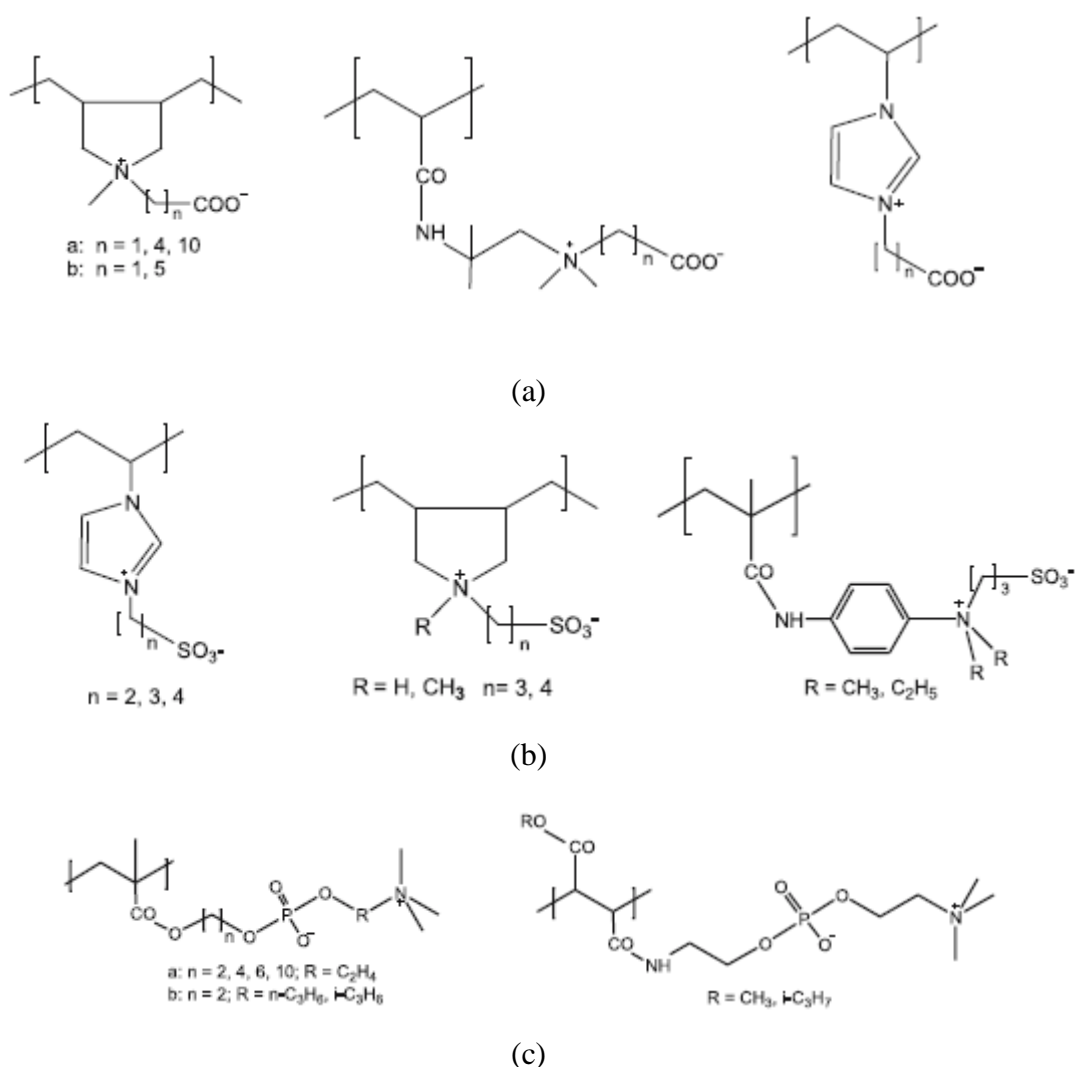
Figure 1.7. Polycarboxybetaines (a), polysulfobetaines (b), and polyphosphobetaines (c).

Similar to polycarboxybetaines, the chemical structure of polysulfobetaines comprises quaternary polypyrrolidinium compounds, quaternary esters or amides of (meth)acrylic acid, polyvinylpyridinium or polyvinylimidazolium compounds bearing an alkylsulfonate group (Figure 1.7b). The polyphosphobetaines are polymeric analogues of the phospholipids (Figure 1.7c). One of the main features of the betaine-type polyampholytes is the tendency of the zwitterionic fragments to form a cyclic conformation via the interaction of the cationic and anionic groups of the neighboring monomer residues (intragroup), or the head-to tail stacking (intrachain) within a single macromolecule and

interchain ion contact between macromolecules. This results in the formation of ionically cross-linked polymer networks (Figure 1.8).
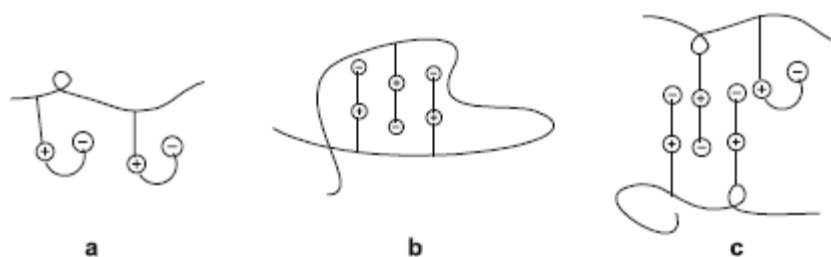
Figure 1.8. Intragroup (a), intrachain (b), and interchain (c) salt bonds in polybetaines.

Therefore, polymeric betaines are considered to be in a collapsed coil form in water below their UCST due to the intra- and/or inter-chain associations.[42] By increasing the temperature these associates unfold towards individual polymer chains and results in the solubilization of the polymer chains. The collapsed state is also disrupted by addition of salt, thereby allowing the chain expansion and solubilization due to screening effects.[43]

1.1.3   Light Responsive Polymers

In the recent decades considerable attention has been paid to the study of the properties of the so-called "bistable" compounds, which upon application of a certain external stimulus rearrange reversibly between two thermodynamically stable states A and B (**Figure 1.9**).
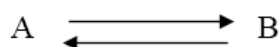
Figure 1.9 The two thermodynamically stable states of a "bistable" compound.

This interconversion can be related to different phenomena such as photochromism, thermochromism and electrochromism.[44] The term photochromism, derived from the Greek words *phos* (light) and *chroma* (color), is related to the application of electromagnetic radiation to the system which causes the reversible rearrangement of the molecules between the two forms, A and B, accompanied with changes in the absorption spectra of the compounds.[44] Upon application of electromagnetic irradiation the electrons of the molecules are promoted from the lowest electronic state to higher energy levels or

11

excited states and subsequently relax back to the ground state by radiative pathways such as fluorescence or phosphorescence or by non-radiative pathways such as energy transfer to the solvent or other molecules. However, when a molecule is photochromic it absorbs this energy to change conformation[45] usually accompanied by molecular structural modifications e.g. cis-trans isomerization, bond scission (homolytic or heterolytic) or tautomerism. Therefore, for photochromism to occur the interconversion between the states A and B should be faster than the other deactivation pathways. Thermochromism is related to thermal induced rearrangement of the molecules characterized by a color change, while electrochromism which is also accompanied by switching between different colors is induced by the generation of different redox states of the compounds possessing different electronic absorption bands.[44] On the other hand, solvatochromism is a phenomenon related to color changes due to pronounced changes in the position (and sometimes intensity) of the UV/Vis absorption bands, induced by variations in the polarity of the environment surrounding the compounds. A hypsochromic (or blue) shift in the spectrum upon increasing the solvent polarity is usually called negative solvatochromism. The corresponding bathochromic (or red) shift is termed positive solvatochromism.[46]

Various families of organic molecules such as spiropyrans, spirooxazines, naphthopyrans, chalcones, diarylethenes, fulgides and azobenzenes exhibit a photochromism behavior (Figure 1.10). These compounds can be classified to the thermally reversible and irreversible molecules upon their thermal behavior. Spiropyrans, spirooxazine, naphthopyrans, and chalcones belong to the first category while diarylethenes and fulgides belong to the second.

Photochromism does not only induce variations in the absorption spectra of the two bistable compounds, but also diverse physical and chemical properties such as refractive indices, dielectric constants, oxidation-reduction potentials and geometrical characteristics.[47] The significant alteration in the properties of the molecules before and after irradiation with light renders them attractive candidates for use in various applications including optical memories, optical switching displays and non-linear optics.

Spirobenzopyran   Spironaphthooxazime   Naphthopyran

Diarylethene   Furylfulgide
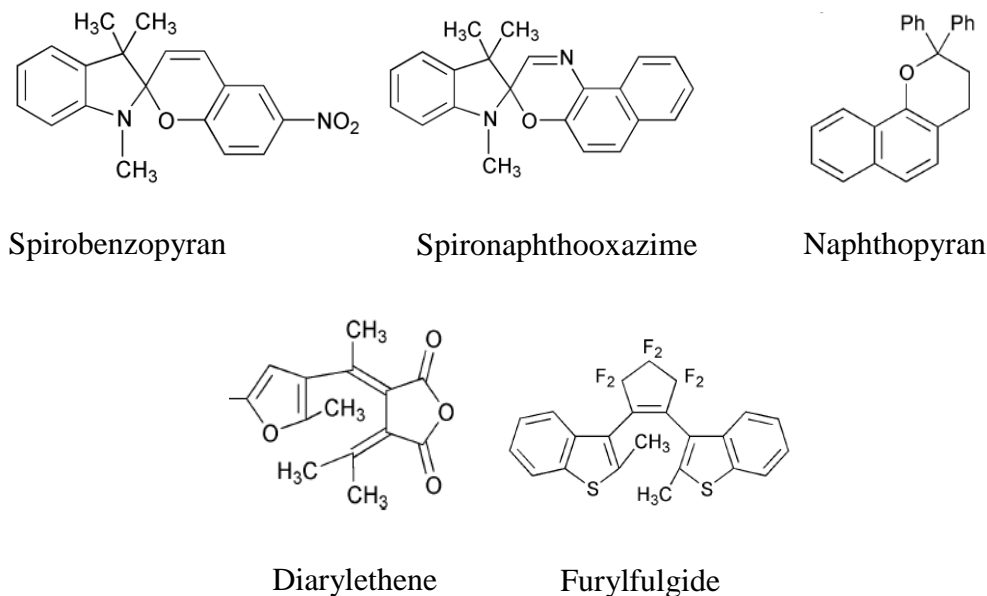
Figure 1.10. Families of molecules that exhibit photochromism.

Spiropyrans comprise one of the most studied and applied family of photochromic compounds. These molecules consist of two orthogonal π-networks which are connected by a tetrahedral carbon center (spiroconjugation).[44] When the nonionic spiropyran (SP) is irradiated with UV light the C-O bond of the benzopyran ring of the molecule is heterolytically cleaved to afford the hydrophilic and bipolar merocyanine (MC) isomer. The isomerisation is reversible and the closed parent molecule can be retrieved either thermally or upon irradiation with green light. (Figure 1.11)

Spiropyran (SP)   Merocyanine (MC)

Figure 1.11. Schematic representation of the photoisomerization of SP to MC.

The initial state of the spiro-compound is an orthogonal colorless compound which is known as the closed spiro form. The important characteristic of this isomer is that the

π-electrons of the benzopyran and indoline ring do not interact and the absorption spectra of the molecules represent a sum of spectra of the two parts.[48] However, upon irradiation with UV light, the C-O spiro bond in the SP form is cleaved heterolytically allowing the rotation of the two moieties of the molecule and thus the "spiro" carbon which was sp^3-hybridized achieves sp^2-hybridization and the molecule becomes planar. This planar isomer known as MC has the ability to absorb photons of visible radiation due to its extended conjugated system and is therefore strongly colored. It has been proved that under continuous irradiation of the liquid or glassy solutions of the SP molecules, all isomers with C-O bonds longer than 1.42 Å can undergo the thermal and photochemical transformations described above, whereas the SPs with shorter C-O bonds, exhibit neither thermochromic nor photochromic properties.[44] On the other hand, MCs are thermally unstable and undergo isomerization to spiropyrans even in dark.[49] However, the rate of the MC-to-SP isomerization is highly depended on the polariry of the environment and the functional substituents on the indoline and the benzopyran ring. In general, MC isomers are stabilized by either a polar environment or specific substituents on the benzopyran and indoline rings. Previous studies have shown that depending on the ring substituents the colored isomers can exist either in the switterionic or in the keto form (Figure 1.12).

$$(1) \qquad\qquad (2)$$

Figure 1.12. Keto (quinodal) (1) and Switterionic (2) form of merocyanine.

1.1.3.1 Solvatochromism

Several reports have indicated that the type of the oxygen of the colored form is determinant for the solvatochromic behavior of the photochromic compound, which can be affected by interactions between the solutes and the solvent media of different polarity. The quinodal character of the oxygen induces positive solvatochromism that is a shift of the absorption maximum of the molecule to longer wavelengths upon increasing the

polarity of the surrounding medium. On the other hand, the switterionic isomers exhibit the opposite trend that is a shift of the absorption maximum to shorter wavelengths upon raising the medium polarity, referred to as negative solvatochromism[50] in accordance with the ground state being more dipolar than the excited state.[51] Thus, the color of the MC isomer depends on the difference in polarity between the photoexcited MC form and the conjugated zwitterionic groud state. In polar solvents, the ground MC state is better solvated than the first excited state and thus the ground state dipole moment is larger than that of the excited state, leading to a blue shift in the visible absorption band (Figure 1.13a).[44]

(a)   (b)
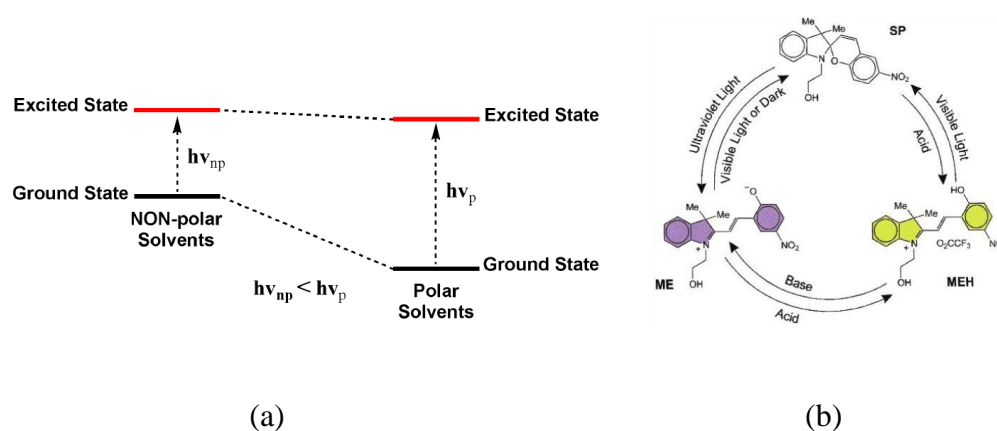
Figure 1.13. Schematic representation of the energy difference between the ground and the excited state of MC in polar and non-polar solvents (a), and switching cycle describing the transition conditions between the three states **SP**, **MC**, and **MEH** (b).

Apart from the polarity of the solvent, the solution pH can also affect significantly the structure of the MC form (Figure 1.13). In particular, when the colorless SP isomer (absorption band around 400 nm) is irradiated with UV light the colored form MC is generated as indicated by the purple color of the solution (absorption band at 563 nm and emission band at 647 nm) (Figure 1.13b). Addition of CF_3COOH in the irradiated solution of the molecule resulted in the protonation of the MC form and the formation of the yellow-green MEH isomer (absorption band at 401 nm), while increase of the solution pH effected by addition of K_2CO_3 induced the reversible reformation of the purple MC form which upon irradiation with visible light afforded the parent SP molecule.[52-53]

1.1.3.2 Substituent Effect

Control of the photochromic isomerization rates is essential for the commercialization of such compounds. One way to improve the control of these systems is the introduction of substituents on the rings of the chromophores. Studies on spirooxazines[50] have indicated the existence of different mechanisms; namely the "push-pull" and the "pull-push" mechanism depending on the substituents of the two perpendicular aromatic systems. In particular, in the "push-pull" mechanism when electrons are pushed toward the benzopyran ring, by the attachment of electron-releasing groups onto the indoline moiety and electron withdrawing groups onto the benzopyran moiety, the molecules adopt the switterionic structure. In the "pull-push" mechanism when electrons are pushed toward the indoline part, by the attachment of electron-releasing groups in the benzopyran moiety and electron withdrawing groups onto the indoline moiety, the chromophores prefer the quinodial structure (Figure 1.14).[50,54-55] The neutral systems behave in an intermediate way. A recent report concluded to a slightly different result according to which introduction of an electron releasing group onto the indoline part stabilizes the biporal stuctrure, while the existence of an electron-releasing group onto the benzopyran ring stabilizes the quinoidal form.

(1)	(2)
"Push-Pull"	"Pull-Push"
Switterionic Merocyanine	Quinodial Merocyanine
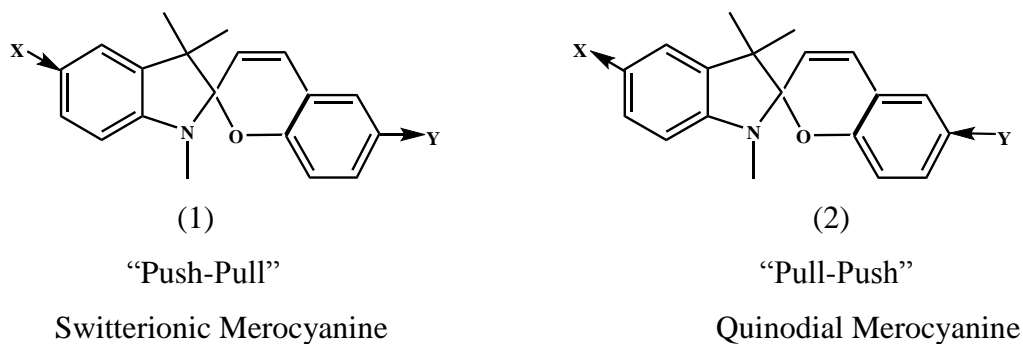
Figure 1.14. Effect of the substituents on the structure of the MC form (1) X= electron-releasing groups, Y=electron withdrawing group (2) Y= electron-releasing groups, X=electron withdrawing group.

The introduction of specific substituents such as crown ethers onto the spiropyrans (Figure 1.15) can lead to the formation of metal ion responsive photochromic

molecules.[56] Even though the charged phenolic oxygen atom of the merocyanine form could bind to a metal center in cooperation with other chelating functions attached at the 8'-position, the complexation does not inhibit the photoisomerization of the molecule but only affects the absorption maximum of the MC form.[57] On the other hand, when SP molecules are carrying crown ether moieties the photoisomerization can be affected by the affinity of the metal ions for the crown ether moiety.
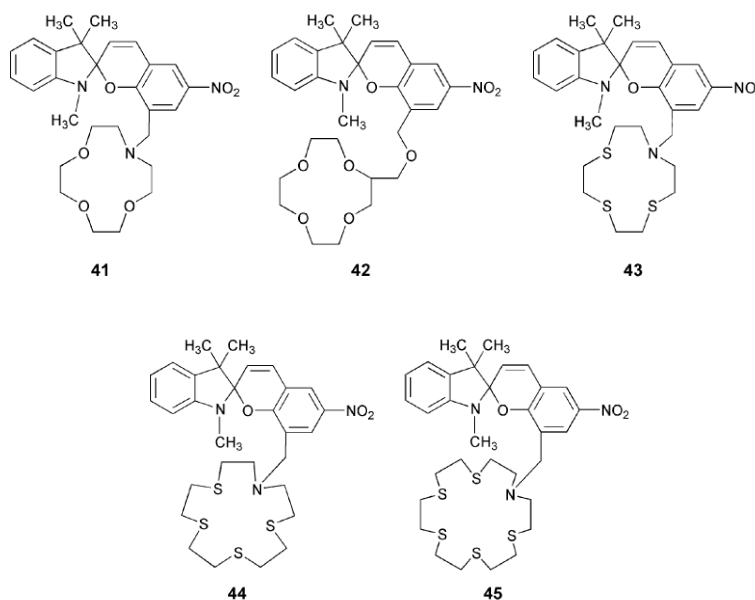
Figure 1.15. Introduction of crown ethers as substituents onto spiropyran molecules.

1.1.3.3   Isomeric forms of Merocyanine

Although eight possible isomers of the open merocyanine structure have been reported in the literature, only four of them are stable and exhibit a local energy minimum.[48] The studies of Nakamura et al.[58] as well as the thermodynamic calculations of Maeda at al.[59] revealed that the trans-trans-cis (TTC) and the cis-trans-cis (CTC) isomers were the most stable (Figure 1.16). This is attributed to the interaction between the central hydrogen and the carbonyl oxygen. According to calculations[60] the most stable merocyanine isomers of naphthoxazine (Figure 1.16) TTC and CTC, exhibit much larger dipole moments (3.6 and 4.3 D, respectively) compared to the closed form (0.6 D). This observation gives a reasonable explanation for the stabilization of the merocyanine isomers in polar media as predicted by calculations and proved by experimental data.[44]
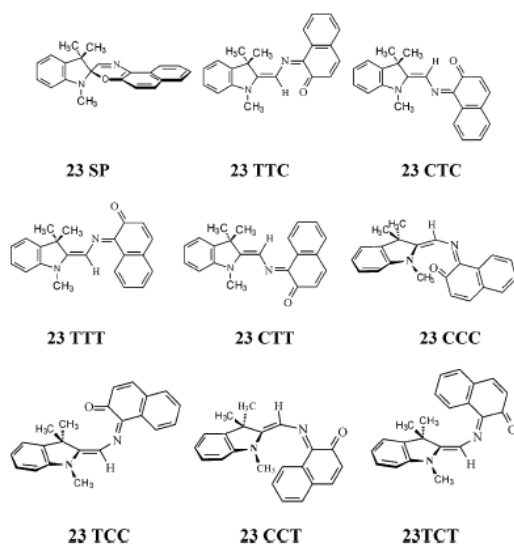
Figure 1.16. Possible isomers of the open merocyanine structure.

1.1.3.4 Aggregation Mechanism

An important property of the MC isomers is their tendency to aggregate into a stack-like arrangement[61-63] (Figure 1.17). This phenomenon is very usual and rather stable aggregates can be observed even in diluted systems or in polymeric films. The giant molecular MC-MC stacks formed in solution are known as Scheibe aggregates. Two types of stacks, the H- and the J-aggregates, have been identified so far which exhibit a distinct maximum in the absorption spectrum. When the molecular dipoles of the MC species are arranged in a parallel orientation (head-to-head arrangement), J-stacks are formed which exhibit an absorption maximum shifted to longer wavelengths (red-shifted) compared to that of the parent MC isomer. On the other hand, if the alignment of the molecular dipoles of the MC isomers is anti-parallel (head-to-tail arrangement) the formation of the H-stacks is promoted which are characterized by an absorption maximum shifted to shorter wavelengths (blue-shifted) compared to that of the free MC species.
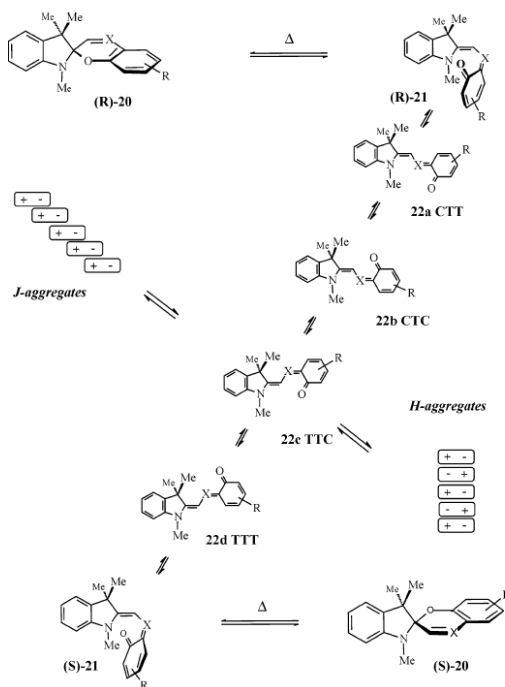
Figure 1.17. Formation of MC-MC Scheibe Aggregates (J- and H-aggregates).

The aggregates are considered to have tilted deck-of-cards, brickwork or herring-bone structure. Studies of H- and J-aggregates in polymer films revealed that at low degrees of association the MC molecules are organized in a rather loose H-stack, structure which allows thermal conversion back to spiropyrans. The retardation of this back reaction as well as the hypsochromic shift depends on the degree of association. On the contrary, J-stack formation leads to a high degree of merocyanine association, a bathochromic spectral shift and phase separation of the J-stacks embedded in the polymer matrix. The stabilization of the MC form in J-stacks is so strong that the dye appears to be indefinitely stable and cannot be converted back to spiropyran without degradation. This stabilization is related to the strong interactions between the MC molecules in the J-stacks and the regular structure of the J-aggregates.[64] Moreover, the colored MC molecules can interact with SP molecules to give A_nB (n=1,2) complexes. The A_2B absorption bands in the visible region are shifted bathochromically with respect to the AB bands. The A_2B complexes form highly dipolar microcrystals having a molecular stack structure. These microcrystals are coated with amorphous material composed of AB complexes and give

rise to a colloidal suspension of globules of about 0.1-0.4 μm in diameter. The microcrystalline nuclei of these globules are responsible for their optical and electrical anisotropy.[65]

Even though the ability of the MC isomers to aggregate can be counted as a major disadvantage, their controlled formation can become a useful tool for various applications. For example, the study of J-aggregates formed in non-polar solvents after irradiation of the SP isomer with UV light, indicates that the stacks exhibit very narrow absorption bands, which is a significant parameter for the design of wavelength-multiplexed memory systems.[66] Moreover it has been proved that the formation of aggregates affect the refractive index of the materials and this might be a useful effect that should be taken into account for the synthesis of tunable photonic band-gap materials.[67]

1.1.3.5   Spiropyran Containing Materials

During recent years, the incorporation of SP chromophores into organic and inorganic matrices has provided a great tool for the development of advanced materials. The need for introducing these molecules in matrices have arisen from two limitations, related to the nature of the chromophores, which restricted their use as independent units; the first is the short life-time of the colored MC species in solution which are thermally unstable and revert back to the parent SP molecules, and the second is their oxygen catalyzed degradation. Thus, the incorporation of these photochromic systems into rigid matrices such as polymers and sol-gels is expected to restrict the mobility of the MC form as well as the diffusion of oxygen.[68]

Two main approaches have been used so far for the preparation of polymer-spiropyran hybrids; the doping method and the covalent attachment method due to its simplicity. The doping approach has been reported in various systems such as organic polymers, inorganic materials and in inorganic/organic matrices.[69-70] Incorporation of photosensitive compounds in matrices with domains of different polarity was proved to be very interesting since it allowed the migration of the molecule to the most compatible-domain depending on the polarity of the isomeric form adopted. Moreover, the concentration of the chromophores embedded in the matrix was proved to be a determinable parameter for the available free volume of the molecules which affects

significantly the conformational changes and the decoloration rate of the chromophores.[71] On the other hand, the covalent attachment of spiropyran molecules within matrices is synthetically more demanding compared to the doping method and requires the incorporation of a polymerizable moiety in the chromophore.[71] Two parameters are crucial and should be considered in this approach; the concentration of the photosensitive nolecules and the length of the spacer which will link the chromophore to the polymeric backbone. It has been proved that closely bound chromophores exhibit slow decoloration rate due to the restricted free volume that hinders the photochromic transition.[72-74] The decoloration rate of the molecules can also be affected by the number of polymerizable groups introduced in the molecule. In particular, when chromophores bearing two polymerizable units were covalently linked in a polymer matrix, a more complicated decoloration behavior was observed attributed to restrictions imposed by the polymer matrix.[75] Comparative studies of the two methods have revealed several debates. Even though negligible differences have been reported in some cases for the two methods, Hu and coworkers[71] as well as Lyubimov et al.[75] have established significant differences among the two approaches.

The isomerization rates of the spiropyran molecules in a given environment are generally affected directly by three factors; polarity, rigidity and free-volume. The effect of the polarity of the matrix is divergent from that in solution. The increase of the polarity in a matrix results in the decrease of the bleaching rate of the molecules due to the effective stabilization of the MC form which in highly polar environments is the most stable state. The effect of matrix rigidity on the isomerization rate of the chromophores was also proved to be important. Studies in a wide range of polymer matrices ranging from flexible, low T_g polymers to rigid glassy systems showed that the increase in the rigidity of the system results in lower decoloration rate of the chromophores. It was recently shown that the attachment of flexible low T_g oligomers such as poly(dimethylsiloxane) to photochromic dyes increases significantly their switching speeds in a rigid polymer matrix.[76] The effect of free volume was also proved to be critical for the decoloration rate of the molecules. The MC-to-SP isomerization is a spatially demanding process since a *ca.* 90° rotation of one-half of the molecule is required for the close SP isomer to reform. Thus, the fading rate of the molecules

increases with the free-volume when the rotation of the colored isomer is favored. On the other hand, a spatially restricted environment and thus the low free volume stabilizes the chromophores over thermal relaxation. It was reported that the incorporation of merocyanine molecules in a phenylsiloxane resin improved the thermal stability of the colored form by a factor of 10^4 in comparison with their stability in ethanol solution.[77]

Recently, the synthesis of spiropyran-based materials is of particular interest due to the multireponsive nature of the molecule. However, the incorporation of the chromophores into materials requires first their modification either with polymerizable moieties or other functional groups and the study of their responsive behavior. Shumburo and Biewer[68] reported the synthesis of a series of *N*-substituted nitro-spiropyran compounds and investigated their photoisomerization rates in polar and non-polar solvents and in organogels (Figure 1.18).
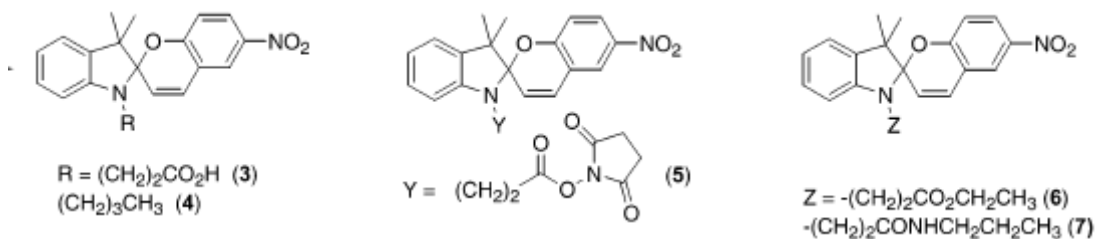
Figure 1.18. *N*-Substituted nitro-spiropyran molecules.

The decoloration rates of the molecules in polar solvents were relatively slow due to the effective stabilization of the colored form, while the incorporation of the spiropyran molecule carrying a succinimidyl group into an organogel showed the stabilization of the colored isomer over thermal relaxation by more than 195 times compared to solution (Figure 1.18-5). The restricted environment of the organogel hinders the MC-to-SP isomerization and increases significantly the life-time of the bipolar species. The retardation of the SP recovery upon photoexcitation was also reported by Hirano et al.[78] who showed the effective stabilization of the colored isomer of a chromophore (Figure 1.19b) in polar solvents (DMSO and methanol). Even though the decoloration of the colored species is slow in environments with low free-volume, however, the SP-to-MC ring-opening reaction is not suppressed as proved when the acrylamide-spiropyran

monomer d (Figure 1.19) was copolymerized with NIPAM and then incorporated in a silica gel.[79]
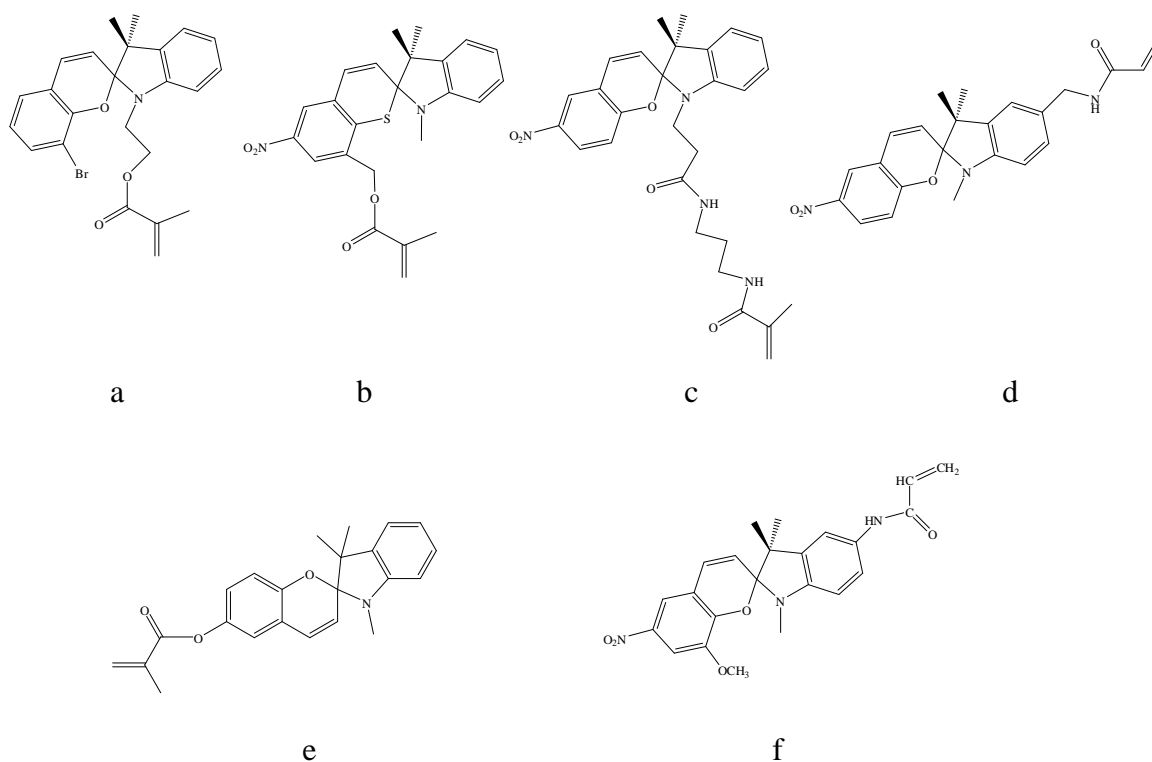
Figure 1.19. Photochromic monomers used for the synthesis of spiropyran-based materials.

A series of spiropyran-based polymers have been synthesized so far upon polymerization of different photoresponsive monomers such as 1',3',3'-trimethyl-6-methacryloyloxy-spiro(2H-1-benzopyran-2,2'-indoline)[80] (Figure 1.19e) and 5-acrylamido-1,3,3-trimethylindolino-6'-nitro-8'-methoxy spiropyran (Figure 1.19f)[81] with acrylates, methacrylates and styrenics by conventional free radical polymerization. McCoy et al.[82] (Figure 1.20a) and Elizalde et al.[83] (Figure 1.20b) in an effort to extend the work on spiropyran-based polymers, synthesized and studied the responsive behavior of *N*-substituted T-type spiropyran molecules which can be further utilized for copolymerization with either vinyl or acrylate-based monomers. The compounds exhibited solvent-depended absorption properties. In particular, only the nitro-substituted compounds undergo the photoinduced SP-to-MC isomerization in acetone while in dichloromethane non- and nitro-substituted molecules showed stack-formation (Figure

1.20a). It is worth noting that the number of methylene groups in the polymerizable spacer had a negligible effect on the photoisomerization rate.
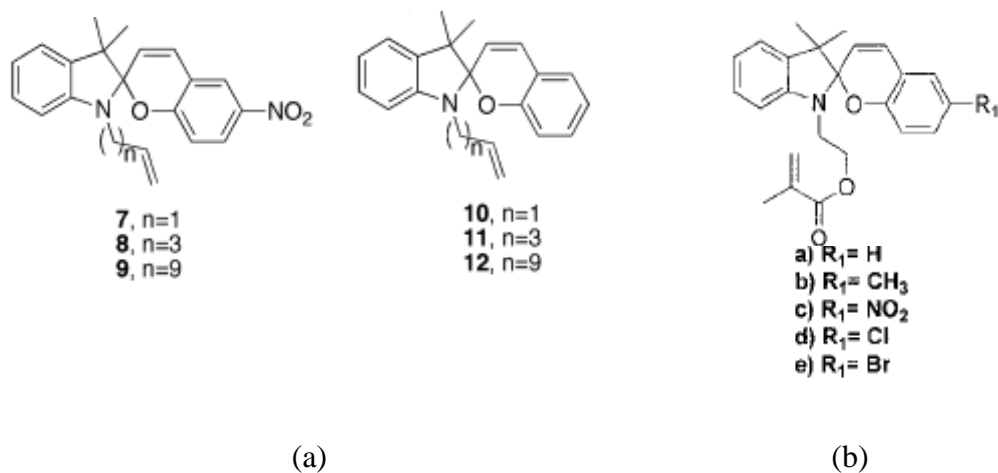
Figure 1.20. T-Monomers

Major was the contribution of Krongauz and Goldburt[65] in the establishment of the stack-like behavior of spiropyran molecules when they are covalently incorporated in a polymeric backbone. For this purpose, a spiropyran-based monomer (Figure 1.19a) was homo- and copolymerized with methyl methacrylate by conventional free radical polymerization and the absorption properties of the materials were studied in the solution and in the solid state and compared to that of the parent molecule. The monomer spectra in solution showed the presence of MC moieties and SP_2-MC complexes. However, the corresponding polymers in solution exhibited insignificant aggregation since only few MC_n and MC-SP stacks were observed due to macromolecular coiling (intramolecular interactions) (Figure 1.21). On the other hand, the aggregation behavior of the polymers was completely different in the bulk where the formation of three-dimensional domains was observed due to the interaction between merocyanine side groups of different macromolecule chains (intermolecular interactions) with a degree of crystallinity of about 40%. The increase in the polarity of the surrounding medium favored further ordering of the molecules due to the effective SP-to-MC interconversion. This mechanism is known as "Zipper Crystallization."[84] Goldburt et al.[84] studied further the aggregation behavior of spiropyran molecules within polymer matrices. For this purpose, spiropyran-based

24

monomers carrying spacers of variable length for connection along the macromolecular chain were copolymerized with methacrylates, acrylates and styrenics. Studies of the isomerization behavior of the photoresponsive units in solution and in bulk showed that the photo-switching of the molecules is highly affected by the length of the spacer connecting the SP moiety to the main polymer chain. The longer the spacer the higher the reaction rate due to the increased flexibility of the MC side groups. These studies also showed the existence of two types of MC species in the materials; the long- and the short-lived MCs. Long-lived MCs belong to molecular stacks formed in loops or other "close"-packed segments. Their long lifetime originates from the fact that their transformation to SP molecules requires either the escape of the MC moiety from the stack or the cleavage of the structure. Better solvation of the polymer results in looser polymer coils and in short-lived MC moieties that fade faster. The "Zipper crystallization" resulted in the formation of more regular intermolecular stacks among the chromophore units in accordance with the studies of Krongauz and Goldburt discussed above.
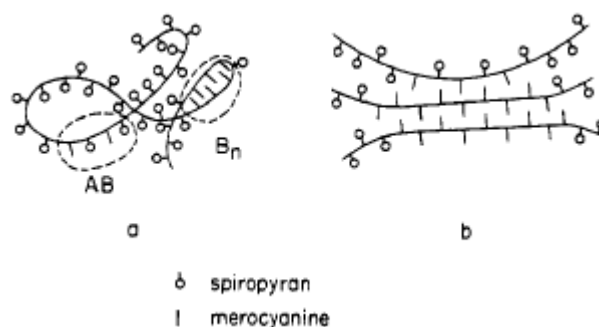
Figure 1.21. Interactions of the polymeric side groups in solution (a), and in the bulk (b).

Despite the tendency of the SP molecules to form aggregates under certain circumstances as discussed previously, spiropyran-based materials can find various applications such as in optical data storage units, in biological fluorescence labeling, as molecular switches, in light-induced detachment of cells, etc. Spiropyran-containing membranes have been successfully used in bio-separation and more specifically in the filtration of specific proteins from complex liquid mixtures.[85] The preparation of the membranes was accomplished via the photopolymerization of vinyl spiropyran, [1'-(2-(propylcarbamylmethacrylamide) ethyl)-3',3'-dimethyl-6-nitrospiro[2H-1]benzo-pyran-

2,2'-indoline] (Figure 1.19c) onto poly(ether sulfonate) membranes. The SP-to-MC isomerization of the chromophores upon photoexitation accompanied with the increased polar character of the MC isomers compared to the apolar SP species allowed tuning of the membrane polarity and wettability. The "closed" SP isomers showed a higher affinity to bovine serum albumin (BSA) binding and adsorbed 26% more protein compared to the open MC form. Thus, the "closed" configuration of the SP molecule on the membrane showed 17% lower phosphate buffered saline (PBS) permeation flux compared to the "open" configuration. These membranes can be proved useful in waste water treatment, in targeted drug delivery applications and in the development of surface valves to control the liquid flow into a lab-on-chip device. The inherent property of the SP chromophores to undergo a significant increase in their polarity upon isomerization to the MC form has been successfully used for the mild detachment of cells from surfaces and their isolation under mild conditions without the need for heat treatment.[86] For this purpose nitrobenzospiropyran-*co*-MMA random copolymers were synthesized by a conventional route and were studied as coating on glass plates for the controlled UV-regulated detachment of platelets, mesenchymal stems and fibrogens. The cells were detached from the photosensitive surface upon light irradiation due to the increased hydrophilic character arisen from the SP-to-MC isomerisation of the chromophores in contrast to the control poly(methyl methacrylate)-coated glass plates which did not show any response. These surfaces can be potentially used in surface marker analysis using flow cytometry.

The chemical attachment of SP dimers in polymeric chains can provide a useful tool for the development of controlled molecular machines in sensing and delivery systems (Figure 1.22).[87] Upon SP-to-MC photoisomerization the polar MC form can interact strongly with ionic species which can then be easily released in a controlled manner via irradiation with visible light due to the reformation of the non-polar SP isomers. The polymeric component can function as a scaffold and prevent the precipitation of the insoluble MC form and its aggregates in a good solvent for the polymer resulting in the formation of self-assembled structures.
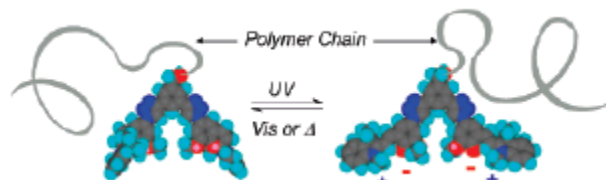
Figure 1.22. Light induced photochromism of the spiropyran dimer-polymer conjugate.

The reversible and abrupt increase in the hydrophilicity of the SP chromophores due to the SP-to-MC isomerization and the remote nature of the light stimulus which provides spatial and temporal control can be used as a tool for regulating remotely the hydration of microgels (Figure 1.23a).[88] It was shown that the incorporation of SP chromophores into PNIPAM-allylamide copolymer microgels affect their temperature-induced volume phase transition. In particular, the photogeneration of the MC isomers within the microgels increased the volume phase-transition temperature of the colloids which swelled due to the increased solvation of the MC species by water, resulting in increased osmotic pressure within the gel. However, when the colloids were irradiated with visible light the closed, non-polar SP species were formed which increased the hydrophobicity of the microgels and favored the decrease of the volume phase-transition temperature. The incorporation of SP moieties within microgels not only affects the physical properties of the colloids but it can also be proved beneficial for the enhancement of the optical properties of the chromophores (Figure 1.23b).[89] The encapsulation of SP species in polymeric nanoparticles comprising an outer hydrophilic PNIPAM shell and a hydrophobic polystyrene core, cross-linked with divinylbenzene, was proved to reinforce the fluorescence of the MC species by more than 200 times in aqueous media. That was attributed to the isolation and the protection of the fluorophores within the hydrophobic polymer cavities from nonradiative decay or electron transfer pathways generated by collisions with the media components. Moreover, the high quantum yield was attributed to the restricted conformational flexibility of the molecules which were trapped in the polymeric matrix. The latter minimized nonradiative relaxation through internal motions of the excited molecules. Furthermore, the immobilization of a photochromic molecule in a hydrophobic cavity offers protection over fatigue effects arising from photochemical switching. These materials are attractive for use as optical

digital storage units based on either absorption or fluorescence read-outs and for biological fluorescence labeling.

The property of the SP molecules to form aggregates upon irradiation with UV light has been applied to control the magnetic properties of composite materials (Figure 1.23c).[90] Iron oxide nanoparticles have been intercalated into photoresponsive nanocapsules formed by the self-assembly of SP-containing amphiphiles. Irradiation of the nano-assemblies with UV light resulted in the SP-to-MC isomerization of the chromophore units and the formation of J-aggregates which induced the increased magnetization of the system. However, the irreversible nature of the stacks formed, hindered the reversible modulation of the magnetization. Formation of J-aggergates was also observed for hybrid organic-inorganic nanoparticles comprising photochromic spiropyran molecules intercalated in a layered $MnPS_3$ material when cast from an organic solution in the presence of a polymer to form thin films. These films exhibited rewritable photoimaging properties suggesting their use for rewritable optical memory media or imaging processes.[91]

(a)

(b)

(c)

Figure 1.23. Photochromic spiropyran molecules (a) immobilized onto the surface of a polymeric sphere (b) embedded in the hydrophobic cavity of a polymeric nanoparticle (c) as part of an amphiphile forming an organic assembly for the intercalation of iron oxide nanoparticles.

The combination of photochromic SP molecules with a helical supramolecular structure offers the opportunity for varying the optical properties of these materials upon the application of external fields (electric and magnetic) and light irradiation.[92] Bobrovsky et al. proposed the copolymerization of SP-based monomers with comonomers carrying nematogenic phenyl benzoate and chiral cholesterylside side groups. The presence of phenyl benzoate and the cholesteryl groups allows the development of a chiral nematic mesophase capable of light reflection at a certain wavelength, while the spiropyran groups render this mesophase responsive to light irradiation. These systems are very promising for applications in data recording and optical data storage (Figure 1.24).
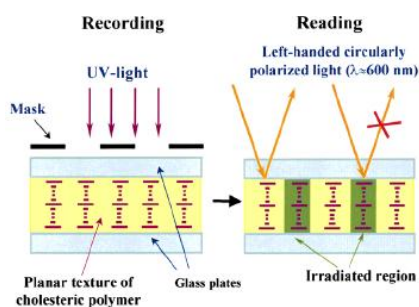
Figure 1.24. Optical data recording (left part) and reading (right part) of the information from the same photochromic-cholesteric polymeric film

The isomerization rate of the ring-closure MC-to-SP reaction is highly affected by the microenvironmet of the chromophores and has been widely used as probe for several processes. Hachisako et al.[93] evaluated the critical gelation concentration of L-glutamic acid by employing lipids with SP head groups and monitoring the first-order kinetics of the thermal MC-to-SP isomerization, which is sensitive to the dispersion state of the lipids and thus enables the determination of their critical aggregation concentration.

Lately, scientists have used the ability of the SP chromophores to complexate with metals in order to prepare photochromic metal-absorbing honeycomb structures. A SP molecule carrying a hydroxyl functionality was coupled to a poly(acrylic acid) linear polymer and the resulting photochromic polymer was used to form ordered honeycomb materials by the breath (BF) technique. Due to the ability of the MC isomers to

complexate with metals the honeycomb structures were embedded with palladium ions, which upon reduction afforded hybrid organic/inorganic porous networks. Calcination of the hybrid material resulted in the formation of unique palladium microrings. This method provides a generalized strategy for preparing hybrid structures incorporating a range of metals.[94]

Recently, the property of the SP molecules to act as mechanopores, that is their mechanochemical response to stress, was studied by incorporating the molecules into polyurethane via step growth polymerization. The stress induced a 6-π electrocyclic ring-opening to the colored MC form of the mechanophore which was quantified by measuring the change in the absorbance of the polymer. The absorption intensity of the material was proved to increase linearly with strain, while when the strain was held constant the MC form did not revert back to the thermodynamically preferred SP form. Thus SP mechanophores can impart the unique functionality of visual stress detection to polymers and have potential for use in smart materials with self-sensing capabilities.[95]

1.1.4 *Multiresponsive materials*

The synthesis of "smart", multiresponsive materials that can recognize independently or synergetically more than one stimulus exhibiting collective responses, accompanied with the formation of hierarchical self-assemblies or/and changes in the volume, shape of surface characteristics of the materials is of particular scientific interest for a wide range of potential applications in drug delivery, tissue engineering, self-healing materials, bioseperations, sensors and actuators. However, the development of synthetic systems being capable to cooperatively respond to multiple external stimuli resulting in an output in a controllable and predictable fashion still possesses a significant challenge. The last years the scientific community has boosted the synthesis and characterization of multiresponsive polymers utilizing robust synthetic techniques such as click chemistry and controlled/living polymerization methods in an effort to elucidate structure-to-property complexity in a controlled manner. Most studies are focused on dual responsive materials which are in the form of linear or graft polymers, polymer or hybrid particles, physical or chemical gels and polymers surfaces or interfaces being sensitive to pH and temperature variations, whereas light-, redox- and competitive host/guest-responsive

materials have been also reported but in a much lesser extent. In this section the focus will be on materials being sensitive to two or more stimuli or exhibiting cooperative dual responsiveness to non-classical stimuli resulting in increased functional complexity in a synergistic manner.

Linear polymers although being simple in terms of architecture, they can exhibit functional complexity and fascinating properties upon choosing the appropriate starting materials and the suitable synthetic pathway with respect to their final application is chosen. A beautiful example of a triply stimulus-sensitive block copolymer assembly, consisting of a temperature-sensitive PNIPAM block and an acid sensitive tetrahydropyran (THP)-protected 2-hydroxyethyl methacrylate (HEMA) part connected by a redox sensitive disulfide functionality was recently reported. The amphiphilic block copolymers which self-assemled into micellar structures in water at RT, flocculated above the LCST of PNIPAM when the block became hydrophobic. The disruption of the self-associated structures was also induced by the hydrolysis of the cyclic acetal functionality of the protected HEMA block under mildly acidic conditions which resulted in the formation of the hydrophilic HEMA units and created an imbalance in the hydrophilic/lipophilic balance of the block copolymers. In a reducing environment, the scission of the intervening disulfide bond connecting the two blocks was promoted leading to the cleavage of the block copolymers into their constituent parts and the disassembly of the polymeric micelles as manifested by controlled release experiments of a model dye molecule.[96] The self-associated behavior of triply sensitive PNIPAM chains carrying tetrathiafulvalene (TTF) end-groups which were able to respond to multiple stimuli including temperature, redox processes and host-guest interactions was also studied. Due to their hydrophobic and hydrophilic nature, TTF and PNIPAM units respectively favored the self-assembly of the polymers in water affording polymeric micelles. Chemical oxidation of the TTF moieties to its TTF^{2+} derivatives resulted in the disruption of the micellar architecture due to the increase in the hydrophilic character of the TTF core. Interesting results were also observed when these researchers studied the host-guest interactions of the TTF moieties with π-rich-electron molecules such as tetracationic macrocycle cyclobis(paraquat-p-phenylene) ($CBPQT^{4+}$, $4Cl^-$). It was found that the minute addition of $CBPQT^{4+}$ resulted in efficient micelle disruption, as evidenced

by controlled release experiments using Nile red loaded micelles, due to the increase of the hydrophilic nature of the TTF moiety upon complexation with $CBPQT^{4+}$.[97] An example of a multi-bio-responsive polymer was reported by the Ulijn group who synthesized novel polyoxazoline based block copolymers. Polyoxazolines are known to exhibit LCST close to physiological temperature. Ring opening polymerization using an alkyne functional initiator was employed to produce an alkyne terminated 2-isopropyl-2-oxazoline block. The complementary azide terminated block was prepared by coupling a fluorenylmethoxycarbonyl-tyrosine (FMOC) with 11-azido-3,6,9-trioxaundecan-1-amine by carbodiimide coupling. The two blocks were linked by ''click'' chemistry to afford the final polymer with one polyoxazoline and one phosphatase- sensitive block, respectively. The polymer exhibited interesting self-assembly properties in aqueous solutions derived either by the application of a temperature stimulus or by the presence of phosphatase which could cleave the phosphate groups of the FMOC containing block with subsequent alternation of the nanoassemblies size.[98] Recently, multiresponsive polymers being sensitive to light for various potential applications, have attracted considerable attention due to the remote character of the stimulus providing temporal and spatial control. Spiropyrans are uniquely attractive compounds since apart from their photo-responsiveness they also show sensitivity towards a number of other stimuli such as solvent polarity, pH and temperature. Thus, their proper combination with other smart functionalities in a single system can open new avenues for the development of multisensitive materials. Recently, we have reported the synthesis of multiresponsive PDMAEMA-*co*-PSP random copolymers synthesized by ATRP, whose optical properties are highly affected by the DMAEMA comonomer, and their physicochemical properties can be modulated upon varying independently four different stimuli; namely the medium polarity, the solution temperature and pH and electromagnetic radiation of specific wavelength. These materials also showed excellent cooperative response to temperature and light stimulation resulting in one controllable output.[99] In a similar study Zhao et al. investigated the temperature-responsive behavior of block copolymers carrying two different photoisomerizable moieties, SPS and azobenzenes (Azo), on the same polymer backbone along with hydrophilic thermosensitive segments, before and after stimulation with electromagnetic radiation of specific wavelength. The isomerization of the Azo and

SP units exerted a significant influence on the temperature-induced phase transition behavior of the block copolymers which exhibited a single transition being shifted as a function of the relative photoisomerization degree of the two chromophores.[100]

Lately, significant progress has been made in the construction of multiresponsive particles carrying various functionalities aiming at different applications, spanning form biosensing and biophotonics and intelligent delivery applications. The development of novel thermosensitive PNIPAM nanogels bearing water-sensitive fluorophores (BDD-AA units), which can be potentially used as intracellular thermometers, was accomplished via emulsion polymerization. In particular, the fluorescent intensity of the nanogels, being proportional to the potassium cation concentration and independent of pH variation, could be finely tuned across a temperature range near the LCST of the polymeric component, where it became dehydrated and quenching from the surrounding water molecules was avoided. This system has been used for measuring the exact temperature within the cytosol of COS7 cells by detecting changes in the fluorescent intensity with an accuracy of ca. 0.5 ^{o}C.[101] In a related study, a more complicated system comprising PNIPAM microgels carrying photocleavable 5-(2'-(dimethylamino)ethoxy)-2-nitrobenzyl acrylate (DMNA) units and fluorescent resonant energy transfer (FRET) donors 4-(2-acryloyloxyethylamino)-7-nitro-2,1,3-benzoxadiazole (NBDAE) and Rhodamine B-based acceptors (RhBEA) was synthesized by free-radical emulsion polymerization. The incorporation of the FRET pair within the nanoparticles allowed the in-situ monitoring of the volume phase transitions of the particles by means of FRET efficiency. More specifically, the thermo-induced phase transition behavior of the PNIPAM and the UV-regulated cleavage of the DMNA units, to give sodium carboxylate residues, led to swelling of the colloids and to variations in the donor-acceptor distance and thus the fluorescence output.[102] Based on the same principle, replacement of the photocleavable DMNA moieties with K^+-sensitive 4-acrylamidobenzo-18-crown-6 residues (B18C6Am) in the same system, allowed the fabrication of ratiometric fluorescent K^+ sensors. The presence of the FRET pairs within the microgels allowed the facile in-situ monitoring of the thermo- and K^+-induced variations in the microgel volume phase transition by fluorescent spectroscopy.[103]

Hydrogels are attractive materials for the development of intelligent devices and components for various applications including drug delivery, tissue engineering and control in membrane permeability. Even though the majority of materials reported so far focus on dual-sensitive hydrogels being sensitive to pH and temperature changes recently some elegant examples of hydrogels being responsive to other stimuli such as light, competitive host/guest and solvent stimuli have been also reported. A multiresponsive hydrogel was synthesized via the cross-linking of NIPAM and a photosensitive vinyl monomer bearing a spiropyran residue by conventional free radical polymerization. This material was proved to be sensitive to pH and temperature variations and to irradiation with blue light. In particular, in the presence of protons the SP species underwent a ring-opening reaction and became protonated leading to a significant expansion of the gels. However, irradiation of the hydrogel with blue light promoted the deprotonation of the chromophores and their ring-closure reaction which was accompanied with the drastic volume shrinkage of the material and increased the conductivity derived from the protons dissociation from the hydrogel. The photoresponsive hydrogel was further introduced to the surface of a porous membrane, to develop a photo- and thermoresponsive gate membrane and examine its application in mass transfer control.[104] An alternative type of multiresponsive materials, which received considerable interest is that of the so-called supramolecular hydrogels which are of non-permanent nature and can reversibly undergo an abrupt sol-to-gel transition upon stimulation with the appropriate trigger. Alvarez-Lorenzo et al, achieved the synthesis of dual responsive supramolecular hydrogels by mixing the photoresponsive poly(N,N-dimethylacrylamide-*co*-methacryloyloxyazobenzene)(DMA-MOAB) copolymer with a temperature-responsive Pluronic F127 (F127) copolymer in water. Under dark conditions, when the photoresponsive copolymers were self-associated due to their amphiphilic nature, the interactions with F127 were minimal. However, photoexcitation of the molecules with UV light resulted in the trans-to-cis isomerization of the azobenzenes and the increase of the polarity of the copolymers, which promoted the disruption of the micellar structures and the interaction of the photosensitive unimers with F127 to form mixed micelles and undergo a sol-to-gel transition. This light and temperature induced sol-to-gel transition hinder the diffusion of solutes such as methylene blue. Addition of hydroxypropyl-*β*-

34

cyclodextrin in the medium, which hosted the cis azobenzene in the sugar cavities, disrupted the interaction of the photosensitive polymer with F127 and the gel formation. Therefore, variations in the concentration of hydroxypropyl-β-cyclodextrin can be used to modulate the response of the copolymer blends to light.[105] Another nice example of multiresposnive gels was reported by Yu et al. who showed the preparation of reversible gels based on a carboxylic azobenzene polymer being sensitive to various stimuli such as temperature, solvent polarity and light. The driving force for the organogel construction was the formation of H-aggregates and hydrogen bonds in highly polar solvents such as DMSO at low temperature leading to the packing of the chromophore moieties. The addition of a solvent of lower polarity or the increase of the solution temperature resulted in the dissociation of the structure and the disruption of the polymer network. The "melting" of the organogel within minutes was also induced upon UV irradiation, due to the cis-to-trans isomerization of the azobenzene chromophores. The gel was restored in dark, but in a much slower rate compared to the "melting process." The novelty of this work relies on the facile disruption/reconstruction of the organogel in response to a number of different stimuli.[106] An alternative method to construct multiresponsive gels is based on the polymerization/cross linking of functional monomers in the interstitial space of colloidal crystal templates arising from the 3D ordered structure of colloidal particles resulting in periodically ordered interconnecting structures known as inverse opal hydrogels (IHO). A dual temperature- and light-sensitive PNIPAM-4-acryloylaminoazobenzene (AAB) gel exhibiting a periodically ordered interconnecting porous structure was synthesized using as template a colloidal crystal with FCC lattice composed of close-packed monodispersed amorphous silica particles. The gel exhibited an abrupt isotropic volume change when the temperature was altered due to the LSCT behavior of PNIPAM and a light-triggered rapid two-state switching between two arbitrary structural colors due to the trans-to-cis isomerization of the azobenzene moieties upon photoexcitation of the chromophores in a temperature-controlled environment. These results suggest that it is possible to tune the structural color of a porous gel rapidly between two arbitrary states using the light stimulus at a controlled temperature.[107]

The development of multiresponsive surfaces which can controllably alter their wetting properties in response to external stimuli is of particular interest. Control over the

surface properties utilizing a remote stimulus is even more advantageous especially for the operation of microfluidic devices and the development of surfaces of controlled friction. Toward this direction, azobenzene containing copolymers were synthesized by the random copolymerization of *N*,*N*-dimethylacrylamide and 4-phenylazophenyl acrylate by conventional free radical polymerization and were further grafted onto silicon wafers to afford dual temperature and light responsive surfaces. Wettability studies showed an increase in the contact angle of the surface upon raising the temperature around the LCST of the polymer. However, upon UV irradiation, the azobenzene groups of the polymer coating switched from the less polar trans to the more polar cis configuration causing a simultaneous shift of the LCST to higher temperatures and an increase in the hydrophilicity of the surface.[108] Multiresponsive surfaces which respond to more than two stimuli are exceptional advantageous since they exhibit fine tuning of their properties in a complex environment. Jiang et al. reported multi-stimulus responsive surfaces being synergistically sensitive to glucose, temperature and pH variations by grafting a PNIPAM-*co*-[poly(acrylamidophenylboronic acid)] (PPBA) copolymer from a rough silicon surface by ATRP. The PNIPAM-*co*-PBA thin films exhibited multiresponsive switching between hydrophobicity and hydrophilicity under external stimuli; namely by either cooling the surface at neutral pH or increasing the pH at low temperature in the presence of glucose or alternatively by exposing the surface to glucose at neutral pH and low temperature. The observed changes in the wettability of the surface were supported by the increase of the LCST of the copolymers at neutral and high pH with the glucose concentration.[109] The use of responsive polymer brushes has been also proved to be attractive in molecular recognition gate membranes to maintain a specific substance concentration and prevent toxic substance leakage or transfer chemical signals. To this direction, Yamaguchi et al. prepared a membrane by plasma graft copolymerization, by filling the pores of a porous polyethylene film with a copolymer of NIPAM (N-isopropylacrylamide) and BCAm (benzo[18]crown-6-acrylamide). The crown moieties trapped specific ions and resulted in an increase of the LCST of the copolymer due to the hydrophilicity of the charged species. Thus, at temperatures above the LCST when the polymer is collapsed on the pore walls a solution free of ions exhibited a high flux through the membrane while in the presence of specific anions (i.e.

Ba^{2+}), below the LCST, the flux of the solution decreased by about 2 orders of magnitude due to the swelling of the copolymer. It is worth noting that the pore size changed uniformly in all pores, upon swelling and shrinking of the polymer, resulting in a clear cut-off value of the solute size leading to high performance membranes.[110-111]

Despite the progress in the design and synthesis of multiresponsive ''smart'' materials, this area still possesses tremendous challenges and is highly intriguing. The synthesis of new monomers with multiresponsive properties which will allow the straightforward preparation of complex systems and the adoption of biomimetic strategies in the design synthesis and engineering of such systems can provide a great potential for the development of a new generation of multiresponsive materials.

1.2 Polymer Brushes

Polymer brushes are polymeric chains attached by one end through an anchor group to a surface, to an interface, to a backbone of other polymer molecules, to the interface between two liquids, between a liquid and air or between melts or solutions of polymer.[112] The tethering occurs in such a way that the grafting density of the polymers is high enough and thus the attached chains are stretched away from the surface in a brush-like conformation (Figure 1.25).[113-114]
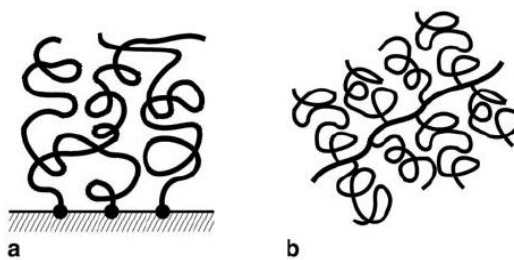
Figure 1.25. Polymer brushes attached on a solid surface (a) and a polymeric backbone (b).

Polymer brushes constitute a central model for many polymer systems that have a common feature: they possess polymer chains with deformed configurations. These systems include polymer micelles, block copolymers at fluid-fluid interfaces, grafted polymers on a solid surface, adsorbed diblock copolymers and graft copolymers at fluid-fluid interfaces (Figure 1.26).[112] Depending on the "grafting density" which is defined as the inverse distance of two neighboring surface-attached polymer molecules, three

regimes are distinguish (Figure 1.27). In the first two cases (a and b) the distance between anchoring points is larger than the size of the molecules and the surface-attached molecules do not overlap. If the molecule tends to be absorbed by the surface the macromolecule has a flat "pancake-like" conformation. In the case when a "non-absorbing" macromolecule is attached on the surface (low grafting density regime) a "mushroom conformation" is observed. When the grafting density increases, the crowding leads to stretching of the chains which adopt the "brush-like" conformation.
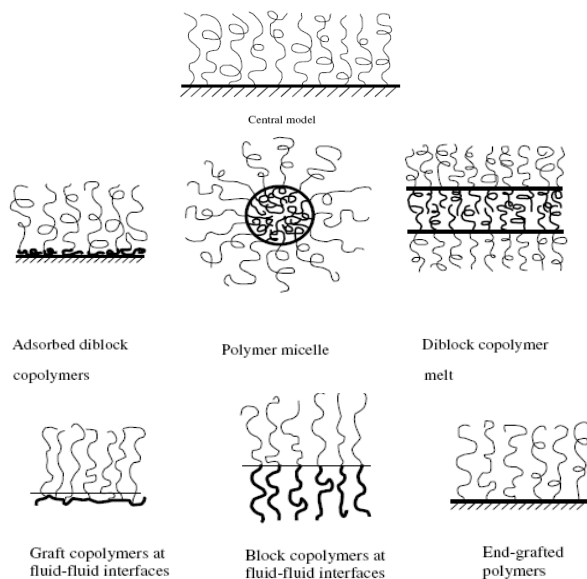
Figure 1.26. Polymer systems that have polymer brushes as their central model.
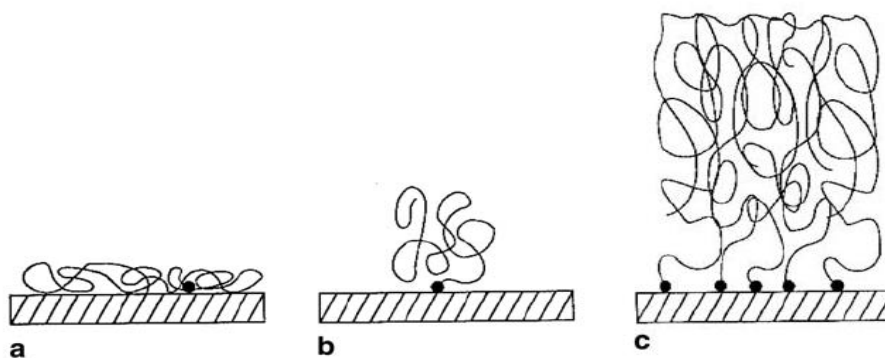
Figure 1.27. Schematic representation of end-attached polymer conformations on a surface: (a) "pancakes", (b) "mushrooms", (c) "brushes".

Genzer and co-workers showed that the crossover between the mushroom and the brush regime occurred at $\sigma \approx 0.065$ nm^{-2}.[115] Solvent molecules can be either present or absent

in the polymer brushes. In the presence of a good solvent the macromolecules try to maximize their contact with the solvent molecules and to avoid the contact with each other. In the melt (absence of solvent) the polymers chains are stretched away from the interface.

In terms of polymer chemical composition, polymer brushes can be divided into homopolymer, mixed homopolymer, random copolymer and block copolymer brushes (Figure 1.28). Homopolymer brushes refer to an assembly of tethered polymer chains consisting of one type of repeat units. Homopolymer brushes can be neutral (a_1) or charged (a_2) depending on the type of the repeat unit. Moreover, polymer brushes can be classified in terms of the rigidity of the polymeric chain to the flexible (a_1), semiflexible (a_4) and liquid crystalline (a_3) polymer brushes. Mixed homopolymer brushes comprise two or more types of homopolymer chains (b).[116] Random copolymer brushes consist of two types of repeat units that are randomly distributed along the tethered polymeric chains (c).[117] Block copolymer brushes refer to an assembly of tethered polymer chains consisting of two or more homopolymer chains that are covalently connected to each other at one end (d).[118]

(a₁) Flexible homopolymer brush   (b) Mixed homopolymer brush   (c) Random copolymer brush   (d) Block copolymer brush

(a₂) Charged homopolymer brush   (a₃) Liquid crystalline polymer brush   (a₄) Semifexible polymer brush
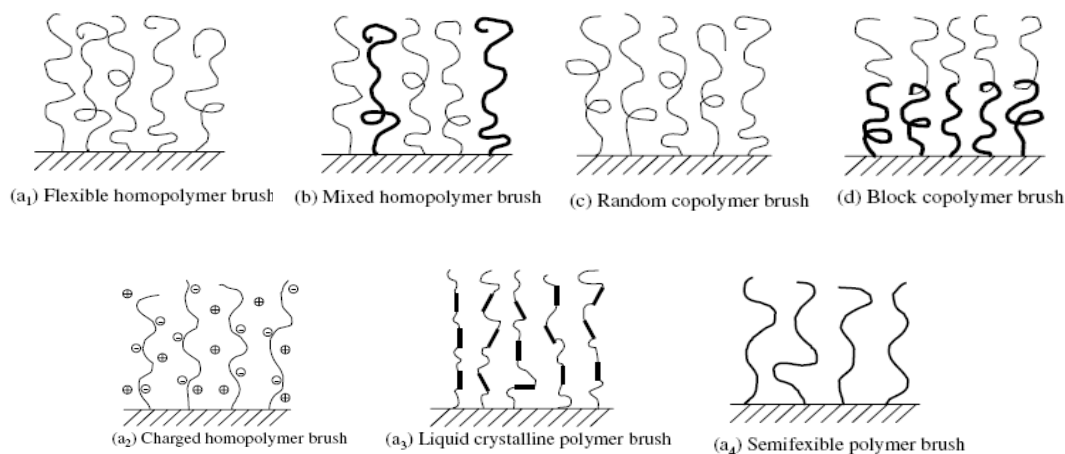
Figure 1.28. Linear polymer brushes (a₁-a₄) homopolymer brushes, (b) mixed homopolymer brushes, (c) random copolymer brushes, (d) block copolymer brushes.

1.2.1 Synthesis of polymer brushes

Two methods have been used for the tethering of polymer brushes onto a surface: physisorption and covalent attachment. Physisorption is characterized by reversibility, while the covalent attachment provides a permanent and stable immobilization on the surface. Covalent attachment includes the "grafting to" and the "grafting from" technique.

A. PHYSISORPTION

Physisorption is achieved by the self-assembly of polymeric surfactants or end-functionalized polymers onto a solid substrate (Figure 1.29).[112,119] Physisorption of block or graft polymers takes place in the presence of a selective solvent or selective surface leading to selective solvation or selective adsorption, respectively. In general, the structure of the polymer brush that arises is a function of some critical parameters such as the selectivity of the solvent, the nature and the architecture of the copolymers, the length of each block and the interactions between the blocks and the surface. In the case of a selective surface, the adsorption of one block onto the surface is favored, while the other block contributes to the formation of the polymer brush.[120] In the case of a selective solvent, one of the blocks is solubilized due to its favorable interactions with the solvent medium while the other block tends to avoid the contact with the solvent forming an anchoring layer.[121] Even though, the adsorption of a block copolymer from a selective solvent or surface is not very difficult the brushes exhibit instability that leads to reversibility of the brush formation. This instability originates from the thermal and solvolytic effect due to weak interactions between the surface and the block copolymers.[118] In most cases the interactions that induce chemisorption are hydrogen bonds and Van den Wals forces. When the system is exposed to other good solvents desorption or displacement of the adsorbed polymers by other macromolecules can be induced. Moreover, when heating the polymeric film at high temperature (above the glass transition temperature) polymer droplets are often formed on the formerly homogeneous substrate due to the dewetting effect.[122-123]
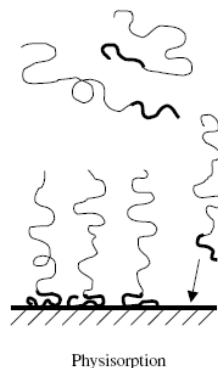
Physisorption

Figure 1.29. Preparation of polymer brushes by "physisorption"

B. COVALENT ATTACHMENT

B1. Polymers Brushes via Chemisorption ("grafting to" method)

The "grafting to" method uses specifically synthesized end-functionalized macromolecules that are chemically attached to appropriate reactive sites on the substrate. End-functionalized polymers with narrow polydispersity can be synthesized by living anionic, cationic, radical, group transfer and ring opening metathesis polymerization.[112] Polymeric molecules with chlorosilane and alkoxysilane end groups have been prepared and immobilized on glass and silicon surfaces while polymers with thiol and sulfide groups have been attached on gold surfaces. This has been used for the modification of both flat and curved surfaces. For example polystyrene sulfonate (PSS) terminated with trichlorosilane anchor groups have been attached both on spherical[124] and planar silicon oxide surfaces.[125-127]

Method limitations

Even though this method is very simple for the preparation of polymer monolayers it has serious limitations. (1) Only relatively simple polymer molecules such as polystyrene can be attached on the surface since the high reactivity of the anchor group prevents the coexistence of more functional groups in the polymer. For example, chlorosilane end-groups would not tolerate any amino, hydroxyl or acid groups. (2) The thickness of the surface-attached monolayer is limited.[128-129] At the beginning of the procedure, when only a small percentage of the surface is occupied by polymeric chains, free chains can easily diffuse towards the surface and react with their counterparts on the surface. Once the

surface becomes very crowded further diffusion of chains becomes very slow. This diffusion barrier leads to a strong kinetic hindrance that limits the film thickness (Figure 1.30).
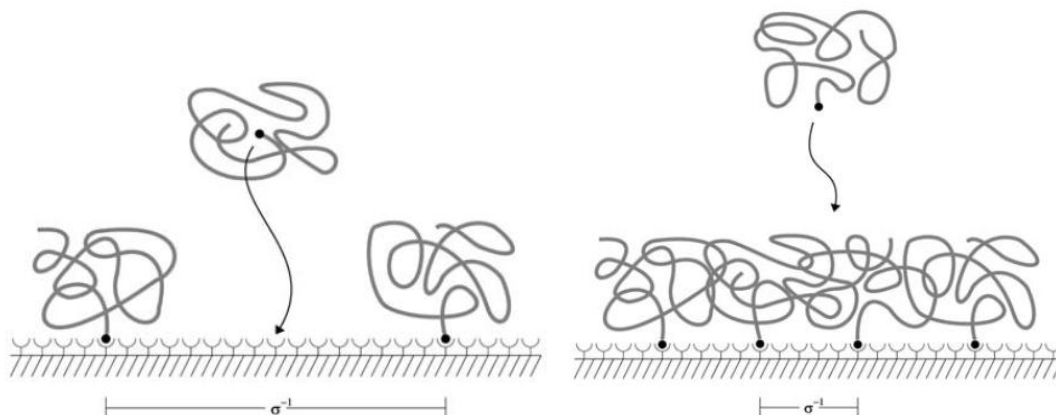
Figure 1.30. Schematic representation of the "grafting to" method.

The macromolecules that have been attached on the surface have to stretch in order to facilitate the approach of more chains near the surface. Consequently, the attachment of further molecules is energetically costly, and even if the kinetic limitations can be circumvented, the grafting density will be limited for thermodynamic reasons. Usually the polymer monolayers that arise from this tethering method adopt the "mushroom" or "brush"conformation. However, in the case of the brush conformation the grafting density and the film thickness are low while the chain stretching is weak.

The synthetic procedure for the synthesis of polyelectrolyte brushes by this method usually involves two steps. In the first step a neutral brush system is formed while in the second step the charged sites are introduced. The modification of the polymer brushes in the second step sometimes gives rise to side reaction, while sometimes the transformation is not quantitative.

B2. Polymer Brushes via surface-initiated polymerization ("grafting from" method)

Surface initiated polymerization or the "grafting from" method overcomes some of the disadvantages of the "grafting to" method since the polymeric chains are grown directly from the surface of the substrate utilizing a pre-prepared monolayer of covalently bonded initiator molecules (Figure 1.31).
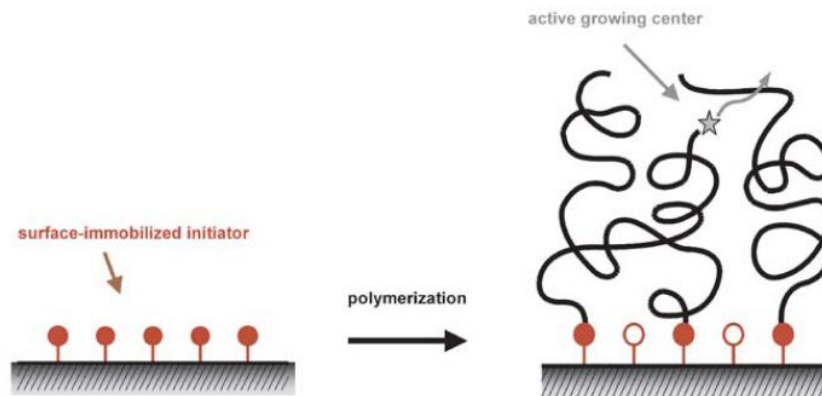
Figure 1.31. Schematic representation of the "grafting from" process.

This method circumvents the diffusion barrier that exists in the "grafting to" method since only monomers have to diffuse to the growing chain ends. Consequently, this procedure leads to the formation of thick polymer layers. It also provides control of functionality, density and thickness of the polymer brushes with almost precise molecular weight.[130] A variety of different initiators as well as polymerization techniques have been involved in this method for the preparation of polymer brushes onto either spherical or planar substrates. A significant parameter that should be taken into account in this technique is the appropriate choice of the initiator functionality that will ensure the anchoring of the initiator monolayer onto the surface of the chosen substrate i.e. thiols on gold, silanes on glass and Si/SiO_2.[130]

In order to achieve a controllable brush density, polydispersity and composition and the requirement for the preparation of block copolymers onto the surface, a controlled polymerization must be employed. Over the last few years a number of controlled polymerization techniques have been used, such as "living" ring opening polymerization, "living" anionic and cationic polymerization, ring opening metathesis polymerization (ROMP), nitroxide-mediated polymerization (NMP), reversible addition-fragmentation chain transfer polymerization (RAFT) and atom transfer radical polymerization (ATRP). In the recent years, ATRP has been the most widely employed technique for the synthesis of neutral and polyelectrolyte polymer brushes via surface-initiated polymerization onto planar and curved surfaces.[130] ATRP offers many advantages in comparison with the other techniques that have been used until today. For example, ATRP is compatible with a variety of functional monomers while the living/controlled character of the

43

polymerization process yields polymers with low polydispersity that are also end-functionalized and thus can be used for the further synthesis of di- and triblock copolymers. Moreover, the synthesis of the thiol and silane initiators that will be bound onto the surface is easier than the AIBN-silane derivative or the nitroxide silane derivative used in free radical, RAFT and NMP polymerizations.

The grafting "from" technique can be applied to grow polymer brushes from both flat and curved surfaces. Even though the principle followed in both cases is similar, however differences can be detected both in the experimental conditions adopted for the synthesis of the materials and the properties of the final grafted surfaces. Nanoparticles which exhibit high curvature and thus high surface-to-volume ratio, posses an appreciable number of sites capable of initiating a polymerization leading to high polymer grafting densities.[131] Consequently, a significant amount of polymer is grown from the surface which can be further isolated upon dissolving the colloidal core to provide the molecular characteristics of the grafted macromolecules. On the other hand, flat surfaces exhibit a lower concentration of initiating sites,[131] compared to the curved surfaces, resulting in lower polymer grafting densities. This particular feature of the planar surfaces leads to a small amount of grafted polymer which is inadequate to provide the molecular characterization of the grafted chains and thus create the necessity of adding free initiator during polymerization which will provide the molecular characterization for the system. The peculiar properties of the curved polymerization templates provide unique properties to the final materials. In particular, in polymer brushes grown from colloidal particles two major types of particle architecture can be distinguished depending on the density and the conformation of the surface bound polymer chains; the concentrated brush regime characterized by high grafting densities and stretched conformations and the intermediate brush regime characterized by a reduced grafting density and relaxed polymer conformations (Figure 1.32).[132] On the other hand, polymer brushes grown from flat surfaces exhibit a sterically homogeneous environment and grafting density. This property of the spherical brushes has affected significantly the thermoresponsive behavior of PNIPAM-coated colloidal particles which exhibited two distinct LCSTs corresponding to the less and more hydrated concentrated and intermediate regimes, respectively.[133-134]
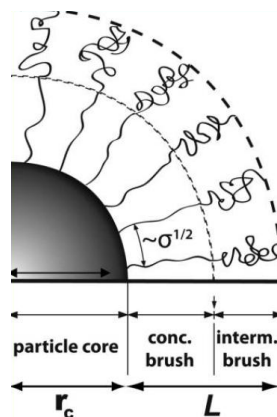
Figure 1.32. Schematic representation of the brush regimes on grafted-colloidal particles; Concentrated and Intermediate brush regime.[132]

1.2.2 *Atom transfer radical polymerization (ATRP).*

An ATRP system is a multicomponent system that involves an initiator with a transferable (pseudo)halogen, a catalytic system, comprising a transition metal species which is coordinated with a suitable ligand, and the monomer. A schematic representation of such a system is illustrated in Figure 1.33.

Mt^m = transition metal
L_n = complexing ligand
R-polymer chain
X = Br or Cl
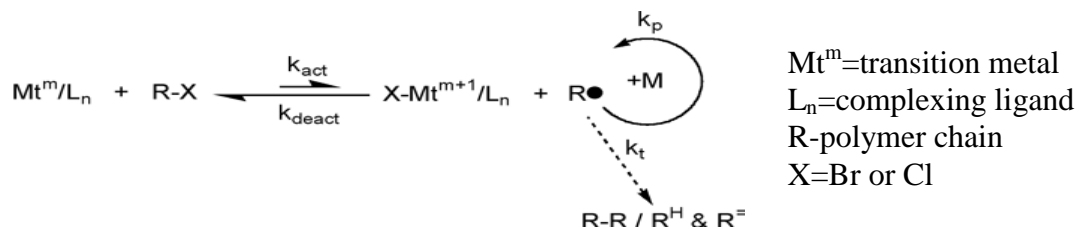
Figure 1.33. General mechanism of ATRP

The name of ATRP originates from this atom transfer step which is the key elementary reaction responsible for the uniform growth of the polymeric chains. Mechanistically, ATRP is based on the inner sphere electron transfer process which involves a reversible (pseudo) halogen transfer between a dormant species (R-X) and a transition metal complex (Mt^m/L_n). This transfer results in the formation of propagating radicals (R·), while the transition metal complex adopts a higher oxidation state ($X-Mt^{m+1}/L_n$). Radicals react reversibly with oxidized metal complexes $X-Mt^{m+1}/L_n$ to reform the dormant species and the transition metal complexes Mt^m/L_n in the lower oxidation state, the activator. This

45

process occurs with a rate constant of activation k_{act} and deactivation k_{deact}. Polymer chains grow by the addition of the intermediate radicals to monomers in a manner similar to a conventional radical polymerization with the rate constant of propagation, k_p. Termination reactions (k_t) also occur in ATRP mainly through radical coupling and disproportionation.[135]

The three steps of the mechanism of an ATRP process are illustrated in Figure 1.34.

Initiation:

$$R-X \; + \; L_nM_t^{+z} \; \underset{}{\overset{K'_{eq}}{\rightleftharpoons}} \; R\bullet \; + \; L_nM_t^{+(z+1)}X$$
$$[X = Cl, Br]$$

$$R\bullet \; + \; \overset{}{\underset{R}{=}} \; \xrightarrow{k'_p} \; P_1\bullet$$

Propagation:

$$P_n-X \; + \; L_nM_t^{+z} \; \underset{}{\overset{K_{eq}}{\rightleftharpoons}} \; P_n\bullet \; + \; L_nM_t^{+(z+1)}X$$

$$P_n\bullet \; + \; \overset{}{\underset{R}{=}} \; \xrightarrow{k_p} \; P_{n+1}\bullet$$
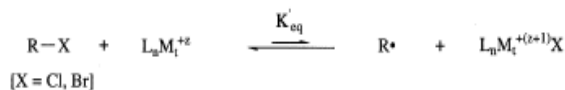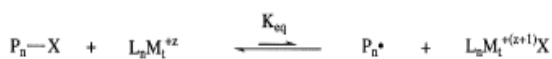
$$R_p = k_{app}[M] = k_p[P^\bullet][M] = k_pK_{eq}[In]\frac{[Cu^I]}{[Cu^{II}X]}[M]$$

$$\text{where } K_{eq} = \frac{k_{act}}{k_{deact}} = \frac{[P^\bullet][Cu^{II}X]}{[Cu^I][PX]}$$

Termination:

$$P_n\bullet \; + \; P_m\bullet \; \xrightarrow{k_t} \; P_{n+m} \; + \; \left(P_n^{=} \; + \; P_m^{H} \right)$$
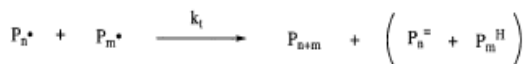
Figure 1.34. General mechanism of ATRP and propagation rate constant

The irreversible termination in these polymerizations can be minimized but cannot be excluded from the mechanism. Therefore these polymerization methods do not meet the strict definition of a *living* polymerization and are more properly termed controlled/living polymerizations in order to take into account the unavoidable irreversible termination. Moreover, above some certain molecular weight values that are specific for the polymerization of each monomer, all controlled/living polymerizations cannot be considered as controlled since some reactions such as termination and chain transfer that were slow become significant.[136]

The mechanism that ATRP utilizes for the minimization of the termination reactions is the replacement of the irreversible termination that is usual in the common

radical polymerizations with the fast, reversible deactivation of the growing radical to a dormant specie. This dormant species can be activated reversibly to produce free radicals that are capable for propagation. The advantage of this mechanism is that only a small concentration of free radicals is employed at any time to propagate a large number of chains. However, there are two main conditions that should govern the equilibrium in order to achieve this controllable mechanism. First, the equilibrium between the dormant and the active species should be shifted to the side of the dormant species in order to ensure that the concentration of the radicals will be low and the rate of the irreversible termination will be negligible relative to the apparent rate of polymerization. The second condition is that the rate of exchange between the dormant and the active species must be faster than the rate of propagation in order to ensure that the possibility of propagation is the same for all the polymer chains.[136]

The bimolecular rate constants for coupling and disproportionation for most organic radicals are near the diffusion–controlled limit (10^8 to 10^{10} $M^{-1}s^{-1}$) so these processes become slow only at radical concentrations below 10^{-7} M. The concentrations of Cu(I) and the halide end groups will remain approximately constant during the polymerization. Consequently, from the expression of the propagation rate constant the product of the radical and deactivator concentrations must remain constant and equal to $[R^{\cdot}][CuBr_2] = K_{eq}[RX][CuBr] = 4*10^{-10}$ M^2. At the initial stages of the reaction the radical and the deactivator concentrations will increase and will reach a value around 10^{-6} M. At these concentrations the radicals will be rapidly coupled. More radicals and deactivator will be formed and further radical combinations will occur until the radicals and the deactivator will reach the crucial concentrations of 10^{-7} and 10^{-3}, respectively. At these concentrations the rate at which radicals combine ($k_{term}[R^{\cdot}]^2$) will be much slower than the rate at which radicals will react with the copper(II) complex ($k_{deact}[R^{\cdot}][Cu^{II}]$) in the deactivation process. Consequently, a controlled/living polymerization will be achieved. During the initial non-stationary process only 5% of the polymer chains will be terminated, while the rest 95% will be further polymerized. The percentage of the terminated chains can be reduced if a small amount of deactivator (10 mole % with respect to the Cu(I) activator) is added initially in the reaction mixture.[136]

1.2.2.1 The Role of the ATRP Components

1.2.2.1.1 Initiators

The role of the initiator in a metal-catalyzed living radical polymerization is to form an initiating radical species by homolytic cleavage of its labile C-halogen bond. Two parameters are very important for a successful ATRP initiating system. First the initiation should be fast in comparison with propagation. Second the probability of side reactions should be minimized. Most of the initiators that have been employed successfully are organic halides which possess surplus halogens or conjugated constituents such as allyl, aryl, carbonyl and cyano groups for the stabilization of the generated radicals by the inductive and/or resonance effects. However, an extensive stabilization of the initiating radical may disturb its addition to the monomers and thus result in slow initiation.[135] The general order of bond strength in the alkyl halides is R-Cl > R-Br>R-I. Therefore alkyl chlorides should be the least efficient initiators and alkyl iodides the most efficient. However, bromide and chloride are the halogens that provide the best molecular weight control.[137-139] In general the structure of the organic halide that is chosen as an initiator in an ATRP process should be similar to that of the dormant chain end of the polymer. That provides similar activity of the carbon-halogen bond with that of the dormant polymer terminal.[135] A wide range of initiators have been used in ATRP reactions including haloalkanes, allyl halides, (haloalkyl)benzenes, haloketones, haloesters, haloamides and halonitriles (Figure 1.35).

A haloalkane initiator is carbon tetrachloride (I-1), which was the first initiator employed for the metal-catalyzed living radical polymerization of MMA using a ruthenium based catalyst.[140] One possible problem with polyhalogen compounds is that they can act as multifunctional initiators to give star polymers. Allyl halides produce relative stable allyl radicals due to the conjugation of a vinyl group with the carbon-centered radical. Allyl chloride and bromide (I-11) were employed as initiators for the controlled radical polymerization of styrene in combination with a Cu catalyst.[141] (Haloalkyl)benzenes (I-12 – I-15) were proved very effective especially for the polymerization of styrene and its derivatives since the benzyl radical is very similar with the growing radical chain ends. Haloketones (I-16 – I-18) favor the formation of the radical due to the presence of the carbonyl group (electron-withdrawing group and

conjugating substituent) in the α-position relative to the C-halogen bonds). However, these initiators are very reactive with copper-catalyzed systems and result in non-controlled polymerizations. This may be induced by the reduction of the electrophilic radical species into ions by the active Cu(I) catalyst. Haloesters (I-21 – I-28), possess the ester group which is a less electron withdrawing group. Consequently, they can activate the carbon-halogen bond without making the resulting radical too electrophilic. This type of initiator can be versatile for various monomers such as styrenics, methacrylates, acrylates, etc.

Haloamines (I-29 – I-30) can be very efficient initiators for the polymerization of acrylamides, while halonitriles are usually employed in the polymerization of acrylonitriles with copper halides.[135]

1.2.2.1.2 Monomers

The successful ATRP of various monomers such as styrene, (meth)acrylates, (meth)acrylamides, dienes, acrylonitrile and other monomers that contain substituents which stabilize the propagating radicals has been reported. Each monomer has its unique atom transfer polymerization constant for its active and dormant species ($K_{eq}=k_{act}/k_{deact}$). Essentially the product of $K_{eq}k_p$ determines the polymerization rate.

Styrenics

The majority of styrene ATRP polymerizations have been performed using copper-based catalyst systems, while the use of other catalytic systems such as iron, ruthenium and rhenium has been also reported. Initiators such as 1-phenylethyl halide, benzylic and allylic halides, functional α-haloesters, polyhalogenated alkanes and arenesulfonyl chlorides have been used for the copper mediated polymerization of styrene, while nonpolar media are the preferred solvents. Polystyrene exhibits a glass transition temperature around 100 °C so the polymerization temperature should be set higher than 100 °C. Moreover, at this temperature range the solubility of the catalyst increases. Monomers that have a similar chemical structure with styrene (dispose electro-withdrawing groups as substituents) showed higher polymerization rates since the atom transfer equilibrium is shifted more towards the active species site.[142]
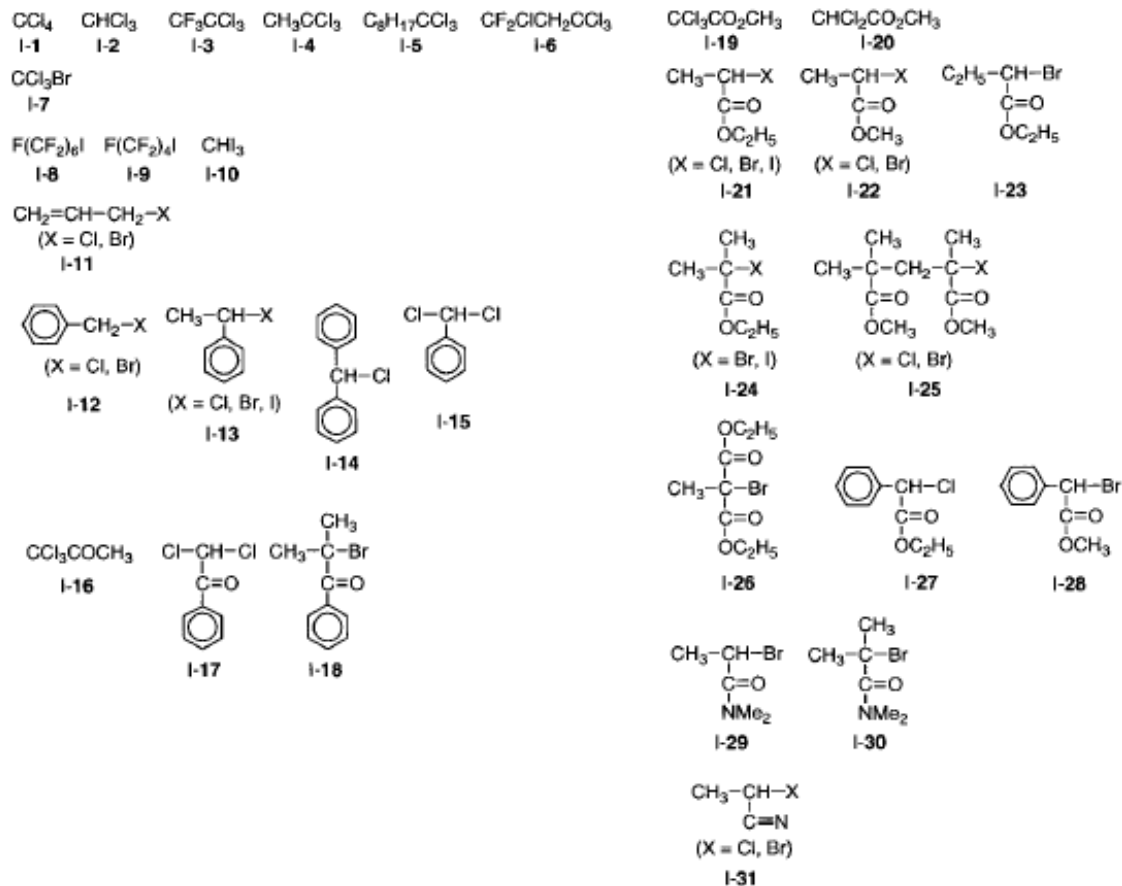
Figure 1.35. ATRP initiators.

(Meth)acrylates[135]

A variety of methacrylate monomers have been polymerized by ATRP (Figure 1.36) using various complexes including ruthenium, iron, copper, nickel, palladium and rhodium. Polymerizations utilizing R-Cl/Ru, R-Br/Ni, R-Br/Cu and RSO_2Cl/Cu components were reported to be well controlled systems. The carbon-halogen bonds derived from methacrylates are highly reactive since the generated radicals are well stabilized due to the high substitution of the carbon atom. This also explains the use of mild metal complexes such as ruthenium and nickel during ATRP. However, for polymerizations taking place in polar solvents the use of the copper/bipyridyl catalytic system is normally used. Methyl methacrylate dormant species are very easily activated and high values of the ATRP equilibrium constant are observed. That can explain the

facile polymerization of MMA as well as the wide range of catalytic systems that have been used. However, some catalysts such as Me$_6$TREN induce very high equilibrium constants leading to non-controlled ATRP polymerizations.
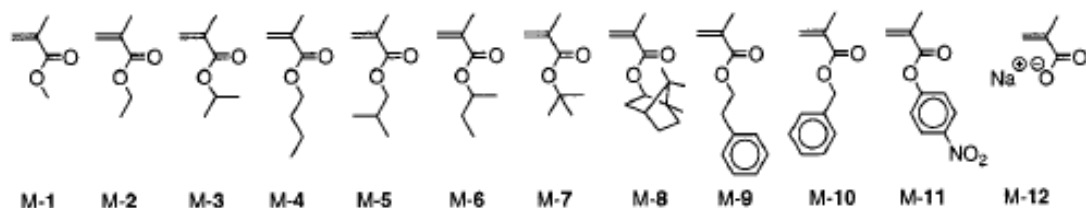
Figure 1.36. Methacrylate monomers that have been polymerized by ATRP.

Initiators that are frequently used for the polymerization of methacrylate monomers are I-24 and I-25 since they are unimer and dimer models of poly(methyl methacrylate). Monomers such as 4-nitrophenyl methacrylates (M-11) can be polymerized in a controlled fashion and the synthesized polymers can be converted easily into poly(methacrylic acid) via deprotection of the nitrophenyl group. Finally, sodium methacrylate (M-12) an ionic monomer can be polymerized directly into the poly(methacrylic acid) sodium salt with controlled molecular weight utilizing a water soluble bromide initiator in water under alkaline conditions (Figure 1.36).[143]Acrylates also generate highly reactive radical species but the carbon-halogen bond is less reactive than that of the methacrylates. Consequently, acrylate monomers demand the use of an active catalyst with lower redox potentials. Suitable initiators for these polymerizations are unimer models of poly(acrylates) such as 1-21.

1.2.2.1.3 Transition-Metal Catalysts

The transition metal complex is one the most important components in ATRP polymerizations. As a catalyst, the complex induces homolytic cleavage of the dormant carbon-halogen bond at the polymer terminal via a one-electron redox reaction of the metal centre. During this process the metal attacks the halogen of the chain end and is oxidized via a single electron transfer followed by halogen abstraction. Later on, the oxidized metal center will undergo reduction giving the halogen back to the growing chain. In the literature several reports concluded that there is a relationship between the

metal center, catalyst structure or ligand and their catalytic activities. In general, it was suggested that the catalytic activity increases with increasing the electron density of the metal center or by decreasing the redox potential of the complex since after the generation of the radical the catalyst should give one electron to the terminal halide.[135] Various transition metals have been employed as the catalytic center of ATRP reactions including ruthenium, iron, copper, nickel, palladium, rhodium, rhenium and molybdenum. Copper is one of the most widely used metals. Moreover, several compounds have been utilized as ligands for the preparation of active catalytic complexes such as nitrogen, phosphorous and other miscellaneous compounds. The main role of the ligand in ATRP is to solubilize the transition-metal salt in the solvent media and also to control the redox potential of the metal center and thus adjust the reactivity and the dynamics of the atom transfer. Nitrogen ligands have been used in copper and iron- mediated ATRP. For copper-mediated polymerizations nitrogen-based ligands work particularly well. Some typical nitrogen based ligands are illustrated in Figure 1.37.
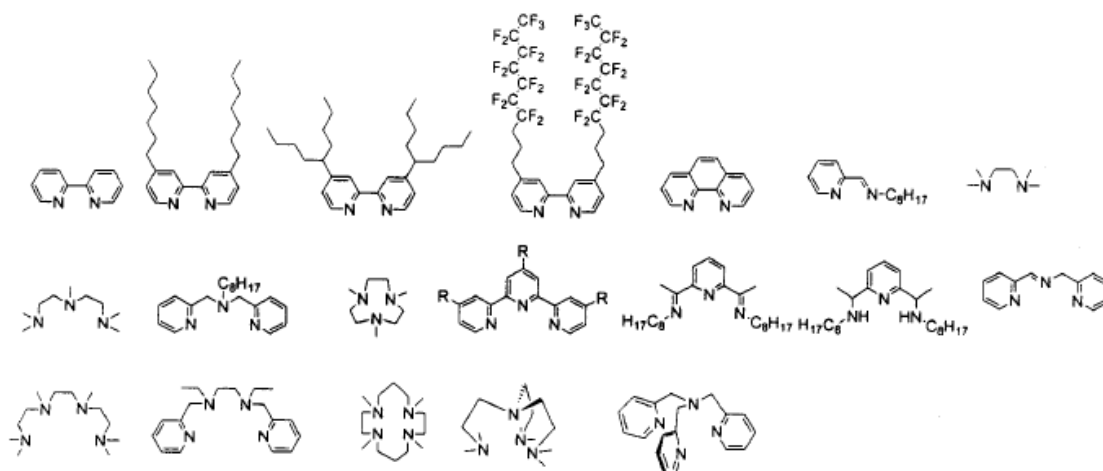
Figure 1.37. Typical N-based ligands used in ATRP.

The electronic and steric effect of the ligands is important. Reduced catalytic activity is observed when there is excessive steric hindrance around the metal-center or when the ligand has strongly electron-withdrawing substituents. The activity of N-based ligands decreases with the number of coordinating sites $N_4>N_3>N_2>>N_1$ and with the number of linking C-atoms $C_2>C_3>C_4$.

1.2.3   Surface-Initiated ATRP

A significant feature of "living/controlled" polymerizations such as ATRP is that they provide the ability of the simultaneous growing of chains from multifunctional cores and surfaces (Figure 1.38).[131] These surfaces can be flat such as silicon wafers[144] and gold surfaces[145-146] or curved such as inorganic particle/colloids or organic latexes.[147] Nanopatterned networks, dendrimers and highly functional linear polymers have also been modified by ATRP.[131]
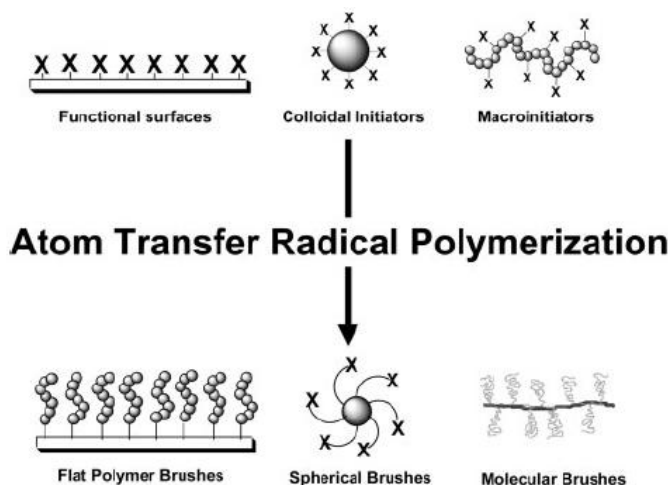
Figure 1.38. Examples of polymer brushes synthesized by ATRP on different surfaces (flat wafers, particles, colloids and polymers) utilizing the "grafting from" techinique (X-halogen).

The advantage of ATRP over the other "controlled/living" techniques is the convenient functionalization of the surface with commercially available molecules such as α-haloesters or benzyl halides circumventing the multistep synthesis of other initiator molecules. Ideally, when multifunctional initiators are used in ATRP star polymers or brushes that employ a number of tethered chains respective to the number of the initiating sites are produced. Nevertheless, low or high percentage of termination reactions can lead to different functionality and molar mass distribution of the tethered chains. In the literature two kind of termination reactions have been reported the intermolecular and intramolecular coupling (Figure 1.39). Intermolecular coupling of the growing radicals forms functional initiators with a different number of initiating sites and can result in

crosslinking, while intramolecular termination of neighboring radicals lowers the overall concentration of the initiator in the system and may lead to tethered chains with various degrees of polymerization (DP).
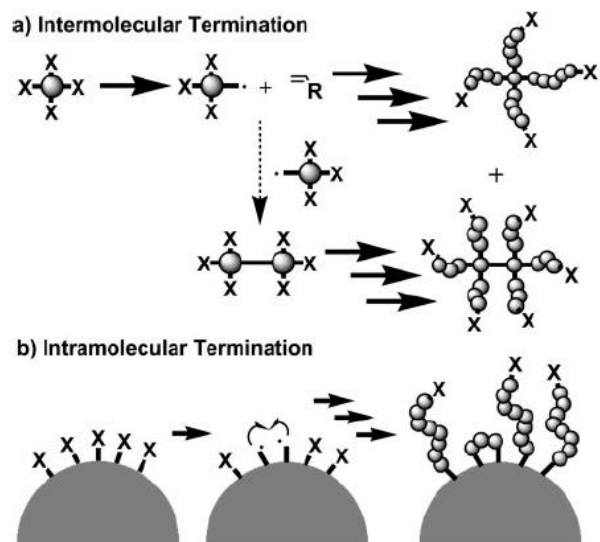
Figure 1.39. Two modes of termination intermolecular (a) and intramolecular (b) termination.

1.2.3.1 Controlled ATRP from Flat and Curved Surfaces
Controlled ATRP from flat surfaces

Flat surfaces are characterized by low surface area, low concentration of the initiator and moreover by small amounts of persistent radicals (deactivator) that are generated after the activation of the initiator sites (homolytic cleavage of C-X bond). If the concentration of the deactivator is very low the propagating radicals are trapped leading to uncontrolled chain growth. Various methods have been developed to overcome this inherent difficulty such as the addition of persistent radicals (deactivator) or "sacrificial initiator" at the beginning of the reaction.

Addition of a Persistent Radical (deactivator)

As predicted from the persistent radical effect the addition of radical-deactivating complexes at the beginning of the reaction facilitates exchange reactions between active radicals and dormant oligo/polymeric halides. ATRP of styrene and methyl acrylate in

the presence of deactivator has led to a gradual increase of the brush film thickness from a flat surface with time.[148]

Addition of "sacrificial" initiator

Fukuda et al.[144] as well as Hawker et al.[149] proved that the addition of untethered small molecule initiators in an ATRP reaction from functional flat surfaces is beneficial for both synthetic and characterization proposes. When a free initiator is added in the system a sufficient concentration of persistent radicals (deactivator) is generated by the termination of radicals formed in solution. Moreover, the final DP of the tethered chains on the surface is determined by the concentration of sacrificial initiator added. Furthermore, since it was proved that polymer brushes cleaved from surfaces had similar molecular masses and polydispersities with the polymer formed in solution, characterization of the free polymers by SEC and ^{1}H NMR can give a good estimation for the molecular masses, the polydispersity and the composition of the polymers brushes.[149]

Controlled ATRP from curved surfaces

Nanoparticles have attracted considerable attention nowadays due to their fascinating electronic, optical, magnetic and/or catalytic properties which are associated with their nano- or quantum–scale dimensions. Such nanoparticles include metals (Au, Pt, Pd, Cu, etc.), semiconductors (CdS, CdSe, ZnS, etc.) and semiconductor oxides (Fe_2O_3, Al_2O_3, TiO_x, SiO_x, etc.).[150] The development of polymer/nanoparticle composite materials is of greater interest due to the combination of the properties of the inorganic nanoparticles with those of the polymer (solubility, film formation, and chemical activity).[151] The development of such polymer/nanoparticles composite materials can be achieved by the synthesis of polymer brushes onto the surface of such nanoparticles. ATRP synthesis of polymer brushes can be accomplished from functionalized nanoparticles serving as colloidal initiators. One interesting aspect of such spherical brushes is the possibility to attain high grafting density of polymer chains due to the high surface/to volume ratio which arises from the high curvature of the particles. In addition, the use of preformed colloidal initiators allows the control of the brush length by changing the ratio of monomer to initiating sites while maintaining a core of stationary dimensions. A variety

of spherical particles that differ in chemical composition such as organic latex colloid emulsions, shell-crosslinked micelles, metal and inorganic particles have been decorated with polymer brushes utilizing ATRP. Moreover, polymer brushes have interesting applications in the colloidal and interfacial phenomena of the particles. Polymer chains in a good solvent can resist overlapping between neighboring particles resulting in colloidal stabilization. The repulsive force arises from the high osmotic pressure inside the brush.[150] Consequently, the organic polymer shell determines the external chemical properties of such materials and their interactions with the environment while their physical properties are governed by both the size and the shape of the inorganic core and the surrounding organic layer.[152]

1.2.3.2   *Functionalization of inorganic particles by ATRP*

1.2.3.2.1   *Polymer-grafted metal-oxide semiconducting nanoparticles*

The functionalization of low-dimensional semiconductor materials such as metal oxide (TiO_2, ZnO, SnO_2) nanoparticles, nanotubes and nanowires with grafted polymer chains has attracted particular attention owing to their intriguing physical properties and their potential use in a wide range of applications. For example hybrid TiO_2 particles can be incorporated into capacitors and thin film transistors leading to the enhancement of the dielectric constant (K) and to mobilities approaching 0.2 $cm^2/V \times s$.[153] However, the surface chemistry of these materials is rather complex and thus the immobilization of small organic molecules or long polymer chains, is not necessarily straightforward.

1.2.3.2.1.1   *Polymer-grafted TiO$_2$ nanoparticles*

The surface of TiO_2 nanoparticles can be modified by the "grafting through" the "grafting from" or the "grafting to" method. The use of initiator functionalized particles has been investigated for the growth of polymer coatings directly from the nanoparticles surface (Table 1). However, the surface chemistry of the TiO_2 particles is different to that of silica and thus the development of new initiator anchoring groups is required. The attachment of organic moieties to the surface of these particles by strong covalent bonding requires the use of highly reactive organic groups such as carboxylic acid,[154-155] phosphoric acid[156] and catechol derivatives.[157] Recently, an approach involving the
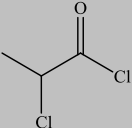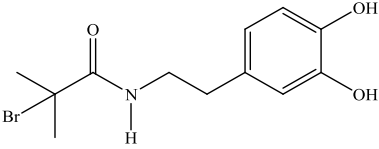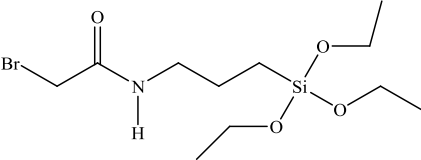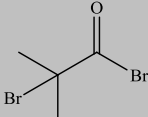
reaction of an acid chloride-terminated initiator with the nanoparticle surface was also applied for the immobilization of an ATRP initiator onto the nanoparticles surface.[158] Three possible coordination mechanisms have been proposed for the binding of the carboxylic acid groups onto the TiO_2 surface; the monodentate, the chelating and the bridging coordination mode. The preferred coordination mechanism is highly dependent on the nanoparticle size which affects the coordinate states of the surface Ti atoms of the nanoparticle. Biomimetic catechol binding sites are advantageous because they facilitate the intramolecular ligand-to-particle charge transfer within the surface Ti-catechol complex.[159] This approach has been used for the growth of metal-binding polymer chains on the surface of the titania nanoparticles followed by the templated growth of metal nanoparticles within the polymer shell to prepare a ternary nanostructure with electrocatalytic properties.[160]

Another route for the preparation of initiator-functionalized metal oxide nanoparticles involves the use of metal alkoxides appropriately derivatized to carry polymerization initiating sites. Upon hydrolysis and condensation of these precursor molecules, amorphous titanium, zirconium and vanadium oxo clusters bearing surface initiating sites are obtained which can serve as multifunctional initiators for si-ATRP.[161-162]

1.2.3.2.1.2 *Polymer-grafted ZnO nanoparticles*

Si-ATRP has been also employed for the functionalization of ZnO nanoparticles with grafted polymer chains. The nanoparticles were pre-functionalized with an appropriate organic initiator using two different anchoring chemistries (Table 1); silane condensation or carboxylic acid coordination. Both hydrophobic[163] and hydrophilic[164-165] polymers have been grown from the surface of the ZnO nanoparticles by ATRP. Moreover, hyperbranched polymer-functionalized ZnO particles were obtained by surface-initiated self-condensing vinyl polymerization (si-SCVP) from initiator-functionalized nanoparticles.[166]

Table 1. Initiator molecules grafted on the surface of TiO$_2$ and ZnO nanoparticles

No	Initiators	Polymer	Ref.
1	O⫽ / Cl / Cl 2-Chloropropionyl chloride	POEMA, PSS	158
2	2-Bromo-2-methyl-N-[2-(3,4-dihydroxyphenyl)ethyl]propionamide	PMMA, PDMAEMA	159-160
3*	(silane initiator structure)	PHEA	164,166
4*	2-bromoisobutyryl bromide	MeO-PEGMA, PMMA, PCEMA	163,165

* Initiators used for ZnO functionalization

However, the surface functionalization of metal-oxide nanoparticles is far from being resolved. There are undoubtedly still many challenges to be meet in the synthesis, functionalization, characterization and potential applications of these materials.
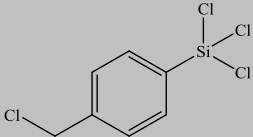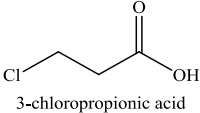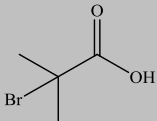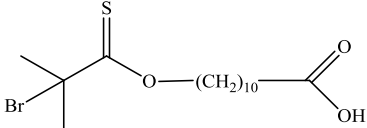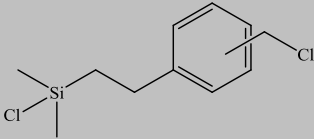
1.2.3.2.2 *Polymer-grafted magnetic nanoparticles*

Magnetic nano-objects have been deemed to hold immense promise for use in in-vivo biomedical applications including magnetic resonance imaging (MRI) contrast enhancement,[167-170] targeted drug delivery,[171-172] hyperthermia,[173-174] magnetic field assisted radionuclide and cancer therapy,[175] in vitro automated separations and isolation of biomolecules and cells[176-178] and magnetically separable nanocatalytic systems.[179-180]However, due to van der Waals attraction forces and their anisotropic dipolar attraction, the magnetic nanoparticles tend to agglomerate into larger clusters and the properties associated with their nanometer dimensions are eliminated. Their

functionalization with organic stabilizers [181-182] can prevent aggregation and improve their dispersion and the confinement of the inorganic material in a polymer matrix.[183-184]

Several reports have described the surface functionalization of magnetic nanoparticles with initiating sites (Table 2) for the growth of polymeric stabilizers utilizing CRP techniques and showed that the magnetic properties were not significantly affected. [185-186]

Table 2. ATRP initiators anchored on the surface of magnetic nanoparticles

No	Initiators	Ref.
1	[4-(chloromethyl)phenyl]trichlorosilane	187
2	3-chloropropionic acid	188
3	2-bromo-2-methylpropionic acid (BMPA)	189-194
4	10-carboxydecanyl 2-bromo-2-methyl-thiopropanoate	195
5	((chloromethyl)phenylethyl)-dimethylchlorosilane (CDS)	185

Lattuada and Hatton proposed a flexible methodology for the preparation of magnetic nanoparticles coated with poly(lactic acid) end-tethered chains grown by surface-initiated ROP and poly(methacrylate) end-grafted chains obtained by ATRP.[196] Poly(2-dimethylamino)ethyl methacrylate) (PDMAEMA) end-grafted chains were also

synthesized from the surface of γ-F$_2$O$_3$ nanoparticles by ATRP affording an "amphibious" character to the hybrids. These core-shell nano-objects being soluble in both aqueous and common solvents remain in the bulk phase in water/oil biphasic systems.[194] F$_2$O$_3$[189] and MnFe$_2$O$_4$[188] core-PS shell hybrids were synthesized by surface-initiated ATRP utilizing an initiator bearing a carboxyl anchoring group. However, the non-covalent linkage of the macromolecules onto the surface facilitated the exchange of the polymer chains with other competing molecules from the solution possessing –COOH groups. One way to overcome this problem is by cross-linking the PS chains onto the nanoparticle surface.[195]

Recently, Xu et al. studied the self-assembly process of nanocomposite films consisting of a lamellar-forming PS-*b*-PMMA copolymer and PMMA-coated magnetite nanoparticles as a function of the concentration of the nanoparticles and the molecular weight of the polymer chains.[197] The particles coated with short PMMA chains were dispersed at low particle concentration and aggregated only upon increasing the concentration of the nanoparticles. However, the increase of the molecular weight of the end-tethered PMMA chains induced nanoparticle aggregation even at low particle concentration. The size of these aggregates was larger than the copolymer domain size and forced the block copolymer to form an onion-like morphology around the aggregates. PMMA-coated magnetic nanoparticles synthesized by ATRP were also introduced in a thin polymer film of a symmetric P2VP-*b*-PMMA copolymer. The structural polymorphism of the film was studied in the presence of carbon tetrachloride vapor, leading to the formation of hexagonal and lamellar microphase-separated morphologies at different exposure times due to the selective solvation of the PMMA block in the solvent. The colloidal hybrids segregated in the PMMA domains of the diblock copolymer due to the affinity of the PMMA-shell for the PMMA block. However, the self-assembled morphology of the film disappeared upon application of a magnetic field generated by the interaction of a magnetized atomic force microscopy tip with the magnetic nanoparticles.[198]

Tuning the composition and functionality of the macromolecules introduced onto the surface of the nanocolloids allows the tailoring of the novel physical, chemical and biological functions of the nanoparticles. In particular, the functionalization of Fe$_3$O$_4$

particles with poly(ethylene glycol methacrylate) (PEGMA) chains did not only improve the dispersability of the nanoparticles in an aqueous solution, but also increased the in-vivo circulation time of the magnetic nanoparticles. PEGMA rendered the surface neutral and hydrophilic and increased its resistance to the adsorption of proteins or macromolecules bearing receptors recognized by the macrophages, thus preventing the endocytosis/phagocytosis of the particles by the macrophase cells.[187] Fe_3O_4/SiO_2-g-poly(styrene sulfonate sodium salt) hybrids were also proposed for use as solid supports for the immobilization of enzymes such as pectinase. Biochemical studies proved that the enzyme retained its activity for 30 days, at a wider pH and temperature range compared to the free enzyme.[199]

A challenging issue that has emerged lately is the formation of clusters, comprising polymer-coated magnetic nanoparticles, in response to an external trigger. These clusters are advantageous for certain potential applications as for example in high gradient magnetic separation processes in which clustering enables the facile scavenging of the particles after the adsorption process.[200] The development of such "smart" hybrids which undergo relatively large and abrupt changes in their physical and/or chemical and colloidal properties in response to external environmental conditions requires the functionalization of magnetic nano-objects with a polymer shell being sensitive to an external stimulus such as the temperature, pH, ionic strength, magnetic field, etc. The thermo-responsive dispersion of F_3O_4@PHEMA hybrids in methanol,[190] F_3O_4@PS particles in cyclohexane[192-193] and poly(ε-caprolactone) (PCL)-coated colloids in dimethyl sulfoxide [191] has been studied. The solubility of the polymer as a function of the solvent quality is determined by the enthalpy and the entropy of the system and is described by the Florry and Huggins theory.[201] Below a critical temperature known as the theta temperature (T_θ) the polymer chains are in a collapsed state due to the predominant attractive forces between the polymer segments. At T_θ the entropy determines the polymer chain conformation which behaves as an ideal chain. Above T_θ the dominant forces are the repulsive interchain and the favorable chain-solvent interactions causing the polymer chains to expand. This thermo-responsive behavior of PS-coated superparamagnetic nanoparticles allowed the development of magneto-responsive Pichering emulsions in a cyclohexane/water mixture above the T_θ of PS,[192] which offer new opportunities for the

encapsulation and controlled release of lipophilic compounds using the magnetic heating of the emulsion in an ac magnetic field to break the emulsion on demand.

Of particular interest is the ability to control the aggregation of core-shell systems by employing the property of several polymers to collapse in aqueous media upon heating above the LCST. This approach has been used to enhance the contrast in magnetic resonance imaging by introducing temperature sensitive Fe_3O_4 nanoparticles into blood cells and causing their reversible agglomeration in response to temperature changes.[202] The hybrid-loaded cells exhibited better magnetic response and enhanced magnetic contrast above the LCST due to aggregation. Besides, the direct temperature change of the hybrid dispersion, the application of an AC magnetic field to generate heat, which is transferred to the temperature-responsive polymer-shell, can be also used to indirectly cause the aggregation of the nanocolloids.[203] A great challenge in this field is the ability to control the cluster size upon aggregation. Janus particles possessing stimuli responsive polymer coatings were shown to meet these requirements. Due to their asymmetric surface functionalization these nano-objects become amphiphilic and self-assemble into well-defined clusters in response to an external stimulus. Janus magnetite nanoparticles coated at one hemisphere with a pH-responsive polymer and on the second hemisphere with a pH-independent or a temperature-responsive polymer can self-assemble into micelle-like structures of finite-size at low pH or high temperatures driven by the individual response of each of the polymer coatings.[204] Moreover, polyampholyte Janus nanoparticles comprising acidic and basic hemispheres have shown an interesting pH-responsive behavior forming clusters at low pH-values due to the excess charge on the one hemisphere of the nanoparticles, followed by aggregation and precipitation of the nanocolloids at intermediate pH-values. due to charge neutralization on the particle surface.[200]

1.2.3.2.3   *Polymer-grafted metal nanoparticles*
1.2.3.2.3.1   *Hybrid gold nanocolloids*
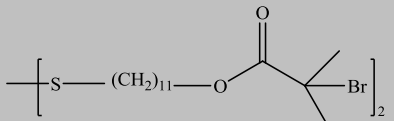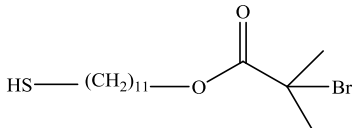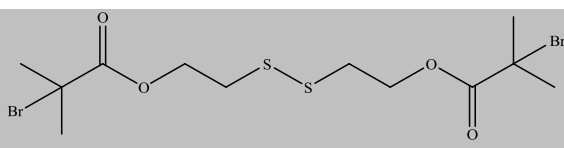
Functionalized metal nanoparticles such as Au, Ag, Pt, and Cu have been the subject of intense research activity over the last decade. The unique electrical properties of these particles[205-209] as well as their optical and photophysical features   (size-controlled

plasmon absorbance, photonic electron–hole pair generation, and fluorescence) have attracted great attention.[210-211] Gold nanoparticles are probably the most attractive metal colloids for potential applications, in electronic and optical materials[212-218] and in biomedicine due to their biocompatibility and non-toxicity.[219-220] However, gold nanoparticles have a high tendency for aggregation which is usually accompanied by a red-shift and a broadening of their plasmon band thus limiting their use in the above applications.[221] The modification of the surface properties of gold nanoparticles was thus urged by the need to stabilize them in both organic and/or aqueous media. Polymeric stabilizers have been employed using either the "grafting to" or the "grafting from" approach and were shown to effectively prevent nanoparticle aggregation.

Gold nanoparticle core nanostructures with a dense polymer layer of well-defined homopolymers and copolymers were easily prepared using controlled/living ATRP to grow polymer chains from initiator functionalized gold nanoparticles (Table 3). Among the syntheses used, si-ATRP from self-assembled monolayers of bromofunctionalized thiolates on gold nanoparticles appears as the most versatile and facile method for the development of structurally controlled hybrids with a gold core of several nanometers in diameter and a shell of variable thickness composed of well-defined, dense polymer brushes.[222-223] These highly grafted hybrids exhibit an intense surface plasmon absorption band which is blue shifted when increasing the grafted polymer chain length, suggesting the improved stabilization of the gold colloids as the size of the polymer stabilizer increases.[224] Moreover, they can form a 2D array with a high degree of structural order due to their long range interparticle interactions which are comparable to the full length of the grafted polymer chains.[225]

Among the different polymer shells, stimuli-responsive polymers are particularly attractive because they allow the manipulation of the optical signal obtained from the gold nanoparticles by external triggers. Cationic, pH-responsive polymer brushes grown from gold nanoparticles, via si-ATRP, were shown to exhibit a reversible shrinkage of the polymer chains which wrap around the gold particle surface. A careful investigation of the pH-response of the grafted polymer chains revealed a two-step transition ascribed to the initial polymer collapse, which induced nanoparticle agglomeration in a second stage. [226]

Table 3. ATRP Initiators immobilized on the surface of gold nanoparticles

No	Initiator	Polymer	Ref.
1	11,11'-dithiobis[1-(2-bromo-2-methylpropionyloxy)undecane] (DTBU)	P4VP, PMMA, P(MeO-PEGMA)-*b*-PNIPAM, PNIPAM, PDMAEMA-*co*-PDEAEMA-*co*-P(PEGMA)	224-231
2		PMMA, P*n*BA, P*t*BA	222-223,232
3	2,2'-dithiobis[1-(2-bromo-2-methylpropionyloxy)ethane] (DTBE)	PDMAEMA	230

These hybrids can serve as pH-stimuli bimetallic catalysts because they can entrap transition metal ions by their efficient coordinating segments followed by in situ metal reduction.[227] Polymer coated gold nanoparticles have been also used for the development of pH sensitive, colloidally stable, hydrophilic polymer capsules which are attractive for the controlled encapsulation and release of drug molecules. The capsules were obtained by first cross-linking the polymer shells followed by the cleavage of the Au-S bonds to remove the gold cores.[230] Temperature-responsive polymers, PNIPAM and poly(*N*-cyclopropylacrylamide) (PCYPAAM), exhibiting an LCST behavior have been also grown from gold nanoparticles using ATRP.[233] The optical properties of these gold particles can be varied by temperature, based on the thermal-responsive behavior of the polymer monolayer. During the collapse of the PNIPAM grafts the surface plasmon not only decreases in intensity, but also blue shifts due to the decrease of the hydrophilicity of the nanoparticle surface as it becomes covered by the collapsed polymer.[234]

Besides the growth of linear polymers, the synthesis of cross-linked temperature responsive gels onto the surface of gold nanoparticles has been explored. Gold

nanoparticles coated with a cross-linked PNIPAM shell have been proposed for use in nanoparticle trapping using the thermo-modulated "breathing process" of the polymer shell.[231]

Moreover, Janus gold-nanoparticles with two types of different polymer chains decorated on the opposite sides of the nanoparticles are accessible. A novel approach was employed which combined a "solid-state grafting-to" method for the immobilization of crystalline polymer chains on one hemisphere and a "grafting-from" technique for the growth of a second type of polymer from the "free" surface of the nanoparticles. The symmetric decoration of the Janus hybrids was confirmed by the selective in-situ formation of platinum nanoparticles on one of the hemispheres.[232] Although this solid-state approach has a higher throughput compared to the self-assembled monolayers it is limited to the grafting of crystalline polymers in one of the two hemispheres.

Finally, binary thermo-sensitive nanocomposites can be obtained by the growth of block copolymers comprising two thermo-responsive blocks on the surface of the gold nanoparticles. These core-shell nanostructures possess two transition temperatures corresponding to the thermally induced conformational transition of the inner and the outer polymer, respectively. Upon cross-linking the polymer shells, the nanostructures can be used as temperature-sensitive catalytic systems with tunable catalytic activity of the incorporated metal nanoparticles as a function of the solution temperature.[235]

1.2.3.2.3.2   *Polymer-coated platinum nanoparticles*

Similar to gold nanoparticles, platinum nanoparticles have a high surface-to-volume ratio and consequently a large fraction of metal atoms are exposed at the surface and are accessible to reactant molecules. Few reports in the literature have described the synthesis of polymer chains from the surface of platinum nanoparticles using the "grafting from" method in combination with a CRP technique. Recently, Carrot et al. have grown poly(butyl methacrylate) (P*n*BMA) chains from initiator-derivatized platinum nanoparticles using ATRP. Small-angle neutron scattering studies in solution showed that the hybrid structure is closer to a star architecture rather than a dense polymer corona surrounding the inorganic core. The formation of 2D arrays (Langmuir film) of these polymer-grafted-platinum hybrids at the air-water interface was shown, in

which the interparticle distance was controlled, by the polymer chain length and the surface pressure in the range of tens of nanometers to a few nanometers.[236]

1.2.3.2.3.3   Polymer-grafted quantum dots

Nanometer-sized semiconductor nanoparticles or quantum dots such as CdSe, CdTe, CdS, and ZnS have been extensively studied and still remain an active research area because of their unique size- and surface-dependent nonlinear optical, physicochemical, and electronic properties.[237] Due to their size in the nanometer range, quantum dots show interesting physical behavior which is totally different to that found in bulk materials. This effect is known as the quantum confinement effect.

Because of these unique electronic and optical properties, including their broad absorption spectra, narrow absorption profiles and their discrete energy bands, semiconductor nanoparticles are candidates for many applications in sensors, solar cells, biological imaging, diagnostics, data storage, light-emitting diodes, single-molecule transistors, and substrates for biological tags and detection devices.[238-246] The modification of the surface of the nanoparticles with polymers is highly advantageous since the polymer endows the quantum dots with new physical and chemical properties including solubility, processability, chemical and biological stability, biocompatibility, and further functionalization possibility.

One of the first attempts for the surface modification of quantum dots came from Patten and Farmer who encapsulated CdS quantum dots in a silica shell and polymerized PMMA chains from the silica surface by ATRP.[247] These hybrid nanoparticles were casted into films which retained the photoluminescence of the precursor CdS nanoparticles and showed good dispersion of the polymer-coated CdS/SiO_2 hybrids throughout the PMMA matrix. However, advances in CRP techniques, which are accompanied with low radical concentrations, have allowed the growth of functional polymers from the surface of quantum dots. "Unprotected" quantum dots without the intermediate silica layer have been used lately as substrates for the development of core-shell hybrids providing an intimate connection of the polymer to the nanoparticle core. An approach involved the use of activators generated by electron transfer (AGET) ATRP in a miniemulsion system to synthesize well-defined polymer chains from the surface of

pre-functionalized CdS nanoparticles.[248] The hybrids exhibited a high homogeneity, while quantum confinement effects were revealed by a blue shift at the onset of the trioctylphosphine oxide (TOPO) quantum dot absorption compared to the absorption of bulk CdS.

Finally, hydroxyl-terminated germanium nanoclusters have been also appropriately functionalized to yield polymer coated nanoclusters via ATRP. The original nanoclusters retained their photophysical properties upon altering the termination group which was consistent with a stable nanocluster surface.[249]

1.2.3.2.4 *Polymer-grafted Silsequioxane nanoparticles*

A lot of synthetic effort has focused on the preparation and properties of polyhedral oligomeric silsesquioxanes (POSS)-polymer hybrid materials due to the observed enhancement of the properties of the organic matrix (increased thermal stability, reduced flammability and dielectric constant) upon incorporation of the POSS molecules.[250-255] POSS molecules have a cage-shaped three-dimensional structure with a general chemical formula $(RSiO_{1.5})_n$. Among them, octasilsesquioxanes $(R_8Si_8O_{12})$ ($n=8$) have been widely investigated owing to their precise molecular structure; they consist of a rigid, cubic silica core with a 0.53 nm side length, and an organic group attached to each of the eight corners. These organic groups can be either inert or reactive, and control the reactivity and the solubility of the POSS molecules [256-257]. Intense research effort has recently led to the preparation of POSS-containing hybrid polymers of different topological structures such as star-shaped, block and tadpole-shaped hybrid polymers. Telechelic and hemitelechelic POSS-containing hybrids have been also synthesized.

1.2.3.2.4.1 *Star-shaped hybrids*

Star-like hybrids with inorganic POSS cores can be prepared by the "core-first" method in which the polymerization is initiated by appropriately functionalized POSS molecules. Well-defined end-tethered homopolymers and block copolymers were grown from the polysilsesquioxane $(SiO_{1.5})$ nanoparticles by ATRP leading to layered core-shell structures.[258-259] A similar method employed POSS macroinitiators with about 58 functions to grow water soluble glycopolymer functionalized silsequioxane particles of

approximately 25 arms. Such well-defined branched structures are attractive for a wide range of applications in biosciences as well as hybrid thickeners in coatings and paints.

An interesting approach was followed for the synthesis of a unique hybrid architecture comprising a POSS core surrounded by four macrocyclic polymer arms to form quatrefoil-shaped star-cyclic PS. The synthesis involved a combination of ATRP chemistry to form an 8-arm star with a POSS core and eight end-functionalized polymer arms carrying azide functionalities. Click reaction between the azide functionalities and a difunctional linker yielded a polymer loop with both ends attached on the POSS molecule. The star-cyclic PS processed a higher glass transition temperature compared to the star-linear PS due to the absence of chain ends in the former molecule [260]. These molecules are also expected to exhibit interesting rheological properties and dynamics related to the ring polymer structure.

1.2.3.2.4.2 *Tadpole-shaped hybrids*

An interesting POSS-based hybrid architecture combines a particle with one covalently bound polymer chain in a single entity. Initial work focused on the growth of methacrylate polymers from a functionalized POSS however, low degrees of polymerization[261] were obtained attributed to the steric hindrance by the bulky POSS molecule.[262] Recently, tadpole-shaped polymeric hybrids with an inorganic POSS "head" and a well-defined polymer "tail" were synthesized using an incompletely condensed POSS molecule bearing a highly reactive trisodium silanolate group as the efficient and versatile initiator for copper-mediated ATRP. This allowed the synthesis of POSS-polymer hybrids with good control over the polymer molecular weight and molecular weight distribution and gave hybrid materials with enhanced degradation and glass transition temperature compared to those of the model polymers without the POSS moiety.[263]

Tadpole-shaped fluorinated POSS molecules bearing well-defined grafted PMMA chains were blended in a PMMA matrix and were shown to migrate at the air/polymer interface with the outermost layer of the film covered almost completely by the POSS heads. Owing to this unique structure, the films exhibited strong resistance against Ar^+

ion etching, despite their low overall POSS content[264] and are attractive for various applications.

Recently, responsive polymer-POSS hybrids comprising temperature-responsive or polyelectrolyte polymer chains have been prepared leading to amphiphilic tadpole-shaped structures. These molecules self-assemble into well-defined temperature-responsive POSS-core micelles or pH-responsive particulate aggregates in aqueous media[265-266] and are proposed for use in controlled drug delivery.

1.2.3.2.5   Silica particles
1.2.3.2.5.1   "Hairy" homopolymer and block copolymer silica particles

The surface hydroxyl groups exposed on the periphery of silica permit their facile derivatization to appropriate initiating moieties (Table 4) for the controlled growth of polymer chains from the surface of the nanoparticles (Figure 1.40). The si-ATRP from silica nanoparticles was first reported by Patten et al. to polymerize styrene and methyl methacrylate.[267-268]   Since   then,   a   variety   of   polymeric   stabilizers   including homopolymers and copolymers of styrenes, meth(acrylates) and acrylamides have been grown from the surface of spherical silica colloids.[131,269-277] Recently, the controlled polymerization of dense PMMA chains, with a very narrow molecular weight distribution from a silica core was achieved by ATRP in bulk. A high grafting-density hydrophobic brush was successfully prepared using an initiator carrying a triethoxysilane anchor group.[278] The control of the grafting density resulted in the formation of a colloidal crystal, when the hybrids were suspended in a good solvent for the polymer in a certain concentration range, which decreased with increasing the grafted polymer chain length, L_c. Long polymer chains led to a nearest neighbor interparticle distance, D_{dis}, within the crystal in the micrometer length scale. The colloidal crystal included both hexagonal close-packed (hcp) and face-centered cubic (fcc) lattice arrangements with the fcc arrangement likely to increase when increasing the polymer chain length. This transition of the crystalline structure from a nearly random stacking to an fcc arrangement was ascribed to a qualitative change of the conformation of the grafted chains and hence the interparticle potential curve at the crossover of the concentrated polymer brush to the semidilute polymer brush in the effective grafting density of the polymer layer.[279-280]
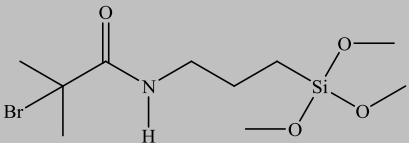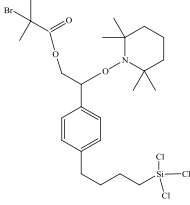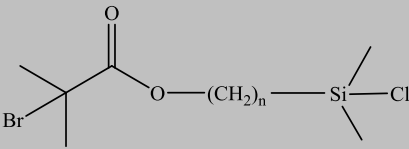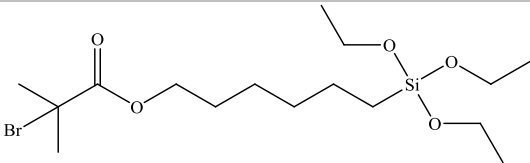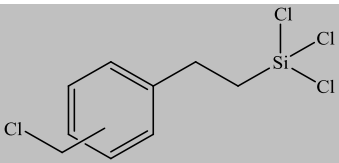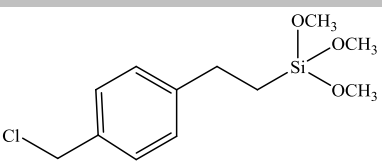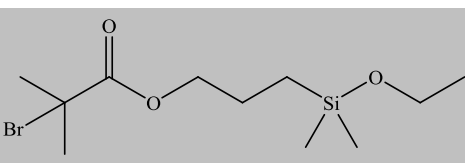
Moreover, the grafting density of the polymer had a significant effect on the "softness" of the hybrid colloids. Significant interpenetration of the grafted polymer chains took place for particles in the intermediate brush regime and decreased as the polymer grafting density increased. As a result, the threshold concentration for graft polymer interpenetration of dense particle brushes was found to increase by about an order of magnitude as compared to the intermediate brush analogue. [132,281] These finding offer unique possibilities for fundamental and applied research of colloidal systems for application in photonic materials, sensors and elsewhere.
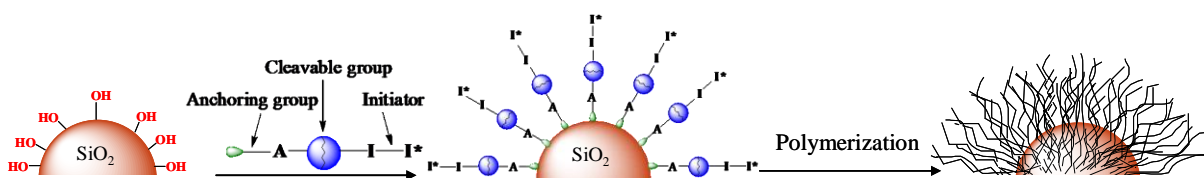
Figure 1.40. Schematic representation of the synthetic procedure followed for the preparation of the silica-polymer core-shell hybrids using the "grafting from" method

The synthesis of hydrophilic methacrylate polymers from the surface of silica particles via ambient temperature ATRP in protic media, utilizing a siloxane-grafted initiator,[282] have been shown to suffer from the hydrolytic cleavage of the grafted polymer chains from the nanoparticle surface.[283] To overcome this problem and circumvent the need for surface pre-treatment of the silica sol with siloxane initiators prior to the polymerization, a cationic ATRP initiator was electrostatically absorbed onto ultrafine anionic silica for subsequent polymer grafting of hydrophilic methacrylates in protic media at ambient temperature. Nonionic and cationic monomers have been polymerized directly in a one-pot synthesis with reasonably high conversions, however the growth of anionic polymers was hindered due to the electrostatic interactions between the negatively charged monomer with the cationic macroinitiator-particles.[284-285] Furthermore, this approach also allowed the synthesis of zwitterionic polymer coatings[286] which are highly resistant to nonspecific protein adsorption in complex media and improve the bio-interfacial properties of the silica particles protecting them against aggregation in complex physiological conditions.[287]

Table 4. Initiator molecules grafted on the surface of silica particles

No	Initiator	Ref.
1	 3-(2-bromoisobutyramido)propyl(trimethoxy)silane	286, 288-295
2		296-297
3		298-301
4	 (2-Bromo-2-methyl)propionyloxyhexyltriethoxysilane	278, 302
5	 2-(m,p-chloromethylphenyl)ethyltrichlorosilane	303-306
6	 (4-(chloromethyl)phenethyl)trimethoxysilane	307
7	 3-(dimethylethoxysilyl)propyl-2-bromoisobutyrate	282-283

Another hybrid system was developed by the si-ATRP of acrylonitrile from the surface of silica nanopartricles. The "hairy" silica-polyacrylonitrile (PAN) hybrids were used as precursors for the synthesis of nanoporous carbon thin films with appreciable adsorption capacities after the pyrolysis of the PAN stabilizers, followed by the removal of silica by HF etching.[308] Using a similar protocol, mesoporous carbons were obtained by the surface polymerization of acrylonitrile from ordered and disordered mesoporous silica templates carrying surface initiating sites, followed by the stabilization of the polymer layer under air and its subsequent carbonization at higher temperatures.[309]

Silica-polymer core-shell hybrids are particularly advantageous for the facile preparation of uniform hollow polymer microspheres by the removal of the silica core of the hybrids using HF etching. Homopolymer and block copolymer coated particles have been used as precursors to obtain polymeric hollow spheres of uniform size and good dispersibility in aqueous or organic media. The structural integrity of the hollow shell or capsule is preserved by either cross-linking the polymer chains,[302,310] or by dispersing the hollow structure in a bad solvent for the polymer.[307] Such hollow capsules are very attractive for the encapsulation and controlled delivery of active compounds in drug delivery and other biomedical applications.

1.2.3.2.5.2 Pickering emulsions and Janus nanohybrids

Janus particles, which are characterized by an asymmetric structure, have attracted particular attention, because they can self-assemble into fascinating hierarchical structures and can serve as building blocks for complex superstructures. The preparation of such synthetic asymmetric particles is effectively assisted by Pickering emulsions, which are emulsions stabilized by particles rather than surfactant molecules. Pickering emulsions can be effectively stabilized by hybrid core-shell particles based on strong polyelectrolyte brushes grown from the surface of silica colloids. Anionic poly(styrenesulfonate) chains have been used because they are "quenched" [311] and highly charged and can thus form long-term stabilized oil-in-water emulsions which are stable against coalescence even at low particle concentrations. The emulsifying properties of the particles are based on the hydrophilic character of the polymer charged side-groups and the hydrophobic character of the polymer backbone which drive their absorption at the

oil/water interface.[304] Amphiphilic Janus particles were prepared in a one-step synthesis by the adsorption of azide-modified silica spheres around the monomer droplets of a styrene/water emulsion with one hemisphere being immerse in the aqueous phase and the other in the organic phase. The emulsion-assisted synthesis of amphiphilic Janus particles comprising PS- and poly(sodium methacrylate)-coated hemispheres used initiator-modified particles to simultaneously grow the polymer chains from the surface of the particles in the two hemispheres. These hybrids can form supramolecular assemblies upon dispersion in solvents being selective for only one hemisphere.[312]

A challenge in the development of Janus particles is the ability to affect their self-organization properties by the application of an external stimulus. Following the Pickering emulsion approach of Granick and co-workers,[313] stimuli-responsive oppositely charged Janus nanoparticles were synthesized using a sequential "grafting from"/"grafting to" approach to decorate the particles with temperature and/or pH responsive polymer chains, respectively. These switchable Janus particles form hierarchically structured aggregates upon altering the solution pH and are proposed for use in the controlled stabilization of emulsions and the regulation of molecular transport across the interface of two immiscible phases.[289]

1.2.3.2.5.3 *Responsive nanohybrids*

1.2.3.2.5.3.1 *pH- and temperature-sensitive core-shell systems*

Recent advances in the field of responsive materials focus on the coating of flat or curved surfaces with polymers exhibiting a stimuli-sensitive behavior and changing their properties in response to an applied stimulus. External stimuli, i.e. temperature, pH and solvent quality, have been investigated leading to changes in the grafted polymer chain conformation and the physicochemical properties of the surface. Silica nanoparticles coated with responsive polymers are attractive building blocks for the development of "smart", environmentally responsive nanostructured materials. The most extensively studied system is PNIPAM grafted polymer chains onto silica nanoparticles which were shown to exhibit a non-conventional temperature-induced double phase transition behavior.[295] The phase transition at lower temperature is ascribed to the cluster-induced collapse of the inner region of the PNIPAM brushes, close to the silica surface, which

posses a high chain density, while the transition at higher temperature is attributed to the outer region of the PNIPAM shell where the chain density is lower. The thermo-induced phase transition of the grafted polymer chains is shifted to lower temperatures and occurs over a broader temperature range compared to that of the free polymer in solution. This is attributed to interchain interactions in the brush layer.[298] The characteristic dehydration of temperature-sensitive polymers in densely-packed brushes can be crucial for the application of such systems as a thermo-responsive stationary phase in chromatography for the separation of active molecules. It was shown that the retention time of steroids increased over a broad range of temperatures for highly grafted PNIPAM-silica hybrids, while at lower grafting densities the retention time increased only in a narrow range around the LCST of the polymer.[303]

The surface-initiated polymerization of responsive monomers has also been used for the modification of the pore properties of mesoporous materials. PNIPAM chains were grown in the pore walls of mesoporous silica leading to materials with temperature responsive pore properties. The long-range ordered hexagonal mesostructure and the thermo-responsive behavior of PNIPAM were retained after the synthesis of the interpenetrating silica-PNIPAM network rendering these materials attractive for use in bioseparations or molecular transport switches.[314]

Another interesting effect induced by the stimuli responsive behavior of the polymer coating is the reversible transportation of stimuli-sensitive core-shell hybrids between two immiscible phases due to the reversible hydration-dehydration of the polymer shell. The reversible migration of temperature-sensitive polymer-grafted silica nanoparticles from an aqueous to an immiscible organic phase upon heating and cooling the system, respectively, was shown,[299,315] which is consistent with the de Gennes concept.[316]

Recently, it was proposed that pH-sensitive core-shell structures can be used as transducers of signals in logic operation systems. More specifically, "smart" signal-responsive hybrid systems with built-in Boolean logic were developed by grafting poly(2-vinyl pyridine) chains onto the surface of silica particles. The hybrids were coupled with an enzyme-based system and were used to detect signals induced by the enzyme function. The biochemical input signals, that is pH changes originated from the

AND/OR logic operations of the enzyme systems, were detected by the self-assembly changes of the pH-sensitive hybrids in solution[317] rendering these materials very promising for use in the development of biochips and other biomedical devices.

Another responsive system of particular interest are "hairy" silica nanoparticles comprising mixed homopolymer brushes These hybrids posses interesting responsive properties induced by changes of the solvent quality. To ensure the uniformity of the mixed polymer layer on the surface of the nanoparticles Y-shaped multifunctional colloidal initiators carrying dual initiating functionalities have been employed. A combination of ATRP followed by NMP chemistry resulted in the formation of the mixed brush by sequential polymerization. The phase behavior of the mixed poly(*t*-buyl acrylate) (P*t*BA)/PS brushes on the silica nanoparticles showed a lateral phase separation of the two polymers under equilibrium melt conditions which resulted in worm-like patterns with a feature size of around 10 nm.[297] Furthermore, hydrolysis of the *tert*-butyl groups produced amphiphilic mixed poly(acrylic acid) (PAA)/PS brushes which rendered the particles dispersible in both chloroform which is a selective solvent for the PS chains and in methanol which is selective for the PAA grafts via the chain reorganization on the surface of the "hairy" particles.[296]

1.2.3.2.5.3.2 Hybrids with gating properties

An ongoing challenge in materials science relies on the development of hybrid assemblies displaying gating properties. It was recently shown, that transport through colloidal nanoporous assemblies can be effectively modulated by modifying the surface of the colloids with "smart", environmentally-responsive polymer brushes in such a way to mimic the gating function in biological nanoporous systems. The first example in this field was reported by Schepelina and Zharov. They used poly(acrylamide) brushes grown by ATRP to modify the surface of the nanopores in films of closed-packed face-centered cubic (fcc) lattices of submicrometer silica spheres. Flux measurements of redox species across these opal films verified that the polymer film thickness increased with the polymerization time leading to a decrease of the pore size.[305] The use of temperature-responsive PNIPAM brushes allowed tuning the flow as a function of temperature, while the film thickness had also a significant effect on the diffusion through the nanopores.

Nanopores bearing a thin PNIPAM layer possessed a positive gating behavior and the diffusion rates increased with increasing temperature, while the nanopores with the thicker PNIPAM layers exhibited the opposite effect (negative gating behavior) and diminished the flow through the nanopores at higher temperatures due to the dehydration of the densely packed polymer inside the nanopores.[306] An alternative approach to develop "smart" hybrid materials displaying gating properties involves the simple modification of ordered mesoporous networks or porous nanocolloids with stimuli responsive end-grafted polymer chains. The temperature-dependent uptake and release of small molecules by these porous materials was modulated by the polymer phase transition and the porosity of the materials. The presence of the hydrated and extended polymer within the porous structure at low temperature inhibited the transport of solutes, while at higher temperatures the collapse of the hydrophobic polymer in the globule conformation within the pores allowed solute diffusion.[318] The inherent disadvantage of the above system was the leakage of the active molecules even at low temperatures. To overcome this problem a different mode of action has been targeted which relies on the uptake and release of the actives below rather than above the LCST. This was achieved by "grafting to" temperature-responsive polymer chains onto the surface of micro-to-mesoporous silica nanoparticles. Below the LCST, the grafted polymer chains adopted a random coil configuration and facilitated the uptake and release of the molecules through the pores. However, upon increasing the temperature above the LCST the polymer chains collapsed, blocked the pores and retarded the diffusion of the molecules.[319]

Finally, pH-responsive polymer coatings that exhibit a rather complex pH- and ion-responsive flux[320] behavior, which is dependent on the pH, the charge of the active species and the ionic strength of the medium, have been developed as gating materials. The stretching of the polymer chains due to the ionization of the monomer repeat units block the nanopores and decrease the diffusion rate. The flow can be restored by increasing the salt concentration which screens the electrostatic repulsion forces.[292] pH-responsive polymer shells were proposed for the development of organic-inorganic hybrid membranes exhibiting high proton conductivity. To this direction, sintered silica and self-assembled nanoporous silica colloidal crystals modified with surface-bound polymer brushes carrying acidic groups were shown to exhibit high water uptake and

proton conductivity. However, despite the superior proton conductivity of the self-assembled membranes their poor mechanical properties limit their use for practical purposes.[293]

1.2.3.2.5.3.3 Photo-responsive hybrids

Core-shell hybrids carrying photo-responsive groups, whose properties can be reversibly altered by applying a remote stimulus such as light of specific wavelength, are highly attractive nowadays. Poly(spirobenzopyran)-*co*-poly(methyl methacrylate) (PSP-*co*-PMMA) copolymer brushes have been synthesized onto the surface of silica particles by ATRP. A progressive decrease of both the coloration and decoloration rates of the SP moieties incorporated in the polymer chains was observed, accompanied by the H-stacking of the chromophore moieties in dense polymer brushes upon irradiation.[300] This effect is very attractive and has been used for the formation of 2D and 3D structures by a light induced assembly and phase separation of the hybrid nanocolloids. The latter is based on the UV induced isomerization of the spiropyran (SP) moieties to merocyanine (MC) groups which exhibit a high dipolar moment and form SP-MC interchain complexes in less polar media leading to the aggregation of the particles. Both the SP content of the polymer and the solvent polarity were shown to affect the photo-induced aggregation of the polymer shell.[321] 2D patterned colloid assemblies were obtained via the appropriate modification of a flat substrate with a PSP-*co*-PMMA polymer film, which was next immersed in a stable colloidal dispersion of the photo-responsive hybrids. Upon UV irradiation, the MC moieties formed on the flat surface due to the SP photo-isomeriation, aggregate with the SP moieties of the polymer brushes of the colloidal hybrids and hold the two surfaces together.[322] Analogous 3D porous structures have been fabricated by direct laser writing of a dense colloidal suspension of the photo-responsive spheres. A two photon absorption process at a focal point of a near-IR pulsed laser, focused tightly in the colloidal dispersion, induced gelation of the hybrids and the isomerization of the SP photo-responsive moieties of the polymer brush to MC groups. The MC-SP and MC-MC *H*-aggregates formed, induce strong intermolecular and interparticle bonding in the system and lead to the 3D structure fabrication.[323] Recently, a similar photo-responsive core-shell hybrid system was proposed for use as a sensitive

ratiometric fluorescent thermometer. The hybrid comprised silica particles coated with a densely grafted PNIPAM shell, labeled with a fluorescence resonance energy transfer (FRET) donor in its inner layer and a photo-responsive SP acceptor in the outer layer. Upon irradiation with UV the non-fluorescent SP form isomerized to the fluorescent MC form and facilitated the FRET process between the donor and the acceptor moieties. The thermo-modulated collapse/swelling of the PNIPAM shell can be used as a temperature probe which tunes the relative distance of the donor and the acceptor in the polymer shell and influences the FRET efficiency.[294]

1.3   Scope of this work

The aim of this work was to synthesize and investigate the responsive behavior of novel spiropyran-based materials including random copolymers, core-shell hybrids and nanocapsules.

Multiresponsive spiropyran-based PDMAEMA-*co*-PSP copolymers, with varying content of the photosensitive moieties (1.3 - 10 mol %), were synthesized by the random copolymerization of DMAEMA and the in-house synthesized SP monomer 1',3',3'-trimethyl-6-methacryloyloxy-spiro(2*H*-1-benzopyran-2,2'-indoline) by copper-mediated ATRP in solution. A PMMA-*co*-PSP copolymer containing 19 mol% SP was also synthesized using the same method and its absorption properties were compared to those of the PDMAEMA-*co*-PSP copolymers. The solvatochromic, pH, temperature and light responsive behavior of the PDMAEMA-*co*-PSP polymers in solution were monitored by UV/vis spectroscopy. The ability of the SP species of the copolymers to undergo coloration in solution in the absence of a photo-trigger, known as "reverse photochromism", created the need to synthesize materials which exhibit "normal photochromism" and whose chromophores could reversibly isomerize between the SP and MC forms upon applying the appropriate photo-trigger. For this purpose, the photoresponsive molecule, 2-(3',3'-dimethyl-6-nitro-3'H-spiro[chromene-2,3'-indol]-1'-yl)-ethanol (SP-OH) was first synthesized via a three-step reaction and was further functionalized with a methacrylate moiety to obtain the photosensitive monomer,1´-(2-methacryloxyethyl)-3´,3´-dimethyl-6-nitrospiro-(2H-1-benzopyran-2,2´-indoline) monomer (SPMA). A photoresponsive PDMAEMA-*co*-PSPMA random copolymer

carrying 6.1 mol% chromophore units was further synthesized via the random copolymerization of DMAEMA and SPMA by ATRP in bulk. The ability of the copolymer to respond to a light and pH-trigger and the fluorescent properties of the copolymer upon irradiation with UV light were studied by UV/vis and fluorescent spectroscopy, respectively.

Next, well-defined photoresponsive spherical polymer brushes were synthesized by the random copolymerization of DMAEMA and SPMA from the surface of initiator-coated silica particles via copper-mediated ATRP in bulk. Three core-shell particles were synthesized; two SiO_2-g-(PDMAEMA-co-PSPMA) hybrids bearing 4.8 and 6.1 mol% SPMA units, and a third sample with a SPMA content of 11.5 mol%. The photo- and pH-responsive behavior of the SiO_2-g-(PDMAEMA-co-PSPMA) core-shell particles carrying 6.1 mol% SPMA and their fluorescent properties were investigated in water by UV/vis and fluorescent spectroscopy, respectively. The effect of biomolecules such as proteins and aminoacids on the fluorescent properties of the hybrid particles upon stimulation of the system with UV light and in the dark, was also studied.

Finally, the ability of the SiO_2-g-(PDMAEMA-co-PSPMA) core-shell particles to be used as precursors for the light-regulated supramolecular engineering of polymeric nanocapsules (NCPs) was also investigated. The engineering of the NCPs was based on the UV-induced formation of non-covalent π-π interactions among the MC isomers in the sterically crowded polymer shell layer which can be reversibly disrupted upon irradiation with visible light. The size and the morphology of the NCPs derived upon HF etching of the silica core of the hybrids were studied at low and high pH by field-emission scanning electron microscopy (FESEM), transmission electron microscopy (TEM) and dynamic light scattering (DLS). The inherent fluorescent properties of the NCPs in the aqueous medium were studied by fluorescent spectroscopy and microscopy. The ability of the NCPs to dissociate to their constituent polymer chains upon irradiation with vis light was monitored by DLS.

1.4 References

(1)   Gil, E. S.; Hudson, S. M. *Prog. Polym. Sci.* **2004**, *29*, 1173-1222.

(2)   McCormick, C. L.; Kirkland, S. E.; York, A. W. *Polymer Reviews* **2006**, *46*, 421-443.

(3)   Galaev, I. Y.; Mattiasson, B. *Trends Biotechnol.* **1999**, *17*, 335-340.

(4)   Gupta, P.; Vermani, K.; Garg, S. *Drug Discov. Today* **2002**, *7*, 569-579.

(5)   Kikuchi, A.; Okano, T. *Prog. Polym. Sci.* **2002**, *27*, 1165- 1193.

(6)   Qiu, Y.; Park, K. *Adv. Drug Delivery. Rev.* **2001**, *53*, 321-339.

(7)   Sershen, S.; West, J. *Adv. Drug Delivery. Rev.* **2002**, *54*, 1225-1235.

(8)   Sharma, S.; Kaur, P.; Jain, A.; Rajeswari, M. R.; Gupta, M. N. *Biomacromolecules* **2003**, *4*, 330-336.

(9)   Yokoyama, M. *Drug Discov. Today* **2002**, *7*, 426-432.

(10)   Dobrynin, A. V.; Colby, R. H.; Rubinstein, M. *J. Polym. Sci., Part B: Polym. Phys.* **2004**, *42*, 3513-3538.

(11)   Ayres, N.; Cyrus, C. D.; Brittain, W. J. *Langmuir* **2007**, *23*, 3744-3749.

(12)   Creutz, S.; Teyssié, P.; Jérôme, R. *Macromolecules* **1997**, *30*, 6-9.

(13)   Goloub, T.; de Keizer, A.; Cohen Stuart, M. A. *Macromolecules* **1999**, *32*, 8441-8446.

(14)   Varoqui, R.; Tran, Q.; Pefferkorn, E. *Macromolecules* **1979**, *12*, 831-835.

(15)   Lowe, A. B.; Billingham, N. C.; Armes, S. P. *Macromolecules* **1998**, *31*, 5991-5998.

(16)   Creutz, S.; van Stam, J.; De Schryver, F. C.; Jérôme, R. *Macromolecules* **1998**, *31*, 681-689.

(17)   Kamachi, M.; Kurihara, M.; Stille, J. K. *Macromolecules* **1972**, *5*, 161-167.

(18)   Chen, W.-Y.; Alexandridis, P.; Su, C.-K.; Patrickios, C. S.; Hertler, W. R.; Hatton, T. A. *Macromolecules* **1995**, *28*, 8604-8611.

(19)   Patrickios, C. S.; Hertler, W. R.; Abbott, N. L.; Hatton, T. A. *Macromolecules* **1994**, *27*, 930-937.

(20)   Philippova, O. E.; Hourdet, D.; Audebert, R.; Khokhlov, A. R. *Macromolecules* **1997**, *30*, 8278-8285.

(21)   Torres-Lugo, M.; Peppas, N. A. *Macromolecules* **1999**, *32*, 6646-6651.

(22)   Tonge, S. R.; Tighe, B. J. *Adv. Drug Delivery. Rev.* **2001**, *53*, 109-122.

(23)   Park, S. Y.; Bae, Y. H. *Macromol. Rapid Commun.* **1999**, *20*, 269-273.

(24)   Kang, S. I.; Bae, Y. H. *J. Control. Release* **2003**, *86*, 115-121.

(25)   Liu, S.; Weaver, J. V. M.; Tang, Y.; Billingham, N. C.; Armes, S. P.; Tribe, K. *Macromolecules* **2002**, *35*, 6121-6131.

(26)   Lee, A. S.; Bütün, V.; Vamvakaki, M.; Armes, S. P.; Pople, J. A.; Gast, A. P. *Macromolecules* **2002**, *35*, 8540-8551.

(27)   Sutton, R. C.; Thai, L.; Hewitt, J. M.; Voycheck, C. L.; Tan, J. S. *Macromolecules* **1988**, *21*, 2432-2439.

(28)   Seymour, L. W. *J. Control. Release* **1994**, *31*, 201-206.

(29)   Guo, X.; Szoka Jr, F. C. *Bioconjugate Chem.* **2001**, *12*, 291-300.

(30)   Heller, J.; Chang, A. C.; Rodd, G.; Grodsky, G. M. *J. Control. Release* **1990**, *13*, 295-302.

(31)   Potineni, A.; Lynn, D. M.; Langer, R.; Amiji, M. M. *J. Control. Release* **2003**, *86*, 223-234.

(32)   Lynn, D. M.; Amiji, M. M.; Langer, R. *Angew. Chem., Int. Ed.* **2001**, *40*, 1707-1710.

(33)   De Las Heras Alarcón, C.; Pennadam, S.; Alexander, C. *Chem. Soc. Rev.* **2005**, *34*, 276-285.

(34)   Schild, H. G. *Prog. Polym.Sci.* **1992**, *17*, 163-249.

(35)   Gan, L. H.; Gan, Y. Y.; Deen, G. R. *Macromolecules* **2000**, *33*, 7893-7897.

(36)   Gan, L. H.; Roshan Deen, G.; Loh, X. J.; Gan, Y. Y. *Polymer* **2001**, *42*, 65-69.

(37)   Peng, S.; Wu, C. *Macromolecules* **2001**, *34*, 568-571.

(38)   Lau, A. C. W.; Wu, C. *Macromolecules* **1999**, *32*, 581-584.

(39)   Lee, S. B.; Russell, A. J.; Matyjaszewski, K. *Biomacromolecules* **2003**, *4*, 1386-1393.

(40)   Vamvakaki, M.; Billingham, N. C.; Armes, S. P. *Macromolecules* **1999**, *32*, 2088-2090.

(41)   Alexandridis, P.; Alan Hatton, T. *Colloids and Surfaces A: Physicochemical and Engineering Aspects* **1995**, *96*, 1-46.

(42)   Kudaibergenov, S.; Jaeger, W.; Laschewsky, A. *Adv. Polym. Sci.* **2006**, *201*, 157-224.

(43)   Chen, L.; Honma, Y.; Mizutani, T.; Liaw, D. J.; Gong, J. P.; Osada, Y. *Polymer* **2000**, *41*, 141-147.

(44)   Minkin, V. I. *Chem. Rev.* **2004**, *104*, 2751-2776.

(45)   Such, G.; Evans, R. A.; Yee, L. H.; Davis, T. P. *J. Macromol. Sci. Polym. Rev.* **2003**, *43*, 547-579.

(46)   Reichardt, C. *Solvents and solvent effects in organic chemistry*; Wiley, 2003.

(47)   Lee, I. J. *J. Photochem. Photobiol., A* **2002**, *146*, 169-173.

(48)   Ernsting, N. P.; Arthen-Engeland, T. *J. Phys. Chem.* **1991**, *95*, 5502-5509.

(49)   Tamai, N.; Miyasaka, H. *Chem. Rev.* **2000**, *100*, 1875-1890.

(50)   Metelitsa, A. V.; Lokshin, V.; Micheau, J. C.; Samat, A.; Guglielmetti, R.; Minkin, V. I. *Phys. Chem. Chem. Phys.* **2002**, *4*, 4340-4345.

(51)   Wojtyk, J. T. C.; Wasey, A.; Kazmaier, P. M.; Hoz, S.; Buncel, E. *J. Phys. Chem. A* **2000**, *104*, 9046-9055.

(52)   Raymo, F. M.; Giordani, S. *J. Am. Chem. Soc.* **2001**, *123*, 4651-4652.

(53)   Wojtyk, J. T. C.; Wasey, A.; Xiao, N.-N.; Kazmaier, P. M.; Hoz, S.; Yu, C.; Lemieux, R. P.; Buncel, E. *J. Phys. Chem. A* **2007**, *111*, 2511-2516.

(54)   Voloshin, N. A.; Metelitsa, A. V.; Micheau, J. C.; Voloshina, E. N.; Besugliy, S. O.; Shelepin, N. E.; Minkin, V. I.; Tkachev, V. V.; Safoklov, B. B.; Aldoshin, S. M. *Russ. Chem. Bull.* **2003**, *52*, 2038-2047.

(55)   Voloshin, N. A.; Metelitsa, A. V.; Micheau, J. C.; Voloshina, E. N.; Besugliy, S. O.; Vdovenko, A. V.; Shelepin, N. E.; Minkin, V. I. *Russ. Chem. Bull.* **2003**, *52*, 1172-1181.

(56)   Tanaka, M.; Ikeda, T.; Xu, Q.; Ando, H.; Shibutani, Y.; Nakamura, M.; Sakamoto, H.; Yajima, S.; Kimura, K. *J. Org. Chem.* **2002**, *67*, 2223-2227.

(57)   Shao, N.; Zhang, Y.; Cheung, S.; Yang, R.; Chan, W.; Mo, T.; Li, K.; Liu, F. *Anal. Chem.* **2005**, *77*, 7294-7303.

(58)   Nakamura, S.; Uchida, K.; Murakami, A.; Irie, M. *J. Org. Chem.* **1993**, *58*, 5543-5545.

(59) Maeda, S.; Mitsuhashi, K.; Osano, Y. T.; Nakamura, S.; Ito, M. *Mol. Crys. Liq. Cryst. Sci. Tech. Mol. Cryst. Liq. Cryst.* **1994**, *246*, 223-230.

(60) Horii, T.; Abe, Y.; Nakao, R. *J. Photochem. Photobiol. A* **2001**, *144*, 119-129.

(61) Onai, Y.; Mamiya, M.; Kiyokawa, T.; Okuwa, K.; Kobayashi, M.; Shinohara, H.; Sato, H. *J. Phys. Chem.* **1993**, *97*, 9499-9505.

(62) Li, Y.; Zhou, J.; Wang, Y.; Zhang, F.; Song, X. *J. Photochem. Photobiol. A* **1998**, *113*, 65-72.

(63) Berkovic, G.; Krongauz, V.; Weiss, V. *Chem. Rev.* **2000**, *100*, 1741-1753.

(64) Eckhardt, H.; Bose, A.; Krongauz, V. A. *Polymer* **1987**, *28*, 1959-1964.

(65) Krongauz, V. A.; Goldburt, E. S. *Macromolecules* **1981**, *14*, 1382-1386.

(66) Junichi, H.; Kumiko, M.; Masa-aki, S.; Yoshio, K. *Thin Solid Films* **1992**, *210-211, Part 2*, 562-564.

(67) Gu, Z.-Z.; Hayami, S.; Meng, Q.-B.; Iyoda, T.; Fujishima, A.; Sato, O. *J. Am. Chem. Soc.* **2000**, *122*, 10730-10731.

(68) Shumburo, A.; Biewer, M. C. *Chem. Mater.* **2002**, *14*, 3745-3750.

(69) Schaudel, B.; Guermeur, C.; Sanchez, C.; Nakatani, K.; Delaire, J. A. *J. Mater. Chem.* **1997**, *7*, 61-65.

(70) Wirnsberger, G.; Yang, P.; Scott, B. J.; Chmelka, B. F.; Stucky, G. D. *Spectrochim. Acta A* **2001**, *57*, 2049-2060.

(71) Hu, A. T.; Wang, W. H.; Lee, H. J. *J. Macromol. Sci. Pure Appl Chem.* **1996**, *A33*, 803-810.

(72) Krongauz, V. *Mol. Cryst. Liq.Cryst. Sci. Tech. Mol. Cryst. Liq. Cryst.***1994**, *246*, 339-346.

(73) Zelichenok, A.; Buchholtz, F.; Yitzchaik, S.; Ratner, J.; Safro, M.; Krongauz, V. *Macromolecules* **1992**, *25*, 3179-3183.

(74) Allcock, H. R.; Kim, C. *Macromolecules* **1991**, *24*, 2846-2851.

(75) Lyubimov, A. V.; Zaichenko, N. L.; Marevtsev, V. S. *J. Photochem. Photobiol. A* **1999**, *120*, 55-62.

(76) Evans, R. A.; Hanley, T. L.; Skidmore, M. A.; Davis, T. P.; Such, G. K.; Yee, L. H.; Ball, G. E.; Lewis, D. A. *Nat. Mater.* **2005**, *4*, 249-253.

(77) Kobatake, S.; Irie, M. *Ann. Rep. Prog. C* **2003**, *99*, 277-313.

(78)   Hirano, M.; Osakada, K.; Nohira, H.; Miyashita, A. *J. Org. Chem.* **2001**, *67*, 533-540.

(79)   Imai, Y.; Adachi, K.; Naka, K.; Chujo, Y. *Polym. Bull.* **2000**, *44*, 9-15.

(80)   Moniruzzaman, M.; Fernando, G. F.; Bellamy, A. J. *Eur. Polym. J.* **2006**, *42*, 1455-1466.

(81)   Mistry, B. B.; Patel, R. G.; Patel, V. S. *J. Appl. Polym. Sci.* **1997**, *64*, 841-848.

(82)   McCoy, C. P.; Donnelly, L.; Jones, D. S.; Gorman, S. P. *Tetrahedron Lett.* **2007**, *48*, 657-661.

(83)   Elizalde, L. E.; Ledezma, R.; López, R. G. *Synth. Commun.* **2005**, *35*, 603-610.

(84)   Goldburt, E.; Shvartsman, F.; Fishman, S.; Krongauz, V. *Macromolecules* **1984**, *17*, 1225-1230.

(85)   Nayak, A.; Liu, H.; Belfort, G. *Angew. Chem., Int. Ed.* **2006**, *45*, 4094-4098.

(86)   Higuchi, A.; Hamamura, A.; Shindo, Y.; Kitamura, H.; Yoon, B. O.; Mori, T.; Uyama, T.; Umezawa, A. *Biomacromolecules* **2004**, *5*, 1770-1774.

(87)   Fukushima, K.; Vandenbos, A. J.; Fujiwara, T. *Chem. Mater.* **2007**, *19*, 644-646.

(88)   Garcia, A.; Marquez, M.; Cai, T.; Rosario, R.; Hu, Z.; Gust, D.; Hayes, M.; Vail, S. A.; Park, C.-D. *Langmuir* **2007**, *23*, 224-229.

(89)   Zhu, M.-Q.; Zhu, L.; Han, J. J.; Wu, W.; Hurst, J. K.; Li, A. D. Q. *J. Am. Chem. Soc.* **2006**, *128*, 4303-4309.

(90)   Taguchi, M.; Li, G.; Gu, Z.; Sato, O.; Einaga, Y. *Chem. Mater.* **2003**, *15*, 4756-4760.

(91)   Zhang, H.; Yi, T.; Li, F.; Delahaye, E.; Yu, P.; Clement, R. *J. Photochem. Photobiol. A* **2007**, *186*, 173-177.

(92)   Bobrovsky, A. Y.; Boiko, N. I.; Shibaev, V. P. *Liq. Cryst.* **2000**, *27*, 57-62.

(93)   Hachisako, H.; Ihara, H.; Kamiya, T.; Hirayama, C.; Yamada, K. *Chem. Commun.* **1997**, 19-20.

(94)   Connal, L. A.; Franks, G. V.; Qiao, G. G. *Langmuir* **2010**, *26*, 10397-10400.

(95)   Lee, C. K.; Davis, D. A.; White, S. R.; Moore, J. S.; Sottos, N. R.; Braun, P. V. *J. Am. Chem. Soc.* **2010**, *132*, 16107-16111.

(96)   Klaikherd, A.; Nagamani, C.; Thayumanavan, S. *J. Am. Chem. Soc.* **2009**, *131*, 4830-4838.

(97)   Bigot, J.; Charleux, B.; Cooke, G.; Delattre, F.; Fournier, D.; Lyskawa, J.; Sambe, L.; Stoffelbach, F.; Woisel, P. *J. Am. Chem. Soc.* **2010**, *132*, 10796-10801.

(98)   Caponi, P.-F.; Qiu, X.-P.; Vilela, F.; Winnik, F. M.; Ulijn, R. V. *Polymer Chemistry* **2011**, *2*, 306-308

(99)   Achilleos, D. S.; Vamvakaki, M. *Macromolecules* **2010**, *43*, 7073-7081.

(100)   Zhao, Y.; Tremblay, L.; Zhao, Y. *J. Polym. Sci., Part A: Polym. Chem.* **2010**, *48*, 4055-4066.

(101)   Gota, C.; Okabe, K.; Funatsu, T.; Harada, Y.; Uchiyama, S. *J. Am. Chem. Soc.* **2009**, *131*, 2766-2767.

(102)   Yin, J.; Hu, H.; Wu, Y.; Liu, S. *Polymer Chemistry* **2011**, *2*, 363-371

(103)   Yin, J.; Li, C.; Wang, D.; Liu, S. *J. Phys. Chem. B* **2010**, *114*, 12213-12220.

(104)   Sumaru, K.; Ohi, K.; Takagi, T.; Kanamori, T.; Shinbo, T. *Langmuir* **2006**, *22*, 4353-4356.

(105)   Alvarez-Lorenzo, C.; Deshmukh, S.; Bromberg, L.; Hatton, T. A.; Sández-Macho, I.; Concheiro, A. *Langmuir* **2007**, *23*, 11475-11481.

(106)   Chen, D.; Liu, H.; Kobayashi, T.; Yu, H. *J. Mater. Chem.* **2010**, *20*, 3610-3614.

(107)   Matsubara, K.; Watanabe, M.; Takeoka, Y. *Angew. Chem., Int. Ed.* **2007**, *46*, 1688-1692.

(108)   Yuan, W.; Jiang, G.; Wang, J.; Wang, G.; Song, Y.; Jiang, L. *Macromolecules* **2006**, *39*, 1300-1303.

(109)   Xia, F.; Ge, H.; Hou, Y.; Sun, T.; Chen, L.; Zhang, G.; Jiang, L. *Adv. Mater.* **2007**, *19*, 2520-2524.

(110)   Ito, T.; Hioki, T.; Yamaguchi, T.; Shinbo, T.; Nakao, S.-i.; Kimura, S. *J. Am. Chem. Soc.* **2002**, *124*, 7840-7846.

(111)   Yamaguchi, T.; Ito, T.; Sato, T.; Shinbo, T.; Nakao, S.-i. *J. Am. Chem. Soc.* **1999**, *121*, 4078-4079.

(112)   Zhao, B.; Brittain, W. J. *Prog. Polym. Sci.* **2000**, *25*, 677-710.

(113)   Halperin, A.; Tirrell, M.; Lodge, T. P. *Adv. Polym. Sci.* **1991**, *100*, 30-71.

(114)   Szleifer, I.; Carignano, M. A. *Adv. Chem. Phys.* **1996**, *94*, 165-260.

(115)   Wu, T.; Efimenko, K.; Genzer, J. *J. Am. Chem. Soc.* **2002**, *124*, 9394-9395.

(116)   Soga, K. G.; Zuckermann, M. J.; Guo, H. *Macromolecules* **1996**, *29*, 1998-2005.

(117) Mansky, P.; Liu, Y.; Huang, E.; Russell, T. P.; Hawker, C. *Science* **1997**, *275*, 1458-1460.

(118) Zhao, B.; Brittain, W. J. *J. Am. Chem. Soc.* **1999**, *121*, 3557-3558.

(119) Bug, A. L. R.; Cates, M. E.; Safran, S. A.; Witten, T. A. *J. Chem. Phys.* **1987**, *87*, 1824-1833.

(120) Guzonas, D.; Boils, D.; Hair, M. L. *Macromolecules* **1991**, *24*, 3383-3387.

(121) Parsonage, E.; Tirrell, M.; Watanabe, H.; Nuzzo, R. G. *Macromolecules* **1991**, *24*, 1987-1995.

(122) Yerushalmi-Rozen, R.; Klein, J.; Fetters, L. J. *Science* **1994**, *263*, 793.

(123) Reiter, G.; Schultz, J.; Auroy, P.; Auvray, L. *Europhys. Lett.* **1996**, *33*, 29-34.

(124) Mir, Y.; Auroy, P.; Auvray, L. *Phys. Rev. Lett.* **1995**, *75*, 2863-2866.

(125) Tran, Y.; Auroy, P.; Lee, L. T.; Stamm, M. *Phys. Rev. E* **1999**, *60*, 6984-6990.

(126) Tran, Y.; Auroy, P.; Lee, L. T. *Macromolecules* **1999**, *32*, 8952-8964.

(127) Tran, Y.; Auroy, P. *J. Am. Chem. Soc.* **2001**, *123*, 3644-3654.

(128) Zajac, R.; Chakrabarti, A. *Phys. Rev. E* **1995**, *52*, 6536-6549.

(129) Kopf, A.; Baschnagel, J.; Wittmer, J.; Binder, K. *Macromolecules* **1996**, *29*, 1433-1441.

(130) Edmondson, S.; Osborne, V. L.; Huck, W. T. S. *Chem. Soc. Rev.* **2004**, *33*, 14-22.

(131) Pyun, J.; Kowalewski, T.; Matyjaszewski, K. *Macromol. Rapid Commun.* **2003**, *24*, 1043-1059.

(132) Voudouris, P.; Choi, J.; Dong, H.; Bockstaller, M. R.; Matyjaszewski, K.; Fytas, G. *Macromolecules* **2009**, *42*, 2721-2728.

(133) Shan, J.; Chen, J.; Nuopponen, M.; Tenhu, H. *Langmuir* **2004**, *20*, 4671-4676.

(134) Wu, T.; Zhang, Y.; Wang, X.; Liu, S. *Chem. Mater.* **2008**, *20*, 101-109.

(135) Kamigaito, M.; Ando, T.; Sawamoto, M. *Chem. Rev.* **2001**, *101*, 3689-3745.

(136) Patten, T. E.; Matyjaszewski, K. *Adv. Mater.* **1998**, *10*, 901-915.

(137) Wang, J.-S.; Matyjaszewski, K. *J. Am. Chem. Soc.* **1995**, *117*, 5614-5615.

(138) Wang, J.-S.; Matyjaszewski, K. *Macromolecules* **1995**, *28*, 7901-7910.

(139) Matyjaszewski, K.; Patten, T. E.; Xia, J. *J. Am. Chem. Soc.* **1997**, *119*, 674-680.

(140) Kato, M.; Kamigaito, M.; Sawamoto, M.; Higashimura, T. *Macromolecules* **1995**, *28*, 1721-1723.

(141) Nakagawa, Y.; Matyjaszewski, K. *Polymer Journal* **1998**, *30*, 138-141.

(142) Matyjaszewski, K.; Xia, J. *Chem. Rev.* **2001**, *101*, 2921-2990.

(143) Ashford, E. J.; Naldi, V.; O'Dell, R.; Billingham, N. C.; Armes, S. P. *Chem. Commun.* **1999**, 1285-1286.

(144) Ejaz, M.; Yamamoto, S.; Ohno, K.; Tsujii, Y.; Fukuda, T. *Macromolecules* **1998**, *31*, 5934-5936.

(145) Kim, J.-B.; Bruening, M. L.; Baker, G. L. *J. Am. Chem. Soc.* **2000**, *122*, 7616-7617.

(146) Huang, W.; Kim, J.-B.; Bruening, M. L.; Baker, G. L. *Macromolecules* **2002**, *35*, 1175-1179.

(147) Bontempo, D.; Tirelli, N.; Feldman, K.; Masci, G.; Crescenzi, V.; Hubbell, J. A. *Adv. Mater.* **2002**, *14*, 1239-1241.

(148) Matyjaszewski, K.; Miller, P. J.; Shukla, N.; Immaraporn, B.; Gelman, A.; Luokala, B. B.; Siclovan, T. M.; Kickelbick, G.; Vallant, T.; Hoffmann, H.; Pakula, T. *Macromolecules* **1999**, *32*, 8716-8724.

(149) Husseman, M.; Malmström, E. E.; McNamara, M.; Mate, M.; Mecerreyes, D.; Benoit, D. G.; Hedrick, J. L.; Mansky, P.; Huang, E.; Russell, T. P.; Hawker, C. J. *Macromolecules* **1999**, *32*, 1424-1431.

(150) Advincula, R. C. *J. Dispersion Sci. Technol.* **2003**, *24*, 343-361.

(151) Liu, P.; Tian, J.; Liu, W.; Xue, Q. *Polym. Int.* **2004**, *53*, 127-130.

(152) Kickelbick, G. *Prog. Polym. Sci.* **2003**, *28*, 83-114.

(153) Maliakal, A.; Katz, H.; Cotts, P. M.; Subramoney, S.; Mirau, P. *J. Am. Chem. Soc.* **2005**, *127*, 14655-14662.

(154) Zhang, Q.-L.; Du, L.-C.; Weng, Y.-X.; Wang, L.; Chen, H.-Y.; Li, J.-Q. *J. Phys. Chem. B* **2004**, *108*, 15077-15083.

(155) Lowes, B. J.; Bohrer, A. G.; Tran, T.; Shipp, D. A. *Polym. Bull.* **2009**, *62*, 281-289.

(156) Clearfield, A. In *Prog. Inorg. Chem.* 1998; Vol. 47, p 371-510.

(157) Rajh, T.; Saponjic, Z.; Liu, J.; Dimitrijevic, N. M.; Scherer, N. F.; Vega-Arroyo, M.; Zapol, P.; Curtiss, L. A.; Thurnauer, M. C. *Nano Lett.* **2004**, *4*, 1017-1023.

(158)   Park, J. T.; Koh, J. H.; Koh, J. K.; Kim, J. H. *Appl. Surf. Sci.* **2009**, *255*, 3739-3744.

(159)   Fan, X.; Lin, L.; Messersmith, P. B. *Compos. Sci. Technol.* **2006**, *66*, 1195-1201.

(160)   Ye, Q.; Wang, X.; Hu, H.; Wang, D.; Li, S.; Zhou, F. *J. Phys. Chem. C* **2009**, *113*, 7677-7683.

(161)   Kickelbick, G.; Holzinger, D.; Brick, C.; Trimmel, G.; Moons, E. *Chem. Mater.* **2002**, *14*, 4382-4389.

(162)   Holzinger, D.; Kickelbick, G. *Chem. Mater.* **2003**, *15*, 4944-4948.

(163)   Sato, M.; Kawata, A.; Morito, S.; Sato, Y.; Yamaguchi, I. *Eur. Polym. J.* **2008**, *44*, 3430-3438.

(164)   Liu, P.; Wang, T. *Curr. Appl Phys.* **2008**, *8*, 66-70.

(165)   Peng, X.; Chen, Y.; Li, F.; Zhou, W.; Hu, Y. *Appl. Surf. Sci.* **2009**, *255*, 7158-7163.

(166)   Liu, P.; Wang, T. *Polym. Eng. Sci.***2007**, *47*, 1296-1301.

(167)   Yan, F.; Xu, H.; Anker, J.; Kopelman, R.; Ross, B.; Rehemtulla, A.; Reddy, R. *J. Nanosci. Nanotechnol.* **2004**, *4*, 72-76.

(168)   Perez, J. M.; Simeone, F. J.; Tsourkas, A.; Josephson, L.; Weissleder, R. *Nano Lett.* **2003**, *4*, 119-122.

(169)   Bulte, J. W. M. *J. Magn. Magn. Mater.* **2005**, *289*, 423-427.

(170)   Lacava, L. M.; Lacava, Z. G. M.; Da Silva, M. F.; Silva, O.; Chaves, S. B.; Azevedo, R. B.; Pelegrini, F.; Gansau, C.; Buske, N.; Sabolovic, D.; Morais, P. C. *Biophys. J.* **2001**, *80*, 2483-2486.

(171)   Häfeli, U. O. *Int. J. Pharm.* **2004**, *277*, 19-24.

(172)   Lübbe, A. S.; Bergemann, C.; Riess, H.; Schriever, F.; Reichardt, P.; Possinger, K.; Matthias, M.; Dörken, B.; Herrmann, F.; Gürtler, R.; Hohenberger, P.; Haas, N.; Sohr, R.; Sander, B.; Lemke, A. J.; Ohlendorf, D.; Huhnt, W.; Huhn, D. *Cancer Res.* **1996**, *56*, 4686-4693.

(173)   Hilger, I.; Katrin, F.; Andrä, W.; Hiergeist, R.; Hergt, R.; Kaiser, W. A. *Acad. Radiol.* **2002**, *9*, 198-202.

(174)   Moroz, P.; Jones, S. K.; Gray, B. N. *Int. J. Hyperth.* **2002**, *18*, 267-284.

(175) Jordan, A.; Scholz, R.; Wust, P.; Fähling, H.; Felix, R. *J. Magn. Magn. Mater.* **1999**, *201*, 413-419.

(176) Nam, J. M.; Thaxton, C. S.; Mirkin, C. A. *Science* **2003**, *301*, 1884-1886.

(177) Patolsky, F.; Weizmann, Y.; Katz, E.; Willner, I. *Angew. Chem., Int. Ed.* **2003**, *42*, 2372-2376.

(178) Gu, H.; Ho, P.-L.; Tsang, K. W. T.; Wang, L.; Xu, B. *J. Am. Chem. Soc.* **2003**, *125*, 15702-15703.

(179) Teunissen, W.; De Groot, F. M. F.; Geus, J.; Stephan, O.; Tence, M.; Colliex, C. *J. Catal.* **2001**, *204*, 169-174.

(180) Lu, A. H.; Schmidt, W.; Matoussevitch, N.; Bönnemann, H.; Spliethoff, B.; Tesche, B.; Bill, E.; Kiefer, W.; Schuth, F. *Angew. Chem., Int. Ed.* **2004**, *43*, 4303-4306.

(181) García, I.; Zafeiropoulos, N. E.; Janke, A.; Tercjak, A.; Eceiza, A.; Stamm, M.; Mondracon, I. *J. Polym. Sci., Part A: Polym. Chem.* **2007**, *45*, 925-932.

(182) Marutani, E.; Yamamoto, S.; Ninjbadgar, T.; Tsujii, Y.; Fukuda, T.; Takano, M. *Polymer* **2004**, *45*, 2231-2235.

(183) García, I.; Tercjak, A.; Zafeiropoulos, N. E.; Stamm, M.; Mondragon, I. *Macromol. Rapid Commun.* **2007**, *28*, 2361-2365.

(184) García, I.; Tercjak, A.; Rueda, L.; Mondragon, I. *Macromolecules* **2008**, *41*, 9295-9298.

(185) Ninjbadgar, T.; Yamamoto, S.; Fukuda, T. *Solid State Sci.* **2004**, *6*, 879-885.

(186) Gravano, S. M.; Dumas, R.; Liu, K.; Patten, T. E. *J. Polym. Sci., Part A: Polym. Chem.* **2005**, *43*, 3675-3688.

(187) Hu; Neoh, K. G.; Cen, L.; Kang, E.-T. *Biomacromolecules* **2006**, *7*, 809-816.

(188) Vestal, C. R.; Zhang, Z. J. *J. Am. Chem. Soc.* **2002**, *124*, 14312-14313.

(189) Wang, Y.; Teng, X.; Wang, J.-S.; Yang, H. *Nano Lett.* **2003**, *3*, 789-793.

(190) Gelbrich, T.; Feyen, M.; Schmidt, A. M. *Macromolecules* **2006**, *39*, 3469-3472.

(191) Kaiser, A.; Gelbrich, T.; Schmidt, A. M. *J. Phys. Condens. Matter* **2006**, *18*, S2563-S2580.

(192) Kaiser, A.; Liu, T.; Richtering, W.; Schmidt, A. M. *Langmuir* **2009**, *25*, 7335-7341.

(193) Kaiser, A.; Schmidt, A. M. *J. Phys. Chem. B* **2008**, *112*, 1894-1898.

(194) Duan, H.; Kuang, M.; Wang, D.; Kurth, D. G.; Möhwald, H. *Angew. Chem., Int. Ed.* **2005**, *44*, 1717-1720.

(195) Li, G.; Fan, J.; Jiang, R.; Gao, Y. *Chem. Mater.* **2004**, *16*, 1835-1837.

(196) Lattuada, M.; Hatton, T. A. *Langmuir* **2007**, *23*, 2158-2168.

(197) Xu, C.; Ohno, K.; Ladmiral, V.; Milkie, D. E.; Kikkawa, J. M.; Composto, R. J. *Macromolecules* **2009**, *42*, 1219-1228.

(198) García, I.; Tercjak, A.; Gutierrez, J.; Rueda, L.; Mondragon, I. *J. Phys. Chem. C* **2008**, *112*, 14343-14347.

(199) Lei, Z.; Ren, N.; Li, Y.; Li, N.; Mu, B. *J. Agric. Food Chem.* **2009**, *57*, 1544-1549.

(200) Lattuada, M.; Hatton, T. A. *J. Am. Chem. Soc.* **2007**, *129*, 12878-12889.

(201) Huggins, M. L. *J. Am. Chem. Soc.* **2002**, *64*, 1712-1719.

(202) Edwards, E. W.; Chanana, M.; Wang, D. *J. Phys. Chem. C* **2008**, *112*, 15207-15219.

(203) Wakamatsu, H.; Yamamoto, K.; Nakao, A.; Aoyagi, T. *J. Magn. Magn. Mater.* **2006**, *302*, 327-333.

(204) Isojima, T.; Lattuada, M.; Vander Sande, J. B.; Hatton, T. A. *ACS Nano* **2008**, *2*, 1799-1806.

(205) Hicks, J. F.; Zamborini, F. P.; Osisek, A. J.; Murray, R. W. *J. Am. Chem. Soc.* **2001**, *123*, 7048-7053.

(206) Hicks, J. F.; Miles, D. T.; Murray, R. W. *J. Am. Chem. Soc.* **2002**, *124*, 13322-13328.

(207) Chen, S.; Murray, R. W. *J. Phys. Chem. B* **1999**, *103*, 9996-10000.

(208) Hicks, J. F.; Zamborini, F. P.; Murray, R. W. *J. Phys. Chem. B* **2002**, *106*, 7751-7757.

(209) Chen, S.; Murray, R. W.; Feldberg, S. W. *J. Phys. Chem. B* **1998**, *102*, 9898-9907.

(210) Daniel, M.-C.; Astruc, D. *Chem. Rev.* **2003**, *104*, 293-346.

(211) Shipway, A. N.; Katz, E.; Willner, I. *ChemPhysChem* **2000**, *1*, 18-52.

(212) Vossmeyer, T.; Guse, B.; Besnard, I.; Bauer, R. E.; Müllen, K.; Yasuda, A. *Adv. Mater.* **2002**, *14*, 238-242.

(213) Storhoff, J. J.; Elghanian, R.; Mucic, R. C.; Mirkin, C. A.; Letsinger, R. L. *J. Am. Chem. Soc.* **1998**, *120*, 1959-1964.

(214) Wohltjen, H.; Snow, A. W. *Anal. Chem.* **1998**, *70*, 2856-2859.

(215) Demaille, C.; Brust, M.; Tsionsky, M.; Bard, A. J. *Anal. Chem.* **1997**, *69*, 2323-2328.

(216) Al-Rawashdeh, N. A. F.; Sandrock, M. L.; Seugling, C. J.; Foss, C. A. *J. Phys. Chem. B* **1998**, *102*, 361-371.

(217) Evans, S. D.; Johnson, S. R.; Cheng, Y. L.; Shen, T. *J. Mater. Chem.* **2000**, *10*, 183-188.

(218) Maier, S. A.; Brongersma, M. L.; Kik, P. G.; Meltzer, S.; Requicha, A. A. G.; Atwater, H. A. *Adv. Mater.* **2001**, *13*, 1501-1505.

(219) Shukla, R.; Bansal, V.; Chaudhary, M.; Basu, A.; Bhonde, R. R.; Sastry, M. *Langmuir* **2005**, *21*, 10644-10654.

(220) Connor, E. E.; Mwamuka, J.; Gole, A.; Murphy, C. J.; Wyatt, M. D. *Small* **2005**, *1*, 325-327.

(221) Fujiwara, H.; Yanagida, S.; Kamat, P. V. *J. Phys. Chem. B* **1999**, *103*, 2589-2591.

(222) Mandal, T. K.; Fleming, M. S.; Walt, D. R. *Nano Lett.* **2002**, *2*, 3-7.

(223) Nuβ, S.; Böttcher, H.; Wurm, H.; Hallensleben, M. L. *Angew. Chem., Int. Ed.* **2001**, *40*, 4016-4018.

(224) Ohno, K.; Koh, K.; Tsujii, Y.; Fukuda, T. *Macromolecules* **2002**, *35*, 8989-8993.

(225) Ohno, K.; Koh, K.; Tsujii, Y.; Fukuda, T. *Angew. Chem., Int. Ed.* **2003**, *42*, 2751-2754.

(226) Li, D.; He, Q.; Yang, Y.; Möhwald, H.; Li, J. *Macromolecules* **2008**, *41*, 7254-7256.

(227) Li, D.; He, Q.; Cui, Y.; Li, J. *Chem. Mater.* **2007**, *19*, 412-417.

(228) Li, D.; Cui, Y.; Wang, K.; He, Q.; Yan, X.; Li, J. *Adv. Funct. Mater.* **2007**, *17*, 3134-3140.

(229) Kim, D. J.; Kang, S. M.; Kong, B.; Kim, W. J.; Paik, H. J.; Choi, H.; Choi, I. S. *Macromol. Chem. Phys.* **2005**, *206*, 1941-1946.

(230) Duan, H.; Kuang, M.; Zhang, G.; Wang, D.; Kurth, D. G.; Mohwald, H. *Langmuir* **2005**, *21*, 11495-11499.

(231) Li, D.; He, Q.; Cui, Y.; Wang, K.; Zhang, X.; Li, J. *Chem. Eur. J.* **2007**, *13*, 2224-2229.

(232) Wang, B.; Li, B.; Zhao, B.; Li, C. Y. *J. Am. Chem. Soc.* **2008**, *130*, 11594-11595.

(233) Roth, P. J.; Theato, P. *Chem. Mater.* **2008**, *20*, 1614-1621.

(234) Raula, J.; Shan, J.; Nuopponen, M.; Niskanen, A.; Jiang, H.; Kauppinen, E. I.; Tenhu, H. *Langmuir* **2003**, *19*, 3499-3504.

(235) Caprioli, L.; Mele, E.; Angilè, F. E.; Girardo, S.; Athanassiou, A.; Camposeo, A.; Cingolani, R.; Pisignano, D. *Appl. Phys. Lett.* **2007**, *91*, art. no. 113113

(236) Carrot, G.; Gal, F.; Cremona, C.; Vinas, J.; Perez, H. *Langmuir* **2009**, *25*, 471-478.

(237) Chen, Y.; Rosenzweig, Z. *Nano Lett.* **2002**, *2*, 1299-1302.

(238) Murray, C. B.; Kagan, C. R.; Bawendi, M. G. *Science* **1995**, *270*, 1335-1338.

(239) Wang, S.; Mamedova, N.; Kotov, N. A.; Chen, W.; Studer, J. *Nano Lett.* **2002**, *2*, 817-822.

(240) Myung, N.; Ding, Z.; Bard, A. J. *Nano Lett.* **2002**, *2*, 1315-1319.

(241) Mattoussi, H.; Radzilowski, L. H.; Dabbousi, B. O.; Fogg, D. E.; Schrock, R. R.; Thomas, E. L.; Rubner, M. F.; Bawendi, M. G. *J. Appl. Phys.* **1999**, *86*, 4390-4399.

(242) Alivisatos, A. P. *Science* **1996**, *271*, 933-937.

(243) Michalet, X.; Pinaud, F. F.; Bentolila, L. A.; Tsay, J. M.; Doose, S.; Li, J. J.; Sundaresan, G.; Wu, A. M.; Gambhir, S. S.; Weiss, S. *Science* **2005**, *307*, 538-544.

(244) Lee, J.; Sundar, V. C.; Heine, J. R.; Bawendi, M. G.; Jensen, K. F. *Adv. Mater.* **2000**, *12*, 1102-1105.

(245) Chan, W. C. W.; Nie, S. *Science* **1998**, *281*, 2016-2018.

(246) Medintz, I. L.; Uyeda, H. T.; Goldman, E. R.; Mattoussi, H. *Nat. Mater.* **2005**, *4*, 435-446.

(247) Farmer, S. C.; Patten, T. E. *Chem. Mater.* **2001**, *13*, 3920-3926.

(248) Esteves, A. C. C.; Bombalski, L.; Trindade, T.; Matyjaszewski, K.; Barros-Timmons, A. *Small* **2007**, *3*, 1230-1236.

(249) Tanke, R. S.; Kauzlarich, S. M.; Patten, T. E.; Pettigrew, K. A.; Murphy, D. L.; Thompson, M. E.; Lee, H. W. H. *Chem. Mater.* **2003**, *15*, 1682-1689.

(250) Kopesky, E. T.; Haddad, T. S.; Cohen, R. E.; McKinley, G. H. *Macromolecules* **2004**, *37*, 8992-9004.

(251) Li, G. Z.; Wang, L.; Toghiani, H.; Daulton, T. L.; Koyama, K.; Pittman, C. U. *Macromolecules* **2001**, *34*, 8686-8693.

(252) Strachota, A.; Kroutilova, I.; Kovarova, J.; Matejka, L. *Macromolecules* **2004**, *37*, 9457-9464.

(253) Matejka, L.; Strachota, A.; Plestil, J.; Whelan, P.; Steinhart, M.; Slouf, M. *Macromolecules* **2004**, *37*, 9449-9456.

(254) Waddon, A. J.; Zheng, L.; Farris, R. J.; Coughlin, E. B. *Nano Lett.* **2002**, *2*, 1149-1155.

(255) Tamaki, R.; Choi, J.; Laine, R. M. *Chem. Mater.* **2003**, *15*, 793-797.

(256) Brown, J. F. *J. Am. Chem. Soc.* **1965**, *87*, 4317-4324.

(257) Sprung, M. M.; Guenther, F. O. *J. Am. Chem. Soc.* **1955**, *77*, 3996-4002.

(258) Pyun, J.; Matyjaszewski, K.; Kowalewski, T.; Savin, D.; Patterson, G.; Kickelbick, G.; Huesing, N. *J. Am. Chem. Soc.* **2001**, *123*, 9445-9446.

(259) Costa, R. O. R.; Vasconcelos, W. L.; Tamaki, R.; Laine, R. M. *Macromolecules* **2001**, *34*, 5398-5407.

(260) Ge, Z.; Wang, D.; Zhou, Y.; Liu, H.; Liu, S. *Macromolecules* **2009**, *42*, 2903-2910.

(261) Pyun, J.; Matyjaszewski, K. *Macromolecules* **2000**, *33*, 217-220.

(262) Pyun, J.; Matyjaszewski, K.; Wu, J.; Kim, G. M.; Chun, S. B.; Mather, P. T. *Polymer* **2003**, *44*, 2739-2750.

(263) Ohno, K.; Sugiyama, S.; Koh, K.; Tsujii, Y.; Fukuda, T.; Yamahiro, M.; Oikawa, H.; Yamamoto, Y.; Ootake, N.; Watanabe, K. *Macromolecules* **2004**, *37*, 8517-8522.

(264) Koh, K.; Sugiyama, S.; Morinaga, T.; Ohno, K.; Tsujii, Y.; Fukuda, T.; Yamahiro, M.; Iijima, T.; Oikawa, H.; Watanabe, K.; Miyashita, T. *Macromolecules* **2005**, *38*, 1264- 1270.

(265) Zhang, W.; Fang, B.; Walther, A.; Müller, A. H. E. *Macromolecules* **2009**, *42*, 2563-2569.

(266) Zhang, W.; Liu, L.; Zhuang, X.; Li, X.; Bai, J.; Chen, Y. *J. Polym. Sci., Part A: Polym. Chem.* **2008**, *46*, 7049-7061.

(267) von Werne, T.; Patten, T. E. *J. Am. Chem. Soc.* **1999**, *121*, 7409-7410.

(268) von Werne, T.; Patten, T. E. *J. Am. Chem. Soc.* **2001**, *123*, 7497-7505.

(269) Carrot, G.; Diamanti, S.; Manuszak, M.; Charleux, B.; Vairon, J. P. *J. Polym. Sci., Part A: Polym. Chem.* **2001**, *39*, 4294-4301.

(270) Böttcher, H.; Hallensleben, M. L.; Nuss, S.; Wurm, H. *Polym. Bull.* **2000**, *44*, 223-229.

(271) El Harrak, A.; Carrot, G.; Oberdisse, J.; Jestin, J.; Boué, F. *Polymer* **2005**, *46*, 1095-1104.

(272) Pyun, J.; Matyjaszewski, K. *Chem. Mater.* **2001**, *13*, 3436-3448.

(273) Carrot, G.; Harrak, A. E.; Oberdisse, J.; Jestin, J.; Boué, F. *Soft Matter* **2006**, *2*, 1043-1047.

(274) Lei, Z.; Bi, S. *Mater. Lett.* **2007**, *61*, 3531-3534.

(275) Savin, D. A.; Pyun, J.; Patterson, G. D.; Kowalewski, T.; Matyjaszewski, K. *J. Polym. Sci., Part B: Polym. Phys.* **2002**, *40*, 2667-2676.

(276) Zhang, K.; Ma, J.; Zhang, B.; Zhao, S.; Li, Y.; Xu, Y.; Yu, W.; Wang, J. *Mater. Lett.* **2007**, *61*, 949-952.

(277) Perruchot, C.; Khan, M. A.; Kamitsi, A.; Armes, S. P.; Watts, J. F.; Von Werne, T.; Patten, T. E. *Eur. Polym. J.* **2004**, *40*, 2129-2141.

(278) Ohno, K.; Morinaga, T.; Koh, K.; Tsujii, Y.; Fukuda, T. *Macromolecules* **2005**, *38*, 2137-2142.

(279) Ohno, K.; Morinaga, T.; Takeno, S.; Tsujii, Y.; Fukuda, T. *Macromolecules* **2007**, *40*, 9143-9150.

(280) Morinaga, T.; Ohno, K.; Tsujii, Y.; Fukuda, T. *Macromolecules* **2008**, *41*, 3620-3626.

(281) Bombalski, L.; Dong, H.; Listak, J.; Matyjaszewski, K.; Bockstaller, M. R. *Adv. Mater.* **2007**, *19*, 4486-4490.

(282) Perruchot, C.; Khan, M. A.; Kamitsi, A.; Armes, S. P.; von Werne, T.; Patten, T. E. *Langmuir* **2001**, *17*, 4479-4481.

(283) Chen, X.; Randall, D. P.; Perruchot, C.; Watts, J. F.; Patten, T. E.; Von Werne, T.; Armes, S. P. *J. Colloid Interface Sci.* **2003**, *257*, 56-64.

(284) Chen, X.; Armes, S. P. *Adv. Mater.* **2003**, *15*, 1558-1562.

(285) Chen, X. Y.; Armes, S. P.; Greaves, S. J.; Watts, J. F. *Langmuir* **2004**, *20*, 587-595.

(286) Jia, G.; Cao, Z.; Xue, H.; Xu, Y.; Jiang, S. *Langmuir* **2009**, *25*, 3196-3199.

(287) Vaisocherov, H.; Yang, W.; Zhang, Z.; Cao, Z.; Cheng, G.; Piliarik, M.; Homola, J. i.; Jiang, S. *Anal. Chem.* **2008**, *80*, 7894-7901.

(288) Zhang, J.; Wang, X.; Wu, D.; Liu, L.; Zhao, H. *Chem. Mater.* **2009**, *21*, 4012-4018.

(289) Berger, S.; Synytska, A.; Ionov, L.; Eichhorn, K.-J.; Stamm, M. *Macromolecules* **2008**, *41*, 9669-9676.

(290) Zhao, H.; Kang, X.; Liu, L. *Macromolecules* **2005**, *38*, 10619-10622.

(291) Mu, B.; Wang, T.; Liu, P. *Ind. Eng. Chem. Res.* **2007**, *46*, 3069-3072.

(292) Schepelina, O.; Zharov, I. *Langmuir* **2008**, *24*, 14188-14194.

(293) Smith, J. J.; Zharov, I. *Chem. Mater.* **2009**, *21*, 2013-2019.

(294) Wu, T.; Zou, G.; Hu, J.; Liu, S. *Chem. Mater.* **2009**, *21*, 3788-3798.

(295) Wu, T.; Zhang, Y.; Wang, X.; Liu, S. *Chem. Mater.* **2007**, *20*, 101-109.

(296) Li, D.; Sheng, X.; Zhao, B. *J. Am. Chem. Soc.* **2005**, *127*, 6248-6256.

(297) Zhao, B.; Zhu, L. *J. Am. Chem. Soc.* **2006**, *128*, 4574-4575.

(298) Li, D.; Jones, G. L.; Dunlap, J. R.; Hua, F.; Zhao, B. *Langmuir* **2006**, *22*, 3344-3351.

(299) Li, D.; Zhao, B. *Langmuir* **2007**, *23*, 2208-2217.

(300) Piech, M.; Bell, N. S. *Macromolecules* **2006**, *39*, 915-922.

(301) Mori, H.; Seng, D. C.; Zhang, M.; Müller, A. H. E. *Langmuir* **2002**, *18*, 3682-3693.

(302) Morinaga, T.; Ohkura, M.; Ohno, K.; Tsujii, Y.; Fukuda, T. *Macromolecules* **2007**, *40*, 1159-1164.

(303) Nagase, K.; Kobayashi, J.; Kikuchi, A.; Akiyama, Y.; Kanazawa, H.; Okano, T. *Langmuir* **2007**, *24*, 511-517.

(304)   Saleh, N.; Sarbu, T.; Sirk, K.; Lowry, G. V.; Matyjaszewski, K.; Tilton, R. D. *Langmuir* **2005**, *21*, 9873-9878.

(305)   Schepelina, O.; Zharov, I. *Langmuir* **2006**, *22*, 10523-10527.

(306)   Schepelina, O.; Zharov, I. *Langmuir* **2007**, *23*, 12704-12709.

(307)   Mandal, T. K.; Fleming, M. S.; Walt, D. R. *Chem. Mater.* **2000**, *12*, 3481-3487.

(308)   Tang, C.; Bombalski, L.; Kruk, M.; Jaroniec, M.; Matyjaszewski, K.; Kowalewski, T. *Adv. Mater.* **2008**, *20*, 1516-1522.

(309)   Kruk, M.; Dufour, B.; Celer, E. B.; Kowalewski, T.; Jaroniec, M.; Matyjaszewski, K. *J. Phys. Chem. B* **2005**, *109*, 9216-9225.

(310)   Fu, G. D.; Zhao, J. P.; Sun, Y. M.; Kang, E. T.; Neoh, K. G. *Macromolecules* **2007**, *40*, 2271-2275.

(311)   Guo, X.; Ballauff, M. *Phys. Rev. E: Stat. Nonlin. Soft Matter Phys.* **2001**, *64*, 0514061-0514069.

(312)   Zhang, J.; Jin, J.; Zhao, H. *Langmuir* **2009**, *25*, 6431-6437.

(313)   Hong, L.; Jiang, S.; Granick, S. *Langmuir* **2006**, *22*, 9495-9499.

(314)   Tian, B.-S.; Yang, C. *J. Phys. Chem. C* **2009**, *113*, 4925-4931.

(315)   Chung, P. W.; Kumar, R.; Pruski, M.; Lin, V. S. Y. *Adv. Funct. Mater.* **2008**, *18*, 1390-1398.

(316)   Wagner, M.; Brochard-Wyart, F.; Hervet, H.; de Gennes, P. G. *Colloid Polym. Sci.* **1993**, *271*, 621-628.

(317)   Motornov, M.; Zhou, J.; Pita, M.; Gopishetty, V.; Tokarev, I.; Katz, E.; Minko, S. *Nano Lett.* **2008**, *8*, 2993-2997.

(318)   Fu, Q.; Rao, G. V. R.; Ista, L. K.; Wu, Y.; Andrzejewski, B. P.; Sklar, L. A.; Ward, T. L.; López, G. P. *Adv. Mater.* **2003**, *15*, 1262-1266.

(319)   You, Y.-Z.; Kalebaila, K. K.; Brock, S. L.; Oupicky, D. *Chem. Mater.* **2008**, *20*, 3354-3359.

(320)   Zhou, L.; Yuan, W.; Yuan, J.; Hong, X. *Mater. Lett.* **2008**, *62*, 1372-1375.

(321)   Bell, N. S.; Piech, M. *Langmuir* **2006**, *22*, 1420-1427.

(322)   Piech, M.; George, M. C.; Bell, N. S.; Braun, P. V. *Langmuir* **2006**, *22*, 1379-1382.

(323) George, M. C.; Mohraz, A.; Piech, M.; Bell, N. S.; Lewis, J. A.; Braun, P. V. *Adv. Mater.* **2009**, *21*, 66-70.

CHAPTER 2

**Multiresponsive and Inherent FRET
Properties of Spiropyran-based Random
Copolymers
Synthesized by Atom Transfer Radical
Polymerization**

2.1.1 Introduction

"Bistable" compounds that can be interconverted, under certain external stimuli, to two thermodynamically stable states of different color have attracted considerable attention lately.[1] The interconversion can be induced by different stimuli and is defined as photochromism, thermochromism, electrochromism and solvatochromism.[1] Photochromism is the light-induced reversible intramolecular rearrangement between two isomeric conformations with different absorption spectra.[2] Organic molecules exhibiting reversible photochromism include azobenzenes, spiropyrans (SPs), spirooxazimes and naphthopyrans[3] with the first being the most extensively studied family of photochromic compounds. Lately, SP molecules, which consist of two orthogonal π-networks that are connected by a tetrahedral carbon centre, have also attracted great interest.[1] Upon UV irradiation, the non-polar, colorless SP molecule undergoes heterolytic cleavage of the C-O bond to form the polar, colored *cisoid* isomer of merocyanine (MC) (see Scheme 2.1.1).

SP   **MC**
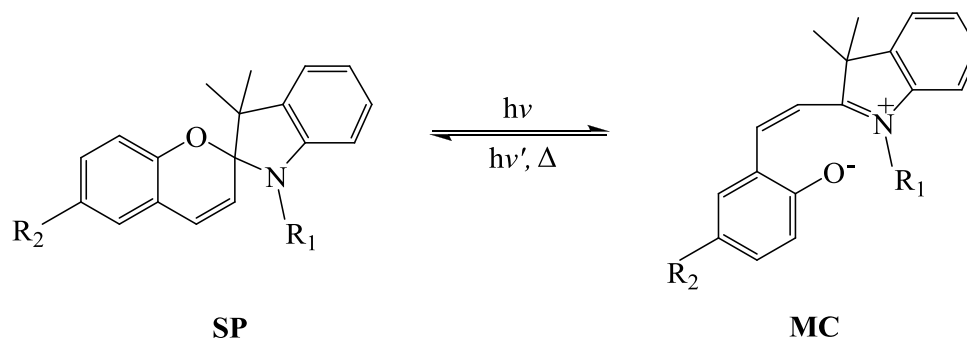
Scheme 2.1.1 Schematic representation of the reversible photo-isomerization process of SP to MC.

The *cisoid* form then isomerizes spontaneously to the thermodynamically stable *transoid* MC form, which is an extended π-conjugated system and absorbs in the visible region. The MC isomer can be converted back to the original SP state either thermally or upon irradiation with visible light. The SP-to-MC interconversion has been investigated for use

in various applications, such as in data recording and optical data storage,[4] sensors,[5-7] microfluidics,[8-9] smart surfaces[10-15] and bioseparation.[16]

The photochromism of SP depends on the polarity of the surrounding medium (solvent or polymer matrix), the solution pH and the presence of ions.[17] Media of low polarity promote the photo-induced isomerization of MC to SP.[18] Moreover, polar media favor the formation of the zwitterionic MC form over the quinoidal isomer.[15] Both of these MC forms exhibit solvatochromism, which is changes in the position and the intensity of their absorption bands induced by variations in the polarity of the surrounding medium. In particular, when the oxygen is in the ionic form the zwitterionic MC exhibits negative solvatochromism upon increasing the polarity of the medium, i.e. a shift of the λ_{max} of MC to shorter wavelengths,[15] accompanied by band broadening and attenuation of the extinction coefficient.[19] However, if the MC oxygen possesses a quinodial character the MC isomer exhibits positive solvatochromism and the λ_{max} is red-shifted.[20] The solution pH also affects the SP-to-MC transformation; low solution pH favors the isomerization of SP to MC and leads to the protonation of the open form, which is accompanied by changes in the absorption spectra of the chromophore, while the SP isomer is recovered in alkaline media.[21-22] The MC form can also bind metal cations, or undergo nucleophilic addition by CN$^-$, which lead to the appearance of blue-shifted MC bands.[5,23-25]

Photochromic copolymers carrying spiropyran side-groups have attracted particular attention lately.[26-30] The chemical linking of the SP moieties can been achieved by two different methods; the covalent attachment of photosensitive dyes to pre-formed polymer chains[31] or the copolymerization of photosensitive compounds carrying polymerizable groups with other vinyl monomers.[32-33] These materials allow to overcome many of the limitations inherent in traditional SP doped polymers such as the phase separation of the colorant and the retardation of the decoloration of the open form.[32,34-35] Matsushima et al. showed that the immobilization of the SP groups onto a polymer backbone suppressed their aggregation and reduced their photodegradation.[36] This is particularly attractive for electronic applications that require high contents of photosensitive compounds and stable performance.[37] Besides, the decoloration rate has been shown to depend on the rigidity, the free volume and the polarity of the polymeric

matrix.[19,38] For example, a low T_g oligomer enhanced the photo-switching rate due to the flexibility of the polymer matrix.[39] At high SP contents the attachment of the photochromic side groups via a long, flexible spacer[40] minimized the retardation of the decoloration which was observed in short spacer systems due to the lack of free volume.[41-42]

The introduction of light-sensitive moieties within responsive polymers has led to the development of sophisticated multi-responsive systems.[26] Spiropyran monomer repeat units have been incorporated within temperature-responsive poly(*N*-isopropylacrylamide) (PNIPAM) chains. The photochromic molecules influenced the phase transition behavior of PNIPAM and reduced its cloud point by more than 10 $^{\circ}$C.[29] On the other hand, PNIPAM-SP microgels were shown to alter their volume phase upon light irradiation.[43] Sumaru et al. reported that the sensitivity of a PNIPAM-*co*-PSP copolymer to light irradiation and temperature changes was dependent on the solution pH.[26] Recently, the photo-induced hydration of the polymer was found to be effective only at low temperatures when the PNIPAM component was sufficiently hydrophilic.[44] This property was applied to develop a colorimetric thermometer based on a PNIPAM-*co*-PSP copolymer, which upon UV irradiation exhibited a continuous bathochromic shift as the temperature increased. The change in the absorption was attributed to the zwitterionic-to-quinodal MC isomerization, induced by the less-polar environment which surrounded the chromophore moieties at higher temperatures.[28]

In this chapter, we report the synthesis of poly[2-(dimethylamino)ethyl methacrylate]-*co*-poly[1',3',3'-trimethyl-6-methacryloyloxy-spiro(2H-1-benzopyran-2,2'-indoline)] (PDMAEMA-*co*-PSP) copolymers that are sensitive to the solvent polarity, temperature, pH and light irradiation. Four different PDMAEMA-*co*-PSP copolymers in which the content of the photosensitive moieties was varied between 1.3 and 10 mol% were prepared by atom transfer radical polymerization (ATRP). A poly(methyl methacrylate)-*co*-PSP (PMMA-*co*-PSP) copolymer containing 19 mol% SP was also synthesized by the same method. The effect of the polarity of the comonomer on the isomerization mechanism of the spiropyran groups was evaluated by comparing the solvatochromic behavior of the PDMAEMA-*co*-PSP and PMMA-*co*-PSP copolymers. To the best of our knowledge, this is the first time that "reverse photochromism" of the

chromophore units, induced by the polarity of the comonomer, is reported. The reversible acid-catalyzed ring-opening process of the photosensitive component of the PDMAEMA-*co*-PSP copolymers in aqueous media was studied. The influence of the copolymer composition and the photo-induced MC-to-SP isomerization on the phase transition temperature of the PDMAEMA-*co*-PSP copolymers was investigated. Finally, the photo-induced decoloration rates of the chromophore moieties of the PDMAEMA-*co*-PSP copolymers were determined in solvents of different polarity. The multi-responsive behavior of the PDMAEMA-*co*-PSP copolymers in addition to their cationic character at low pH, which can induce attractive electrostatic interactions with DNA, enzymes, and polyanionic drugs, are very important and open up new applications of these materials in the areas of chemical and biochemical gates, gene transfer, programmed adsorption of proteins and drug delivery.

2.1.2   *Experimental Section*

Materials.   The monomer, DMAEMA (98%, hydrophilic and ionizable), the ligand, *N,N,N′,N″,N″*-pentamethyldiethylenetriamine (99%, PMDETA), the initiator, ethyl 2-bromoisobutyrate (98%), triethylamine (99%, TEA), the metal salt, copper(I) bromide (99.9%, $Cu^{(I)}Br$) and chloroform (99.8%, $CDCl_3$) were purchased from Aldrich, Germany. The monomer, MMA (99%, hydrophobic), dichloromethane (99.8%, DCM), methacryloyl (97%) and acryloyl (96%) chlorides were purchased from Fluka, Germany. The photochromic spiropyran molecule, 1',3',3'-trimethyl-6-hydroxyspiro(2H-1-benzopyran-2,2'-indoline) (99%, HBPS) was purchased from Acros Organics, Germany and was used without further purification. Toluene (99.7%) and tethahydrofuran (THF, 99.9 %) were purchased from Riedel-de Haën, Germany.

Methods.   The monomers were passed through basic alumina columns to remove inhibitors. The polymerization solvent, THF, was dried being refluxed over potassium for 3 days. All reagents used for the monomer synthesis were stirred over CaH_2, were freshly distilled under vacuum and were kept under a dry nitrogen atmosphere until use. All glassware was dried overnight at 160 °C prior to use.

2.1.2.1 Synthesis of the spirobenzopyran-methacrylate monomer

The synthesis involved an esterification reaction, to produce a spiropyran-based molecule carrying a polymerizable methacrylate moiety. In a typical reaction, HBPS (1.0 g, 3.4 mmol) was transferred in a 250 mL flask and was dried under vacuum for 2 h. Dry dichloromethane (29 mL) was injected in the reaction flask under nitrogen. Next, TEA (1.4 mL, 0.010 mol) was added followed by the dropwise addition of methacryloyl chloride (0.50 mL, 5.2 mmol). The reaction was allowed to proceed for 3 days at RT. The triethylamine hydrochloride salt produced was removed by filtration under nitrogen, while the solvent and the excess amounts of the reagents were eliminated under reduced pressure. The product (1 g, yield: 85%) was dried in a vacuum oven at RT and was characterized by ^{1}H NMR.

2.1.2.2 Polymerizations

A typical polymerization procedure followed for the synthesis of the copolymers is described below (see Scheme 2.1.2).
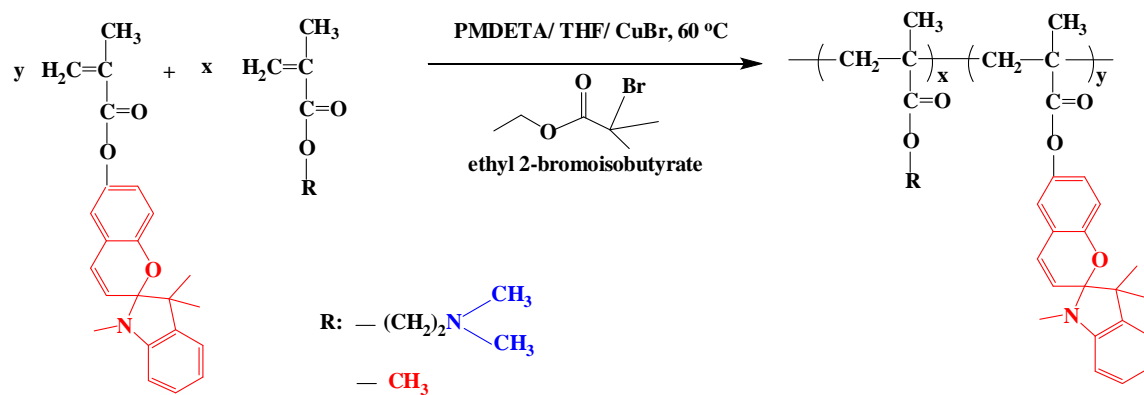
Scheme 2.1.2. Reaction scheme for the ATRP copolymerization of 1',3',3'-trimethyl-6-methacryloyloxy-spiro(2H-1-benzopyran-2,2'-indoline) with DMAEMA and MMA.

The initiator, ethyl 2-bromoisobutyrate (14.7 µL, 9.87×10^{-5} mol), 1',3',3'-trimethyl-6-methacryloyloxy-spiro(2H-1-benzopyran-2,2'-indoline) (0.080 g, 2.21×10^{-4} mol) and DMAEMA (0.147g, 9.35×10^{-4} mol) were transferred in a 100 mL round-bottom flask containing 6 mL dry THF. The reaction was set under a nitrogen atmosphere and subsequently, the ligand PMDETA (124 µL, 5.94×10^{-4} mol) and CuBr (0.0141 g, 9.83 ×

10^{-5} mol) were added under continuous stirring. The polymerization flask was inserted in an oil bath at 60 $^{\circ}$C and the polymerization was allowed to proceed for 24 hrs. The product was isolated by precipitation in hexane and was dried under vacuum at RT. This procedure resulted in a PDMAEMA-*co*-PSP random copolymer containing 10 mol% PSP, with an M_n of around 5,900 g/mol and M_w/M_n equal to 1.56 by gel permeation chromatography (see entry 4, Table 2.1.1) at 84% yield. The other three PDMAEMA-*co*-PSP copolymers were prepared by varying the comonomer ratio at a fixed initiator concentration. A similar procedure was followed for the synthesis of the PMMA-*co*-PSP copolymer which was recovered by precipitation in water.

2.1.2.3 Characterization of the copolymers

Gel Permeation Chromatography (GPC). The molecular weights (MWs) and the molecular weight distributions (MWDs) of the random copolymers were determined by GPC using a mixed-D and a mixed-E column. The mobile phase was THF, delivered at a flow rate of 1 mL min^{-1}. The refractive index signal was measured using a Shodex RI-101 refractive index detector. The calibration curve was based on six narrow MW linear polystyrene standards ranging from 1,310 to 299,000 g $\times$ mol^{-1}.

^{1}H NMR Spectroscopy. The composition of the copolymers was determined by ^{1}H NMR spectroscopy using a 500 MHz Avance Bruker NMR spectrometer. The solvent used was CDCl$_3$ containing tetramethylsilane (TMS) which served as an internal reference. The absolute molecular weight of the PMMA-*co*-PSP copolymer was also determined by ^{1}H NMR spectroscopy.

UV/vis absorption studies. The solvatochromism of the copolymers in a range of solvents of different polarity was monitored by UV/vis spectroscopy. The absorption spectra of 3.3×10^{-2} wt% copolymer solutions in toluene, chloroform, tetrahydrofuran, dichloromethane and water were recorded using a Lambda 25 Perkin-Elmer UV/vis spectrophotometer in the wavelength range 250-850 nm.

The effect of the addition of acid or base on the absorption properties of the PDMAEMA-*co*-PSP3 copolymer in aqueous media was studied. A 1.2×10^{-2} wt% aqueous solution of the photosensitive copolymer was prepared by dissolving the appropriate amount of polymer in Milli-Q water prefiltered through a 0.2 μm syringe

filter. The UV/vis spectra of the aqueous solution were recorded upon the addition of 2.4 μL aliquots of 0.1 M HCl or NaOH solution.

The temperature-induced phase transition behavior of the PDMAEMA-*co*-PSP copolymers was investigated by recording the absorbance of 1 wt% aqueous solutions of the copolymers at 750 nm, while the solution temperature was raised from 25 to 90 ^{o}C at a heating rate of 1 °C/min.

The photo-induced bleaching of the chromophore moieties of the PDMAEMA-*co*-PSP1 copolymer was studied in solvents of different polarity by UV/vis spectroscopy in the wavelength range 250-850 nm. A 5×10^{-2} wt% solution of the copolymer in water and in acetonitrile was prepared and the samples were irradiated with visible light utilizing a Nd:yttrium aluminum garnet (YAG) laser operating at the second harmonic, λ=532 nm (B. M. Industries, Serie 5000). The ~ 100 mJ laser beam was focused in the cuvette to ensure the homogeneous irradiation of the sample. The decoloration rate, k_{obs}, of the chromophore units of the copolymer was calculated by fitting the experimental data to the following equation[45]:

$$\ln(A_t - A_e) = -k_{obs}\, t + \ln(A_o - A_e) \qquad\qquad \text{(eq. 2.1.1)}$$

where A_o, A_t and A_e is the absorbance at the λ_{max} of the MC form at time 0, t and ∞ (taken as the absorbance of the visible irradiation photostationary state), respectively.

2.1.3   Results and Discussion

2.1.3.1 Synthesis of the random copolymers by ATRP

Random copolymers carrying photochromic spiropyran moieties were synthesized by ATRP. A photosensitive molecule exhibiting a singlet excited state was chosen instead of that with a triplet state i.e. nitrospiropyrans, because the latter accelerates the photodegradation process.[46] The polymerizable spiropyran molecule was prepared first The following peaks were identified in the proton nuclear magnetic resonance (^{1}H NMR) spectrum of the synthesized monomer (500 MHz, CDCl$_3$) (see Figure 2.1.1): δ 1.16 (3H, H-3'), 1.31 (3H, H-3'), 2.05 (3H, H-11) 2.73 (3H, H-1'), 5.70 (1H, =CH$_2$, H-9), 5.73 (1H, H-3), 6.31 (1H, =CH$_2$, H-10), 6.52 (1H, H-4), 6.71 (1H, H-7'), 6.79-6.85 (4H, H-5, H-5', H-7, H-8), 7.08 (1H, H-4'), 7.18 (1H, H-6'). The successful synthesis was confirmed by ^{1}H NMR spectroscopy due to the absence of the peak at 4.26 ppm attributed to the –OH

group of the precursor alcohol and the appearance of two new peaks at 5.7 and 6.3 ppm assigned to the protons of the carbon-carbon double bond and a peak at 2.04 ppm which corresponds to the methyl group of the methacryloyl moiety.[47] The peaks attributed to the aromatic protons next to the ester group were also shifted to lower fields following the esterification reaction, and confirmed the synthesis of the monomer.
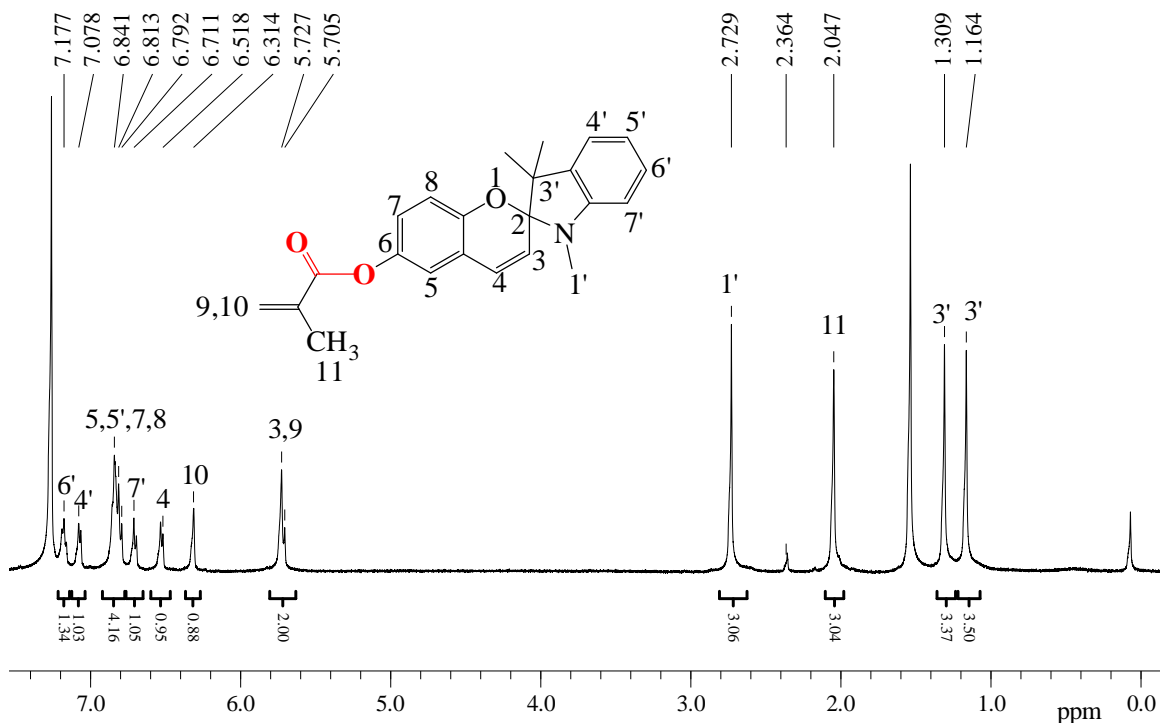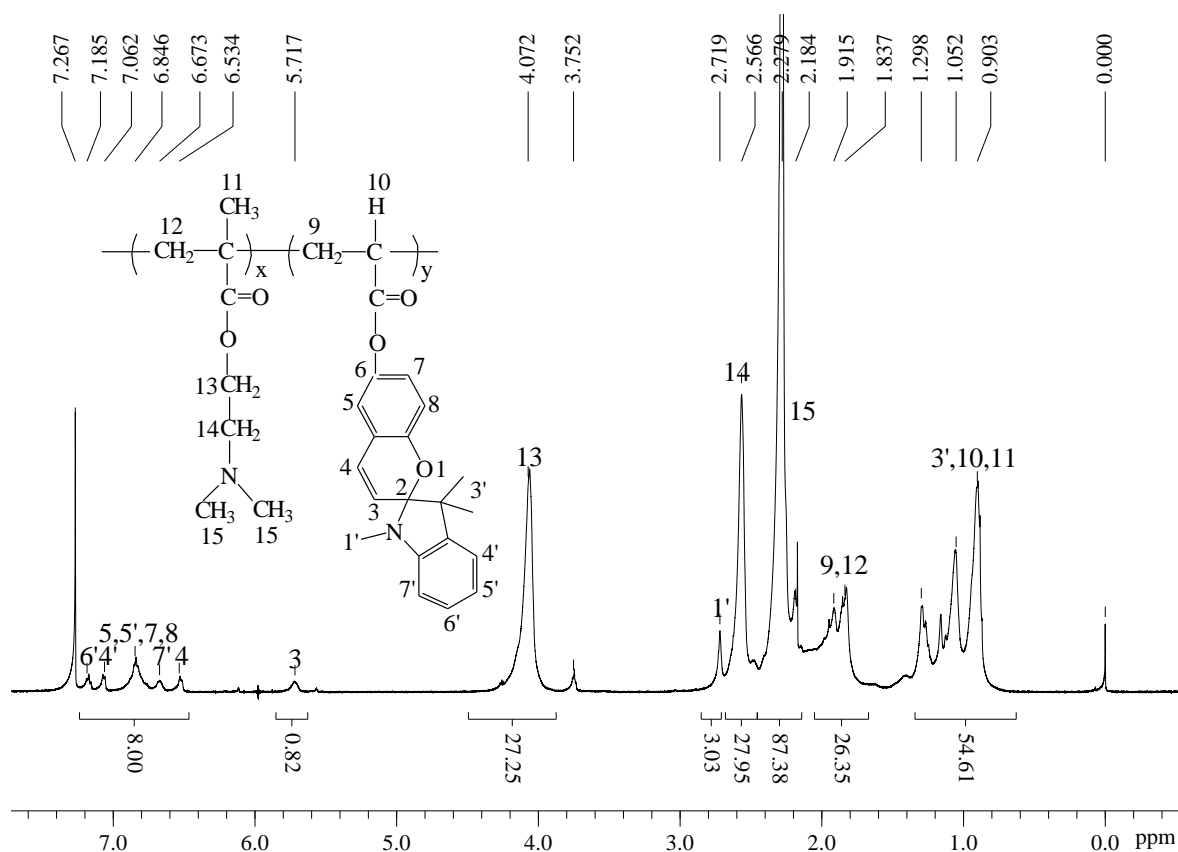

Figure 2.1.1. ^{1}H NMR spectrum (in CDCl$_3$) of the 1',3',3'-trimethyl-6-methacryloyloxy-spiro(2H-1-benzopyran-2,2'-indoline) monomer.

Next, the dye monomer was copolymerized with DMAEMA or MMA by ATRP. Four different copolymers of 1',3',3'-trimethyl-6-methacryloyloxy-spiro(2H-1-benzopyran-2,2'-indoline) with DMAEMA and one with MMA were prepared in THF (see Table 2.1.1). The presence of the peaks due to both monomer repeat units and the significant broadening of the peaks in the ^{1}H NMR spectra of the products (see Figure 2.1.2) confirmed the synthesis of the copolymers.

Table 2.1.1. GPC and ^{1}H NMR characterization data of the spiropyran-based copolymers

Copolymer	GPC results			Composition by ^{1}H NMR (mol% SP)
	M_n	M_w	M_w/M_n	
PDMAEMA-*co*-PSP1	8,900	13,000	1.46	1.3
PDMAEMA-*co*-PSP3	6,600	10,000	1.51	3.0
PDMAEMA-*co*-PSP6	8,300	12,300	1.48	6.0
PDMAEMA-*co*-PSP10	5,900	9,200	1.56	10.0
PMMA-*co*-PSP19	4,200	7,700	1.84	19.0

Figure 2.1.2. ^{1}H NMR spectrum (in CDCl$_3$) of the PDMAEMA-*co*-PSP6 copolymer.

The absolute molecular weight of the PMMA-*co*-PSP copolymer was calculated from ^{1}H NMR spectroscopy by ratioing the peak integrals at 3.59 ppm attributed to the methoxy

protons of the PMMA and at 5.7 ppm due to the proton of the benzopyran phenyl group next to the spiro tetrahedral linkage over that at 4.1 ppm which corresponds to the methylene protons of the initiator. The actual molecular weight of the copolymer was found 1,360 g/mol, which is in good agreement with the theoretical value of 1,840 g/mol, suggesting the "controlled/living" character of the polymerization. However, the actual molecular weights of the PDMAEMA-*co*-PSP copolymers could not be determined by ^{1}H NMR due to the overlap of the peaks attributed to the methylene protons of the initiator and the methylene protons next to the ester group of the DMAEMA monomer repeat units at 3.95-4.35 ppm (see Figure 2.1.2). The apparent molecular weights (M_n's) and the molecular weight distributions (M_w/M_n's, PDIs) of the copolymers were determined by GPC (see Table 2.1.1). The M_n's of the photoresponsive copolymers were found between 4,200 and 8,900 g/mol, while their PDIs ranged between 1.46 and 1.84 which are lower than those reported for spiropyran-based copolymers synthesized by conventional free radical polymerization.[26,48-49] The slightly broader molecular weight distributions of the copolymers, compared to those reported for the controlled polymerization of styrenic and methacrylate monomers,[50-51] are attributed to the low molecular weights of the polymers and the polymerization of highly functional monomers (DMAEMA and SP), and are similar to those reported in the literature for PMMA-*co*-PSP copolymer analogues synthesized by ATRP.[30]

The copolymer composition (see Table 2.1.1) was calculated from the ratio of the peak integrals attributed to the methylene protons next to the ester group of DMAEMA (see Figure 2.1.2, H-13) and the proton of the benzopyran phenyl group next to the spiro tetrahedral linkage (see Figure 2.1.2, H-3), for the PDMAEMA-*co*-PSP copolymers, while the integrals of the peaks corresponding to the methoxy protons of MMA and the benzopyran protons of SP next to the spiro tetrahedral linkage were ratioed to calculate the composition of the PMMA-*co*-PSP copolymer.

2.1.3.2 Solvatochromic behavior of the copolymers

The solvatochromic behavior of the copolymers in solvents of different polarity was examined before irradiation. The polarity of the solvent has been shown to influence the isomerization of the photochromic molecules between the different MC forms and the

thermal fading of the MC isomers to the SP form.[52-53] Figure 2.1.3a shows the UV/vis spectra for five PDMAEMA-*co*-PSP3 copolymer solutions in toluene, chloroform, THF, DCM and water. The absorption band observed in toluene at 558 nm was attributed to the planar zwitterionic MC form.
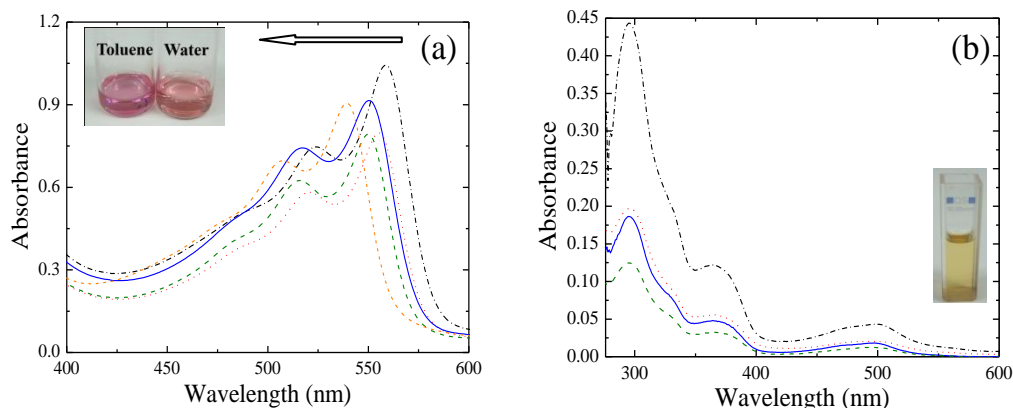
Figure 2.1.3. UV/vis absorption spectra of the PDMAEMA-*co*-PSP3 (a) and PMMA-*co*-PSP (b) copolymers in solvents of different polarity; toluene; (...), chloroform; (…), tetrahydrofuran; (_), dichloromethane; (...) and water (...).

The formation of the colored zwitterionic MC form before irradiation was attributed to the "reverse photochromism", that is the stabilization of the open zwitterionic form of the chromophore in polar media before irradiation, induced by the polar DMAEMA comonomer units.[54-55] Upon increasing the solvent polarity a shift of the MC peak to shorter wavelengths was observed from 558 nm for toluene (SPP scale = 0.655) to 555 nm for chloroform (SPP scale = 0.786), 551 nm for THF (SPP scale = 0.838) and 549 nm for DCM (SPP scale = 0.876), while the lowest value was found for water (539 nm, SPP scale = 0.962). This phenomenon, which is known as "negative" solvatochromism, is related to the stabilization of the planar zwitterionic MC form in the solvent medium and is common in spiropyrans disposing electron-withdrawing groups on the benzopyran moiety, known as pull-type photochromic compounds, such as the molecule used in this study.[20] In polar media, the ground state of the bipolar colored form[56] is stabilized more effectively compared to the excited state ($\mu_{ground} > \mu_{excited}$).[15] This results in a greater energy gap between the two MC states and to a hypsochromic shift of the absorption

bands. A peak with an absorption maximum at 524 nm was also observed in the spectrum in toluene and was attributed to SP-MC and intramolecular MC_n stacks which are of H-type and thus blue-shifted compared to the free MC.[34] These aggregation phenomena are strongly enhanced in systems with high chromophore contents and under conditions which stabilize the planar zwitterionic MC molecules.[57] The H-stacks exhibited a "negative" solvatochromism similar to that of the free MC form, and a blue-shift of the peak was observed upon increasing the polarity of the solvent (524 nm for toluene, 521 nm for chloroform, 517 nm for THF, 515 nm for DCM and 506 for water). The "negative" solvatochromism of the photochromic species of the PDMAEMA-co-PSP3 copolymer upon increasing the polarity of the medium was also observed visually as a small change in the color of the solution from light pink in toluene to light orange in water (see Figure 2.1.3a, inset).

In contrast to the PDMAEMA-co-PSP copolymer, the absorption properties of the PMMA-co-PSP analogue were not influenced by the solvent medium before irradiation (see Figure 2.1.3b). The absorption bands observed in toluene at 296 and 323 nm (shoulder) were attributed to the closed form of the spiropyran molecule. The two halves of the photochromic molecule in the closed form are topologically orthogonal, hence the π-absorption spectrum consists of two localized transitions rather than a single delocalized transition for the molecule as a whole.[58] The former intense peak (296 nm) was attributed to the indoline part and the latter shoulder (323 nm) was assigned to the chromene moiety. However, no peak assigned to the free MC form at 558 nm was observed for this copolymer. This was attributed to the non-polar character of the MMA comonomer which does not stabilize the open MC form and thus favors the "normal photochromism". The very low intensity band at ~500 nm was attributed to the formation of a few H-stacks as discussed above for the PDMAEMA-co-PSP copolymer. However, a new peak at 366 nm was observed attributed to a non-polar MC isomer. It is noted that this peak was not observed for the PDMAEMA-co-PSP copolymers suggesting that the non-polar photoisomer was stabilized by the less polar MMA units. These species showed negligible sensitivity to the polarity of the surrounding medium and the λ_{max} of the peak remained at 366 nm, while a yellow color polymer solution was obtained (see Figure 2.1.3b, inset) for all solvents. The above results suggest that the polarity of the

comonomer affects the solvatochromic properties to the polymer by the selective stabilization of a particular photoisomer. The colored MC form is stabilized by polar comonomers resulting in copolymers which exhibit "reverse photochromism" and "negative solvatochromism", whereas "normal photochromism" is favored by comonomers of lower polarity. The stabilization of specific chromophore isomers by tuning the polarity of the comonomer can be very promising for the development of materials with high specificity in terms of optical properties.

### 2.1.3.3 Acidochromic properties of the spiropyran-based copolymers

The effect of the solution pH on the SP-to-MC isomerization of the chromophore units of the PDMAEMA-*co*-PSP3 copolymer was also investigated. The closed SP form isomerizes to the open MC form and becomes protonated upon the addition of acid leading to the formation of $[MC-OH]^+$ species. A competitive process also takes place, that is the protonation of the closed SP moieties leading to the formation of the positively charged $[SP-NH]^+$ species (see Scheme 2.1.3). Both processes are fully reversible and the closed SP form is recovered upon the addition of base.[22]
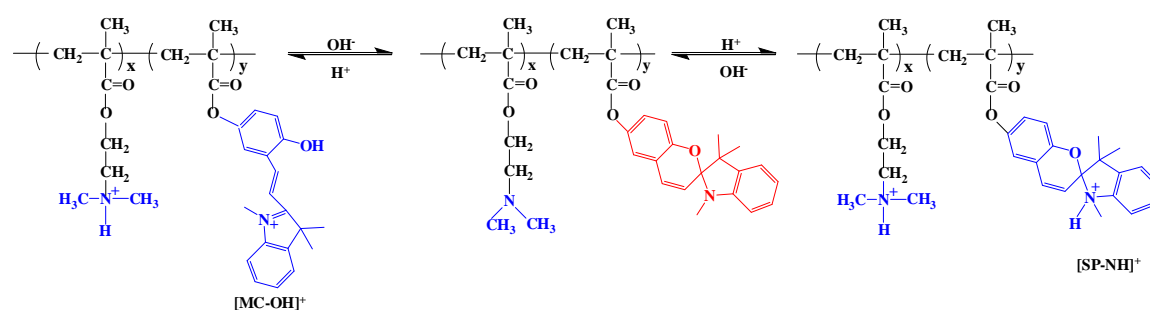
Scheme 2.1.3. Reversible protonation/deprotonation of the PDMAEMA-*co*-PSP copolymers in acidic/basic media.

Figure 2.1.4a shows the absorption spectra of an aqueous solution of the PDMAEMA-*co*-PSP3 copolymer upon the gradual addition of acid. The protonation of both the DMAEMA ($pK_a = 7.0$)[59] and the MC ($pK_a=6-7$)[26] monomer repeat units (see Scheme 2.1.3) was taken into account for the addition of a stoichiometric amount of HCl to fully protonate the copolymer. For low acid contents ($< 9.6\ \mu L$) the intensity of the absorption

band at 296 nm, assigned to the closed SP form, decreased gradually, while the intensity of the absorption peak at 538 nm, which corresponds to the open MC form, increased (see Figure 2.1.4a inset) suggesting the acid-catalysed ring-opening of SP to the MC isomer.[60-61] Further addition of HCl (> 9.6 μL), resulted in the decrease of the intensity of the peak at 538 nm (see Figure 2.1.4a, inset) and the appearance of a new absorption band at 423 nm attributed to the protonated colored MC form.[62-63]
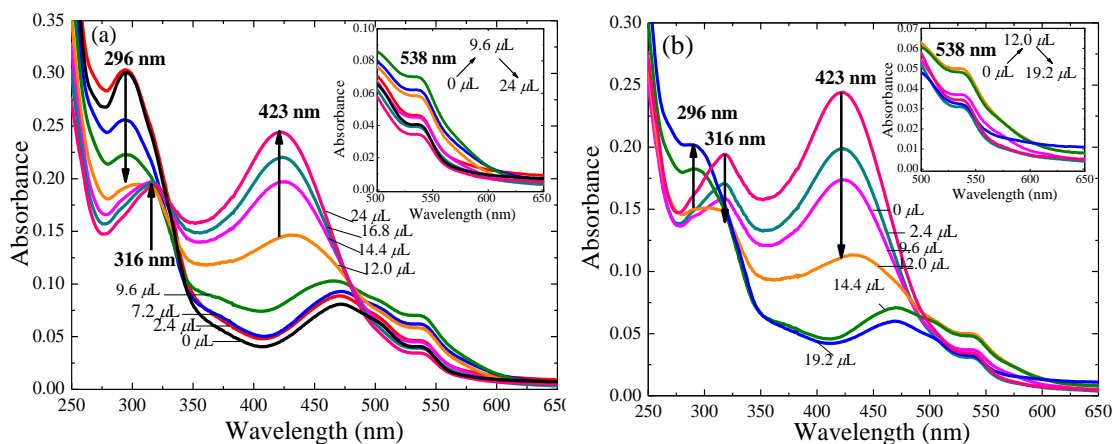
Figure 2.1.4. UV/vis absorption spectra of an aqueous PDMAEMA-*co*-PSP3 copolymer solution upon the addition of acid (HCl) (a) and following the neutralization of (a) with base (NaOH) (b).

This is consistent with the protonation of the open MC species and the formation of the *trans*-[MC-OH]$^+$ form at higher acid concentration. In a competing process, the closed SP species became protonated as evidenced by the appearance of an absorption peak at 316 nm attributed to the protonated closed SP. It is also noted that the intensity of the peak attributed to the MC-MC *H*-type stacks (498 nm), decreased upon the addition of acid. The suppression of aggregate formation via intramolecular interactions in acidic media was attributed to two synergetic effects; the first is the protonation of the phenolate anions of the open MC form which led to a positive net charge on the photochromic side-groups and the second is the protonation of the tertiary amine groups of DMAEMA, both of which resulted in repulsive forces along the polymer chain and prohibited the formation of stacks. The acid-induced process discussed above was fully reversible; addition of base resulted initially, in the deprotonation of the [MC-OH]$^+$ and [SP-NH]$^+$

species, signified by the decrease of the intensity of the peaks at 423 and 316 nm, respectively (see Figure 2.1.4b), while at higher base concentration the closed SP species were recovered due to the MC-to-SP isomerization, leading to an increase of the intensity of the band at 296 nm and a simultaneous decrease of the MC peak at 538 nm (see Figure 2.1.4b inset). Figures 2.1.5a and 2.1.5b summarize the absorbance intensity changes for the PDMAEMA-*co*-PSP3 copolymer solution upon the addition of acid and base, respectively. The concentration of acid in the solution is normalized over the total concentration of ionizable species (DMAEMA and SP) defined as α_{eff} = [HCl]/[DMAEMA+SP monomer units]. α_{eff} represents the theoretical fraction of protonated DMAEMA and SP monomer repeat units, if one assumes that all H^+ from the added HCl protonate the DMAEMA and SP species of the copolymer, and takes values in the range $0 < \alpha_{eff} < 1$ (see Figure 2.1.5a).[64]
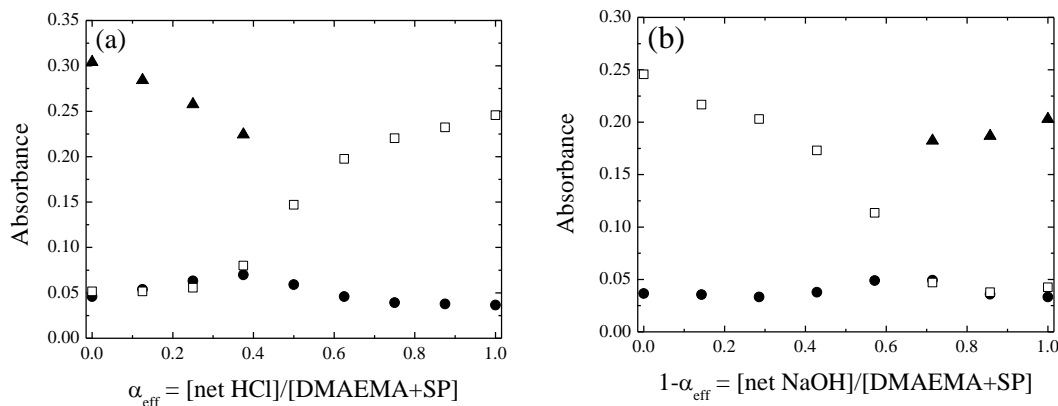
Figure 2.1.5. Absorption intensities of the chromophore species in an aqueous solution of the PDMAEMA-*co*-PSP3 copolymer as a function of the ratio α_{eff} = [HCl]/[DMAEMA+SP monomer units] (a) and $(1-\alpha_{eff})$ = [NaOH]/ [DMAEMA+SP monomer units] (b); SP; (▲), MC; (●), [MC-OH]$^+$; (□).

For the addition of base (see Figure 2.1.5b) $1-\alpha_{eff}$ = [NaOH]/[DMAEMA+SP monomer units] is defined as the fraction of the deprotonated ionizable groups (DMAEMA and SP), assuming that all OH^- from the added NaOH deprotonate the monomer repeat units, and takes values in the range $0 < (1-\alpha_{eff}) < 1$. As shown in Figure 2.1.5a the addition of HCl resulted initially $(0 < \alpha_{eff} < 0.4)$ in a decrease of the SP species accompanied by a

simultaneous increase of the MC moieties due to the acid-induced isomerization of SP to the open MC form. Further addition of acid ($0.4 < \alpha_{eff} < 1$) gave rise to a sharp increase of the intensity of the [MC-OH]$^+$ species accompanied by a decrease of the intensity of the MC units, suggesting the protonation of the latter moieties. On the other hand, Figure 2.1.5b shows that the addition of base resulted in a completely reversible process; first the neutralization of the protonated MC species by NaOH and the formation of the open MC moieties took place for $0 < 1-\alpha_{eff} < 0.6$, followed by the isomerization of MC to the closed SP species in strong alkaline media ($0.6 < 1-\alpha_{eff} < 1$).

The reversible acidochromic behavior of the PDMAEMA-*co*-PSP3 copolymer in water was also observed visually. At high acid concentration the formation of the [MC-OH]$^+$ moieties was evidenced by the appearance of a yellow color attributed to the absorption of the protonated MC form at 423 nm, while upon addition of base the deprotonation of the [MC-OH]$^+$ species resulted in a light red color attributed to a low concentration of remaining MC species in the solution.

2.1.3.4 Temperature-induced phase transition of the PDMAEMA-co-PSP copolymers

PDMAEMA is a well known temperature sensitive polymer which exhibits a LCST in the range between 32 and 46 ^{o}C.[59,65] In this study we investigated the effect of the photosensitive comonomer on the LCST of the PDMAEMA-*co*-PSP copolymers. The phase transition behavior of the four copolymers containing 1.3, 3, 6 and 10 mol% chromophore units was studied in water. Figure 2.1.6 shows the absorbance at 750 nm for the four copolymer solutions in the temperature range 30-90 ^{o}C. The PDMAEMA-*co*-PSP1 copolymer exhibited a LCST of 44 ^{o}C. Furthermore, an increase of the chromophore content of the copolymer to 3 mol% resulted in a 14 ^{o}C increase of the LCST, while for chromophore contents above 6 mol% the LCST was eliminated and the copolymers remained soluble in the aqueous medium over the whole temperature range. The increase in the LCST of the copolymer with the chromophore content was attributed to the hydrophilic open MC form of the photosensitive moieties the presence of which was verified by UV/vis spectroscopy (data not shown). The polar MC species increase the hydrophilicity of the copolymer and hence the LCST of the polymer.[43] Sumaru and coworkers reported that the MC-to-SP conversion in thermally responsive PNIPAM-*co*-

PSP copolymers can become very important in the dark as the temperature increases and can hinder the tuning of the LCST of the copolymers.[26]
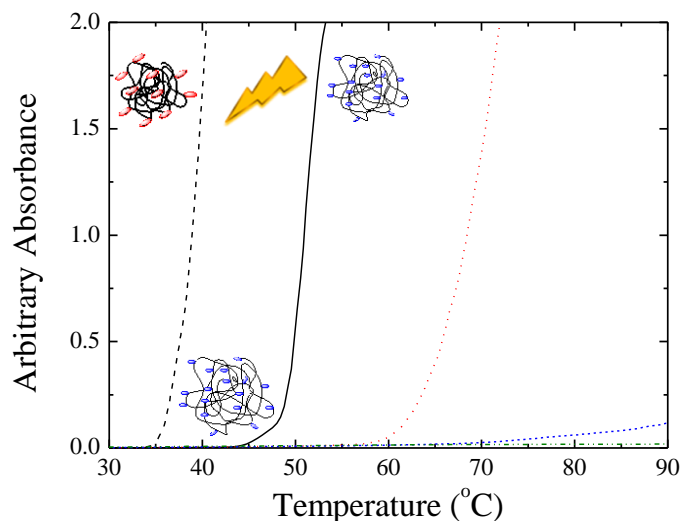

Figure 2.1.6. Turbidimetry *vs* temperature curves obtained for aqueous solutions of the PDMAEMA-*co*-PSP copolymers at neutral pH; PDMAEMA-*co*-PSP1; (–), PDMAEMA-*co*-PSP3; (...), PDMAEMA-*co*-PSP6; (--), PDMAEMA-*co*-PSP10; (....), PDMAEMA-*co*-PSP1 following irradiation with visible light (---). The cloud points were determined from tangents constructed from the turbidimetry curves.

However, the stabilization of the open MC form by the polar DMAEMA comonomer units in the PDMAEMA-*co*-PSP copolymers is believed to retard the thermal fading of the chromophore units in the dark and allow tuning the phase transition temperature of the copolymers. Moreover, irradiation of the PDMAEMA-*co*-PSP1 copolymer with visible light resulted in the significant decrease of the LCST to 34 °C (see Figure 2.1.6) which is lower compared to that reported in the literature for a PDMAEMA homopolymer of similar molecular weight.[59,65] This is attributed to the hybrophobic SP moieties formed upon irradiation of the copolymer with visible light (see discussion below), which increase the hydrophobicity of the copolymer.[43] Therefore, the photo-induced MC-to-SP isomerization of the chromophore units of the copolymers can be conveniently used to tune their phase transition behavior, which could be particularly advantageous for certain applications such as catalyst recovery, waste capture and others.

2.1.3.5 Photoresponsive behavior of the PDMAEMA-co-PSP copolymer

Figure 2.1.7 shows the UV/vis spectra for an aqueous PDMAEMA-*co*-PSP1 copolymer solution upon successive visible light irradiation.
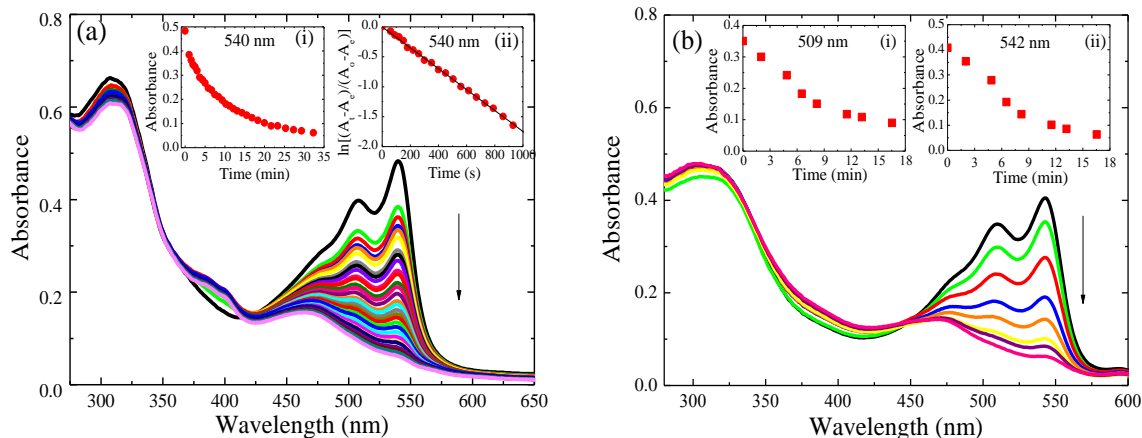
Figure 2.1.7. UV/vis absorption spectra of a PDMAEMA-*co*-PSP1 copolymer in water (a) and in acetonitrile (b) upon successive irradiation with visible light. Inset (a_i) and (b_{ii}) shows the decay of the absorption at the MC maximum as a function of irradiation time and inset (a_{ii}) is the rate constant plot for the first-order decoloration reaction of the photochromic MC moieties of the copolymer. Inset (b_i) shows the decay of the absorption band at 509 nm attributed to the *H*-stacks of the MC moieties.

A gradual decrease of the intensity of the absorption band at 540 nm, attributed to the bipolar MC isomer, was observed due to the isomerization of MC to the colorless SP form. A simultaneous decrease of the intensity of the absorption band at 507 nm, attributed to the *H*-type MC aggregates, was also observed, upon irradiation with visible light, suggesting the effective MC-to-SP isomerization of the MC moieties of the aggregates. Inset (i) in Figure 2.1.7a shows the intensity of the absorption band at 540 nm as a function of irradiation time. After 32 min of irradiation the absorbance at 540 nm reached a plateau suggesting that the chromophores attained a photostationary state.[66] Similar results were obtained upon irradiating a PDMAEMA-*co*-PSP1 copolymer solution in acetonitrile with visible light (see Figure 2.1.7b); the intensity of the absorption bands at 509 nm (see Figure 2.1.7b, inset (i)) and 542 nm (see Figure 2.1.7b, inset (ii)) attributed to the *H*-type MC stacks and the MC isomer, respectively, decreased

progressively with irradiation time. However, the photostationary state was reached only after 17 min of irradiation in acetonitrile (see Figure 2.1.7b insets (i) and (ii)). The rate constants for the visible bleaching, k_{obs}, of the colored MC moieties of the copolymer in water and in acetonitrile were calculated by fitting the experimental data to eq. 2.1.1 (see Figure 2.1.7a, inset ii). k_{obs} in water was calculated to be 1.8×10^{-3} s^{-1}, whereas in acetonitrile the photo-bleaching process exhibited a higher kinetic value of 3.4×10^{-3} s^{-1}. The lower kinetic constant found in water suggests that the ring-closing process is suppressed in the polar aqueous environment (SPP scale = 0.962) due to the effective stabilization of the MC isomer. The latter results in a higher energy barrier for the MC-to-SP isomerization which requires an energerically unfavored rotation around the central double bond of the molecules.[15,18] On the contrary, acetonitrile is a less polar solvent (SPP scale = 0.895) compared to water and thus, the MC form is less effectively stabilized and the MC-to-SP isomerization is energetically favored, resulting in a higher kinetic value. Similar results have been reported in the literature for spiropyran molecules in organic solvents of different polarity.[15]

2.1.4   Conclusions

In this study, we report the synthesis of multi-responsive spiropyran-based copolymers by ATRP. The polarity of the comonomer affected the stabilization of a certain isomer of the photosensitive moieties and thus the "normal" *vs* "reverse" photochromism of the PSP-based copolymers. In particular, DMAEMA, a polar comonomer, induced "reverse photochromism" and stabilized the planar zwitterionic form which exhibited a hypsochromic shift upon increasing the solvent polarity, known as "negative solvatochromism". On the other hand, the less polar MMA comonomer, exhibited "normal" photochromism and stabilized a non-polar photoisomer, before irradiation, which was not affected by the polarity of the solvent. The PDMAEMA-*co*-PSP copolymers also exhibited a reversible pH-induced SP-to-MC isomerization and protonation/deprotonation of the MC form accompanied by a color change of the polymer solution. A strong influence of the copolymer composition and the photo-induced MC-to-SP isomerization of the chromophore moieties on the phase transition behavior of the PDMAEMA-*co*-PSP copolymers was found, with an increase of the LCST with the

117

hydrophilic MC chromophore content and a decrease of the transition temperature following the photo-induced MC-to-SP isomerization of the chromophores due to the hydrophobic character of the SP moieties. Finally, the PDMAEMA-*co*-PSP copolymers exhibited a photo-induced decoloration, upon irradiation with visible light, which was faster in acetonitrile compared to water due to the more effective stabilization of the bipolar MC isomer in polar media. These multi-sensitive polymers create new perspectives for the development of multi-responsive materials for biological and environmental applications.

2.1.5   References

(1)   Minkin, V. *Chem. Rev.* **2004**, *104*, 2751-2776.

(2)   Minkin, V. I. *Theor. Exp. Chem.* **1995**, *31*, 140-152.

(3)   Kobatake, S.; Irie, M. *Annu. Rep. Prog. Chem., Sect. C: Phys. Chem.* **2003**, *99*, 277-313.

(4)   Bobrovsky, Y.; Boiko, N. I.; Shibaev, V. P. *Liq. Cryst.* **2000**, *27*, 57-62.

(5)   Shao, N.; Zhang, Y.; Cheung, S.; Yang, R.; Chan, W.; Mo, T.; Li, K.; Liu, F. *Anal. Chem.* **2005**, *77*, 7294-7303.

(6)   Voloshin, N. A.; Chernyshev, A. V.; Metelitsa, A. V.; Besugliy, S. O.; Voloshina, E. N.; Sadimenko, L. P.; Minkin, V. I. *Arkivoc* **2004**, *xi*, 16-24.

(7)   Radu, A.; Scarmagnani, S.; Byrne, R.; Slater, C.; Lau, K.; Diamond, D. *J. Phys. D: Appl. Phys.* **2007**, *40*, 7238-7244.

(8)   Caprioli, L.; Mele, E.; Angilè, F. E.; Girardo, S.; Athanassiou, A.; Camposeo, A.; Cingolani, R.; Pisignano, D. *Appl. Phys. Lett.* **2007**, *91*, art. no. 113113

(9)   Koide, T.; Takei, G.; Kitamori, T.; Kim, H.-B. *7th international Conference on Miniaturized Chemical and Blochemlcal Analysts Systems, October 5-9, 2003, Squaw Valley, Callfornla USA* **2003**, 769-772.

(10)   Lahann, J.; Langer, R. *MRS Bull.* **2005**, *30*, 185-188.

(11)   Athanassiou, A.; Lygeraki, M.; Pisignano, D.; Lakiotaki, K.; Varda, M.; Mele, E.; Fotakis, C.; Cingolani, R.; Anastasiadis, S. *Langmuir* **2006**, *22*, 2329-2333.

(12)   Mele, E.; Pisignano, D.; Varda, M.; Farsari, M.; Filippidis, G.; Fotakis, C.; Athanassiou, A.; Cingolani, R. *Appl. Phys. Lett.* **2006**, *88*, 203124.

(13)   Wang, S.; Song, Y.; Jiang, L. *J. Photochem. Photobiol. C Photochem. Rev.* **2007**, *8*, 18-29.

(14)   Gras, S.; Mahmud, T.; Rosengarten, G.; Mitchell, A.; Kalantar-Zadeh, K. *ChemPhysChem* **2007**, *8*, 2036-2050.

(15)   Wojtyk, J. T. C.; Wasey, A.; Kazmaier, P. M.; Hoz, S.; Buncel, E. *J. Phys. Chem. A* **2000**, *104*, 9046-9055.

(16)   Nayak, A.; Liu, H.; Belfort, G. *Angew. Chem., Int. Ed.* **2006**, *45*, 4094-4098.

(17)   *Chemistry and Applications of Leuco Dyes*; 1st ed.; Nakazumi, H., Ed.; Springer: New York, 1997.

(18)   Sheng, Y.; Leszczynski, J.; Garcia, A. A.; Rosario, R.; Gust, D.; Springer, J. *J. Phys. Chem. B* **2004**, *108*, 16233-16243.

(19)   Guglielmetti, R. In *Elsevier Science*, 2nd ed.; Dürr, H., Bous-Laurent, H., Eds.; Elsevier Science Publishing House: Amsterdam, 2003; Vol. 40, p 314-466.

(20)   Ortica, F.; Favaro, G. *J. Phys. Chem. B* **2000**, *104*, 12179-12183.

(21)   Raymo, F. M.; Giordani, S. *J. Am. Chem. Soc.* **2001**, *123*, 4651-4652.

(22)   Wojtyk, J. T. C.; Wasey, A.; Xiao, N. N.; Kazmaier, P. M.; Hoz, S.; Yu, C.; Lemieux, R. P.; Buncel, E. *J. Phys. Chem. A* **2007**, *111*, 2511-2516.

(23)   Chibisov, A. K.; Görner, H. *Chem. Phys.* **1998**, *237*, 425-442.

(24)   Wojtyk, J. T. C.; Kazmaier, P. M.; Buncel, E. *Chem. Commun.* **1998**, 1703-1704.

(25)   Shiraishi, Y.; Adachi, K.; Itoh, M.; Hirai, T. *Org. Lett.* **2009**, *11*, 3482-3485.

(26)   Sumaru, K.; Kameda, M.; Kanamori, T.; Shinbo, T. *Macromolecules* **2004**, *37*, 4949-4955.

(27)   Kameda, M.; Sumaru, K.; Kanamori, T.; Shinbo, T. *Langmuir* **2004**, *20*, 9315-9319.

(28)   Shiraishi, Y.; Miyamoto, R.; Hirai, T. *Org. Lett.* **2009**, *11*, 1571-1574.

(29)   Ivanov, A. E.; Eremeev, N. L.; Wahlund, P. O.; Galaev, I. Y.; Mattiasson, B. *Polymer* **2002**, *43*, 3819-3823.

(30)   Piech, M.; Bell, N. S. *Macromolecules* **2006**, *39*, 915-922.

(31)   Labsky, J.; Koropecky, I.; Nespurek, S.; Kalal, J. *Eur. Polym. J.* **1981**, *17*, 309-313.

(32) Hu, A.; Wang, W.-H.; Lee, H.-J. *J. Macromol. Sci., Part A: Pure Appl. Chem.* **1996**, *33*, 803-810.

(33) Davis, D. A.; Hamilton, A.; Yang, J.; Cremar, L. D.; Van Gough, D.; Potisek, S. L.; Ong, M. T.; Braun, P. V.; Martinez, T. J.; White, S. R.; Moore, J. S.; Sottos, N. R. *Nature* **2009**, *459*, 68-72.

(34) Krongauz, V. A.; Goldburt, E. S. *Macromolecules* **1981**, *14*, 1382-1386.

(35) Lukyanov, B. S.; Metelitsa, A. V.; Voloshin, N. A.; Alexeenko, Y.; Lukyanova, M. B.; Vasilyuk, G. T.; Maskevich, S. A.; Mukhanov, E. L. *Int. J. Photoenergy* **2005**, *7*, 17-22.

(36) Matsushima, R.; Nishiyama, M.; Doi, M. *J. Photochem. Photobiol., A* **2001**, *139*, 63-69.

(37) Krongauz, V.; Zelichonok, A.; Buchholz, F.; Ratner, J. *US Patent 5905148* **1999**, *5,322,945*.

(38) Such, G.; Evans, R. A.; Yee, L. H.; Davis, T. P. *J. Macromol. Sci., Polym. Rev. C* **2003**, *43*, 547-579.

(39) Evans, R.; Hanley, T.; Skidmore, M.; Davis, T.; Such, G.; Yee, L.; Ball, G.; Lewis, D. *Nat. Mater.* **2005**, *4*, 249-253.

(40) Krongauz, V. *Mol. Cryst. Liq. Cryst.* **1994**, *246*, 339-346.

(41) Zelichenok, A.; Buchholtz, F.; Yitzchaik, S.; Ratner, J.; Safro, M.; Krongauz, V. *Macromolecules* **1992**, *25*, 3179-3183.

(42) Goldburt, E.; Shvartsman, F.; Fishman, S.; Krongauz, V. *Macromolecules* **1984**, *17*, 1225-1230.

(43) Garcia, A.; Marquez, M.; Cai, T.; Rosario, R.; Hu, Z.; Gust, D.; Hayes, M.; Vail, S.; Park, C.-D. *Langmuir* **2007**, *23*, 224-229.

(44) Edahiro, J. i.; Sumaru, K.; Takagi, T.; Shinbo, T.; Kanamori, T.; Sudoh, M. *Eur. Polym. J.* **2008**, *44*, 300-307.

(45) Drummond, C. J.; Furlong, D. N. *J. Chem. Soc., Faraday Trans.* **1990**, *86*, 3613-3621.

(46) Malkin, Y. N.; Krasieva, T. B.; Kuzmin, V. A. *J. Photochem. Photobiol., A* **1989**, *49*, 75-88.

(47)   Moniruzzaman, M.; Fernando, G. F.; Bellamy, A. J. *Eur. Polym. J.* **2006**, *42*, 1455-1466.

(48)   Bobrovsky, A. Y.; Boiko, N. I.; Shibaev, V. P. *Adv. Mater.* **1999**, *11*, 1025-1028.

(49)   Kim, C.-H.; Kim, D.; Lee, J.; Lee, K.-S. *Mol. Cryst. Liq. Cryst.* **2001**, *370*, 131-134.

(50)   Ohno, K.; Morinaga, T.; Koh, K.; Tsujii, Y.; Fukuda, T. *Macromolecules* **2005**, *38*, 2137-2142.

(51)   Kwak, Y.; Matyjaszewski, K. *Macromolecules* **2008**, *41*, 6627-6635.

(52)   Kojima, K.; Hayashi, N.; Toriumi, M. *J. Photopolym. Sci. Technol.* **1995**, *8*, 47-54.

(53)   Semyakina, G. M.; Samedova, T. G.; Popova, N. I.; Zakhs; Malkin, Y.; Martynova, V. P.; Barachevskii, V. A.; Topchiev, D. A.; Kabanov, V. A. *Russ. Chem. Bull.* **1983**, *32*, 1153-1157.

(54)   Biteau, J.; Chaput, F.; Boilot, J.-P. *J. Phys. Chem.* **1996**, *100*, 9024-9031.

(55)   Schaudel, B.; Guermeur, C.; Sanchez, C.; Nakatani, K.; Delaire, J. A. *J. Mater. Chem.* **1997**, *7*, 61-65.

(56)   Metelitsa, A. V.; Lokshin, V.; Micheau, J. C.; Samat, A.; Guglielmetti, R.; Minkin, V. I. *Phys. Chem. Chem. Phys.* **2002**, *4*, 4340-4345.

(57)   Eckhardt, H.; Bose, A.; Krongauz, V. *Polymer* **1987**, *28*, 1959-1964.

(58)   Tyer, N.; Becker, R. *J. Am. Chem. Soc.* **1970**, *92*, 1289-1294.

(59)   Bütün, V.; Armes, S. P.; Billingham, N. C. *Polymer* **2001**, *42*, 5993-6008.

(60)   Raymo, F.; Giordani, S. *J. Am. Chem. Soc.* **2001**, *123*, 4651-4652.

(61)   Keum, S. R.; Lee, K. B.; Kazmaier, P. M.; Buncel, E. *Tetrahedron Lett.* **1994**, *35*, 1015-1018.

(62)   Zhou, J.; Lia, Y.; Tanga, Y.; Zhaoa, F.; Songa, X.; Lib, E. *J. Photochem. Photobiol., A* **1995**, *90*, 117-123.

(63)   Roxburgh, C. J.; Sammes, P. G. *Dyes Pigm.* **1995**, *27*, 63-69.

(64)   Vamvakaki, M.; Papoutsakis, L.; Katsamanis, V.; Afchoudia, T.; Fragouli, P. G.; Iatrou, H.; Hadjichristidis, N.; Armes, S. P.; Sidorov, S.; Zhirov, D.; Zhirov, V.; Kostylev, M.; Bronstein, L. M.; Anastasiadis, S. H. *Faraday Discuss. Chem. Soc.* **2005**, *128*, 129-147.

(65)   Fournier, D.; Hoogenboom, R.; Thijs, H. M. L.; Paulus, R. M.; Schubert, U. S. *Macromolecules* **2007**, *40*, 915-920.

(66)   Yoshida, T.; Morinaka, A.; Funakoshi, N. *J. Chem. Soc., Chem. Commun.* **1986**, 437-438.

2.2.1 Introduction

The fluorescence resonance energy transfer (FRET) process, has been extensively adopted the last years as a well characterized photophysical tool for the development of chemo-sensors and labels in biology which are non-toxic, biocompatible and functional in the benign aqueous environment. A great breakthrough in this direction was the coupling in a single system of fluorophores and photoresponsive molecules which can remotely interconvert between a non-fluorescent and a fluorescent form, regulating the quenching or enhancement of the fluorophore emission. Spiropyrans (SPs) are widely used for this purpose since they can be remotely and reversibly interconverted between the non-fluorescent SP and the merocyanine (MC) fluorophore without extreme requirements, switching "on" and "off" the FRET process. The majority of the fabricated FRET polymeric systems rely on the self-assembly of amphiphilic block copolymers, carrying donor-acceptor FRET pairs in distinct blocks, into micellar structures. Advances in "controlled/living" polymerization techniques which provide great synthetic flexibility has given a great potential for the synthesis of well-defined block copolymers capable of forming micellar FRET nano-sized scaffolds. The micelles, derived upon the self-assembly of a triblock copolymer carrying a poly(ethylene oxide) (PEO), a poly(styrene) (PS) and a SP-containing block, were employed as scaffolds for the FRET process in which the fluorescent intensity of a hydrophobic nitrobenzoxadiazolyl (NBD) derivative encapsulated in the micellar core was quenched due to the SP-to-MC inteconversion.[1] The length of the PS block, which suppressed the dissociation of the micellar structures upon the photo-induced SP-to-MC isomerization, was a crucial parameter for the FRET efficiency of the system which was improved upon incorporating moderate PS blocks in the triblock even for short PSP blocks.[2] In another study, a three-state switchable multicolor lumineccence system was developed upon incorporating a 4-(2-acryloyloxyethylamino)-7-nitro-2,1,3-benzoxadiazole (NBDAE) donor and two type of acceptor dyes (PSP and rhodamine B) in a single system, since the fluorescent emission of the former could be easily switched "off" and "on" upon varying the light irradiation (UV/vis) and the solution pH, respectively.[3] A similar system, formed via the self-assembly of amphiphilic diblock copolymers containing NBDAE donors and rhodamine B-based acceptor (RhBHA) groups has been used for the development of multifunctional

ratiometric fluorescent temperature sensors or chemosensors for metal ions (mercury and copper) and pH.[4] The detection of mercury, has been also achieved by monitoring the quenching of the emission intensity of a fluorescein derivative (donor) incorporated within the hydrophobic core of PEO-*b*-PS micelles, when the spirolactam-rhodamine derivative (acceptor) located at the micelle core/corona interface underwent a ring–opening reaction stimulated by mercury cations.[5] To the best of our knowledge, only few examples of polymers, non-assembled into micellar structures, have served as FRET scaffolds among which is a SP-polythiophene conjugate. This system exhibited FRET in THF since the polythiophene moieties serve as donors and transfer energy to the MC fluorophores derived upon the photo-induced isomerization of the non-fluorescent SP groups. Based on that property, these polymers were used for the detection of cyanide anions in the presence of which the FRET process was suppressed.[6]

Herein, we report the synthesis of a photoresponsive PDMAEMA-*co*-PSPMA random copolymer by atom transfer radical polymerization (ATRP). The photochromic and fluorescent properties of the copolymer can be remotely modulated using a light trigger of specific wavelength. The SP moieties of the random copolymer, upon stimulation with UV light, are isomerized to three bipolar species, a non-planar X isomer and two planar MC species, consisting donor-acceptor FRET pairs. The SP interconversion can be employed to modulate the fluorescence of the X fluorophores; their emission intensity is quenched when the photochromic molecules adopt their MC state, while the FRET is switched "off" upon the thermal recovery of the non-fluorescent SP isomer. The random distribution of the donor and acceptor species, which are in close proximity due to the association of the polymer in solution in addition to the adequate spectral overlap of the donor emission and the acceptor absorption bands, promotes the efficient energy transfer from the X to the MC photo-isomers. The advantages of this copolymer as FRET-based nano-sized scaffold rely on its function in the aqueous medium, the controlled quantity of chromophores introduced in the system, and the stabilization of the MC isomers by the polar microenvironment enabling adequate fading rates of the isomers to allow the read-out process. To the best of our knowledge, the development of a nano-sized FRET system based on a random copolymer carrying donor-acceptor pairs derived upon the photostimulation of a single parent molecule, is

unprecedented. The novelty of the present system opens new opportunities for the development of chemo- and biological-sensors.

2.2.2 Experimental Section

Materials. The monomers, 2-(dimethylamino)ethyl methacrylate (DMAEMA) and methacrylic acid (MAA), the ligands, 1,1,4,7,10,10-hexamethyltriethylenetetramine (HMTETA) and 4,4′-dinonyl-2,2′-dipyridyl (dNbpy), the initiator, ethyl 2-bromoisobutyrate (2-(EiB)Br), the metal salt, copper(I) chloride ($Cu^{(I)}Cl$), triethylamine (TEA), chloroform ($CDCl_3$), deuterium oxide (D_2O), 2,3,3-trimethyl-3H-indole, 2-bromoethanol, 2-hydroxy-5-nitrobenzaldehyde, neutral and basic alumina (Al_2O_3), dicyclohexylcarbodiimide (DCC) and 4-dimethylaminopyridine (DMAP) were purchased from Aldrich, Germany. The salt magnesium sulfate ($MgSO_4$), potassium hydroxide and silica gel were purchased from Fluka, Germany. The solvents, dichloromethane (DCM), diethyl ether, ethanol, methanol and petroleum ether were purchased from Fischer scientific, Germany. Chloroform ($CHCl_3$) was purchased from Acros Organics, Belgium, acetonitrile from Panreac, Spain and tetrahydrofuran (THF) from Labscan, Ireland.

Methods. DMAEMA was passed through a basic alumina column to remove the inhibitors before use. All the solvents were stirred over CaH_2, were freshly distilled under vacuum and were kept under a dry nitrogen atmosphere until use. All glassware was dried overnight at 160 °C prior to use. All other reagents were used as received.

### 2.2.2.1 Synthesis of 2-(3',3'-Dimethyl-6-nitro-3'H-spiro[chromene-2,3'-indol]-1'-yl)-ethanol (SP-OH)[7]

1-(2-hydroxyethyl)-2,3,3-trimethyl-3H-indolium bromide (1). In a two-necked flask bearing a side arm and equipped with a condenser, a mixture of 2,3,3-trimethyl-3H-indole (8.9 g, 0.056 mol) and 2-bromoethanol (8.75 g, 0.07 mol) in acetonitrile (75 mL) was refluxed at 75 °C for 50 h under an inert nitrogen atmosphere (Scheme 2.2.1). Next, the reaction mixture was cooled down to RT and the solvent was removed under reduced pressure to obtain a dark red solid. The crude solid product was suspended via sonication and underwent several washing cycles with hexane to remove the unreacted reagents. It

was next isolated via filtration and dried under reduced pressure. The dark pink solid, still containing traces of the initial reactants, was then recrystallized several times from chloroform to afford 13.6 g of the purified pink product in 86% yield which was further characterized by ^{1}H NMR spectroscopy in D_2O.
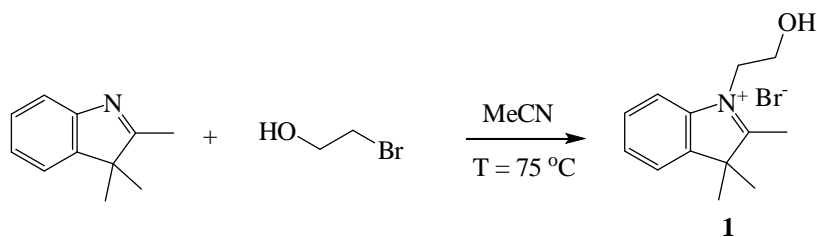

Scheme 2.2.1. Reaction scheme for the synthesis of 1-(2-hydroxyethyl)-2,3,3-trimethyl-3*H*-indolium bromide (1).

9,9,9α-Trimethyl-2,3,9,9α-tetrahydro-oxazolo[3,2-α]indole (2). The 1-(2-hydroxyethyl)-2,3,3-trimethyl-3*H*-indolium bromide (13.6 g, 0.047 mol) was allowed to dissolve in 235 mL water, overnight. The red aqueous solution of compound 1 (Figure 2.2.1) was then reacted with potassium hydroxide (4.2 g, 0.075 mol) for 4 h at RT under continuous stirring (Scheme 2.2.2) to form a yellow oily product which was phase separated in the aqueous medium (Figure 2.2.1). The reaction mixture was then extracted with diethylether (4 × 90 mL), the volume of the organic phase was reduced under reduced pressure and stirred over anhydrous magnesium sulfate to remove water traces. Next, the solution was passed through a 0.2 μm syringe filter to remove the salt and the solvent was evaporated to afford the dry cyclic indoline product (9.5 g) as a yellow oil in 99% yield which was characterized by ^{1}H and ^{13}C NMR spectroscopy in CDCl$_3$.
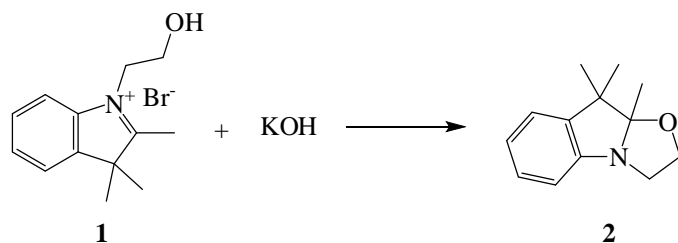
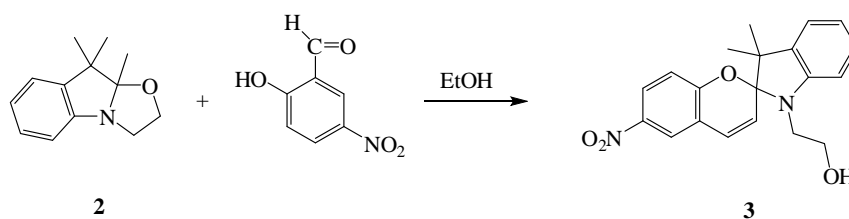**Scheme 2.2.2**. Reaction scheme for the synthesis of 9,9,9α-trimethyl-2,3,9,9α-tetrahydro-oxazolo[3,2-α]indole (2).
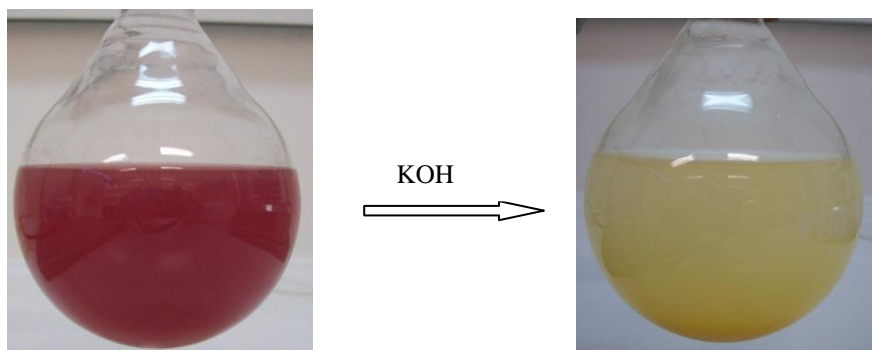
Figure 2.2.1. The red aqueous solution of compound 1 (left) upon reaction with KOH in water forms an oily, cyclic product (2) which phase separated in the aqueous medium (right).

2-(3',3'-Dimethyl-6-nitro-3'H-spiro[chromene-2,2'-indol]-1'-yl)-ethanol (SP-OH) (3)

The procedure followed for the synthesis of the nitro-substituted photochromic spiropyran molecule, consisting of an indoline and a benzopyran ring connected to a tetrahedral carbon center, involved the condensation of an indoline molecule (2) with hydroxynitrobenzaldehyde (Scheme 2.2.3) in ethanolic media according to the literature.[7] In a three-neck flask equipped with a condenser, a solution of 9,9,9α-trimethyl-2,3,9,9α-tetradydro-oxazolo[3,2-α]indole (9.5 g, 0.047 mol) in EtOH (100 mL) was prepared and heated at 40 $^{\circ}$C under nitrogen. Next, 2-hydroxy-5-nitrobenzaldehyde (9.3 g, 0.056 mol) was added under continuous stirring and the reaction mixture was refluxed at 70 $^{\circ}$C for 30 min, at 80 $^{\circ}$C for 1 hour and finally at 90 $^{\circ}$C for 3 hours. The reaction mixture was then cooled down to RT and the product was isolated via filtration. The resulting dark purple solid was further washed with EtOH and dried under reduced pressure to isolate the final product (8.1 g) in 64 % yield which was further characterized by ^{1}H and ^{13}C NMR spectroscopy in CDCl$_3$.
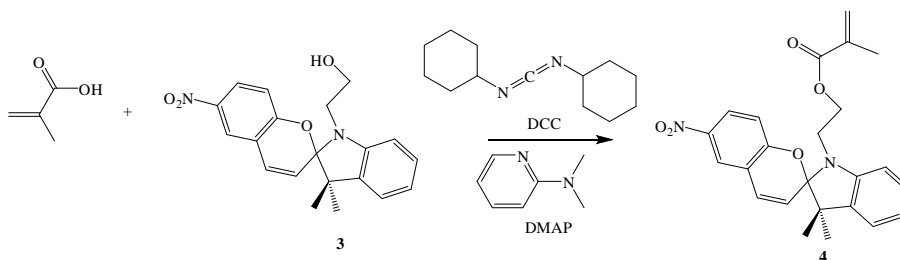
Mechanism
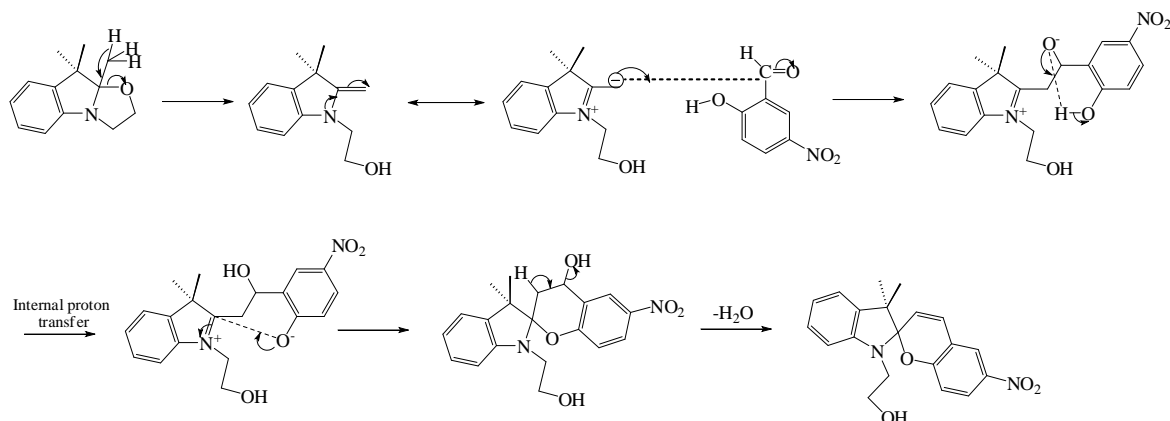
Scheme 2.2.3. Reaction scheme and mechanism for the synthesis of 2-(3',3'-dimethyl-6-nitro-3'H-spiro[chromene-2,2'-indol]-1'-yl)-ethanol (3).
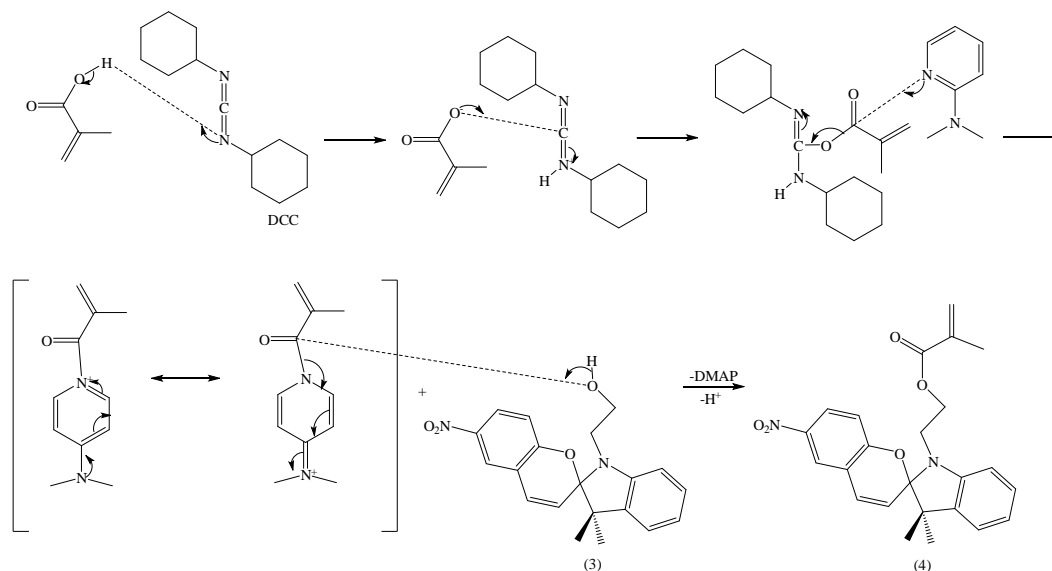
2.2.2.2 Synthesis of the 1´-(2-methacryloxyethyl)-3´,3´-dimethyl-6-nitrospiro-(2H-1-benzopyran-2,2´-indoline) monomer (SPMA) (4).

The spiropyran monomer, SPMA, was synthesized via a Steglich esterification reaction (Scheme 2.2.4).[8] A solution of dicyclohexylcarbodiimide (DCC) (5.83g, 0.028 mol) and methacrylic acid (MAA) (2.2 mL, 0.026 mol) in dry dichloromethane (DCM) (150 mL) was cooled to 0 $^{\circ}$C while stirring under an inert N_2 atmosphere to form an *O*-acylisourea intermediate (Scheme 2.2.4). Next, a catalytic amount of 4-dimethylaminopyridine (DMAP), which acts as a transfer reagent and react with *O*-acylisourea forming an "active" ester, was transferred in the reaction mixture and was further reacted with the photosensitive SP alcohol (3) (6.96g, 0.020 mol) to obtain the final ester. After heating to RT the reaction was allowed to proceed for 2 days. The crude product was isolated under reduced pressure using a rotary evaporator, purified via column chromatography (silica gel, petroleum ether/CH_2Cl_2 95:5, v/v) and crystallized from methanol to afford 5.2 g (0.012 mol) of light green crystals (Figure 2.2.2) in 63% yield which was further characterized by ^{1}H and ^{13}C NMR spectroscopy in $CDCl_3$. Due to SP-to-MC ring-opening of the molecules upon interaction with acidic silica,[9] the silica column was first packed with the same solvent mixture used for the molecule elution in the presence of 7% triethylamine (TEA) to reduce the acidity of the packing material. The chromophore that interacted with the silica was retrieved upon passing pure methanol through the column

(Figure 2.2.3). The direct reaction of SP-OH (3) with methacryloyl chloride for the synthesis of the spiropyran monomer results in low yields according to the literature[10-11] while our previous efforts has also led to a mixture of the product with a chromophore carrying two methacrylate moieties (data not shown) due to the ring-opening reaction of the SP molecule.
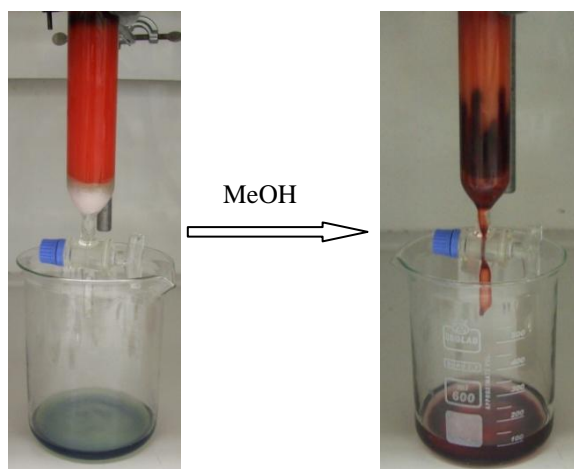

Mechanism

Scheme 2.2.4. Reaction scheme for the synthesis of 1´-(2-methacryloxyethyl)-3´,3´-dimethyl-6-nitrospiro-(2H-1-benzopyran-2,2´-indoline) (4)(SPMA).

Figure 2.2.2. Light-green crystals of the SPMA monomer after purification by column chromatography and crystallization from MeOH.

Figure 2.2.3. The green-colored SPMA after column chromatography is isolated in the mobile phase (left), while the fraction of the molecule adsorbed on the silica (red color) is retrieved upon treating the silica gel with MeOH (right).

2.2.2.3 *Polymerizations.*

PDMAEMA homopolymers.

In a typical solvent-free polymerization, DMAEMA (74.6 g, 0.48 mol), the initiator, ethyl 2-bromoisobutyrate (2-(EiB)Br) (110 μL, 7.42×10^{-4} mol), the ligand, 1,1,4,7,10,10-hexamethyltriethylenetetramine (HMTETA) (404 μL, 1.48×10^{-3} mol) and the metal salt, copper(I) chloride (CuCl) (0.073 g, 7.42×10^{-4} mol) were transferred in the reaction flask under continuous stirring and a dry nitrogen flow (Scheme 2.2.5). The reaction mixture was degassed by five freeze-pump-thaw cycles and the reaction was allowed to proceed at RT until almost complete monomer consumption. Samples were withdrawn from the polymerization flask at various time intervals during the reaction, were exposed to air to quench the reaction and were characterized by ^{1}H NMR spectroscopy and gel permeation chromatography (GPC) to determine the monomer conversion and the molecular weight and molecular weight distribution of the synthesized polymers, respectively. The samples for GPC characterization were immediately frozen with liquid nitrogen, solubilized in THF and precipitated in hexane to be purified from the excess monomer and the ligand in order to avoid chain propagation that takes place even at low temperature in the fridge. The PDMAEMA homopolymers

were purified from copper traces by solubilization in THF and passing through a neutral Al_2O_3 column.
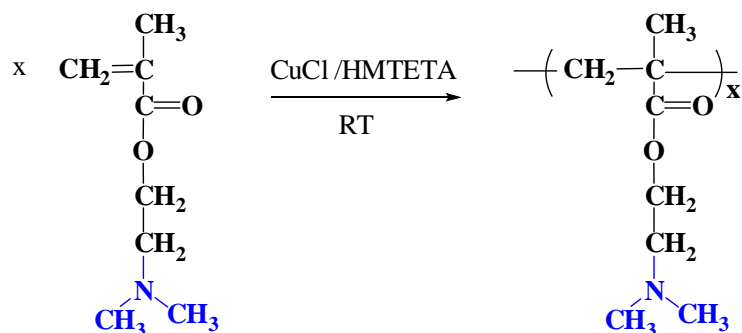
Scheme 2.2.5. Synthetic procedure followed for the synthesis of the PDMAEMA homopolymers in bulk.
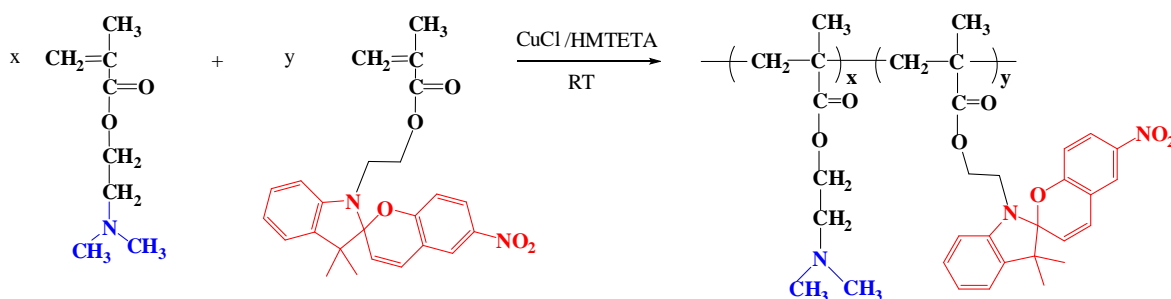

PDMAEMA-b-PSPMA.

A PDMAEMA homopolymer was synthesized and purified following the procedure described above and utilizing DMAEMA (10 g, 0.064 mol), 2-(EiB)Br (94.8 μL, 6.30 $\times$ 10^{-4} mol), HMTETA (346 μL, 1.27 $\times$ 10^{-3} mol) and CuCl (0.063 g, 6.30 $\times$ 10^{-4} mol). Next, the PDMAEMA homopolymer was freeze-dried from benzene to remove any traces of moisture. For the synthesis of the block copolymer a procedure similar to that reported in the literature was followed;[24] 4,4′-Dinonyl-2,2′-dipyridyl (dNbpy) (0.11 g, 2.66 $\times$ 10^{-4} mol), SPMA (0.15 g, 3.56 $\times$ 10^{-4} mol), freeze-dried PDMAEMA (0.2 g, 1.33 $\times$ 10^{-5} mol, M_n = 15370 g/mol and PDI = 1.23), CuCl (0.013 g, 1.33 $\times$ 10^{-4} mol) and anisole (1.4 mL) were transferred in a round bottom flask equipped with a stirrer bar under a dry nitrogen flow (Scheme 2.2.6). Oxygen was removed by five freeze-pump-thaw cycles and the reaction was allowed to proceed at 70 ^{o}C for 50 h. The reaction mixture was then cooled down to RT, opened to air and the product was purified from the non-reacted monomer and metal catalyst by precipitation in hexane. Copper traces were removed by passing a THF solution of the product through a basic Al_2O_3 column.
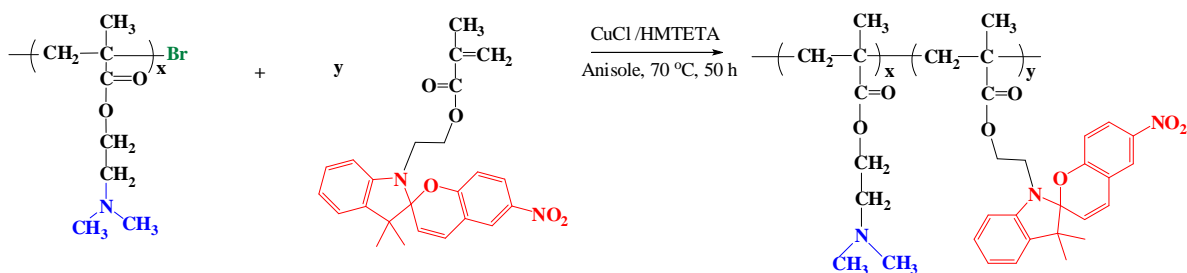
Scheme 2.2.6. Synthetic procedure followed for the synthesis of the PDMAEMA-*b*-PSPMA block copolymers.

PDMAEMA-co-PSPMA.

In a typical solvent-free polymerization, the crystals of the SPMA monomer (0.42g, 9.98 $\times$ 10^{-4} mol) were dissolved in DMAEMA (3.00g, 0.019 mol) under continuous stirring. Next, the initiator, ethyl 2-bromoisobutyrate (2-(EiB)Br) (7.2 μL, 4.85 $\times$ 10^{-5} mol), the ligand, 1,1,4,7,10,10-hexamethyltriethylenetetramine (HMTETA) (26.10 μL, 9.59 $\times$ 10^{-5} mol) and the metal salt, copper(I) chloride (CuCl) (0.005g, 5.05 $\times$ 10^{-5} mol) were transferred in the reaction flask under a dry nitrogen flow (Scheme 2.2.7). The reaction mixture was degassed by five freeze-pump-thaw cycles and the reaction was allowed to proceed at RT until the almost complete consumption of the two comonomers. The polymerization mixture was then exposed to air and the product dissolved in THF while the copolymer was isolated, free of ligand and monomer traces, by precipitation in hexane. The product was further dissolved in THF, passed through an Al_2O_3 column to remove copper traces and characterized by ^{1}H NMR spectroscopy and gel permeation chromatography (GPC).

Scheme 2.2.7. Schematic representation of the procedure followed for the preparation of the PDMAEMA-*co*-PSPMA random copolymer.

2.2.2.4 Characterization of the random copolymers

Gel Permeation Chromatography (GPC). The molecular weight (MW) and molecular weight distribution (MWD) of the random copolymers were determined by gel permeation chromatography (GPC) (Thermo Finnigan). The instrument was equipped with two PL mixed-D and mixed-E columns operating at an oven temperature of 40 $^{\circ}$C. THF was used as the eluent at a flow rate of 1 mL min^{-1}. The refractive index signal was measured using a Shodex RI-101 refractive index detector. A series of narrow MWD linear poly(methyl methacrylate) standards ranging from 850 to 342,900 g × mol^{-1} were used for the GPC calibration.

^{1}H NMR Spectroscopy. The composition of the random copolymers in the two comonomers was calculated by ^{1}H NMR spectroscopy using a 300 MHz Avance Bruker NMR spectrometer. CDCl$_3$ was used as the solvent and tetramethylsilane (TMS) served as the internal reference for the ^{1}H NMR measurements.

Dynamic light scattering (DLS). The hydrodynamic diameter (D_h) of the random PDMAEMA-co-PSPMA copolymer was determined by DLS using a 3D LS Spectrometer from LS Instrument with a HeNe laser operating at 632.8 nm at scattering angles 30°, 50°, 70°, 90°, 110° and 130°. The average particle sizes were obtained from the intensity autocorrelation functions by KWW analysis.

UV/vis absorption studies. The photo-regulated SP-to-MC isomerization of the chromophores units of the PDMAEMA-*co*-PSPMA random copolymer and the ring-closure isomerisation of the MC isomers to the parent SP species as a function of time was studied in water using a Lambda 950 Perkin-Elmer UV/vis spectrophotometer in the wavelength range 200-850 nm. The absorption spectrum of an aqueous 1.2 × 10^{-2} wt % solution of the PDMAEMA-*co*-PSPMA copolymer was recorded upon irradiation with UV light utilizing a Spectroline hand-held UV lamp operating at 365 nm (8 watt) for 49 s. The kinetic rate constants of the thermal fading process of the photoisomers were determined by collecting the absorption spectra of the random copolymer at various time intervals while kept in the instrument's chamber at RT.

The acidochromic properties of the PDMAEMA-*co*-PSPMA random copolymer were studied by monitoring the changes in the UV/vis absorption spectrum of aqueous

6.4×10^{-2} wt% solution of the copolymer upon the addition of 4-50 μL aliquots of 0.1 and 1 M HCl.

Fluorescent Measurements. The FRET process was studied by recording the fluorescence emission spectra of 6.8×10^{-2} wt% aqueous solution of the PDMAEMA-*co*-PSPMA random copolymer before and after illumination with UV light, using a Jobin-Yvon / Horiba Fluoromax-P scanning spectrofluorometer (excitation at 521 nm with a Xenon arc lamp). The slit widths were set at 1 nm for excitation and 5 nm for emission. The kinetic rate constants of the MC bleaching process in dark were calculated by monitoring the emission spectra of the random copolymer kept in the instrument's chamber at RT at various time intervals during the MC thermal relaxation.

2.2.3 Results and Discussion

2.2.3.1 Synthesis of the SP-OH and SPMA molecules.

The spiropyran alcohol (SP-OH) was synthesized in three steps starting from the commercially available 2,3,3-trimethyl-3*H*-indole. Alkylation of 2,3,3-trimethyl-3*H*-indole with bromoethanol derived the salt (1) in high yield, which treatment if the latter with KOH afforded the oxazole derivative (2). The method followed for the synthesis of the spiropyran molecule is similar to that employed in the classical paper of Wizinger where the methylene bases of nitrogen heterocycles (Fisher bases) were boiled with *o*-hydroxy aromatic aldehydes in suitable solvents (most often in alcohols). In our case, the oxazole derivative (2) was refluxed with 2-hydroxy-5-nitrobenzaldehyde in ethanol for several hours to obtain the nitro-substituted chromophore (3). The progress of the reaction was monitored by recording the ^{1}H and ^{13}C NMR spectra of the products, at various time intervals. The ^{1}H NMR spectra of the commercially available starting materials were also recorded and compared to that of the products.

The ^{1}H NMR spectrum of 2-bromoethanol exhibits the following two peaks: (300 MHz, CDCl$_3$) δ 3.52-3.55 (1H, H-1), 3.89-3.93 (2H, H-2) (see Appendix, Figure 1) while the ^{1}H NMR spectrum of the 2,3,3-trimethyl-3H-indole precursor shows five bands: (300 MHz, CDCl$_3$) δ 1.32 (6H, H-6), 2.28 (3H, H-5), 7.19-7.21 (1H, H-3), 7.26-7.32 (2H, H-2, H-4), 7.52-7.54 (1H, H-1) (see Appendix, Figure 2). Upon refluxing the two materials in acetonitrile for several hours under an inert atmosphere and after the purification of the

reaction product, 1-(2-hydroxyethyl)-2,3,3-trimethyl-3H-indolium bromide (1), its ^{1}H NMR spectrum exhibited six signals assigned below: (300 MHz, D_2O) δ 1.62 (6H, H-6), 2.88 (3H, H-5), 4.13-4.16 (2H, H-7), 4.67-4.71 (2H, H-8), 7.65-7.68 (2H, H-1, H-2), 7.77-7.82 (2H, H-3, H-4) (Figure 2.2.4). The appearance of the two signals at 4.13-4.16 and 4.67-4.71 ppm, attributed to the methylene protons of the attached hydroxyethyl moiety, verified the successful alkylation of the indoline molecule.
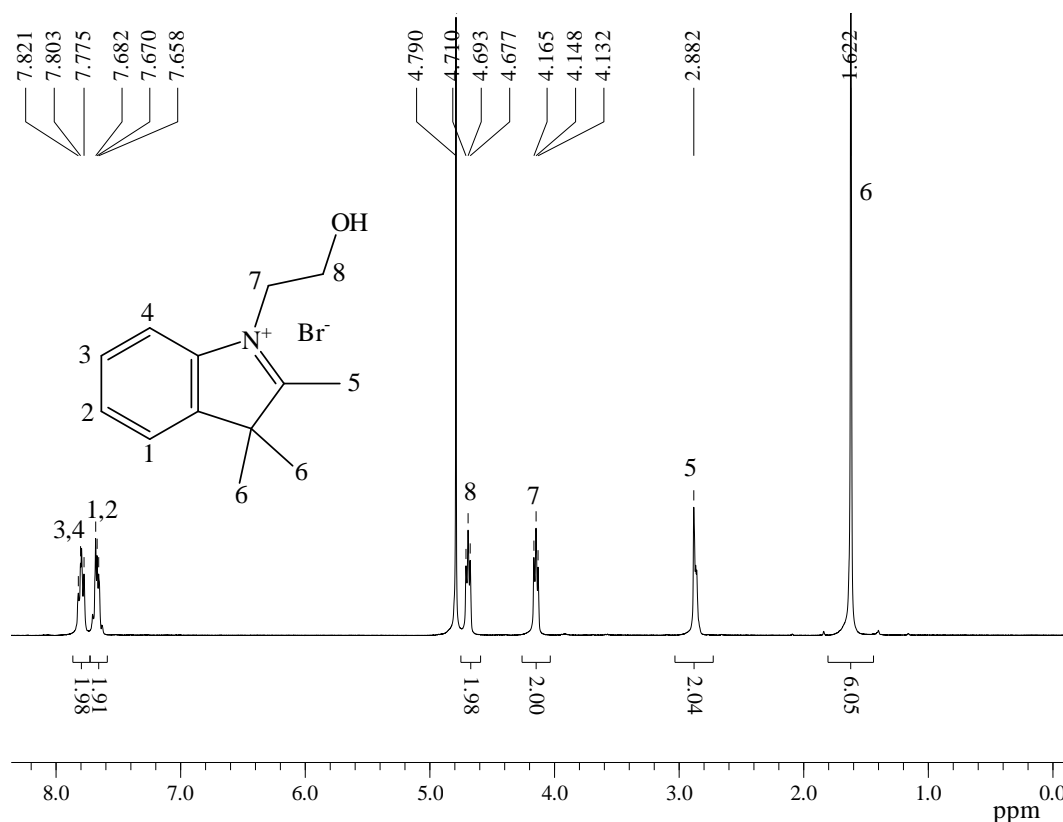

Figure 2.2.4. ^{1}H NMR spectrum of 1-(2-hydroxyethyl)-2,3,3-trimethyl-3H-indolium bromide

The reaction of 1-(2-hydroxyethyl)-2,3,3-trimethyl-3*H*-indolium bromide with KOH and the formation of the cyclic product 9,9,9α-trimethyl-2,3,9,9α-tethadydro-oxazolo[3,2-α]indole had a prominent effect on the ^{1}H NMR chemical shifts of the former molecule as shown in the ^{1}H NMR spectrum of the product (300 MHz, $CDCl_3$) δ 1.18 (3H, H-5), 1.39 (3H, H-6), 1.43 (3H, H-6'), 3.47-3.62 (2H, H-7), 3.67-3.86 (2H, H-8), 6.74-6.77 (1H, H-4), 6.89-6.94 (1H, H-2), 7.06-7.09 (1H, H-1) and 7.11-7.16 (1H, H-3) (Figure 2.2.5). The

H-5 of (1) resonates 1.7 ppm upfield upon the formation of the oxazole derivative (2) while the methyl protons H-6 of (1) observed at 1.62 ppm are splitted to two distinct singlets H-6 and H-6' which are shifted upfiled to 1.39 and 1.42 ppm, respectively, indicating that the formation of the five-membered ring imposes a different environment to the two methyl groups. This effect is also implied by the appearance of two complex multiplets for the two pairs of methylene protons, H-7 and H-8 which are also shifted downfield, by about 0.7 and 1 ppm, respectively. A similar trend was also observed for the aromatic protons of (2) which resonate upfield compared to those of (1). The characteristic chemical shifts of the carbons for the oxazole molecule (Figure 2.2.6) were also assigned in its ^{13}C NMR spectrum (300 MHz, CDCl$_3$) δ 17.60 (1C, C-8), 20.81 (1C, C-8'), 28.09 (1C, C-9), 46.96 (1C, C-7), 50.10 (1C, C-12), 62.98 (1C, C-11), 108.97 (1C, C-10) 111.96 (1C, C-4), 121.16 (1C, C-2), 122.39 (1C, C-1), 127.48 (1C, C-3), 140.02 (1C, C-6), 150.54 (1C, C-5) and verify the successful synthesis of the cyclic oxazole product.
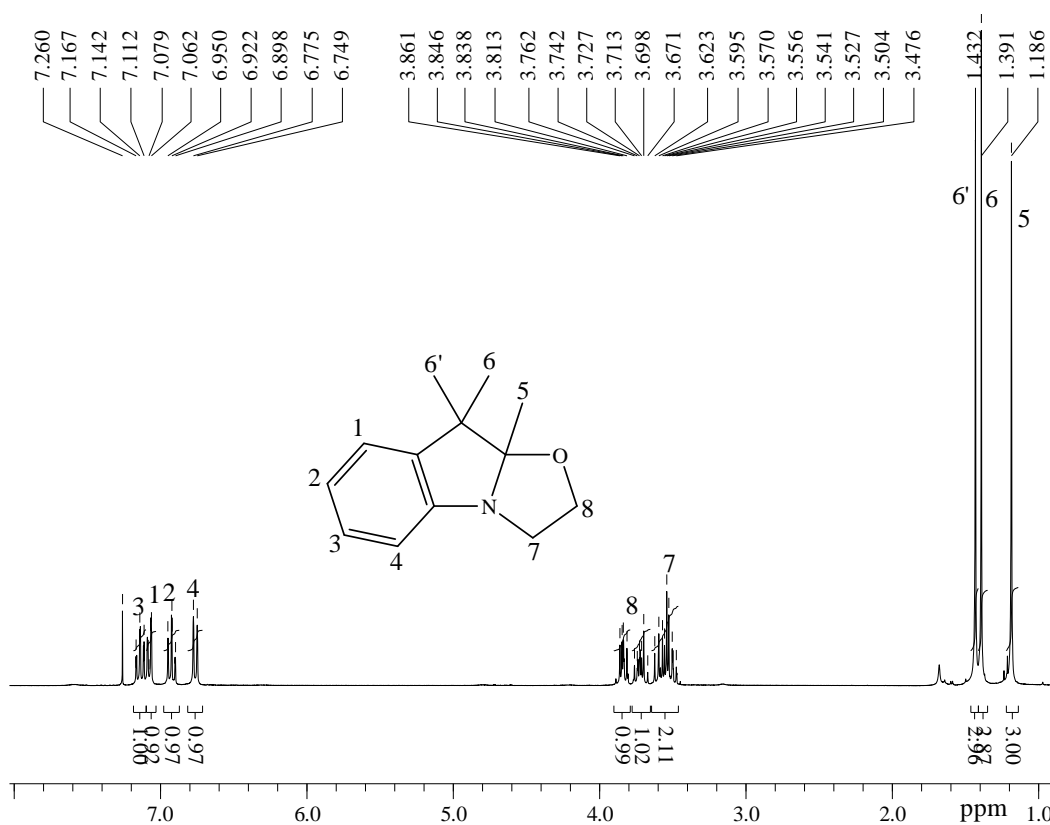

Figure 2.2.5. ^{1}H NMR spectrum of 9,9,9α-trimethyl-2,3,9,9α-tethadydro-oxazolo[3,2-α]indole in CDCl$_3$.
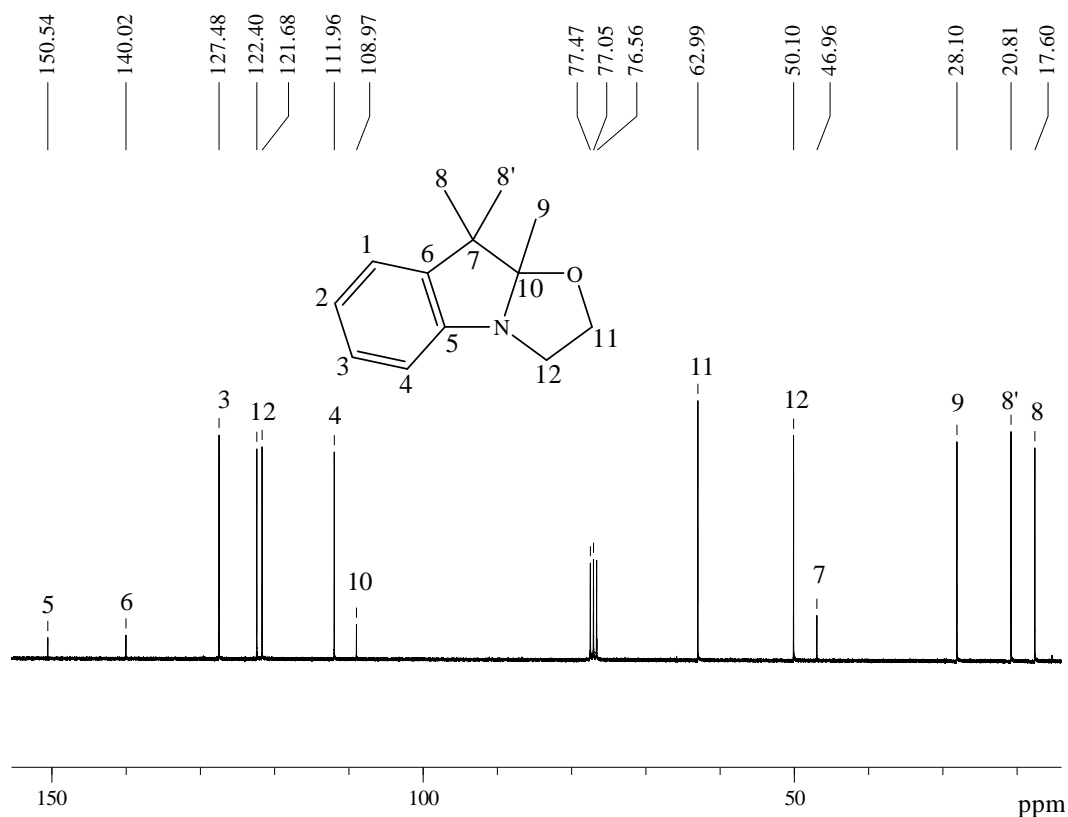
Figure 2.2.6. ^{13}C NMR spectrum of 9,9,9α-trimethyl-2,3,9,9α-tethadydro-oxazolo[3,2-α]indole in CDCl$_3$.

The synthesis of the nitro-substituted spiropyran alcohol was accomplished upon the condensation of the synthesized 9,9,9α-trimethyl-2,3,9,9α-tethadydro-oxazolo[3,2-α]indole with 2-hydroxy-5-nitrobenzaldehyde in ethanol at high temperature. The ^{1}H NMR spectrum of the 2-hydroxy-5-nitrobenzaldehyde precursor shows the following bands: (300 MHz, CDCl$_3$) δ 6.88-7.46 (1H, H-5), 8.4-8.6 (2H, H-3, H-4), 10.0 (1H, H-2), 11.60 (1H, H-1) (see Appendix, Figure 3) while the synthesized 2-(3',3'-dimethyl-6-nitro-3'H-spiro[chromene-2,2'-indol]-1'-yl)-ethanol exhibited the following ^{1}H NMR chemical shifts (300 MHz, CDCl$_3$) δ 1.19 (3H, H-3'), 1.29 (3H, H-3'), 3.29-3.51 (2H, H-9), 3.71-3.84 (1H, H-10), 5.86-5.91 (1H, H-3), 6.66-6.68 (1H, H-4), 6.75-6.78 (1H, H-7'), 6.88-6.92 (2H, H-6', H-5'), 7.09-7.11 (1H, H-4'), 7.17-7.22 (1H, H-8) and 8.00-8.04 (2H, H-5, H-7) (Figure 2.2.7).
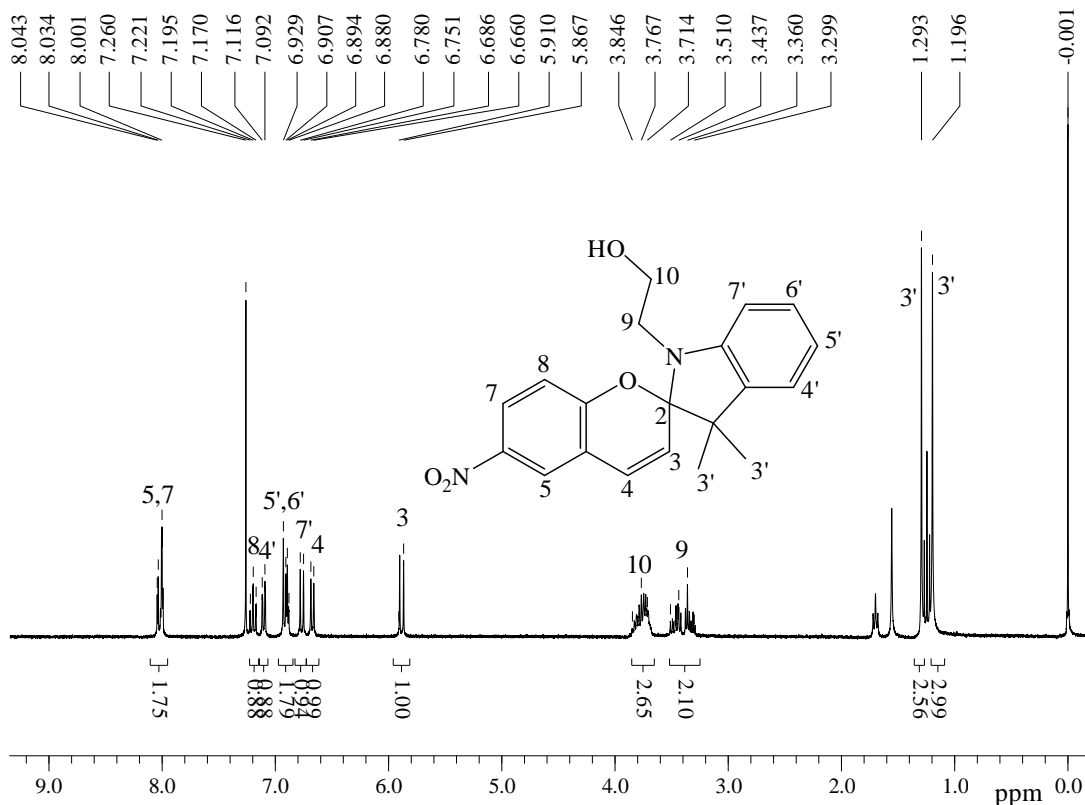
Figure 2.2.7. ^{1}H NMR spectrum of 2-(3',3'-dimethyl-6-nitro-3'H-spiro[chromene-2,2'-indol]-1'-yl)-ethanol in CDCl$_3$.

The synthesis of the nitro-substituted spiropyran alcohol is accompanied by the formation of a chiral spirocenter which connects the two perpendicular aromatic systems, the indoline and the benzopyran ring, as indicated by the appearance of two new signals at 5.86-5.91 and 6.66-6.68 attributed to H-3 and H-4, respectively (Figure 2.2.7). The absence of a signal at 1.18 ppm attributed to the methyl proton H-5 of the oxazolo derivative (Figure 2.2.5) in addition with the disappearance of the bands attributed to the protons of the hydroxyl- and aldehyde-functionalities of the 2-hydroxy-5-nitrobenzaldehyde precursor, observed at 11.6 and 10 ppm, respectively (Figure 3, appendix) was consistent with the synthesis of the desired molecule. The chiral spirocenter imposes a different environment to the methyl protons H-3', resulting in two distinct singlets at 1.19 and 1.29 ppm. The same effect is also observed for the pair of methylene protons, H-9 and H-10, which exhibit two complex multiplets. The successful synthesis of the molecule was also supported by the ^{13}C NMR spectrum of the product

138

(Figure 2.2.8) which exhibited twenty bands attributed to the twenty characteristic carbon atoms of the chromophore compared to the thirteen bands observed in the spectrum of the precursor oxazole derivative (300 MHz, CDCl$_3$) δ 20.05 (1C, C-10'), 25.92 (1C, C-11'), 46.14 (1C, C-12'), 52.84 (1C, C-3'), 60,83 (1C, C-13'), 106.72 (1C, C-2), 106.92 (1C, C-8') 115.54 (1C, C-9), 118.55 (1C, C-6'), 120.01 (1C, C-5), 121.91 (1C, C-4), 121.95 (1C, C-6), 122.78 (1C, C-7'), 125.99 (1C, C-3), 127.86 (1C, C-5'), 128.27 (1C, C-8), 135.89 (1C, C-4'), 141.23 (1C, C-7), 146.94 (1C, C-9'), 159.28 (1C, C-10). The presence of the benzopyran carbons in the spectrum of the product (C3-10) in addition to the appearance of the chiral carbon C-2, connecting the two rings, at 106.72 ppm and the absence of C-9 of the oxazolo precursor (Figure 2.2.6) verified the isolation of the desired product in high purity.
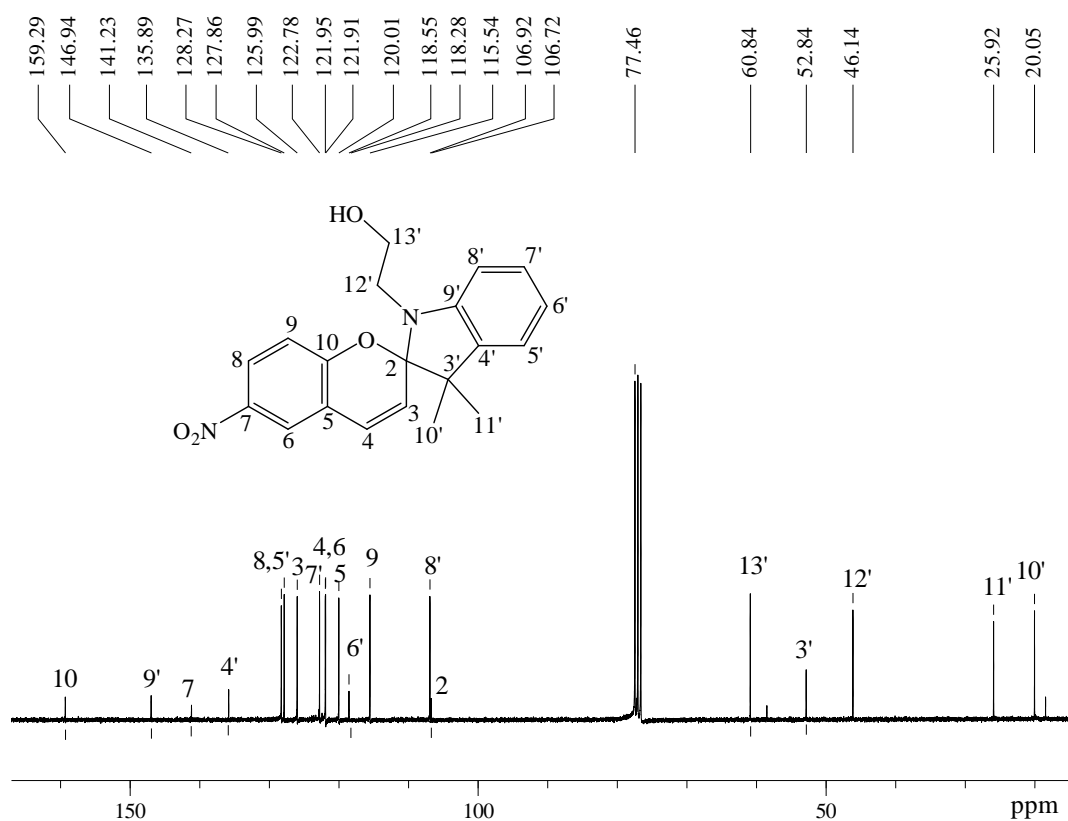
Figure 2.2.8. ^{13}C NMR spectrum of 2-(3',3'-dimethyl-6-nitro-3'H-spiro[chromene-2,2'-indol]-1'-yl)-ethanol in CDCl$_3$.

139

The reversible nature of the SP-to-MC isomerization process of 2-(3',3'-dimethyl-6-nitro-3'H-spiro[chromene-2,2'-indol]-1'-yl)-ethanol in acetonitrile was studied via cycled its irradiation with UV light at 365 nm and following thermal fading of the molecules in dark. Stimulation of the SP chromophores with UV light in acetonitrile, resulted in the evolution of a band at 565 nm attributed to the MC form. Storage of the molecules in dark for 5 min led to the thermal relaxation of the MC isomers and the reformation of the closed SP form (Figure 2.2.9). Even though, the absorption intensity of MC decreased after the first cycle, the chromophores could be switched "on" and "off" at least 7 times without significant photo-degradation effects (Figure 2.2.9, inset).
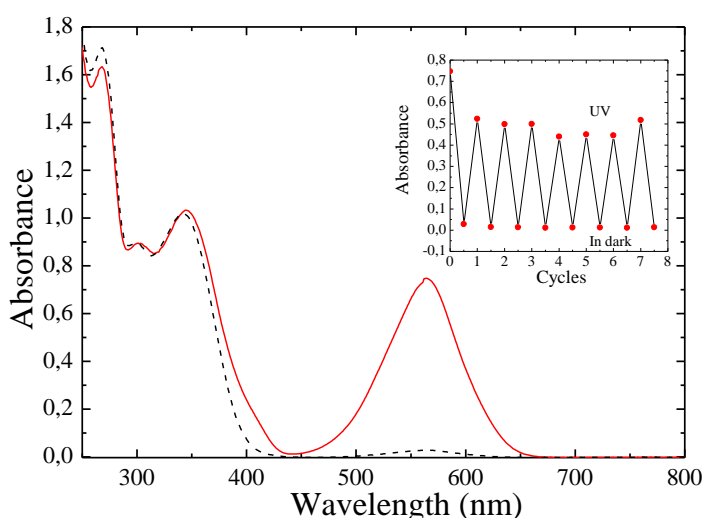
Figure 2.2.9. Absorption properties of the SP alcohol in acetonitrile upon irradiation with UV light (—) and following thermal fading in dark (---). The inset shows the photoswitching cycles of the chromophore.

The functionalization of the spiropyran molecules with a methacrylate moiety was accomplished via the mild Steglich esterification reaction of the precursor spiropyran alcohol with methacrylic acid in the presence of DCC, catalyzed by DMAP. The successful synthesis of the monomer, 1´-(2-methacryloxyethyl)-3´,3´-dimethyl-6-nitrospiro-(2H-1-benzopyran-2,2´-indoline) (SPMA), was confirmed by ^{1}H NMR spectroscopy (Figure 2.2.10).
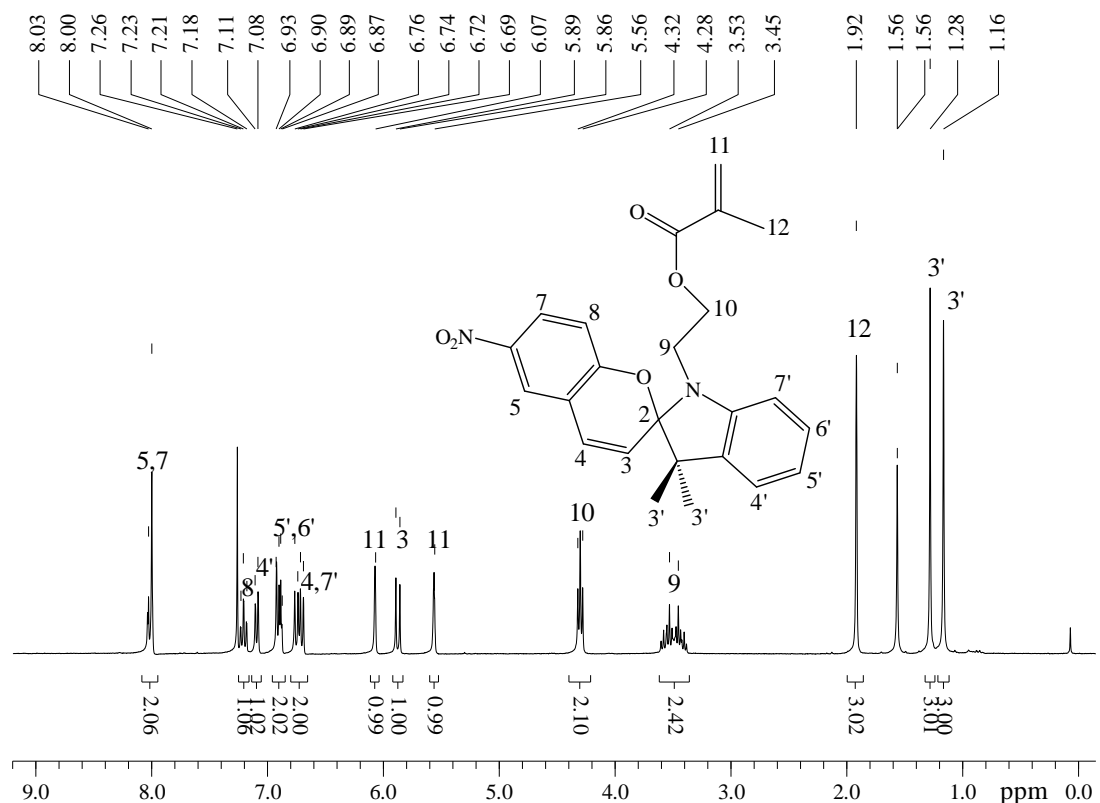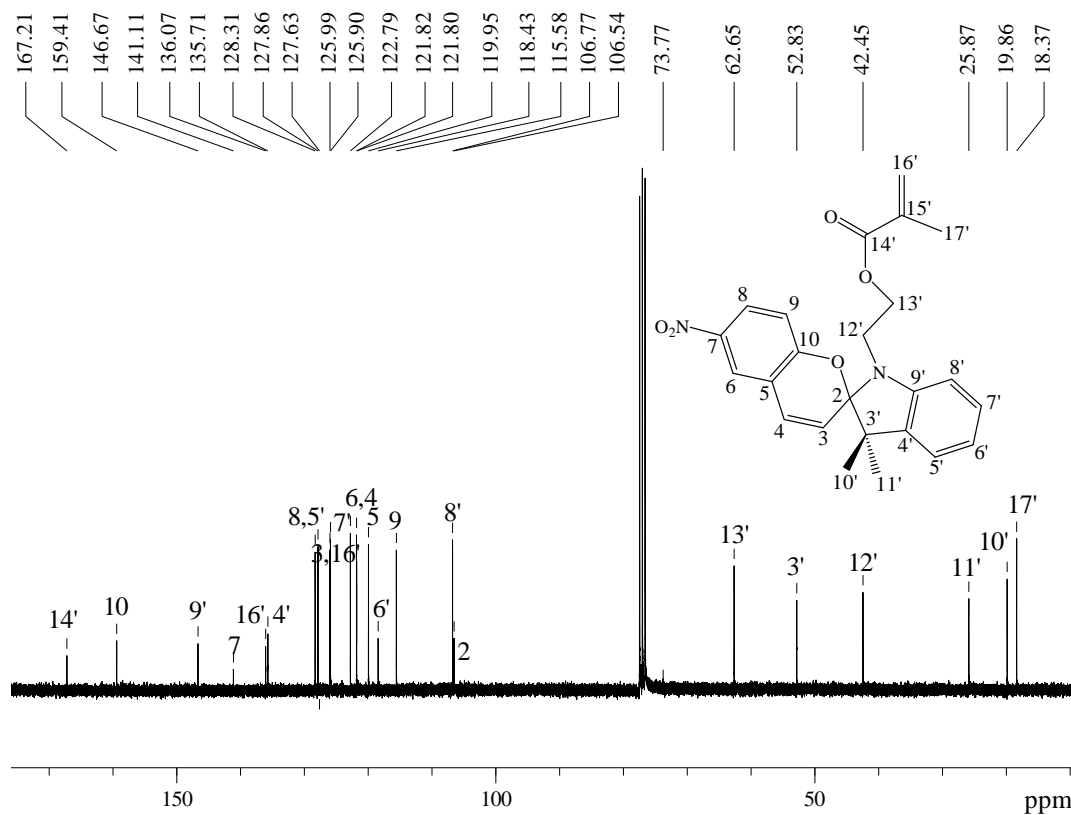
Figure 2.2.10. ^{1}H NMR spectrum (in CDCl$_3$) of 1´-(2-methacryloxyethyl)-3´,3´-dimethyl-6-nitrospiro-(2*H*-1-benzopyran-2,2´-indoline) (SPMA).

The ^{1}H NMR spectrum of the product showed the following resonances (300 MHz, CDCl$_3$): δ 1.16 (3H, H-3'), 1.28 (3H, H-3'), 1.92 (3H, H-12), 3.38-3.60 (2H, H-9), 4.28-4.32 (2H, H-10), 5.56 (1H, H-11), 5.86-5.89 (1H, H-3), 6.07 (1H, H-11), 6.69-6.76 (2H, H-4, H-7'), 6.87-6.13 (2H, H-5', H-6'), 7.08-7.11 (1H, H-4), 7.18-7.23 (1H, H-8), 8.0-8.03 (2H, H-5, H-7). The spectrum indicates that the methylene protons next to the hydroxyl group of the precursor alcohol (H-10, Figure 2.2.7) resonates 0.6 ppm downfield in the ^{1}H NMR spectrum of SPMA after the esterification reaction, while three new peaks appeared; namely two bands at 5.5 and 6.0 ppm, assigned to the protons of the carbon-carbon double bond (H-11) and a peak at 1.9 ppm which corresponds to the methyl group of the methacrylate moiety (H-12). The successful synthesis of the polymerizable SPMA was further supported by the ^{13}C NMR spectrum (Figure 2.2.11) of the molecule (300 MHz, CDCl$_3$): δ 18.37 (1C, C-17'), 19.86 (1C, C-10'), 25.87 (1C, C-11'), 42.45 (1C, C-12'), 52.83 (1C, C-3'), 62,65 (1C, C-13'), 106.54 (1C, C-2), 106.74

(1C, C-8') 115.58 (1C, C-9), 118.43 (1C, C-6'), 119.95 (1C, C-5), 121.80 (1C, C-4), 121.82 (1C, C-6), 122.79 (1C, C-7'), 125.90 (1C, C-3), 125.99 (1C, C-16'), 127.86 (1C, C-5'), 128.31 (1C, C-8), 135.71 (1C, C-4'), 136.07 (1C, C-15'), 141.11 (1C, C-7), 146.67 (1C, C-9'), 159.61 (1C, C-10), 167.21 (1C, C-14'). The appearance of the four carbons of the methacryloyl moiety in the ^{13}C NMR spectrum of SPMA and more importantly, the presence of the carbonyl carbon, C-14' at 167.241 ppm, verified the success of the esterification reaction and the synthesis of the photoresponsive SP monomer.

Figure 2.2.11. ^{13}C NMR spectrum (in CDCl$_3$) of 1´-(2-methacryloxyethyl)-3´,3´-dimethyl-6-nitrospiro-(2H-1-benzopyran-2,2´-indoline) (SPMA).

2.2.3.2 Synthesis of PDMAEMA homopolymers.

The PSPMA monomer was further reacted with DMAEMA to afford block and random copolymers by ATRP. The reaction conditions of the homopolymerization of DMAEMA by ATRP were first optimized. DMAEMA was homopolymerized in bulk at RT utilizing a CuCl/HMTETA transition metal complex as the catalyst system (Scheme 2.2.5). The

142

monomer conversion was monitored by ^{1}H NMR spectroscopy from the samples withdrawn from the reaction flask at various time intervals during polymerization. Calculations were based on the integration of the resonance peaks at 4.23 and 4.0 ppm attributed to the methylene protons next to the ester group of the monomer and the polymer, respectively. Figure 2.2.12 shows the first-order kinetic plot of the monomer concentration, presented as a semilogarithmic plot of monomer conversion *vs* time. Monomer conversion increases with polymerization time and reaches a maximum value of 77 % after 115 h of polymerization. However, the plot is concave upwards with increasing polymerization time indicating a fast reaction, characterized by a kinetic constant of 7.4×10^{-6} s^{-1} for the first 7 hours of polymerization, which becomes much slower $k = 3.5 \times 10^{-6}$ s^{-1} at longer polymerization times. This unusual non-linear behavior was attributed to the increase of the reaction viscosity with the polymer molecular weight which retarded the monomer diffusion and thus the polymer chain growth in accordance to previous reports in the literature on polymerizations carried out in bulk.[12] However, these reaction conditions also suppress the diffusion of the growing polymer radicals and thus hinder bimolecular termination reactions resulting in elimination of polymer termination[12] as evidenced by the linear kinetic plots (Figure 2.2.12).[13]
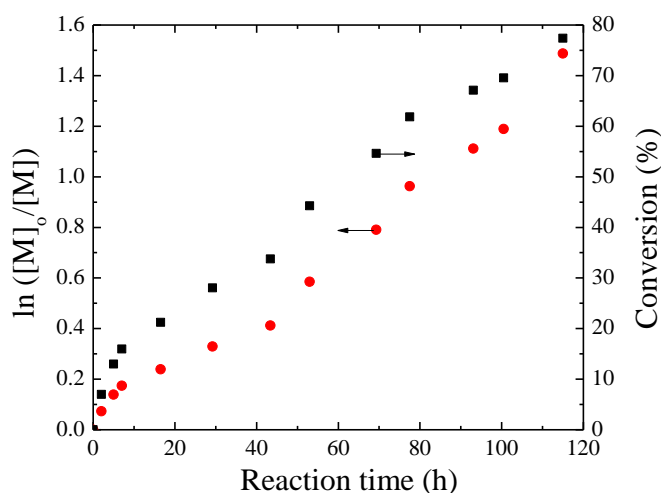
Figure 2.2.12. Semilogarithmic and linear plots of the monomer conversion as a function of the reaction time, for the polymerization of DMAEMA in bulk at RT.
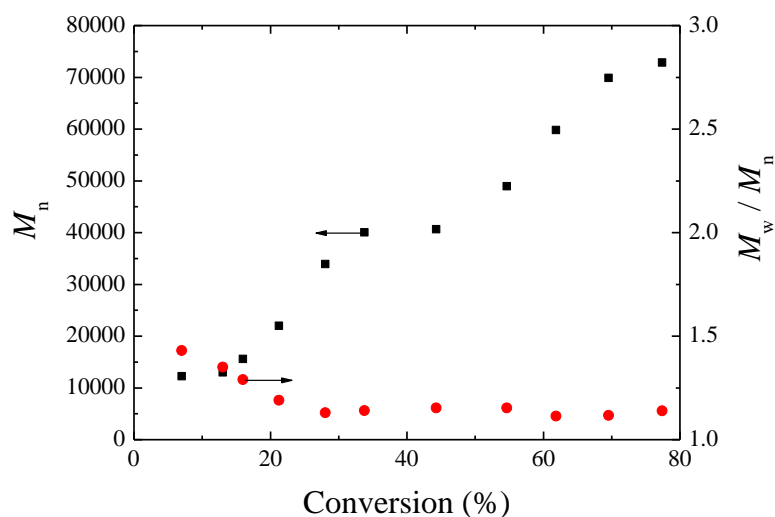
The evolution of the number average molecular weight (M_n) and the molecular weight distribution (M_w/M_n, PDI) of the polymer with time were monitored by GPC analysis. Typical GPC traces of PDMAEMA homopolymers with time are shown in Figure 2.2.13. The elution peaks were shifted to shorter retention times and thus to higher molecular weights upon increasing the reaction time and thus the monomer conversion indicating the successful propagation of the polymerization. A significant narrowing of the GPC traces was also observed upon increasing the reaction time, suggesting the narrowing of the PDIs as the chains grow. The absence of tails at high and low molecular weights was indicative of the absence of termination reactions during the polymerization in bulk.
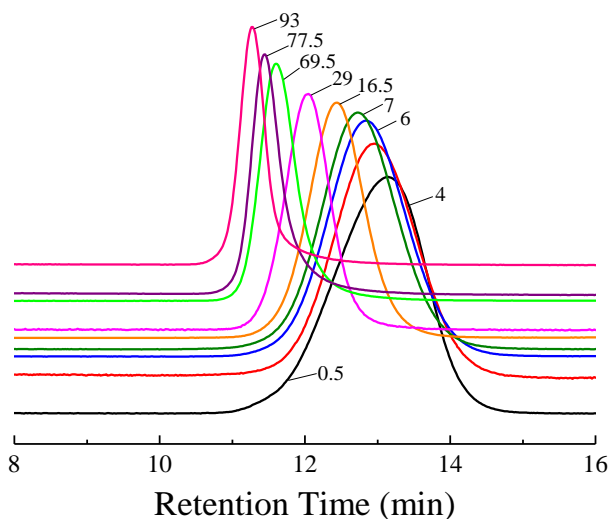
Figure 2.2.13. Evolution of GPC traces with reaction time for the polymerization of DMAEMA in bulk at RT. The numbers denote the time (h) at which the samples were withdrawn from the reaction flask.

Figure 2.2.14 shows the M_n's and the PDIs of the polymers *vs* the monomer conversion. The evolution of the molecular weight of the polymer and the exponential decay of the PDIs as a function of monomer conversion is observed. The linear progression of the molecular weight with monomer conversion indicates the constant concentration of growing radicals and is characteristic for controlled polymerizations. The monomer consumption calculated by ^{1}H NMR is in good agreement with the data derived from GPC analysis; after 7 h of polymerization and monomer conversion about

144

16 % a M_n of 15,600 g/mole and a PDI of 1.29 was found while after 115 h of polymerization, when the monomer conversion approaches 77 % the M_n increases to 72,900 and the PDI decreases to 1.14. These findings in addition with the linear kinetic plots suggest that the ATRP of DMAEMA in bulk at RT proceeds in a "controlled" manner[14] leading to high molecular weight polymer chains of narrow PDIs.

FIgure 2.2.14. Evolution of the number-average molecular weight M_n (■) and the polydispersity index (M_w/M_n) (●) as a function of monomer conversion, for the polymerization of DMAEMA in bulk at RT.

Even though "livingness" and "control" goes in parallel in most ionic polymerization processes this is not the case for the "controlled/living" radical polymerizations.[14] The "living" character of the PDMAEMA chains grown by solvent-free polymerization at RT was investigated by employing the PDMAEMA homopolymer chains (M_n = 15370 g/mol, PDI = 1.23, degree of polymerization (DP) = 98) as macroinitiators to initiate the polymerization of SPMA by copper-mediated ATRP in anisole (Scheme 2.2.6). The GPC curves of PDMAEMA homopolymer and the respective PDMAEMA-*b*-PSPMA block copolymer are shown in Figure 2.2.15. The GPC curve of the polymer after chain extension is shifted towards higher molecular weights; namely the chain-extended polymer exhibited M_n = 16,900 g/mol and PDI=1.46. These results verify the "living" character of the PDMAEMA precursor, while the

increase of the PDI upon the chain extension of the polymer, which is attributed to the tail observed at lower molecular weights suggest that a few termination reactions take place.
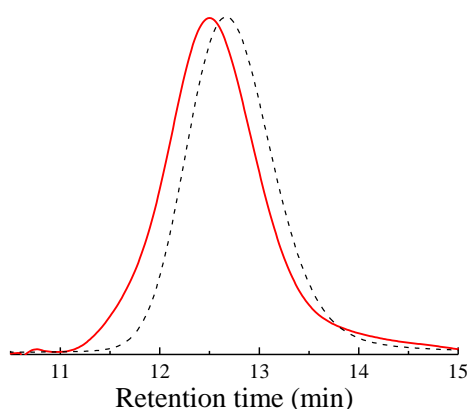
Figure 2.2.15. GPC curves of the PDMAEMA homopolymer (--) and the PDMAEMA-*b*-PSPMA block copolymer (—) after chain extension with SPMA.

The success of the chain extension reaction was also verified by ^{1}H NMR spectroscopy (Figure 2.2.16). The ^{1}H NMR spectrum of the block copolymer exhibited the characteristic resonance peaks of the benzopyran (H-3─H-8) and the indoline (H-3'─H-7') rings of the SPMA comonomer in addition to the DMAEMA peaks. Considering that the integral of the band at 4.07 nm assigned to the methylene protons H-15 of PDMAEMA corresponds to 196 protons (DP = 98), and the integral of the peak at 7.88 ppm attributed to protons H-5 and H-7 of the benzopyran ring of SPMA, the number of SPMA units per chain was calculated to be 7. This finding deviates from GPC results which indicated the presence of 4 SPMA units per chain. The divergence was attributed to the difference in the molecular structure of the PDMAEMA-*b*-PSPMA block copolymer and the PMMA standards used for the GPC calibration, which results in the calculation of an effective M_n for the copolymer.
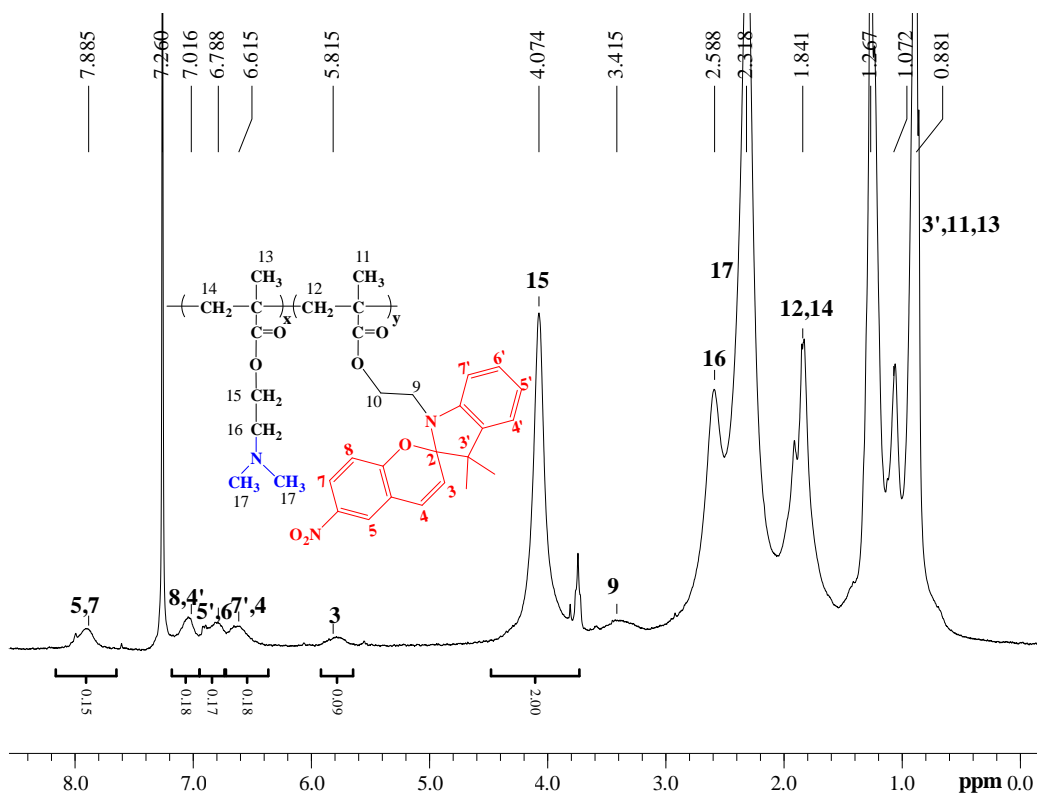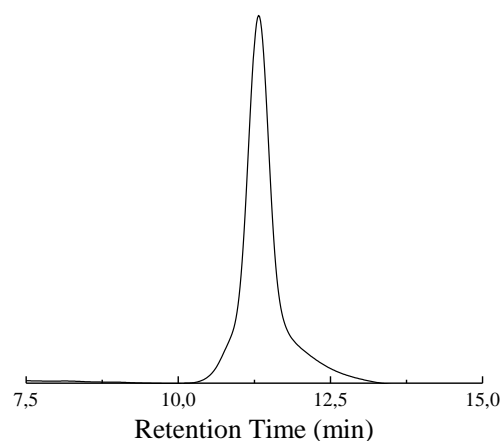
Figure 2.2.16. ^{1}H NMR spectrum (in CDCl$_3$) of the PDMAEMA-*b*-PSPMA copolymer.

The above results verified that the polymerization of DMAEMA in bulk at RT utilizing CuCl/HMTETA as the transition metal complex proceeds in a "controlled" manner and results in high molecular weight PDMAEMA chains bearing "living" chains ends which can re-initiate the ATRP polymerization of other functional monomers such as SPMA. To the best of our knowledge this the first report on the synthesis of PDMAEMA-*b*-SPMA copolymers by sequential ATRP, which opens new possibilities for the development of multiresponsive micellar structures in aqueous media, being sensitive to pH, temperature, light and other variations of the solution properties.

2.2.4   *Synthesis of PDMAEMA-co-PSPMA random copolymer.*

The photosensitive SPMA monomer was next copolymerized randomly with DMAEMA by copper-mediated ATRP in bulk to obtain a PDMAEMA-*co*-PSPMA random copolymer (Scheme 2.2.7). The molecular weight (M_n) and the molecular weight distribution (M_w/M_n, PDI) of the PDMAEMA-*co*-PSPMA random copolymer was found 66,600 g/mol and 1.29, respectively by GPC (Figure 2.2.17). The low PDI of the polymer

147

is in agreement with the "living/controlled" nature of the ATRP process. The PDI of the present copolymer is similar to those reported by Wu at al. for a PSP-*co*-PNIPAM copolymer[10] and lower compared to those we reported recently for PDMAEMA-*co*-PSP copolymers synthesized in solution (THF),[15] and those reported for PMMA-*co*-PSP copolymer and PSP homopolymer chains[11,16] synthesized earlier by ATRP. Much higher PDIs were reported for spiropyran-based copolymers synthesized by conventional free radical polymerization as expected.[17-19]

Figure 2.2.17. GPC trace of the PDMAEMA-*co*-PSPMA random copolymer.

The composition of the PDMAEMA-*co*-PSPMA random copolymer was calculated from its ^{1}H NMR spectrum. In particular, the integral of the peak attributed to the methylene protons next to the ester group of DMAEMA (see Figure 2.2.18, H-15) and that of the benzopyran protons adjacent to the nitro group (see Figure 2.2.18, H-5 and 7) were ratioed to determine a SP content of 6.1 mole % in the copolymer.
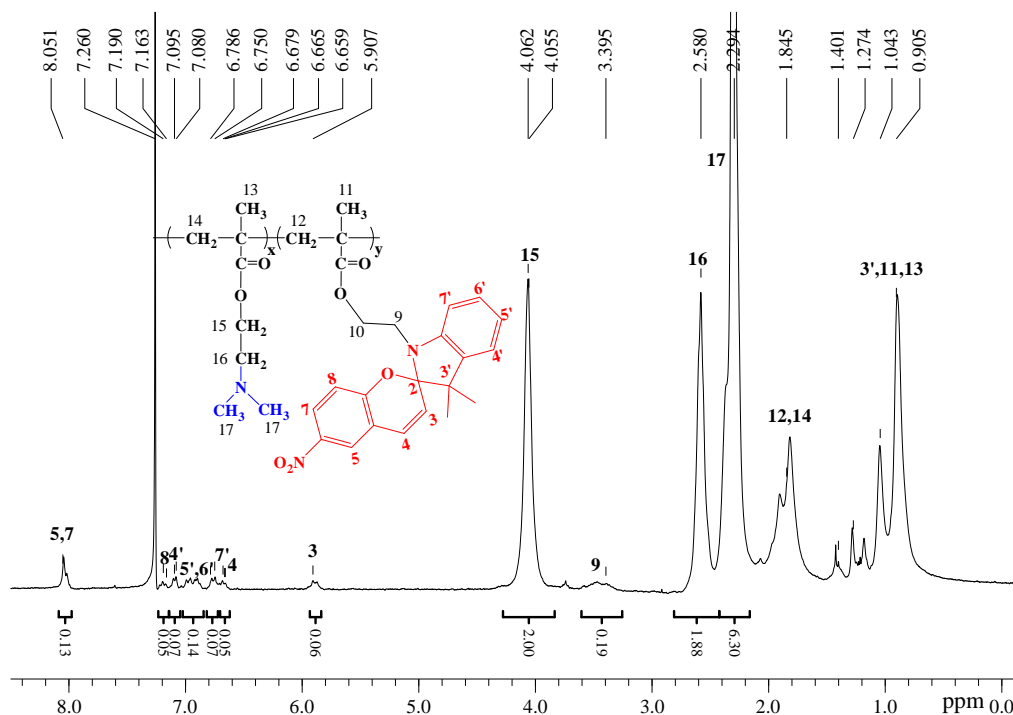
Figure 2.2.18. ^{1}H NMR spectrum (in CDCl$_3$) of the PDMAEMA-*co*-PSPMA random copolymer.

2.2.5 *Photoresponsive behavior of the PDMAEMA-co-PSPMA random copolymer*

The absorption properties of the PDMAEMA-*co*-PSPMA random copolymer were studied in water before and after stimulation with UV light for 49 s (Figure 2.2.19). Before irradiation, the absorption spectrum of the copolymer exhibited three absorption bands; an absorption maximum around 390 mm attributed to the cisoid, non-planar X isomer, and two red-shifted bands at 521 and 553 nm ascribed to different colored merocyanine MC$_1$ and MC$_2$ moieties, respectively.[20-21] The coexistence of the bipolar species in the copolymer before UV irradiation was attributed to the highly polar aqueous medium (SPP scale = 0.962) in addition with the hydrophilic nature of the DMAEMA comonomer which exert great influence and establish a polar microenvironment around the chromophores.[22] The usual photochromic behavior of SPs involves the isomerization of the non-polar parent molecule to a colored planar MC form upon photoexcitation, while in some cases more than one switterionic isomers are obtained.[20-21] The observation of the X isomers is more common in nitrosubstituted SPs[23] while the appearance of two different MC species indicate variations in the microenvironment polarity of the

149

chromophores;[24] a more polar microenvironment stabilizes more effectively the bipolar ground compared to the excited MC state leading to "negative solvatochromism," that is the blue shifting of the MC maximum, while less polar areas are represented by red-shifted MC bands.[25-26]
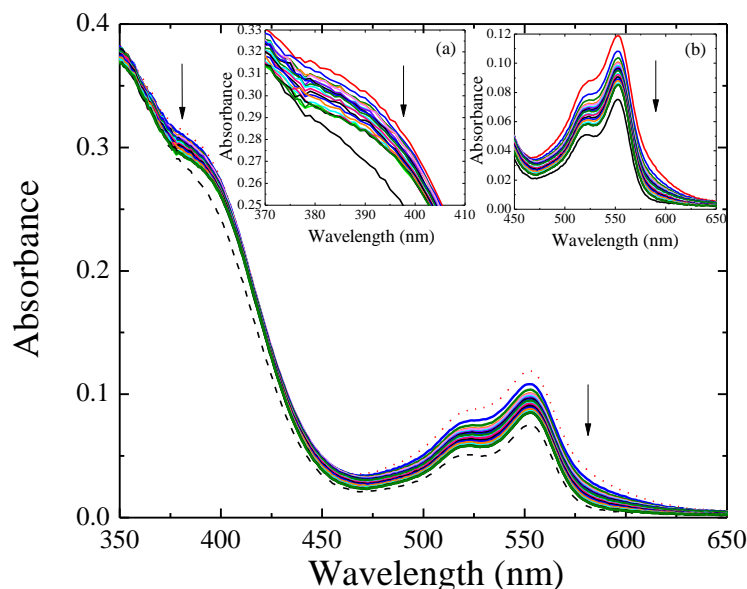
Figure 2.2.19. UV/vis absorption spectra of the PDMAEMA-*co*-PSPMA random copolymer in the dark following irradiation with UV light in an aqueous medium (…). The bands of the X, MC_1 and MC_2 photoisomers can be observed in the absorption spectrum of the copolymer even before stimulation with UV light (---). Insets (a) and (b) show the thermal fading of X and MC species, respectively.

The stimulation of the PDMAEMA-*co*-PSPMA random copolymer with UV light resulted in the enhancement of all three bipolar photoisomers, the X and two distinct MC species (Scheme 2.2.8), as indicated by the simultaneous evolution of three bands in the absorption spectrum of the copolymer at 390, 521 and 553 nm attributed to the X isomer and the two MC species, respectively (Figure 2.2.19). Although the X isomers are usually transient species with a short life-time detected by ultrafast spectroscopy[21] they can be clearly observed in the present system. This is attributed to the microenvironment of the chromophores including the segmental mobility of the polymer chains, the polarity of the comonomer and the surrounded solvent medium which affects the isomerization rates of the species formed, rendering them excellent candidates as environmental probes. The X-

to-SP and MC-to-SP thermal relaxation of the chromophores in the random copolymer was investigated by UV/vis spectroscopy via monitoring the suppress of the absorption intensity of the X isomer at 390 nm and the MC bands at 521 and 553 nm, in dark, following the irradiation of the copolymer with UV light for 49 s (Figure 2.2.19).
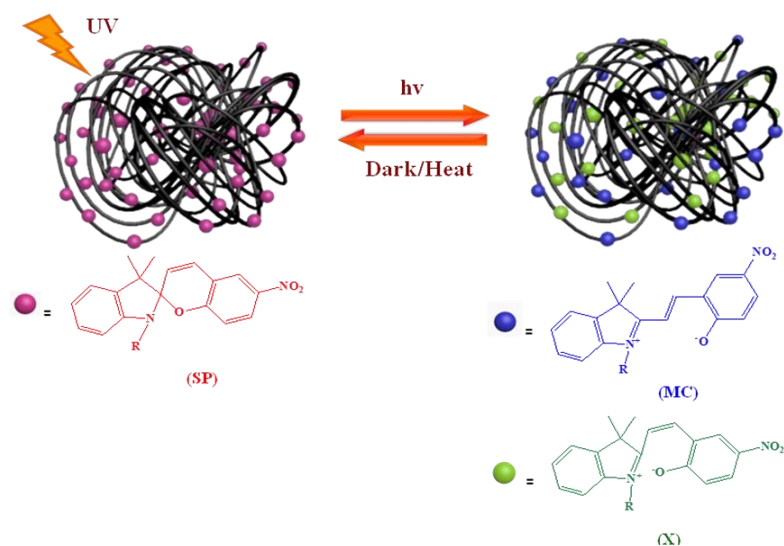
Scheme 2.2.8. Photo-regulated SP-to-MC and SP-to-X isomerization of the photoresponsive moieties of the PDMAEMA-*co*-PSPMA random copolymer. SP is the parent molecule in its ground electronic state, X denotes a bipolar, non-planar isomer and MC represents the several possible planar, merocyanine isomers. The SP form can be retrieved either thermally or upon irradiation with visible light.

The absorption bands of the three isomers diminish slowly with time with no change in the absorption shape. The kinetic constants for the X and MC decoloration process were calculated by fitting the experimental data of the fading process with a biexponential decay function (eq 2.2.1) (Figure 2.2.20).[27]

$$\frac{A_t - A_e}{A_o - A_e} = a\exp(-k_1 t) + (1-a)\exp(-k_2 t) \qquad \text{(eq. 2.2.1)}$$

where A_t and A_o and A_e is the absorption maximum of the X and MC isomers at time 0, t and when the molecules attain their photostationary state (t = ∞). α denotes the fraction of the X and MC isomers fading faster with a rate constant k_1 and (1-α) represents the residual X and MC species bleaching at a slower rate, k_2.
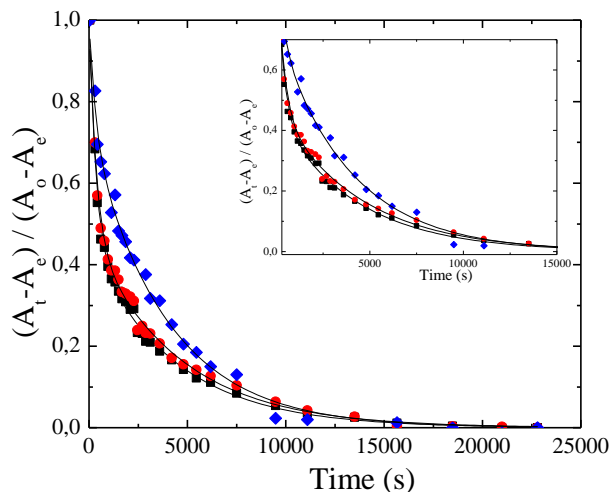
Figure 2.2.20. Kinetics of the MC_1-to-SP (■), MC_2-to-SP (●) and X-to-SP (♦) thermal bleaching process for the PDMAEMA-*co*-PSPMA random copolymer in water. The solid black lines represent the fits of the data using eq. 2.2.1. Inset shows a magnification of the kinetics at shorter fading times.

The non-monoexponential fading behaviour of spiropyran moieties incorporated in polymers has been reported previously for SP molecules embedded in amorphous glassy poly(alkyl methacrylate) films[28-29] and was attributed to the non-homogeneous microenvironment around each chromophore molecule in terms of free-volume and relaxation of the polymeric chain. Variations in the environment surrounding the chromophores derive from various factors including chain segmental mobility, available free volume, polymer polarity, volume change originated from the structure rearrangement of the molecule upon isomerisation, the existence of various isomers and the distribution of the molecules within the polymer matrix.[30] Thus, the polymer matrix imposes a distribution of localized barriers to the system which have to be thermally overcome by the sterically demanding ring-closure process of MC[31] which has to pass through the energetically unfavored rotation around the central double bond of the molecules to form the intermediate cis-isomer and finally the closed SP form.[25] In the present system, a significant contribution to the more complicated fading behavior of the chromophores is derived from the fact that when the PDMAEMA-*co*-PSPMA copolymer is dissolved in water associates leading to the formation of nanoscale assemblies. The hydrodynamic diameter (D_h) of the PDMAEMA-*co*-PSPMA random copolymer in the

aqueous medium was determined by DLS before and after irradiation with UV light (Figure 2.2.21).
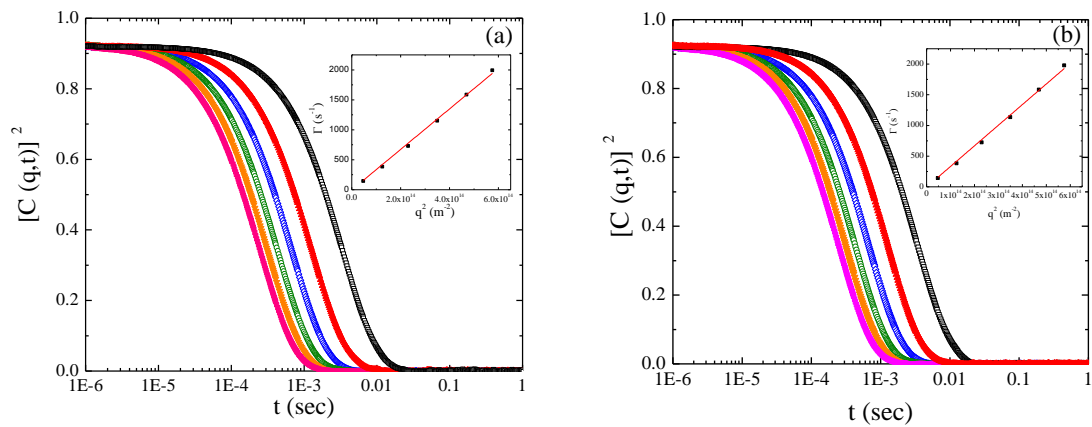
Figure 2.2.21. Intensity autocorrelation functions of the PDMAEMA-*co*-PSPMA copolymer before (a) and after (b) irradiation with UV light for scattering angles 30° (□), 50° (▲), 70° (◊), 90° (○), 110° (▼) and 130° (■). Insets show the Γ *vs* q^2 plots, while red solid lines represent linear fits to the data.

The DLS measurements showed single-exponential decay of the intensity autocorrelation functions at scattering angles 0°, 50°, 70°, 90°, 110° and 130° before UV irradiation, from which a D_h of 142 nm was calculated (Figure 2.2.21a). Similar polymer associates of D_h = 144 nm were observed in water after irradiation of the random copolymer with UV light (Figure 2.2.21b). Thus, the photoregulated SP-to-MC isomerization of the chromophore species of the copolymer does not affect its association in water. This may be attributed to the low SP content of the random copolymer and the fact that some SP moieties were isomerized to the MC form before irradiation with UV light as indicated by UV/vis measurements (Figure 2.2.19). This result suggests that the association of the random copolymers in water may impose variations in the chromophores microenvironment in terms of polarity and free volume leading to a more complicated fading behavior of the chromophores.

Kinetic constants along with the amplitudes (α, 1-α) for all switching processes present in the system are listed in Table 2.2.1.

Table 2.2.1. Rate constants and fractions of the short- and long-lived species for the MC$_1$-to-SP, MC$_2$-to-SP and X-to-SP isomerization process of the PDMAEMA-*co*-PSPMA random copolymer at 25 ^{o}C.

| λ_{max} (nm)[1]	Species	a[2]	b[3]	Rate constants[4]	
				k_1(s^{-1})[5]	k_2(s^{-1})[6]
553	MC$_1$	0.55	0.45	2.78×10^{-3}	2.35×10^{-4}
521	MC$_2$	0.53	0.47	2.74×10^{-3}	2.24×10^{-4}
390	X	0.27	0.73	3.00×10^{-3}	2.58×10^{-4}

[1]Absorption maximum of the X and MC species. [2]fraction of short-lived X and MC species (eq. 2.2.1). [3]fraction of long-lived X and MC isomers (eq. 2.2.1). [4]calculated from UV/vis absorption spectra of the copolymers. [5]k_1 represents the rate constant for the short-lived X and MC isomers. [6]k_2 represents the rate constant for the long-lived species.

The biexponential fitting model reveals that the X isomers exhibit decoloration rates $k_1 = 3.00 \times 10^{-3}$ s^{-1} and $k_2 = 2.58 \times 10^{-4}$ s^{-1} attributed to the short- and -long-lived X species, respectively. MC$_2$ isomers are also fading thermally according to the biexponential model, while the short- and long-lived isomers exhibite isomerization constants $k_1 = 2.74 \times 10^{-3}$ s^{-1} and $k_2 = 2.24 \times 10^{-4}$ s^{-1}, respectively. Similary, the isomerization constants of the MC$_1$ species, were calculated to be $k_1 = 2.78 \times 10^{-3}$ s^{-1} and $k_2 = 2.35 \times 10^{-4}$ s^{-1} for the short- and lond-lived isomers, respectively. It is worth noting that the short-lived X, MC$_1$ and MC$_2$ photoisomers exhibit similar isomerization constants. In addition, similar fractions of short- and long-lived species were observed for the two planar MC isomers, while the majority of X isomers are long-lived (73 %) (Table 2.2.1). Moreover, all long-lived isomers exhibit decoloration rates which are one order of magnitude lower than the short-lived species. This behavior is attributed to the polarity gradient derived from the less polar polymeric backbone and the highly polar tertiary amine side groups which promote a polar microenvironment around the molecules and stabilize the MC switterions while the less polar areas favor the ring-closure reaction and faster isomerization rates.[22,32] Moreover, the association of the polymer in water (Figure 2.2.21) impose a spatially inhomogeneous environment around the chromophores in terms of free volume

and favors the complicated fading behavior of the chromophores which results in long- and short-lived species which are fading thermally with different rates.

2.2.6 *Acidochromic properties of the PDMAEMA-co-PSPMA random copolymer*

The effect of the solution pH on the isomerization process of the SP moieties of the PDMAEMA-*co*-PSPMA random copolymer was investigated upon the gradual addition of acid in an aqueous solution of the copolymer. The addition of a low amount of acid in the solution induces the chemical formation of the switterionic MC isomers due to the ring-opening of the closed SP form induced by the increased polarity of the chromophore microenvironment. Furthermore, at extremely acidic solutions the bipolar species become protonated resulting in the generation of the protonated $[MC-OH]^+$ isomers. A competitive process is also catalyzed by acid that is the protonation of the closed SP isomers, resulting in the formation of the $[SP-NH]^+$ photoisomers (Scheme 2.2.9).
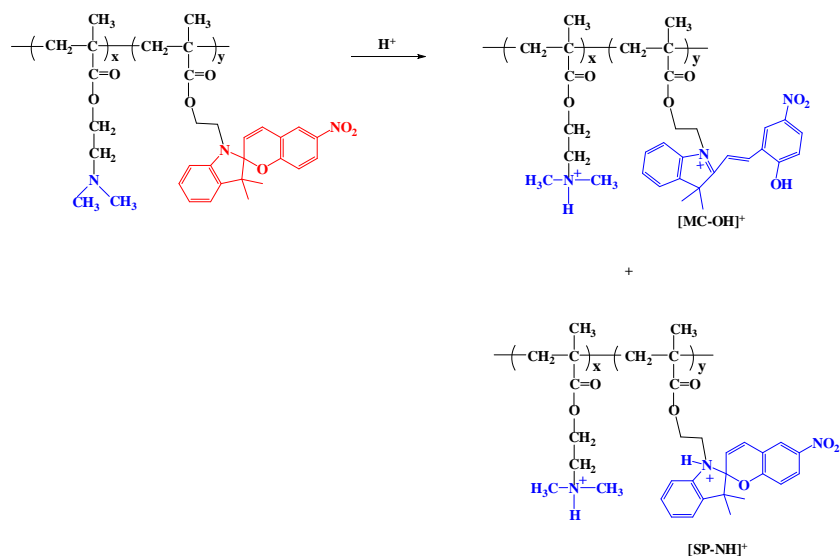
Scheme 2.2.9. Protonation of the PDMAEMA-*co*-PSPMA random copolymer in aqueous medium upon the gradual addition of acid.

All these species exhibiting distinct absorption maxima, and thus their formation can be monitored spectroscopically. On the other hand, the process is fully reversible and neutralization of the system with base leads to the regeneration of the parent SP molecules.[33] In the present system, the acid-induced SP-to-MC ring-opening process and the protonation of the MC switterions (pK_a=6-7)[17] described above are accompanied by

the protonation of the DMAEMA units which exhibit a similar pK_a value ($pK_a = 7.0$)[34] and thus this process is also taken into account for the addition of the appropriate amount of acid. Figure 2.2.22a shows the absorption spectra of the PDMAEMA-*co*-PSPMA copolymer upon the sequential addition of acid.
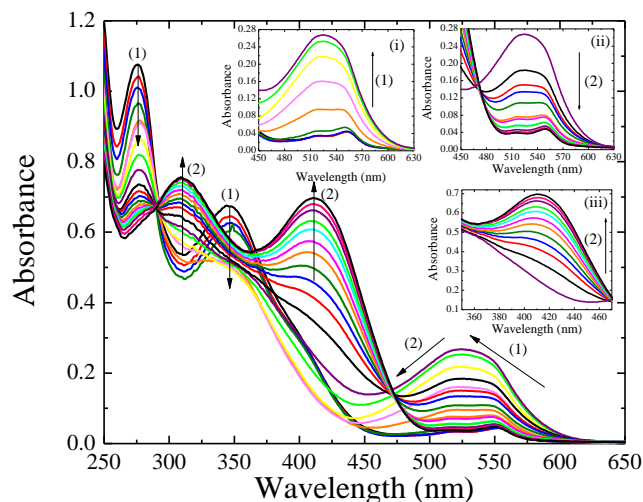
Figure 2.2.22a. UV/vis absorption spectra for an aqueous solution of the PDMAEMA-*co*-PSPMA random copolymer upon the addition of acid (HCl). Inset (i) shows the increase of the intensity at the absorption maximum of MC (527 nm) upon the addition of 3.94×10^{-5} moles HCl. Insets (ii) and (iii) show the decrease of the absorption intensity of MC (527 nm) and the evolution of the [MC-OH]$^+$ band (411 nm), respectively upon the further addition of 2.40×10^{-4} moles HCl.

As discussed in the previous section, variations in the polarity of the microenvironment of the chromophores result in the coexistence of two MC isomers in the copolymer with absorption maxima at 521 and 553 nm in addition with the X isomer observed at 390 nm. In contrast to the photo-stimulated ring-opening process of the chromophores which showed an increase in the absorption intensity of both isomers while retaining their initial relative intensity ratio (Figure 2.2.19), the acid catalyzed ring-opening process had a significant effect on the formation of the more polar MC_2 isomers at 521 nm which gradually attain an intensity similar to that of the less polar MC_1 species leading to the appearance of a broad absorption band between 450 and 620 nm (Figure 2.2.22a, process 1). This is attributed to the increased polarity of the surrounding microenvironment due to

156

presence of protons in the solution and the protonation of the DMAEMA units (Figure 2.2.22a, inset i). The formation of the bipolar species in solution requires the consumption of the parent SP isomers as indicated by the decrease of the SP band at 276 nm (Figure 2.2.22a, process 1). The absorption intensity of the X isomer at 390 nm also decreases upon the addition of acid in the system suggesting its conversion to the open MC switterions (Figure 2.2.22a).[35] Further increase of the acid concentration catalyzed the protonation of the colored isomers leading to the gradual suppress of the MC band at 527 nm (Figure 2.2.22a, inset ii) and the concomitant formation of the *trans*-[MC-OH]$^+$ derivatives observed at 411 nm (Figure 2.2.22a, inset iii).[7] In parallel, pronounced increase in the absorption intensity at 310 nm reveals the generation of the protonated closed [SP-NH]$^+$ isomers (Figure 2.2.22a, process 2). Figure 2.2.22b summarizes the variations in the absorption intensities of the chromophore species as a function of the moles of acid added in the aqueous solution of the random copolymer.
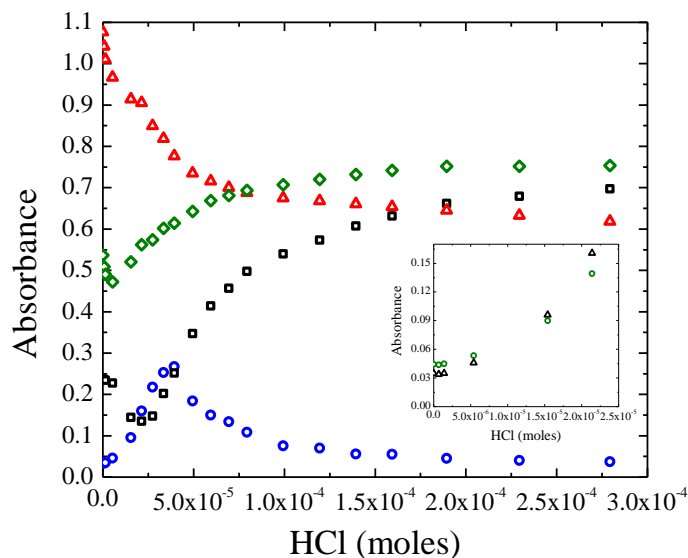

Figure 2.2.22b. Absorption intensities of the chromophore species in an aqueous solution of the PDMAEMA-*co*-PSPMA random copolymer as a function of the moles added HCl; SP; (△), [SP-NH]$^+$; (◊), [MC-OH]$^+$; (□), MC; (○). The inset shows the variations in the absorption intensities of MC$_1$ (○) and MC$_2$ (△) species, at H$^+$ ≤ 2.5 × 10^{-4} mole.

At low acid concentrations, $H^+ \leq 3.94 \times 10^{-5}$ mol, the closed SP isomers undergo a ring-opening reaction to form the colored MC isomers as indicated by the decrease of the absorption intensity of the SP isomers and the concomitant increase of the intensity of the MC band. In parallel, the protonation of the closed SP form leads to the formation of the $[SP\text{-}NH]^+$ isomers as evidenced by the evolution of their absorption intensity at 310 nm. It should be noted that at $H^+ \leq 2.5 \times 10^{-5}$ mole a bimodal band is observed for the MC species indicating the presence of two MC isomers, while the faster evolution of the absorption maximum of the MC_2 isomers at 521 nm compared to the MC_1 isomers at 553 nm (Figure 2.2.22b, inset) leads to the appearance of a broad band between 450 and 620 nm. At low acid concentration ($H^+ \leq 2.2 \times 10^{-5}$ mole) a decrease of the absorption intensity at 411 nm is observed suggesting the isomerization of the X species to the MC form. At higher acid concentrations, 3.94×10^{-5} mole $\leq H^+ \leq 2.79 \times 10^{-4}$ mole, a decrease in the absorption intensity of the MC band was observed suggesting the formation of the $[MC\text{-}OH]^+$ isomers verified by the significant increase in their absorption magnitude at 411 nm.

2.2.7   Fluorescent behavior of the PDMAEMA-co-PSPMA random copolymer

The fluorescent properties of the PDMAEMA-*co*-PSPMA random copolymer in water were investigated before stimulation, upon irradiation with UV light and during thermal relaxation of the chromophores at neutral pH. The emission spectrum ($\lambda_{ex} = 521$ nm) of the random copolymer before UV irradiation (Figure 2.2.23a, spectrum 1) exhibited three separated emission maxima; an intense band at 567 nm attributed to the non-planar isomer X[36] and the red-shifted peaks at 611 and 645 nm assigned to the MC residues of the polymeric chain. The coexistence of a fraction of the bipolar isomers in the copolymer before light stimulation was attributed to the highly polar microenvironment surrounding the chromophores, established by both the aqueous solvent medium and the polar PDMAEMA comonomer, which favors the isomerization of the SP species to the switterionic isomers. This observation is in agreement with the absorption spectrum of the copolymer which showed the generation of more than one photoisomers from the same parent molecule even before photoexcitation (Figure 2.2.19).
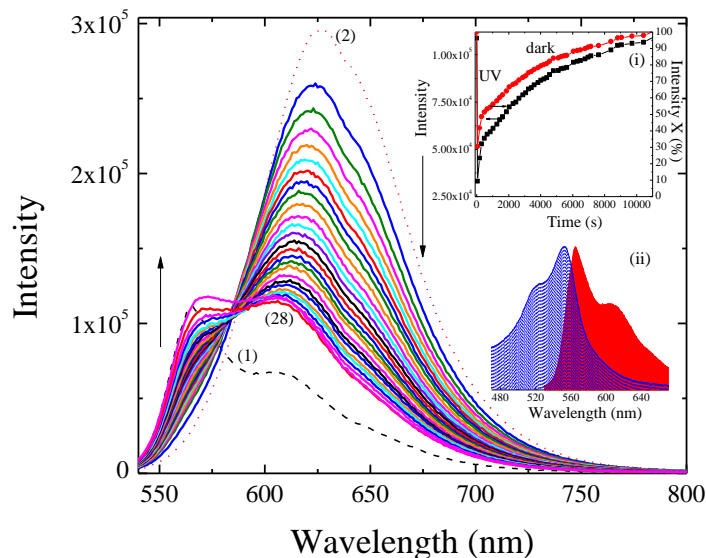
Figure 2.2.23a. Fluorescence emission spectra (λ_{ex} = 521 nm) for the PDMAEMA-*co*-PSPMA random copolymer in water at neutral pH, before (1) and after (2) irradiation with UV light and during thermal relaxation of the chromophores at RT (3-28). Inset (i) shows the absolute (■) and % (●) variations in fluorescence emission intensity of the X species (567 nm) as a function of time. The minimum in the plots represents the fluorescence emission intensity of X upon 49 s irradiation with UV light. Inset (ii) shows the spectral overlap region between the donor (X) emission spectrum (red) and the acceptor (MC) absorption spectrum (blue).

Figure 2.2.23a (spectrum 2) shows the fluorescence emission spectrum (λ_{ex} = 521 nm) of the random copolymer in water at neutral pH following irradiation with UV light for 49 s. The effect of the photo-stimulation of the copolymer with UV light is two-fold; the emission intensity of the X species at 567 nm is quenched by 70 % (Figure 2.2.23a, inset i) giving rise to the significant evolution of a bimodal band with maxima at 626 and 645 nm attributed to two different MC isomers. This result seems in contrast to the absorption spectra which showed the simultaneous generation of the X isomers and the two colored MC species upon irradiation of the copolymer with UV light (Figure 2.2.19). However, the quenching of the formed X isomer emission suggests a fluorescence resonance energy transfer (FRET) from X to the MC isomers. The occurrence of FRET between the photoisomers is determined by two stringent requirements; the absorption band of the energy acceptor to overlap properly with the emission band of the energy

donor and the spatial donor-acceptor distance to be within the Föster radius. The first requirement is successfully fulfilled in the present system since the absorption band of the MC acceptors at 553 nm overlaps significantly with the emission band of the X donors at 567 nm (Figure 2.2.23a, inset ii). Such an energy transfer from the X to the MC species has been reported previously for 1'-octadecyl-3',3'-dimethyl-6-nitrospiro-[2*H*-1-benzopyran-2,2'-indoline) molecules incorporated in Langmuir-Blodgett (LB) films prepared in a mixed film with stearic acid, arachidic acid, and tripalmitine where the chromophores exhibited close proximity, for which the Föster's critical distance R_0 between donors and acceptors has been calculated to be as short as 2 nm.[36] Considering that the R_0 for the X-MC FRET pairs is 2 nm,[36] the energy transfer was calculated by the "rule of thumb" to be effective over distances in the $R_0 \pm 50\% R_0$ range,[37] namely 1 nm ≤ $r \leq 3$nm, where r is the distance between the X donors and the MC acceptors and R_0 the distance between donors and acceptors at which 50% of the excited donors decay via energy transfer, while the rest via alternative radiative or non-radiative ways.[37] The donor-acceptor distance r can be calculated according to equation 2.2.2.

$$r = R_0 \left[\frac{(1-E)}{E} \right]^{1/6} \qquad \text{(eq. 2.2.2)}$$

where R_0 is the critical energy transfer distance and E the FRET efficiency. The FRET efficiency can be determined experimentally form fluorescence spectroscopy data according to equation 2.2.3.

$$E = 1 - \left(\frac{X_t}{X_o} \right) \qquad \text{(eq. 2.2.3)}$$

where X_t is the fluorescent intensity of the donor X after switching "off" the stimulation of the hybrids with UV light and X_o is the fluorescence intensity of the donor X before UV irradiation.[37-39] From the above equations the FRET efficiency in our system was calculated to be 70% and the X-MC distance about 1.74 nm. This is attributed to the photoinduced SP-to-MC and SP-to-X isomerization which leads to significant increase of the abundance of the X and MC moieties, constituting FRET-based donor-acceptor pairs (Scheme 2.2.10).
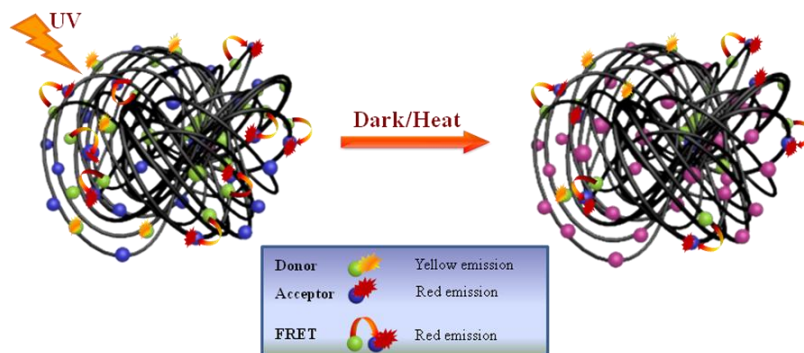
Scheme 2.2.10. Schematic illustration of the photo-regulated FRET process from the X to the MC species for the PDMAEMA-*co*-PSPMA random copolymer. The FRET process is switched "on" and "off" via stimulation of the chromophores with UV light and upon thermal relaxation of the MC species, respectively.

The significant quenching of the X emission intensity is facilitated by the adequate number of MC acceptors derived upon photo-stimulation of the copolymer promoting the high transfer efficiency. The high efficiency of the FRET process is also favored by the close proximity of the chromophores due to the association PDMAEMA-*co*-PSPMA chains in water (Figure 2.2.21).Thus, the random distribution of SP chromophores along a macromolecular chain which associates in solution can facilitate the occurrence of an intra- and inter-chain FRET phenomenon.

The FRET process is gradually switched "off" upon the MC-to-SP thermal relaxation, resulting in the progressive recovery of the intensity of the X species (Figure 2.2.23a). The photoswitchable "on"-"off" fluorescent character of the polymers is based on the fact that the non-fluorescent SP moieties are photoisomerized to the colored, fluorescent MC species facilitating the charge transfer, while the phenomenon is attenuated and finally interrupted upon the thermal-induced elimination of the MC quenchers (Scheme 2.2.10). The emission intensity of the X species which is abruptly suppressed upon irradiation with UV light is gradually retrieved (Figure 2.2.23b).
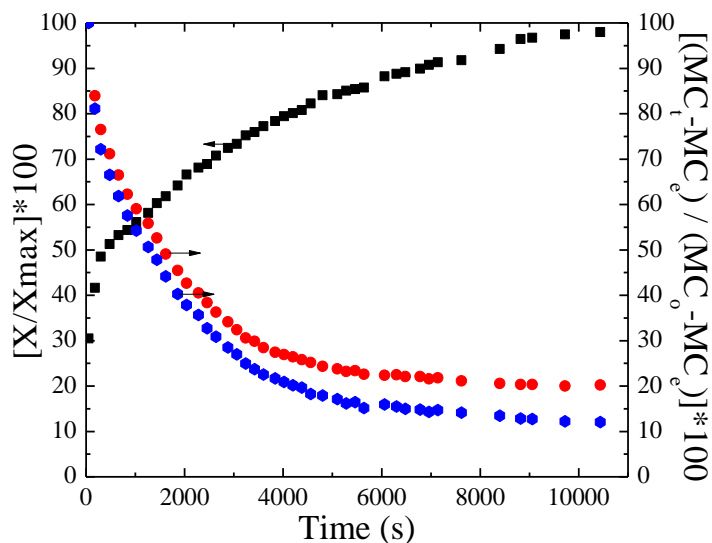
Figure 2.2.23b. Variations in the relative fluorescence intensity of the X isomers (■, λ_{em} = 567 nm) and the MC_1 (●, λ_{em} = 645 nm) and MC_2 (●, λ_{em} = 626 nm) species as a function of time after stimulation of the copolymer with UV light in water.

In particular, 26 % of the fluorescent intensity of X intensity is gained after 1,020 s of thermal relaxation, while in parallel the fluorescent intensities of the MC_1 and the MC_2 species are quenched by 46 and 41 %, respectively, whereas the thermal relaxation of the system for 10,440 s results in the total recovery of the X fluorescent intensity (98%) and the presence of 12 and 20% of MC_1 and MC_2 species. It should be noted that the fluorescence emission at 626 nm is a sum of the contributions from the FRET process and the isolated MC isomers while the relative contribution of the two factors is difficult to be quantified. The fact that the emission intensity of X isomers was recovered before the total quenching of the MC acceptors, although the fading rate constants of the two isomers are similar (Table 2.2.1), indicates an excess of the MC isomers.

Several factors, including the chain segmental mobility, variations in the available free volume derive from the association of the PDMAEMA-*co*-PSPMA chains in water, the microenvironment polarity, the volume change originated from the structure rearrangement of the molecule upon isomerisation and the distribution of the molecules within the polymer matrix favor the stabilization of the bipolar X and MC species by the current system, prolong their life-time (Figure 2.2.23b) and enable the read-out process. To the best of our knowledge, the FRET in polymeric materials carrying X-MC donor-

162

acceptor pairs has not reported previously while the phenomenon was observed only when 1'-octadecyl-3',3'-dimethyl-6-nitrospiro-[2H-1-benzopyran-2,2'-indoline] was mixed with aliphatic acids or tripalmitine to form LB films, and was studied by picosecond time resolved fluorescence spectroscopy due to short lifetime of the X isomer. However, in our system the effective stabilization of both photoisomers over thermal relaxation enable the monitoring of the phenomenon. The increase of the half-life of the MC isomers has been reported previously in the literature for chromophores substituted with a succinyl ester functionality when embedded in a gel derived from 4-*tert*-butyl-1-phenylcyclohexanol[40] or upon incorporation of the molecules within polymer matrices, enabling their use in super-resolution fluorescence imaging.[41]

The rates of the ring closure MC-to-SP reaction, were calculated by following the decrease of the fluorescent maximum of the two MC species as a function of time. The kinetic constants for the SP reformation were calculated by fitting the fluorescent experimental data to eq. 2.2.1 (Figure 2.2.23c).
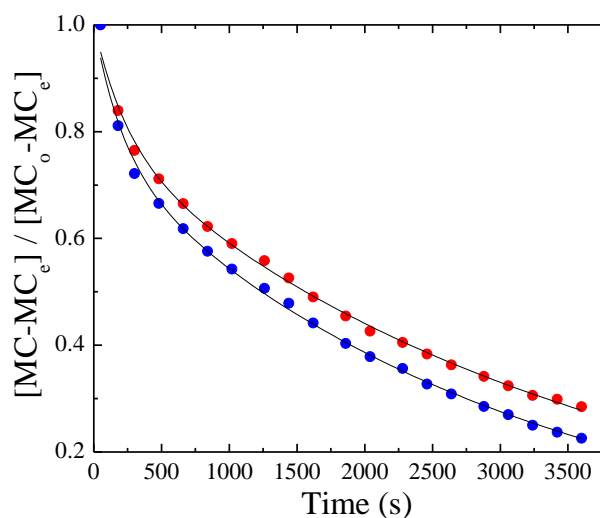
Figure 2.2.23c. Normalized fluorescence intensities of the MC_1 ($\bullet$, λ_{em} = 645 nm) and MC_2 ($\bullet$, λ_{em} = 626 nm) species of the PDMAEMA-*co*-PSPMA random copolymer. The solid black lines represent the fits to the data using eq. 2.2.1.

Both MC isomers follow a biexponential model of thermal relaxation, suggesting the existence of short- and long-lived species which are promoted by polarity

163

inhomogeneities in the microenvironment of the chromophores in accordance with the absorption studies discussed previously (Table 2.2.1) and variations in the free volume derive from the association of the copolymer in water (Figure 2.2.21). The MC_1 isomer with fluorescent maximum at 645 nm exhibited fading constants, $k_1 = 4.68 \times 10^{-3}$ s^{-1} and $k_2 = 3.37 \times 10^{-4}$ s^{-1} attributed to the short- and long-lived species, respectively, with mole ratio 24/76 (Table 2.2.2). The blue shifted mero form (MC_2) with a fluorescence maximum at 626 nm exhibited similar mole ratio of long- and short-lived isomers with MC_1. The fading rate constants of the short- and long-lived MC_2 species were determined to be 4.10×10^{-3} s^{-1} and 2.88×10^{-4} s^{-1}, respectively. These results show that the bleaching rates of the long-lived MC_1 and MC_2 isomers are an order of magnitude lower compared to that of the short-lived chromophores suggesting the significant effect of the microenvironment on the isomerization rates of the chromophores in agreement with the absorption data discussed previously (Table 2.2.1).

Table 2.2.2. Rate constants for the MC-to-SP isomerization process of the chromophores of the PDMAEMA-*co*-PSPMA random copolymer at 25 $^{\text{o}}$C.

λ_{max} (nm)[1]	Species	a[2]	b[3]	Rate constants[4]	
				k_1(s^{-1})[5]	k_2(s^{-1})[6]
645	MC_1	0.24	0.76	4.68×10^{-3}	3.37×10^{-4}
626	MC_2	0.22	0.78	4.10×10^{-3}	2.88×10^{-4}

[1]Fluorescence maximum of the MC band. [2]fraction of short-lived MC species (eq. 2.2.1). [3]fraction of long-lived MC isomers (eq. 2.2.1). [4]calculated from fluorescent emission spectra of the copolymers. [5]k_1 represents the rate constant for the short-lived MCs. [6]k_2 represents the rate constant for the long-lived species.

2.2.8   Conclusions

In this study, we report the synthesis of a photoresponsive random copolymer, comprising DMAEMA and SPMA moieties, by ATRP. The localized barriers inherent of the polymeric matrix establish a non-homogeneous microenvironment around the chromophores and affect both the photosensitive and fluorescent properties of the copolymers. Three bipolar species, X and two MC isomers, coexist in the copolymers

before and after stimulation with UV light and follow biexponential thermal bleaching rates. The presence of both X and MC species in close proximity promoted by the association of the copolymer chains in water, consisting FRET donor-acceptor pairs, facilitates the occurrence of intrachain and interchain energy transfer from the X to the MC isomers, while the polar environment established by polar microenvironment retards their thermal fading, extending the lifetime of the MC acceptors and the duration of the phenomenon. The SP-to-MC isomerization in the present system, can be achieved not only upon application of electromagnetic radiation but also chemically, by the addition of acid in the system accompanied with the formation of closed and open protonated species at higher acid concentrations.

2.2.9   References

(1)   Chen, J.; Zeng, F.; Wu, S.; Zhao, J.; Chen, Q.; Tong, Z. *Chem. Commun.* **2008**, 5580-5582.

(2)   Chen, J.; Zeng, F.; Wu, S. *ChemPhysChem* **2010**, *11*, 1036-1043.

(3)   Li, C.; Zhang, Y.; Hu, J.; Cheng, J.; Liu, S. *Angewandte Chemie* **2010**, *122*, 5246-5250.

(4)   Hu, J.; Dai, L.; Liu, S. *Macromolecules* **2011**, *44*, 4699-4710.

(5)   Ma, B.; Xu, M.; Zeng, F.; Huang, L.; Wu, S. *Nanotechnology* **2011** *22* 065501.

(6)   Park, I. S.; Jung, Y.-S.; Lee, K.-J.; Kim, J.-M. *Chem. Commun.* **2010**, *46*, 2859-2861.

(7)   Raymo, F. M.; Giordani, S. *J. Am. Chem. Soc.* **2001**, *123*, 4651-4652.

(8)   Neises, B.; Steglich, W. *Angew. Chem., Int. Ed.* **1978**, *17*, 522-524.

(9)   Weis, L. D.; Evans, T. R.; Leermakers, P. A. *J. Am. Chem. Soc.* **1968**, *90*, 6109-6118.

(10)   Wu, T.; Zou, G.; Hu, J.; Liu, S. *Chem. Mater.* **2009**, *21*, 3788-3798.

(11)   Wu, Y.; Zhang, C.; Qu, X.; Liu, Z.; Yang, Z. *Langmuir* **2010**, *26*, 9442-9448.

(12)   Ohno, K.; Morinaga, T.; Koh, K.; Tsujii, Y.; Fukuda, T. *Macromolecules* **2005**, *38*, 2137-2142.

(13)   Zhang, X.; Xia, J.; Matyjaszewski, K. *Macromolecules* **1998**, *31*, 5167-5169.

(14)   Fischer, H. *Chem. Rev.* **2001**, *101*, 3581-3610.

(15) Achilleos, D. S.; Vamvakaki, M. *Macromolecules* **2010**, *43*, 7073-7081.

(16) Piech, M.; Bell, N. S. *Macromolecules* **2006**, *39*, 915-922.

(17) Sumaru, K.; Kameda, M.; Kanamori, T.; Shinbo, T. *Macromolecules* **2004**, *37*, 4949-4955.

(18) Bobrovsky, A. Y.; Boiko, N. I.; Shibaev, V. P. *Adv. Mater.* **1999**, *11*, 1025-1028.

(19) Kim, C.-H.; Kim, D.; Lee, J.; Lee, K.-S. *Mol. Cryst. Liq. Cryst.* **2001**, *370*, 131-134.

(20) Yoshida, T.; Morinaka, A.; Funakoshi, N. *J. Chem. Soc., Chem. Commun.* **1986**, 437-438.

(21) Zhang, J. Z.; Schwartz, B. J.; King, J. C.; Harris, C. B. *J. Am. Chem. Soc.* **1992**, *114*, 10921-10927.

(22) Biteau, J.; Chaput, F.; Boilot, J. P. *J. Phys. Chem.* **1996**, *100*, 9024-9031.

(23) Krysanov, S. A.; Alfimov, M. V. *Chem. Phys. Lett.* **1982**, *91*, 77-80.

(24) Wohl, C. J.; Helms, M. A.; Chung, J. O.; Kuciauskas, D. *J. Phys. Chem. B* **2006**, *110*, 22796-22803.

(25) Wojtyk, J. T. C.; Wasey, A.; Kazmaier, P. M.; Hoz, S.; Buncel, E. *J. Phys. Chem. A* **2000**, *104*, 9046-9055.

(26) Vandewyer, P. H.; Hoefnagels, J.; Smets, G. *Tetrahedron* **1969**, *25*, 3251-3266.

(27) Ueda, M.; Kudo, K.; Ichimura, K. *J. Mater. Chem.* **1995**, *5*, 1007-1011.

(28) Kryszewski, M.; Nadolski, B.; North, A. M.; Pethrick, R. A. *J. Chem. Soc., Faraday Trans.* **1980**, *76*, 351-368.

(29) Levitus, M.; Talhavini, M.; Negri, R. M.; Atvars, T. D. Z.; Aramendía, P. F. *J. Phys. Chem. B* **1997**, *101*, 7680-7686.

(30) Hu, A. T.; Wang, W.-H.; Lee, H.-J. *J. Macromol. Sci., A* **1996**, *33*, 803-810.

(31) Richert, R.; Heuer, A. *Macromolecules* **1997**, *30*, 4038-4041.

(32) De Sousa, F. B.; Guerreiro, J. D. T.; Ma, M.; Anderson, D. G.; Drum, C. L.; Sinisterra, R. D.; Langer, R. *J. Mater. Chem.* **2010**, *20*, 9910-9917.

(33) Wojtyk, J. T. C.; Wasey, A.; Xiao, N. N.; Kazmaier, P. M.; Hoz, S.; Yu, C.; Lemieux, R. P.; Buncel, E. *J. Phys. Chem. A* **2007**, *111*, 2511-2516.

(34) Bütün, V.; Armes, S. P.; Billingham, N. C. *Polymer* **2001**, *42*, 5993-6008.

(35)   Zhou, J.; Li, Y.; Tang, Y.; Zhao, F.; Song, X.; Li, E. *J. Photochem. Photobiol., A* **1995**, *90*, 117-123.

(36)   Minami, T.; Tamai, N.; Yamazaki, T.; Yamazaki, I. *J. Phys. Chem.* **1991**, *95*, 3988-3993.

(37)   Sapsford, K. E.; Berti, L.; Medintz, I. L. *Angew. Chem., Int. Ed.* **2006**, *45*, 4562-4588.

(38)   Gouanvé, F.; Schuster, T.; Allard, E.; Méallet-Renault, R.; Larpent, C. *Adv. Funct. Mater.* **2007**, *17*, 2746-2756.

(39)   Chen, J.; Zeng, F.; Wu, S.; Chen, Q.; Tong, Z. *Chem. Eur. J.* **2008**, *14*, 4851-4860.

(40)   Shumburo, A.; Biewer, M. C. *Chem. Mater.* **2002**, *14*, 3745-3750.

(41)   Seefeldt, B.; Kasper, R.; Beining, M.; Mattay, J.; Arden-Jacob, J.; Kemnitzer, N.; Drexhage, K. H.; Heilemann, M.; Sauer, M. *Photochem. Photobiol. Sci.* **2010**, *9*, 213-220.

(42)   Zhu, L.; Zhu, M. Q.; Hurst, J. K.; Li, A. D. Q. *J. Am. Chem. Soc.* **2005**, *127*, 8968-8970.

(43)   Zhu, L.; Wu, W.; Zhu, M.-Q.; Han, J. J.; Hurst, J. K.; Li, A. D. Q. *J. Am. Chem. Soc.* **2007**, *129*, 3524-3526.

(44)   Rosario, R.; Gust, D.; Hayes, M.; Springer, J.; Garcia, A. A. *Langmuir* **2003**, *19*, 8801-8806.

CHAPTER 3

Inherent FRET properties of photoswitchable fluorescent hybrids enhanced by proteins

3.1 Introduction

The last two decades, advanced nanotechnology explores the integration of hard and soft structures into complex multiresponsive nanodevices whose function can be localized at the nanoscale. Highly attractive nowadays, is the synthesis of particles carrying photosensitive moieties, whose properties can be reversibly altered by applying a remote stimulus with spatial and temporal control, such as light irradiation of specific wavelength and known energy. A family of photosensitive molecules used for this purpose are the non-polar spiropyrans (SPs), which upon irradiation with visible light isomerize to the polar merocyanine (MC) form while irradiation of the latter with visible light induces the reformation of the SPs. The incorporation of SP moieties into colloidal particles provides a tool for sensing,[1] for the reversible phase transfer of particles[2] or for the subramolecular engineering of colloidal assemblies.[3] In particular, the SP-to-MC photoswitching of the chromophores within polymer brushes grown from the surface of silica particles has facilitated the formation of intraparticle aggregates and the fabrication of 2D assemblies[4] or 3D structures[5] of the colloids. The same principle has been utilized for the enhancement of the magnetization,[6] and the development of T2 agents[7] due to the photoinduced aggregation of SP-containing magnetic vesicles and iron oxide particles, respectively.

The photo-induced SP-to-MC isomerization has a great impact on the fluorescence properties of the systems. In particular, the SP isomer exhibits no visible absorption and thus no fluorescence while the MC form absorbs in the visible region and imparts red fluorescence with high emission rate and long photobleaching time[8] especially when embedded in hydrophobic cavities of hydrophilic nanoparticles.[9-10] The ability of the spiropyrans to switch reversibly between a non-fluorescent (off-state) and a fluorescent (on-state) is a key for various applications, including fluorescence microscopy, since fluorescence emission comprises a sensitive readout signal with excellent spatial resolution. This property enables the use of spiropyrans in photoactuated unimolecular logical switching attained reconstruction (PULSAR) microscopy to monitor their self-assembly in the nanometer scale.[8,11] Variations in the intensity and the lifetime of the fluorescent MC moieties can also provide a useful tool for studying MC-aminoacid interactions.[1]

Lately, the engineering of photo-modulated fluorescence nanoparticles (PFPs) have aroused tremendous interest due to their application as light addressable nanoscale devices in biotechnology for genetic detection, biological imaging and cell labeling. The fabrication of such systems can be achieved by the covalent incorporation of organic molecules, fluorescent donors and photosensitive acceptors in 3D-polymeric matrices,[12-14] the introduction of fluorescence diads into inorganic nanoparticles,[15] the solubilization of hydrophobic nitrobenzoxadiazolyl (NBD) derivatives in the core of self-assembed triblock copolymer carrying photochromic moieties[16] or the anchoring of photosensitive dyes or biological substances labeled with chromophores onto the surface of fluorescent nanoparticles.[17] SPs can be effectively combined with other fluorescent dyes or nanoparticles to synthesize systems which exhibit photo-regulated fluorescence resonance energy transfer (FRET) since upon photoswiching they can provide an ideal fluorescence switching pair which operates without extreme requirements. However, efficient energy transfer between the species can be achieved only when the emission band of the fluorophore (donor) and the absorption band of the chromophore (acceptor) overlap and their distance is within the Föster radius (generally, 1-10 nm).[18-19] SP-based FRET systems synthesized so far involved the covalent incorporation of different fluorescence donors such as 4-methamino-9-allyl-1,8-naphthalimide (MANI),[20] nitrobenzoxadiazolyl-based[21] or perylene dyes[10] within polymeric nanoparticles carrying spiropyran acceptors. FRET has been also observed when SP molecules[22] or SP-protein complexes[23] were immobilized onto the surface of quantum dots (QDs) causing their fluorescence quenching upon the light-induced SP-to-MC isomerization. The fluorescence quenching of nitrobenzoxadiazloyl derivatives located in the core of self-assembled triblock copolymers carrying SP moieties was also reported upon the photoswitching of the latter species to the MC isomers.[16]

Advancements in controlled radical polymerization (CRP) methods have a new potential in the synthesis of hybrid multiresponsive nanodevices. This is attributed to the fact that CRPs provide a high degree of synthetic flexibility towards the introduction of a variety of functional polymers including photoresponsive polymers onto the surface of different substances.[2,24] Nanoparticles bearing high surface-to-volume area and thus many active sites to initiate polymerization can be used as robust platforms for the

synthesis of polymer brushes bestowed with fluorophores and photoresponsive moieties for the development of efficient FRET systems. The controlled nature of the CRPs resulting in well defined macromolecular characteristics, grafting densities and film thicknesses onto the surface of the particles provides control over the quantity of the dyes covalently incorporated in the polymer shell thus the efficiency of the PFPs in contrast to core-shell particles synthesized by conventional radical polymerization methods. Covalent linkage of the photosensitive moieties within the polymer brush hinters any dye leakage and that is particular advantageous for biological applications. Recently, Shiyong et al. took advantage of the atom transfer radical polymerization (ATRP) synthetic flexibility to fabricate PNIPAM polymers brushes onto the surface of silica particles labeled in the inner and the outer shell with FRET donors 4-(2-acryloyloxyethylamino)-7-nitro-2,1,3-benzoxadiazole (NBDAE) and SP acceptors, respectively. The UV-induced SP-to-MC photoswitching allow the occurrence of a FRET process between the NBDAE and MC moieties while its efficiency was tuned taking into advantage the temperature-induced phase transition of the PNIPAM component to vary the donor-acceptor distance.[25]

Herein, we report a hard-and-soft hybrid nanosystem based on silica particles densely grafted with PSP-*co*-PDMAEMA random copolymer brushes by ATRP whose photochromism and fluorescence can be remotely modulated using a light-trigger of specific wavelength. These hybrids exhibit the unique feature of possessing two different bipolar fluorescent species, X and MC, upon stimulation with UV light, comprising the donor and acceptor dyad, which gained an "on" - "off" FRET process based on the photoinduced SP-to-MC isomerization and vice versa. In particular, the fluorescence emission intensity of the X donors is quenched when the non-fluorescent SP molecules are photoisomerized to the MC fluorophores while the FRET process is switched "off" upon the thermal MC-to- SP relaxation. The efficiency of the FRET process relies on the high degree of overlap of the donor emission and the acceptor absorption bands and the close proximity of the bipolar isomers embedded in the sterically crowded polymer brush. The homogeneous distribution of the donors and acceptors which are not topologically isolated in the outer and inner brush layer promotes higher FRET efficiencies. The advantages of these PFPs rely on the control over the quantity of the

chromophores introduced into the polymer brush, their dispersibility and function in the benign aqueous media of slightly basic pH established by the hydrophilic DMAEMA comonomer which in addition stabilizes the MC isomers and allows adequate switching rates of the photoisomers which enablie the read-out process. To the best of our knowledge, the inherent property of a brush system to exhibit FRET due to the generation and the efficient stabilization of X-MC donor-acceptor pairs by the surrounding microenvironment following the photo-stimulation of one single parent molecule is unprecedented. This property of the nanohybrids can be successfully applied for the detection of biological substances such as proteins and aminoacids. In particular the PFPs show excellent function in the presence of biomolecules such as proteins and aminoacids which however affect the FRET efficiency of the system; namely the presence of bovine serum albumin (BSA) in the aqueous dispersion of the hybrids was proved to enhance significantly the FRET efficiency. These features of the hybrids in addition with the absence of any dye leakage stress their potential applications as biological sensors and optically addressable devices.

3.2   Experimental Section

Materials. The monomer, 2-(dimethylamino)ethyl methacrylate (DMAEMA), the ligands, 1,1,4,7,10,10-hexamethyltriethylenetetramine (HMTETA) and *N,N,N',N'',N''*-pentamethyldiethylenetriamine (PMDETA), the initiator, ethyl 2-bromoisobutyrate (2-(EiB)Br), the metal salt, copper(I) chloride ($Cu^{(I)}Cl$), the aminoacid L-histidine and the protein bovine serum albumin (BSA), thriethoxysilane, triethylamine (TEA), allyl alcohol, the Karstedt catalyst, 2-bromoisobutyryl bromide, sodium bicarbonate ($NaHCO_3$), chloroform ($CDCl_3$) and dimethylformamide (DMF) were purchased from Aldrich, Germany. The salt magnesium sulfate ($MgSO_4$) was purchased from Fluka, Germany. The solvents, dichloromethane (DCM) and acetone were purchased from Fischer scientific, chloroform ($CHCl_3$) from Acros Organics, Belgium and acetonitrile from Panreac, Spain. Silica particles were purchased from Fiber Optic Center Inc. (USA).

Methods. DMAEMA was passed through a basic alumina column to remove the inhibitors before use. All solvents and triethylamine were stirred over CaH_2, were freshly distilled under vacuum and were kept under a dry nitrogen atmosphere until use. All

glassware was dried overnight at 160 °C prior to use. All other reagents were used as received.
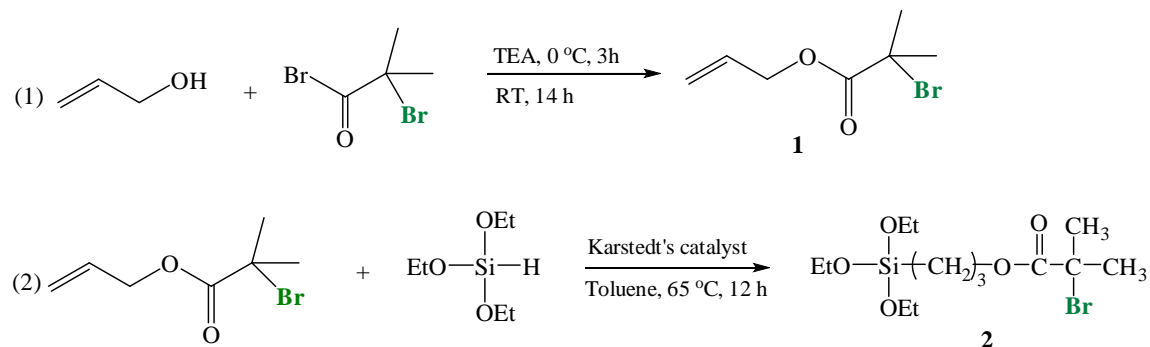
3.2.1 *Synthesis of the ATRP initiator [3-(2-bromoisobutyryl)propyl]triethoxysilane (BPTS).*

The ATRP initiator, [3-(2-bromoisobutyryl)propyl]triethoxysilane (BPTS) was synthesized followed a procedure described previously in the literature.[26-27] The reaction was accomplished in two steps (Scheme 3.1). The first step involves the reaction of allyl alcohol with an acyl bromide while the second step is a hydrosilylation to form the triethoxysilane initiator.

Allyl 2-bromoisobutyrate. For the synthesis of allyl 2-bromoisobutyrate, in a round bottom flask equipped with a side arm the allyl alcohol (1.8 mL, 0.026 mol), dry THF (64 mL) and triethylamine (4.5 mL, 0.032 mol) were transferred under continuous stirring and an inert nitrogen atmosphere. Next, the reaction mixture was cooled to 0 °C in an ice bath and 2-bromoisobutyryl bromide (4.0 mL, 0.032 mol) was added dropwise. The reaction was allowed to proceed for 3h at 0 °C and 14 h at RT. The produced salt was removed by vacuum filtration of the reaction mixture and the crude product was isolated by eliminating the excess of the starting reagent and the solvent via distillation under reduced pressure. The product was cleaned from the acid derived from 2-bromoisobutyryl bromide hydrolysis via fractional distillation utilizing a Glass Oven B-585 Kugelrohr at 95 °C. The compound was further diluted with 30 mL chloroform and washed several times with saturated $NaHCO_3$ aqueous solution (30 mL) and nanopure water (30 mL) to remove all traces of the acid. The solution was then dried over $MgSO_4$ and passed through a 0.2 μm syringe filter to remove the salt, while the solvent was evaporated to dryness to afford 1.8 g of a transparent liquid in 33 % yield which was characterized by ^{1}H NMR spectroscopy.

[3-(2-bromoisobutyryl)propyl]triethoxysilane (BPTS). In a two-necked flask equipped with a side arm the ally-2 bromoisobutyrate alcohol (1.8 g, 0.87 mmol) and dry toluene (4.6 mL) were charged under continuous stirring and nitrogen purging. Next, triethoxysilane (3.32 mL, 0.017 mol) was added in the reaction flask followed by the addition of 90 μL of Karstedt's catalyst solution. The reaction was allowed to proceed for

12 h at 65 °C before the BPTS was isolated by distilling the excess of the reagents and the solvent under reduced pressure and was characterized by ^{1}H NMR spectroscopy.

Scheme 3.1. Synthesis of the BPTS initiator via a two-step reaction; first the synthesis of allyl 2-bromoisobutyrate (1) followed by catalytic hydrosilylation to form the BPTS (2).

3.2.2   *Self-assembled monolayer of the initiator molecules onto the silica particles.*

The surface functionalization of the silica particles with the reactive BPTS molecules was accomplished as following: 10 g of silica particles were dried under vacuum at 110 °C for 12 h and were then suspended in 200 mL of dry chloroform using ultrasonic agitation for 3 h, under an inert atmosphere. Next, 0.25 mL of BPTS were transferred in the particles dispersion and the condensation reaction was allowed to proceed for 2 days at RT (Scheme 3.2).
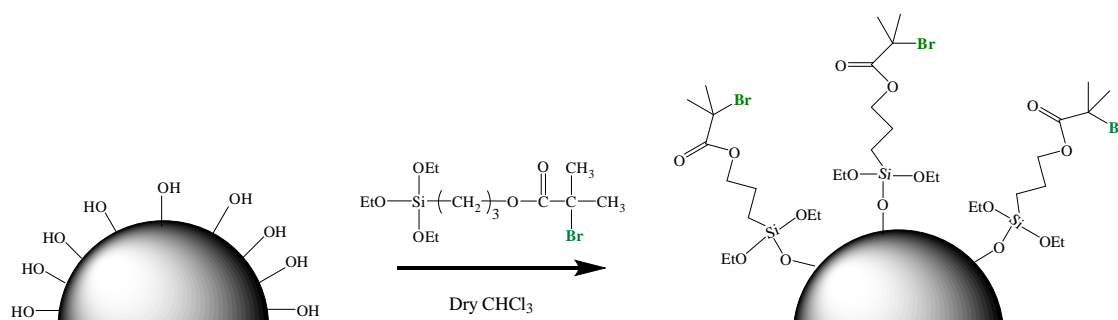

Scheme 3.2. Anchoring of the BPTS initiator onto the curved surface of the silica particles

The initiator-coated particles were purified by a centrifugation/decantation sequence using chloroform (5 cycles) and THF (5 cycles) and were sealed in the dry state, in a dark container, until use.

174

3.2.3 Polymerizations.

3.2.3.1 SiO₂-g-PDMAEMA

Two core-shell SiO$_2$-*g*-PDMAEMA hybrid particles were synthesized by the homopolymerization of DMAEMA from the surface of the initiator-functionalized silica particles via si-ATRP (Scheme 3.3).
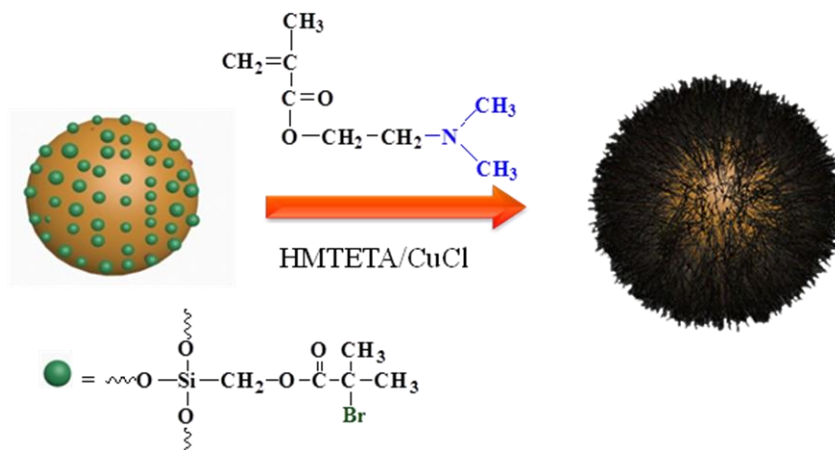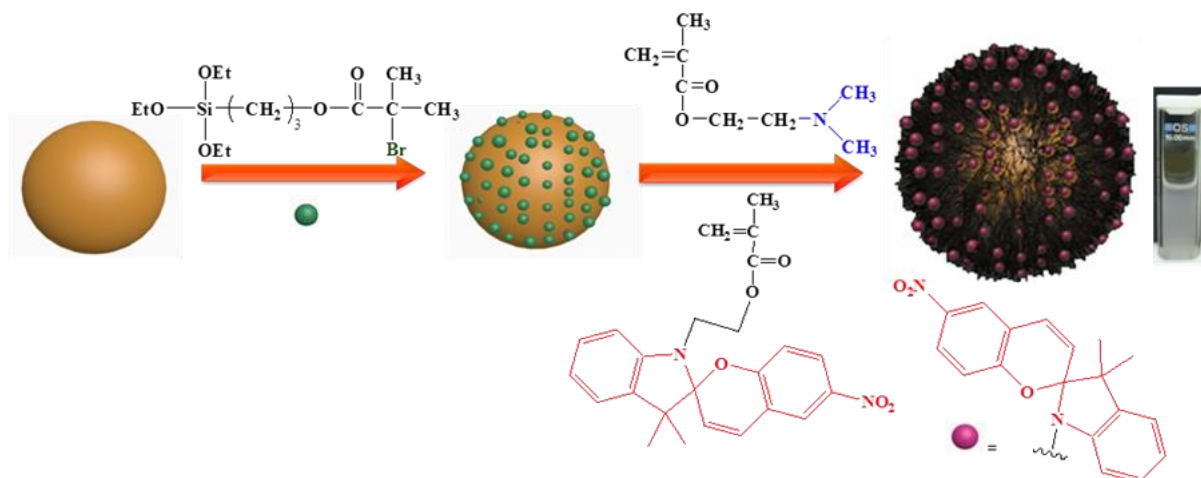

Scheme 3.3. Synthetic procedure followed for the preparation of the SiO$_2$-*g*-PDMAEMA core-shell particles in bulk at RT.

First, 0.40g of initiator-coated SiO$_2$ particles were suspended in 10 mL dry DMF utilizing ultrasonic agitation and were solvent exchanged to DMAEMA by consecutive centrifugation and redispersion cycles. In a typical solvent-free polymerization, the dispersion of the particles in DMAEMA (3.65 g, 0.023 mol) was placed under an inert nitrogen atmosphere and continuous stirring. Next, the free initiator, ethyl 2-bromoisobutyrate (2-(EiB)Br) (7.2 μL, 4.85 × 10^{-5} mol), the ligand, 1,1,4,7,10,10-hexamethyltriethylenetetramine (HMTETA) (79.11 μL, 2.90 × 10^{-4} mol) and the metal salt, copper(I) chloride (CuCl) (0.014g, 1.41 × 10^{-4} mol) were transferred in the reaction flask under a dry nitrogen flow. The reaction mixture was degassed by five freeze-pump-thaw cycles and the reaction was allowed to proceed at RT until the full consumption of the monomer. Next, the polymerization mixture was exposed to air, was diluted with THF and was centrifuged to isolate the polymer-coated particles. The free polymer in the THF supernatant was precipitated in hexane and was characterized by ^{1}H NMR

175

spectroscopy and gel permeation chromatography (GPC). The polymer-coated SiO_2 particles were purified by a centrifugation/decantation sequence using chloroform (4 cycles), DCM (4 cycles), acetonitrile (4 cycles) and a *N,N,N',N'',N''*-pentamethyldiethylenetriamine (PMDETA)/acetonitrile mixture (30:70, v/v) (5 cycles) to remove any residual copper species, ligand and unreacted monomer. The hybrids were dispersed in acetonitrile (1.37 wt % solution) and were sealed in a dark container under N_2, until use. This procedure resulted in SiO_2-*g*-PDMAEMA hybrid particles with 36 wt% polymer content. A similar procedure was followed for the synthesis of the second sample of SiO_2-*g*-PDMAEMA hybrid particles by decreasing the molar concentration of the 2-(EiB)Br free initiator from 33.1 to 12.3 mol % with respect to the total concentration of bound and unbound initiator while keeping the molar ratio of the other reagents constant which resulted in hybrid particles with 45 wt% polymer content.

3.2.3.2   *SiO$_2$-g-(PDMAEMA-co-PSPMA)*

Three SiO_2-*g*-(PDMAEMA-*co*-PSPMA) hybrids were synthesized by the random copolymerization of DMAEMA and SPMA from the surface of the silica particles via si-ATRP (Scheme 3.4). First, 0.40g of initiator-coated SiO_2 particles were suspended in 10 mL dry DMF utilizing ultrasonic agitation and were solvent exchanged to DMAEMA by consecutive centrifugation and redispersion cycles. In a typical solvent-free polymerization, the dispersion of the particles in DMAEMA (3.47g, 0.022 mol) prepared under an inert atmosphere and continuous stirring, were fed with SPMA (0.49g, 1.16×10^{-3} mol). Next, the free initiator, ethyl 2-bromoisobutyrate (2-(EiB)Br) (7.2 μL, 4.85×10^{-5} mol), the ligand, 1,1,4,7,10,10-hexamethyltriethylenetetramine (HMTETA) (79.11 μL, 2.90×10^{-4} mol) and the metal salt, copper(I) chloride (CuCl) (0.014g, 1.41×10^{-4} mol) were transferred in the reaction flask under a dry nitrogen flow. The reaction mixture was degassed by five freeze-pump-thaw cycles and the reaction was allowed to proceed at RT until the full consumption of the two comonomers.

Scheme 3.4. Schematic representation of the synthetic procedure followed for the preparation of the photoresponsive SiO$_2$-*g*-(PDMAEMA-*co*-PSPMA) core-shell structures.

Next, the crude reaction mixture was exposed to air, was diluted with THF and was centrifuged to isolate the polymer-coated particles. The free polymer in the THF supernatant was precipitated in hexane and was characterized by ^{1}H NMR spectroscopy and gel permeation chromatography (GPC). The polymer-coated SiO$_2$ particles were purified by a centrifugation/decantation sequence using chloroform (4 cycles), DCM (4 cycles), acetone (4 cycles), acetonitrile (4 cycles) and a *N,N,N',N'',N''*-pentamethyldiethylenetriamine (PMDETA)/acetonitrile mixture (30:70, v/v) (5 cycles) to remove any residual copper species, ligand and unreacted monomer. The hybrids were dispersed in acetonitrile (1.37 wt% solution) and were sealed in a dark container under N$_2$ until use. A similar procedure was followed for the synthesis and the purification of the other SiO$_2$-*g*-(PDMAEMA-*co*-PSPMA) hybrids while the moles of reagents used for the synthesis of the core-shell structures are summarized in Table 3.1. It should be noted that 0.4 and 0.3 g of initiator-coated silica particles were used for the synthesis of hybrids 1-2 and hybrid 3, respectively.

Table 3.1. Moles of the reagents used for the synthesis of the SiO_2-g-(PDMAEMA-co-PSPMA) hybrids.

Sample	CuCl	HMTETA	BPTS	2-(EiB)Br	Monomer	
					DMAEMA	SPMA
Hybrid 1	1.94×10^{-4}	3.88×10^{-4}	9.70×10^{-5}	9.70×10^{-5}	2.95×10^{-2}	1.55×10^{-3}
Hybrid 2	1.41×10^{-4}	2.82×10^{-4}	9.70×10^{-5}	4.85×10^{-5}	2.22×10^{-2}	1.16×10^{-3}
Hybrid 3	8.49×10^{-5}	1.70×10^{-4}	7.28×10^{-5}	1.21×10^{-5}	1.09×10^{-2}	2.72×10^{-3}

3.2.4 *Characterization of the hybrids*

Gel Permeation Chromatography. The molecular weight (MW) and molecular weight distribution (MWD) of the free polymers were determined by gel permeation chromatography (GPC) (Thermo Finnigan pump). The instrument was equipped with two PL mixed-D and mixed-E columns operating at an oven temperature of 40 ^{o}C. THF was used as the eluent at a flow rate of 1 mL min^{-1}. The refractive index signal was measured using a Shodex RI-101 refractive index detector. A series of narrow MWD linear poly(methyl methacrylate) standards ranging from 850 to 342,900 g $\times$ mol^{-1} were used for the GPC calibration.

^{1}H NMR Spectroscopy. The composition of the hybrids in the two comonomers was calculated by determining the composition of the free polymer by ^{1}H NMR spectroscopy using a 300 MHz Avance Bruker NMR spectrometer operating in a Fourier transform mode. CDCl$_3$ was used as the solvent and tetramethylsilane (TMS) served as the internal reference for the ^{1}H NMR measurements.

Thermogravimetric analysis (TGA). TGA was performed under a nitrogen atmosphere utilizing a Perkin-Elmer TGA analyzer (Diamond Pyris model) at a scan rate of 10 °C/min in the temperature range from 25 to 700 ^{o}C.

Fourier Transform Infrared Spectroscopy. The Attenuated Total Reflectance Fourier Transfer Infrared (ATR FTIR) spectra were recorded on a Nicolet 6700 optical spectrometer equipped with a DTGS KBr detector. The spectra were collected in the range of 400-4000 cm^{-1} at a resolution of 4 cm^{-1} and were analyzed using the Omnic software.

Potentiometric Titration. The titration curve of the SiO$_2$-*g*-(PDMAEMA-*co*-PSPMA) hybrids in the pH range from 2 to 11.5 was obtained by monitoring the increase of the solution pH upon addition of 5 μL aliquots of 0.1 M NaOH to a 0.21 wt % colloidal dispersion.

Scanning Electron Microscopy (SEM). The morphology of the core-shell particles was studied by field emission scanning electron microscopy (FESEM; JEOL JSM 7000F) at an accelerating voltage 10-30 kV. A droplet of the particles dispersion was deposited on a silicon wafer, evaporated at RT and sputter coated with a 10 nm thick Au layer to minimize charging.

Transmission electron microscopy (TEM). TEM images were obtained on a JEOL 200-CX instrument operating at 120 kV. For this purpose, a droplet of the nanoparticles dispersion was placed on a carbon-coated copper grid and dried under atmospheric pressure.

Dynamic light scattering (DLS). The hydrodynamic diameter (D_h) of the precursor silica and the hybrid core-shell particles was determined by DLS using a 3D LS Spectrometer from LS Instrument with a HeNe laser operating at 632.8 nm at scattering angles 30°, 50°, 70°, 90°, 110° and 130°. The average particle sizes were obtained from the intensity autocorrelation functions by KWW analysis.

UV/vis absorption studies. The photoinduced SP-to-MC isomerisation of the chromophores embedded within the PDMAEMA-*co*-PSPMA polymer brushes and the thermal relaxation of the MC isomers as a function of time were studied using a Lambda 25 Perkin-Elmer UV/vis spectrophotometer in the wavelength range 250-850 nm in solvents of different polarity. For this purpose the absorption spectra of 8.7×10^{-2} wt% dispersions of the SiO$_2$-*g*-(PDMAEMA-*co*-PSPMA) in water and in acetonitrile were recorded upon irradiation with UV light utilizing a Spectroline hand-held UV lamp operating at 365 nm (8 watt) for 49 s. The kinetic rate constants of the MC thermal bleaching process were determined by collecting the absorption spectra of a dispersion of the core-shell hybrids kept in the instrument' s chamber, at various time intervals at RT.

The acidochromic properties of the SiO$_2$-*g*-(PDMAEMA-*co*-PSPMA) core-shell hybrids were studied by monitoring the changes in the UV/vis absorption spectrum of

179

4.00×10^{-2} wt% aqueous dispersion of the hybrids upon the addition of 1-7 μL aliquots of 0.1 M and 1 M HCl.

Fluorescence Measurements. Fluorescence emission spectra of 0.11 wt% aqueous dispersion of the hybrids before and after illumination with UV light were recorded on a Jobin-Yvon / Horiba Fluoromax‑P scanning spectrofluorometer following excitation at 521 nm with a Xenon arc lamp. The slit widths were set at 1 nm for excitation and 5 nm for emission. Similarly, the fluorescent emission spectra of the hybrids were recorded in the presence of 87 μM BSA and L-histidine. The kinetic rate constants of the MC bleaching process in the presence and absence of the biological substances were calculated by monitoring the emission spectra of the core-shell hybrids, following their thermal relaxation in the instrument' s chamber, at various time intervals at RT.

3.3   Results and Discussion

3.3.1   *Synthesis of the ATRP initiator [3-(2-bromoisobutyryl)propyl]triethoxysilane (BPTS)*
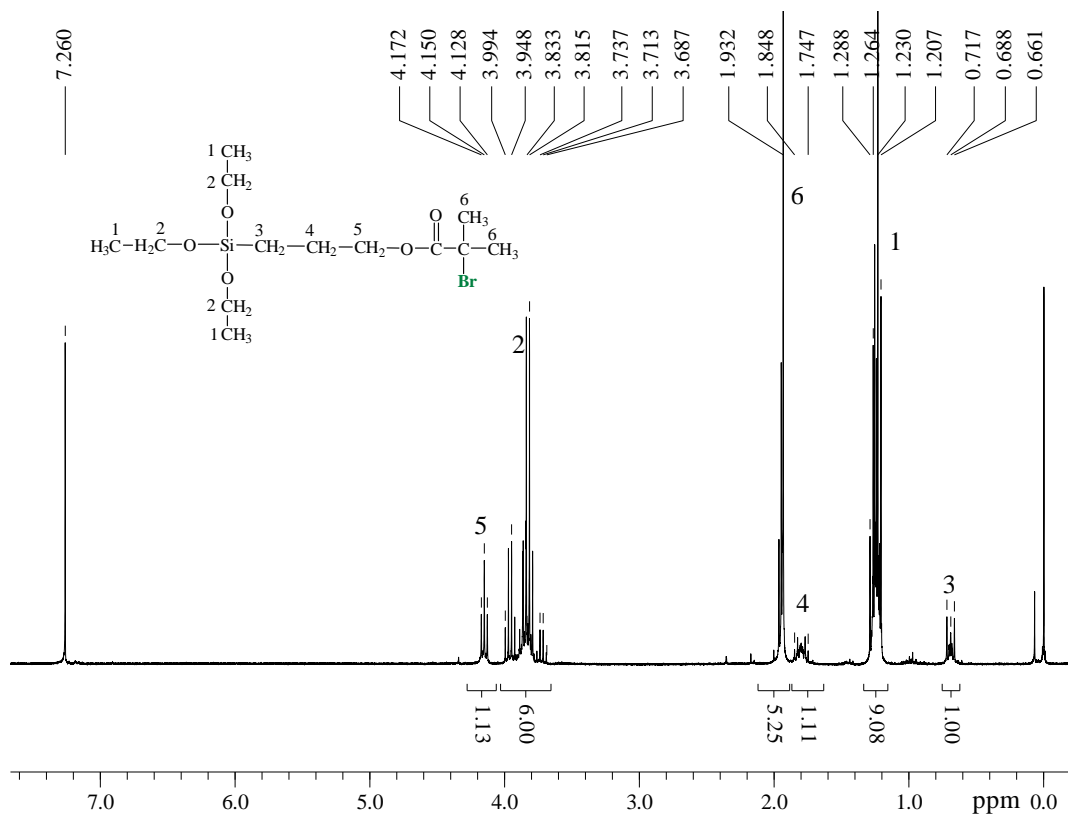
The synthesis of the BPTS initiator, bearing functionalities capable of initiating an ATRP reaction and anchoring onto inorganic substrates, was accomplished via a two step synthesis which involved the esterification reaction of an allyl alcohol with an acid bromide to obtain the allyl 2-bromoisobutyrate, which further underwent a hydrosilylation reaction to afford the BPTS. The successful synthesis was monitored by ^{1}H NMR after each reaction step. Figure 3.1 shows the ^{1}H NMR spectrum of the allyl 2-bromoisobutyrate; (300 MHz, CDCl$_3$) δ 1.95 (6H, H-5) 4.66-4.69 (2H, H-4), 5.26-5.41 (2H, H-1, H-2), 5.87-6.00 (1H, H-3). Comparison of the ^{1}H NMR spectrum of the product to that of the precursor allyl alcohol; (300 MHz, CDCl$_3$) δ 4.15 (2H, H-4), 5.12-5.31 (2H, H-1, H-2), 5.94-6.07 (1H, H-5) (see Appendix, Figure 4), indicated that the methylene protons H-4 of the allyl 2-bromoisobutyrate resonate about 0.5 ppm downfield compared to those of the allyl alcohol. This observation, in addition with the appearance of a new band at 1.95 ppm attributed to the methyl protons H-5 of the bromoisobutyrate group verified the synthesis of the desired molecule.
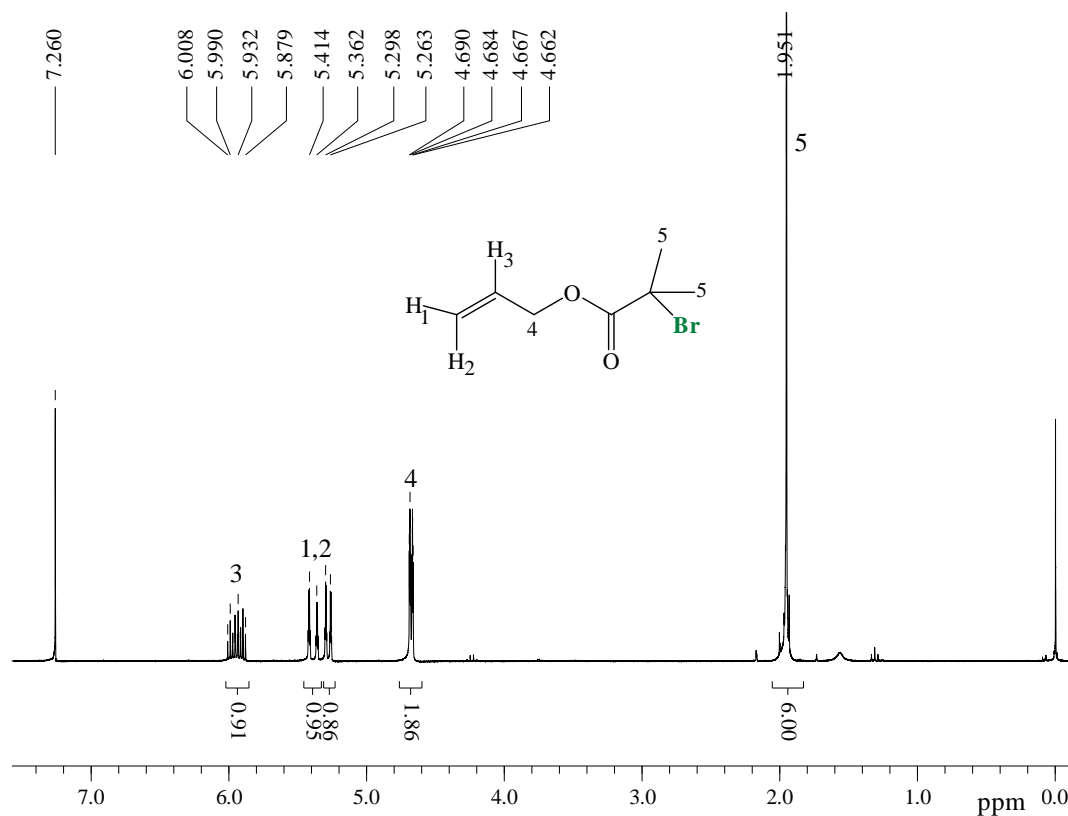
Figure 3.1. ^{1}H NMR spectrum of allyl 2-bromoisobutyrate in CDCl$_3$

The allyl 2-bromoisobutyrate was further reacted with triethoxysilane to afford the BPTS molecule. The ^{1}H NMR spectrum of the product was recorded (300 MHz, CDCl$_3$) δ 0.66 (1H, H-3), 1.20-1.28 (9H, H-1), 1.74-1.84 (2H, H-4), 1.93 (6H, H-6), 3.68-3.99 (6H, H-2), 4.12 (2H, H-5) (Figure 3.2) and compared to that of the precursor triethoxysilane (300 MHz, D$_2$O) δ 1.24 (9H, H-3), 3.82-3.89 (6H, H-2), 4.29 (1H, H-1) (see Appendix, Figure 5) and that of the allyl 2-bromoisobutyrate, discussed above. The disappearance of the vinyl protons H-(1-3) observed in the spectrum of the allyl 2-bromoisobutyrate at 5.26-5.41 and 5.87-6.00 ppm and the appearance of two new signals attributed to the methylene protons H-3 and H-4 at 0.66 and 1.74-1.84, respectively, suggest the successful synthesis of the initiator molecule. Moreover, the upfield shift of the methylene protons H-5 next to the ester group and the appearance of the characteristic signals of the triethoxysilane moiety at 1.20-1.28 and 3.68-3.99 ppm attributed to H-1and H-2, respectively support the above findings.

181

Figure 3.2. ^{1}H NMR spectrum of BPTS in CDCl$_3$

3.3.2 *Synthesis of PDMAEMA homopolymer brushes onto SiO$_2$ particles by ATRP*

The BPTS initiator was further anchored onto the surface of the silica particles via the condensation reaction of the ethoxy groups of the molecule with the hydroxyl functionalities of the inorganic particles. Next, the initiator-coated silica particles were used as multifunctional initiators for the copper-mediated si-ATRP of DMAEMA to obtain core-shell hybrids with PDMAEMA homopolymer chains in the shell (Scheme 3.3).The polymerization was conducted in the presence of free initiator, ethyl 2-bromoisobutyrate (2-(EiB)Br), the content of which was varied in order to obtain colloids with different polymer content; namely two SiO$_2$-*g*-PDMAEMA hybrid core-shell hybrids were synthesized by decreasing the molar concentration of the 2-(EiB)Br from 33.1 to 12.3 mole % with respect to the total concentration of bound and unbound initiator while keeping the degree of polymerization constant.

The successful synthesis of the polymer brushes onto the surface of the silica particles was qualitatively confirmed by ATR-FTIR analysis. Figure 3.3 shows the ATR-

FTIR spectrum of the core-shell hybrids plotted against that of the initiator-coated colloids. The successful synthesis of DMAEMA chains onto the surface of SiO_2 nanoparticles was verified by the appearance of a resonance at 1723 cm^{-1} which is characteristic of the C=O stretching vibration of the ester group.[28] The ATR-FTIR spectrum of the hybrid particles also showed two peaks at 2948 and 2819 cm^{-1} assigned to aliphatic C-H stretching vibrations of the -CH_3 and -CH_2 groups, respectively suggesting the presence of the organic coating onto the surface of the colloids.[29] This finding was further supported by the appearance of the bands at 1485, 1455 and 1393 cm^{-1} assigned to C-H bending vibrations of the aliphatic component.
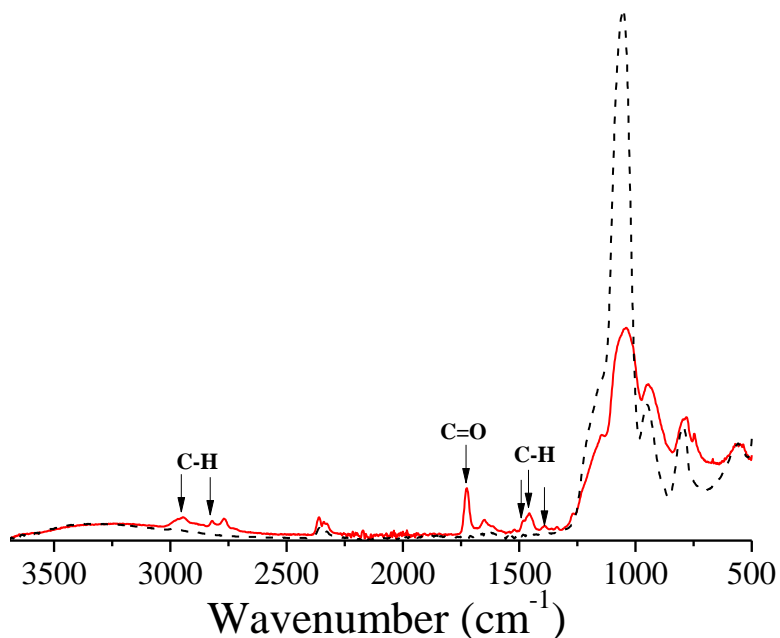
Figure 3.3. ATR-FTIR spectra of the silica particles modified with the BPTS initiator (**...**), and the SiO_2-g-PDMAEMA1 hybrid particles (–).

The molecular weights (M_n's) and the molecular weight distributions (M_w/M_n, PDIs) of the free PDMAEMA chains synthesized in parallel with the grafting of the PDMAEMA chains from the surface of the silica particles were determined by GPC (Figure 3.4). The polymer chains grown from the surface of SiO_2-g-PDMAEMA1 exhibited a M_n of 66,200 g/mol and a PDI of 1.21, while upon decreasing the

concentration of the free initiator in the reaction mixture by 20.8 mol %, longer polymer chains (M_n = 94,200 g/mol, PDI = 1.4) were grown from the surface of the particles for the SiO$_2$-g-PDMAEMA2 hybrid. The PDIs of the polymer chains are comparable with those reported recently for short PDMAEMA chains grafted onto silica particles in acetone[30] and for PDMAEMA chains grown from polystyrene latex particles in an acetone/water mixture by ATRP.[31-32] The increase of the PDI upon decreasing the free initiator content in solution is related with the fact that longer chains were grown from the surface of the particles, leading to extended polymerization times which favor possible side reactions and the broadening of the PDIs.
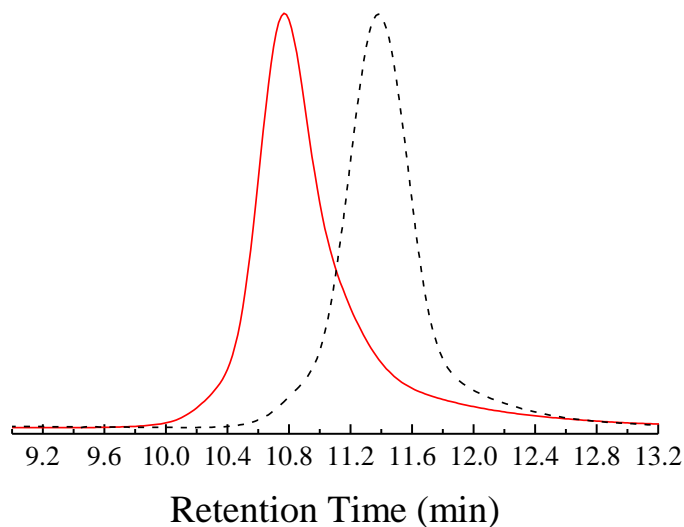
Figure 3.4. GPC traces of the unbound PDMAEMA obtained during the synthesis of the SiO$_2$-g-PDMAEMA1 (---) and the SiO$_2$-g-PDMAEMA2 (–) hybrid particles.

The organic content of the core-shell hybrids was quantitatively determined by TGA. Figure 3.5 shows the TGA thermograms of the PDMAEMA-coated silica particles plotted against the thermogram of the initiator-coated particles and that of a PDMAEMA homopolymer. The hybrids, SiO$_2$-g-PDMAEMA1 and SiO$_2$-g-PDMAEMA2, showed a weight loss of 36 and 45 wt%, respectively, in the temperature range 200-680 $^\circ$C, attributed to the PDMAEMA component. The thermal decomposition of the polymer of the hybrid particles followed a two step weight loss process similar to that of the PDMAEMA homopolymer (Figure 3.5). The polymeric content of the hybrid particles

increased by 9 wt% upon decreasing the molar concentration of the free-initiator from 33.1 to 12.3 mol% in the reaction mixture while keeping the monomer concentration constant. This is because for lower free initiator concentration, longer polymer chains are grown from the surface in order to achieve the full conversion of the monomer leading to the observed increase of the polymer content of the hybrids.
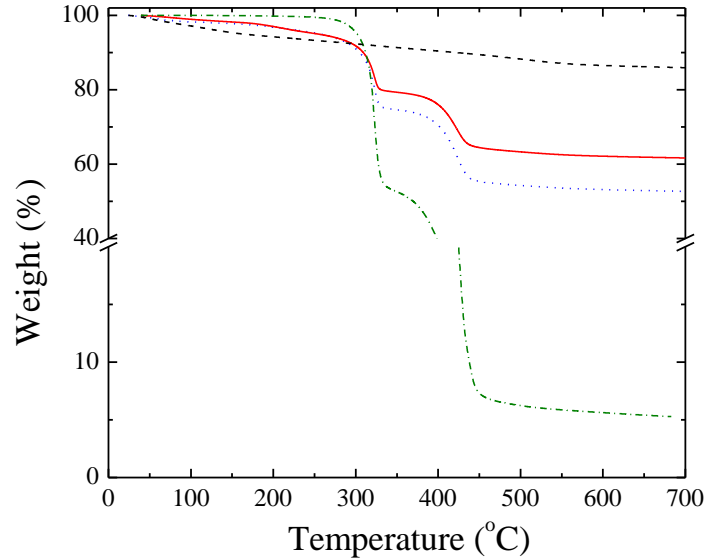
Figure 3.5. TGA thermograms of the silica particles modified with the BPTS initiator (---), the SiO$_2$-g-PDMAEMA1 (—) and SiO$_2$-g-PDMAEMA2 (...) hybrid particles and a PDMAEMA homopolymer (..).

The grafting density σ (chains/nm^2) of the PDMAEMA chains onto the surface of the silica particles was found from the TGA and GPC results to be 0.42 and 0.44 chains/nm^2 for the hybrid SiO$_2$-g-PDMAEMA1 and SiO$_2$-g-PDMAEMA2 particles, respectively, according to equation 3.1:

$$\sigma = \frac{\left(\dfrac{m_{poly.}}{M_n}\right) \times N_A}{m_{part.} \times \left(\dfrac{A}{m}\right)} \qquad \text{(eq. 3.1)}$$

where $m_{poly.}$ and $m_{part.}$ is the mass of the polymer and the silica particles in the hybrids as determined by TGA, M_n is the number-average molecular weight of the chains grafted

185

onto the surface of the nanoparticles measured by GPC, N_A is the Avogadro constant and *A/m* is the surface area of the nanoparticles per gram calculated assuming that the particles are spheres with diameter 250 nm and density 2 g/cm^3 according to equation 3.2:

$$\frac{A}{m} = \frac{4\pi R^2}{\rho \times V}$$
(eq. 3.2)

where *A*, *m*, *R*, ρ and *V* are the surface area, the mass, the radius, the density and the volume of the particles, respectively. This means that the distance between the grafting points is almost constant at 1.5 nm for both samples, while the number of chains per particle was determined to be 83700 and 85425 for the hybrid SiO$_2$-*g*-PDMAEMA1 and SiO$_2$-*g*-PDMAEMA2 particles, respectively by equation 3.3:

$$\text{Number of chains/particle} = (4\pi R^2) \times \sigma$$
(eq. 3.3)

where *R* is the diameter of the particles and σ the grafting density (chains/nm^2) of the chains onto the particles' surface. On the other hand, the grafting density of the BPTS initiator was calculated to be 0.33 nm^2/initiator following eq. 3.1 by determining the initiator and particle mass by TGA and the molecular weight of the initiator taking into account the fact that one ethoxy groups is substracted upon the condensation of the initiator with the hydroxyl groups of the silica surface. Thus, an initiator efficiency of 14.3 and 14.6 % for the hybrid SiO$_2$-*g*-PDMAEMA1 and SiO$_2$-*g*-PDMAEMA2 particles, respectively was found. The above results suggest that the grafting density and thus the distance of the grafting points, the number of chains per particle and the initiation efficiency are similar for the two samples, which differ only on the chain length of the polymer grown from the surface of the nanoparticles as evidenced by GPC.

The morphology of the hybrids was studied by transmission electron microscopy (TEM) and field-emission scanning electron microscopy (FESEM) (Figure 3.6).
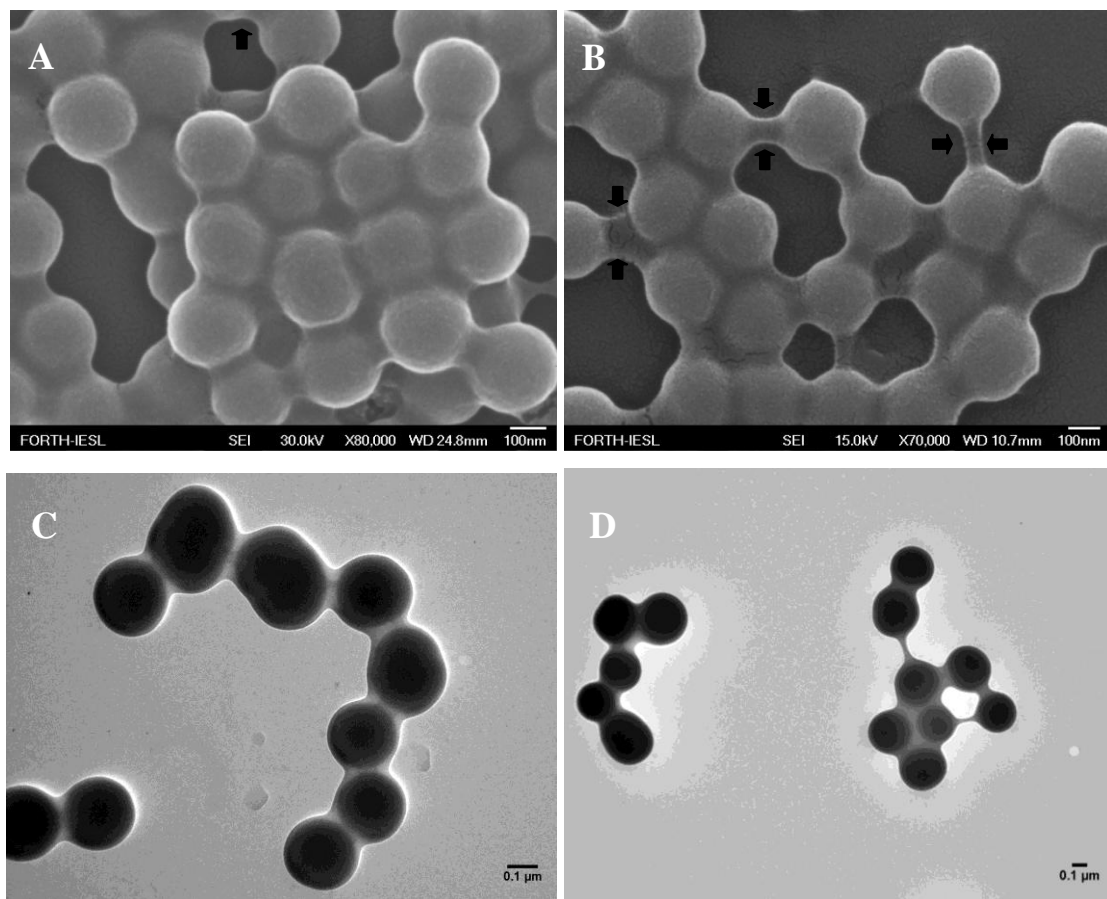
Figure 3.6. FESEM (A and B) and TEM (C and D) images of the SiO$_2$-*g*-PDMAEMA1 (A and C) and SiO$_2$-*g*-PDMAEMA2 (B and D) hybrid particles.

The SEM images (Figure 3.6A and B) showed well defined hybrid particles exhibiting a uniform conformal coating onto the surface of the particles with diameter 237 ± 9 and 247 ± 10 nm for SiO$_2$-*g*-PDMAEMA1 and SiO$_2$-*g*-PDMAEMA2, respectively. At higher concentrations the colloids formed connections between the particles, attributed to the polymer component, as indicated by the arrows in Figures 3.6A and B. The TEM images of the particles (Figure 3.6C and D) showed that the hybrids are regular and of core-shell structure with the lighter color polymer shell surrounding the dark colored silica core. The diameter of the hybrids in the dry state was calculated by TEM to be 233 ± 4 and 301 ± 16 nm for SiO$_2$-*g*-PDMAEMA1 and SiO$_2$-*g*-PDMAEMA2, respectively, which is in good agreement with the SEM results. Moreover, the increase in the size of the hybrid particles for SiO$_2$-*g*-PDMAEMA2 was attributed to the longer polymer chains onto the surface of the inorganic silica particles as indicated by the GPC and TGA data, above.

187

3.3.3 *Synthesis of PDMAEMA-co-PSPMA random copolymer brushes onto SiO₂ particles by ATRP*

The synthesis of PDMAEMA-*co*-PSPMA brushes form the surface of silica particles following the solvent-free polymerization conditions described above was also investigated. For this purpose, multifunctional silica-based ATRP initiators were synthesized via the condensation reaction of [3-(2-bromoisobutyryl)propyl]triethoxysilane (BPTS) with the hydroxyl functionalities of the inorganic colloids and were further reacted with DMAEMA and SPMA in the presence of the CuCl/HMTETA transition metal complex, to obtain the final photoresponsive hybrid particles (Scheme 3.4). Three hybrids were synthesized; two core-shell structures, SiO_2-*g*-(PDMAEMA-*co*-PSPMA)1 and 2, carrying similar SPMA contents, 4.8 and 6.1 mole%, respectively and grafted copolymer chains of M_n = 57,000 and 66,000 g/mol, respectively. However, hybrid 3 carried a higher SPMA content of 11.5 mol % units and longer PDMAEMA-*co*-PSPMA copolymers chains of M_n = 80,500 g/mol.

The successful synthesis of the polymer brushes onto the surface of the silica particles was qualitatively confirmed by ATR-FTIR analysis. Figure 3.7 shows the ATR-FTIR spectrum of the core-shell hybrids plotted against that of the initiator- and PDMAEMA-coated silica particles synthesized following a similar procedure. The appearance of the bands at 2944 and 2820 cm^{-1} assigned to the aliphatic C-H stretching vibrations of the -CH₃ and -CH₂ groups, respectively indicated the presence of the organic component onto the surface of the silica particles. This was further supported by the resonance peak at 1727 cm^{-1} attributed to the ester carbonyl groups and the bands at 1455 and 1389 cm^{-1} assigned to the C-H bending vibration of both constituents. The successful copolymerization of the SP comonomer within the polymer brushes is verified by the appearance of a number of characteristic features of the SP structure in the ATR-FTIR spectrum of the hybrids indicated by the arrows in the inset of Figure 3.7. The bands at 1612 and 1577 cm^{-1} are attributed to the C=C stretching vibrations of the aromatic ring of the molecule while typical symmetric and antisymmetric stretching vibrations of the aryl nitro group are observed at 1521 and 1336 cm^{-1}. The latter band overlaps with the bending vibration modes of the tertiary amine groups of PDMAEMA, observed in the FTIR spectrum of the PDMAEMA-coated silica particles but not in that of the colloids modified with the initiator. The alkyl bending vibrations of the molecule

emerge at 1481 cm^{-1}. Another characteristic SP band comprises the symmetric C-O-C stretching of the cyclic ether at 1267 cm^{-1}.[33-35] Even though the SP content in the polymer brushes is low the characteristic peaks of the molecule can be clearly seen in the FTIR spectra of the hybrids in contrast to what has been reported in previous studies.[25]
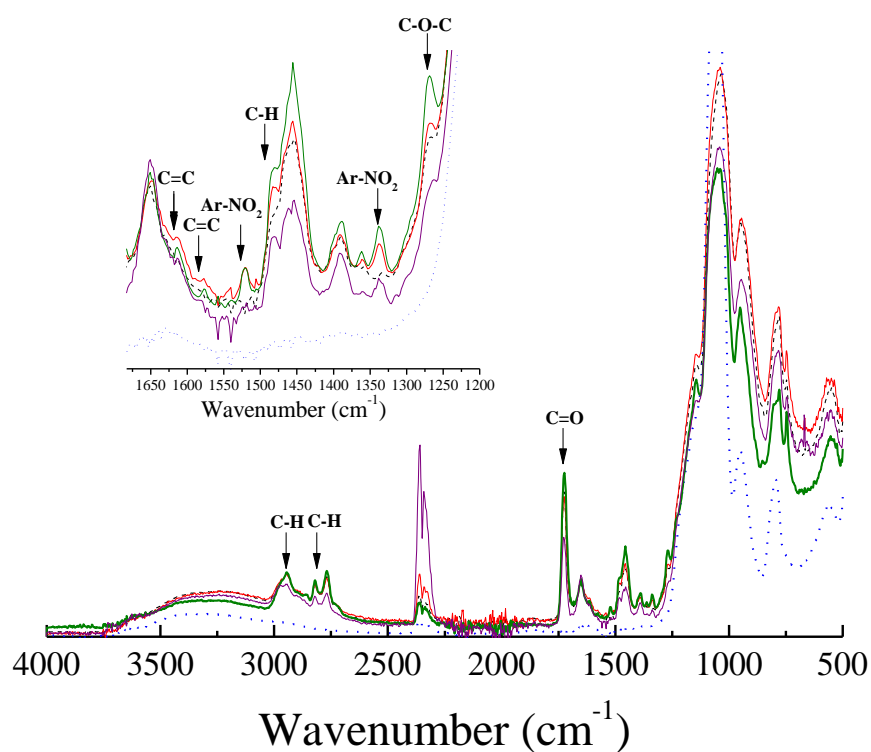
Figure 3.7. ATR-FTIR spectra of the silica particles modified with the BPTS initiator (…), the SiO_2-*g*-PDMAEMA (---) and SiO_2-*g*-(PDMAEMA-*co*-PSPMA)1 (—), SiO_2-*g*-(PDMAEMA-*co*-PSPMA)2 (—) and SiO_2-*g*-(PDMAEMA-co-PSPMA)3 (—) core-shell particles. The inset shows the characteristic vibrations of the SPMA functional groups indicated by the arrows.

The composition of the PDMAEMA-*co*-PSPMA random copolymer brushes was determined from the ^{1}H NMR spectra of the free polymers. In particular, the integrals of the peaks attributed to the methylene protons next to the ester group of DMAEMA (see Figure 3.8, H-15) and the benzopyran protons adjacent to the nitro group (see Figure 3.8, H-5 and H-7) were ratioed and the content of the chromophore moieties within the

189

polymer brush was calculated to be 4.8, 6.1 and 11.5 mol % for SiO$_2$-*g*-(PDMAEMA-*co*-PSPMA)1, 2 and 3, respectively.
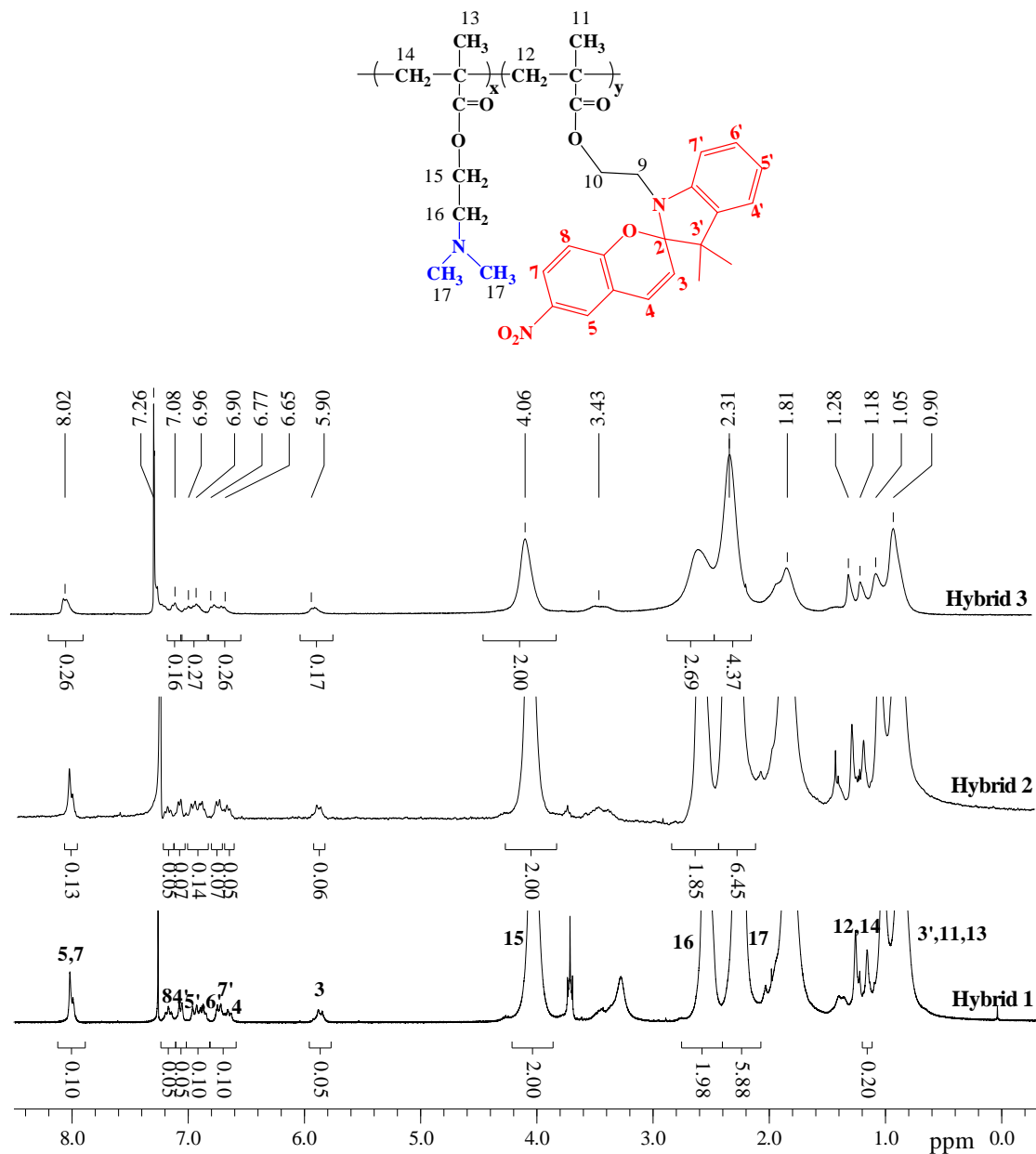
Figure 3.8. ^{1}H NMR spectra (CDCl$_3$) of the free PDMAEMA-*co*-PSPMA random copolymers.

These results are summarized in Table 3.2. The PSPMA content of the hybrids SiO$_2$-*g*-(PDMAEMA-*co*-PSPMA)1 and 2 was found to be in good agreement to the theoretical value calculated from the comonomer feed ratio indicating a good control of the

incorporated chromophores (5 mol %) in the polymer brushes. However, the SiO_2-g-(PDMAEMA-co-PSPMA)3 exhibited a lower PSPMA content compared to the theoretical value (20 mol %) which was attributed to the inability of the DMAEMA comonomer to fully solubilize the solid SPMA comonomer. The above results suggest an efficient copolymerization at low chromophore contents, whereas at higher SPMA contents the copolymer composition diverts from the targeted values.

Table 3.2. TGA, GPC and ^{1}H NMR data for the SiO_2-g-(PDMAEMA-co-PSPMA) hybrids as well as calculated grafting densities, distances between grafting points, initiator efficiency and number of polymer chains per particle.

Sample	2-(EiB)Br[1]	GPC results			SPMA	Polym.[3]	σ^4	d^5	a^6	f^7
		M_n	M_w	M_w/M_n	(mol%)[2]					
Hybrid 1	50.0	57,000	73,300	1.28	4.8	30	0.38	1.62	13	74,575
Hybrid 2	33.1	66,600	86,300	1.29	6.1	36	0.42	1.54	14	83,700
Hybrid 3	14.3	80,500	175,900	2.18	11.5	47	0.55	1.35	18	108,507

[1]mol % of the free initiator. [2]determined by ^{1}H NMR. [3]Polymer content (wt %) of the hybrids determined by TGA. [4]grafting density (#chains/nm[2]). [5]Distance between grafting-points (nm). [6]Initiator efficiency. [7]Number of polymer chains/particle.

The molecular weights (M_n's) and the molecular weight distributions (M_w/M_n, PDIs) of the PDMAEMA-co-PSPMA random copolymers grafted from the surface of the silica particles were determined by GPC and are summarized in Table 3.2. The polymer chains grafted from the surface of the silica particles for the SiO_2-g-(PDMAEMA-co-PSPMA)1 and 2 hybrid particles, exhibit low PDIs, 1.28-1.29 in agreement with the "living/controlled" nature of the ATRP process. The PDIs are comparable with that reported elsewhere for SP-co-PNIPAM polymer brushes containing 0.16 mol % SP.[25] However, the hybrid 3 containing 11.5 mol % of SPMA exhibited a much higher PDI (2.18) comparable to that reported in the literature for homopolymer PSP brushes and PMMA-co-PSP polymer brushes bearing 25 mol % SP.[2,24] The M_n's of the PDMAEMA-co-PSPMA random copolymers grafted onto the surface of the silica particle were determined to be 57,000 and 66,000 g/mol for the hybrids SiO_2-g-(PDMAEMA-co-

PSPMA)1 and 2, respectively, which are higher compared to the M_n of 22,000 g/mol determined for well-defined SP-*co*-PNIPAM polymer brushes.[25] However, the PDMAEMA-*co*-PSPMA chains of the hybrid (PDMAEMA-*co*-PSPMA)3 exhibited a M_n of 80,500 g/mol which denotes the grafting of longer polymer chains from the surface of the particles and is comparable to that determined for PMMA-*co*-PSP polymer brushes exhibiting high polydispersities.[24] The loss of control for the SiO_2-*g*-(PDMAEMA-*co*-PSPMA)3 is two-fold; the higher SPMA content in the reaction medium allows a more efficient complexation of the Cu^{II} species formed at the beginning of the reaction leading to an increase of the Cu^{I}/Cu^{II} ratio which increases the termination reactions. The decrease of the free initiator content in the reaction mixture from 50 to 14.3 mol %, resulted in longer polymerization times allowing more termination reactions to take place. This effect in addition to the fact that the "grafting from" polymerizations often suffer from lower initiation efficiencies inherent to the steric congestion of the 2-bromoisobutyrate groups in comparison to polymerizations in the solution, increased the possibility of side-reactions which facilitate the broader PDI.[36] These findings suggest that the polymerization conditions used result in well-defined hybrids of controlled chromophore content and low PDIs in the presence of at least 33 mol % free initiator and at SPMA contents as high as 5 mol % while at lower 2-(EiB)Br and higher SPMA contents the control is lost.

The organic component of the core-shell hybrids was quantitatively determined by TGA. Figure 3.9 shows the TGA thermograms of the (PDMAEMA-*co*-PSPMA)-coated silica particles plotted against the thermograms of the initiator-coated particles and the SiO_2-*g*-PDMAEMA particles. The photoresponsive hybrids exhibited an organic content of 30-47 wt % in the temperature range 200-700 ^{o}C (Table 3.2). Their thermal decomposition follows a two step weight loss process at 305 and 405 ^{o}C similar to that of the PDMAEMA-coated silica particles. The polymeric component of the SiO_2-(PDMAEMA-*co*-PSPMA) hybrids increases linearly upon decreasing the content of the free-initiator in the reaction mixture (Figure 3.10), while keeping the total degree of polymerization constant (Table 3.1).
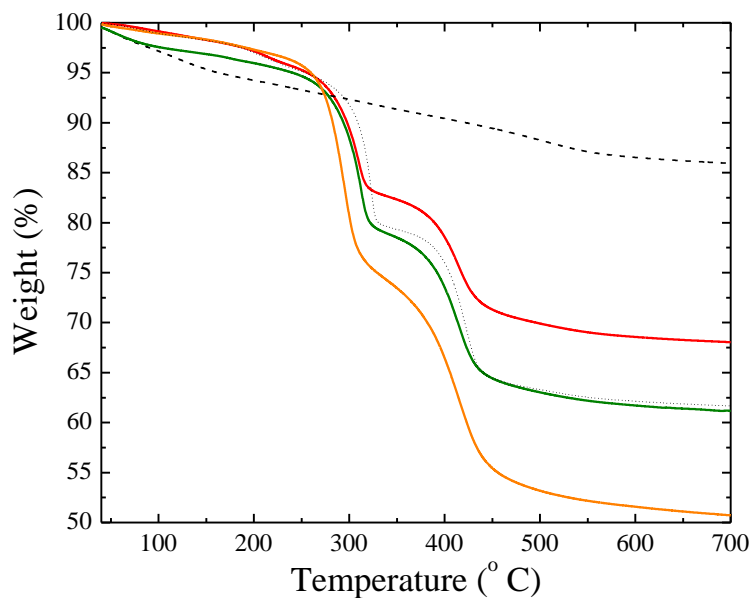
Figure 3.9. TGA thermograms of the SiO$_2$ particles modified with the BPTS initiator (--), the SiO$_2$-*g*-PDMAEMA (…) and the SiO$_2$-(PDMAEMA-*co*-PSPMA)1 (—), 2(—) and 3(—) core-shell particles.
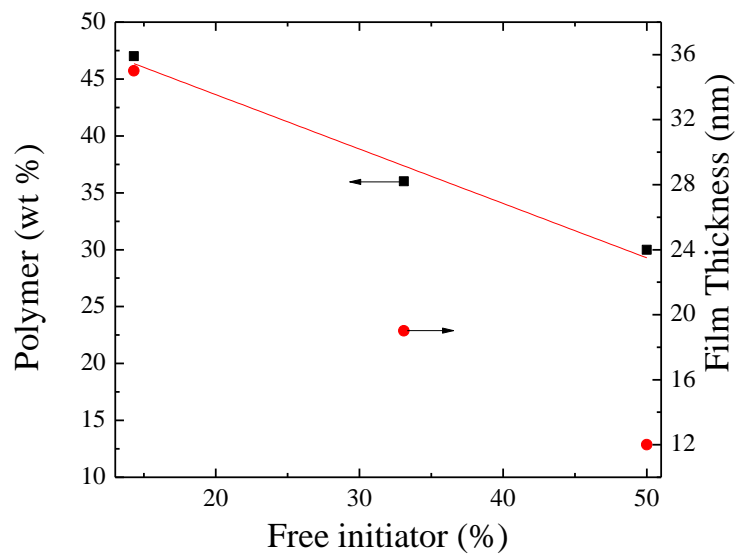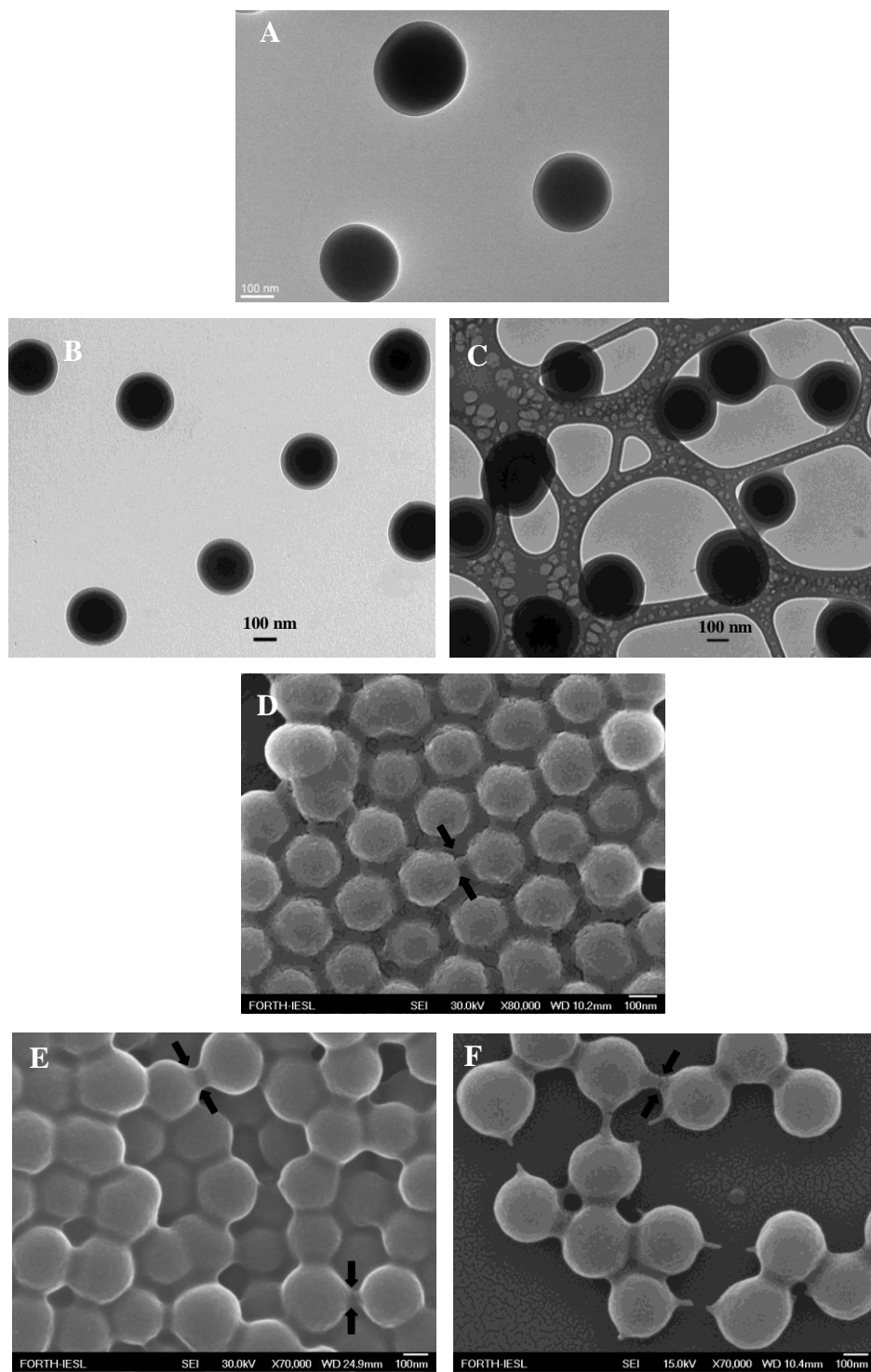

Figure 3.10. Variations in the polymer content (■) and the film thickness (●) of the hybrids determined by TGA and TEM measurements, respectively as a function of the mole concentration of the free initiator 2-(EiB)Br. The red line represents the linear fit to the experimental data.

These findings suggest that upon decreasing the concentration of 2-(EiB)Br in solution, longer chains are grafted from the surface of the silica particles resulting in a higher polymer content of the hybrids. This result is in agreement with the literature where variations in the concentration of the free initiator resulted in control over the film thickness in polymer brushes, with the thicker achieved at the lower concentration of the free initiator.[37]

From the TGA results and the M_n of the grafted polymers determined by GPC (Table 3.2), the grafting density of the PSPMA-*co*-PDMAEMA chains onto the surface of silica nanoparticles was calculated from eq. 3.1 to be in the range of 0.38-0.55 chains/nm^2 and thus the average distance between neighboring grafted chains varied from 1.62 to 1.35 nm (Table 3.2).The number of chains per particle was also calculated and was found between 74,575 and 108,507 from eq. 3.3. A grafting density of the ATRP initiator of about 0.33 nm^2/initiator was also calculated from eq. 3.1 based on the TGA results of the initiator-coated particles, suggesting that the efficiency of the surface-initiated polymerizations were between 13 and 18 %, similar to that reported in the literature for (SPMA-*co*-PNIPAM)-based polymer brushes on silica particles.[25] The grafting density and thus the distance between the anchoring points, the initiator efficiency and the number of chains per particle was almost the same for the SiO$_2$-(PDMAEMA-*co*-PSPMA)1 and 2 hybrid particles. However higher values were determined for the SiO$_2$-(PDMAEMA-*co*-PSPMA)3 hybrid particles, attributed to the fact that the non-"living" character of the PDMAEMA-*co*-PSPMA chains grown from the surface of the silica particles was not taken into consideration for the calculations.

The morphology of the hybrids was studied by transmission electron microscopy (TEM) and field-emission scanning electron microscopy (FESEM) (Figures 3.11 A-C and D-F, respectively). The SEM images showed a uniform conformal coating onto the surface of the particles resulting in well defined hybrids whose diameter ranged from 200 ± 5 to 271 ± 5nm (Table 3.3).

Figure 3.11. TEM and FESEM images of the SiO$_2$-*g*-(PDMAEMA-*co*-PSPMA) hybrids 1-3 (A-C and D-F, respectively).

The size of the hybrids in the dry state was proved to increase upon increasing the polymer content. At high concentrations the colloids formed connections between the particles, as indicated by the arrows in Figures 3.11 D-F, due to the coalescence of the polymer shells of neighboring core-shell hybrids indicating good film formation properties.[38] TEM imaging (Figure 3.11 A-C) indicated that the hybrids are discrete, smooth, and regular in size and shape with diameters ranging from 237 ± 12 to 307 ± 16 nm in good agreement with the SEM results (Table 3.3). The hybrids are of core-shell structure with the lighter color polymer shell surrounding the dark color silica core. The thickness of the polymer shell lies between 12 and 35 ± 3 nm (Table 3.3), and increases upon decreasing the mole concentration of the free 2-(EiB)Br initiator in the reaction mixture, in agreement with the increase of the polymer content of the hybrids determined by TGA. The above results prove that well-defined photosensitive core-shell nanoparticles can be synthesized by si-ATRP from initiating sites on the surface of SiO_2.

Table 3.3. Diameter of the hybrids determined by SEM and TEM and polymer film thickness as calculated by TEM.

Sample	d_1 (nm)[1]	d_2 (nm)[2]	h (nm)[3]
Hybrid 1	200 ± 5	241 ± 12	12
Hybrid 2	245 ± 20	237 ± 12	19 ± 3
Hybrid 3	271 ± 17	307 ± 16	35 ± 4

[1]diameter of the hybrids determined by SEM. [2]diameter of the hybrids determined by TEM. [3] polymer film thickness determined by TEM.

The photoresponsive, acidochromic and fluorescent properties of the hybrids will be discussed in the following sections. For this purpose, the most well defined hybrid containing the higher polymer and SPMA content, that is hybrid SiO_2-g-(PDMAEMA-co-PSPMA)2, was chosen. The solution properties of the core-shell hybrid particles were investigated in water and for that reason the dispersability of the hybrids in the aqueous medium was studied by DLS and compared to that of the bare silica particles (Figure 3.12). DLS measurements of the bare silica particles and the core-shell hybrids in neutral pH water showed a 197 nm increase in size for the initial silica particles from $D_h = 267$

nm to $D_h = 464$ nm for the hybrid core-shell structures after the polymerization (Γ vs q^2 plots, Figure 3.12 (b) and (c)). The hydrodynamic thickness h^{39} of the brush layer was calculated to be 98.5 nm, that five times larger compared to that in the dry state (19 ± 3 nm), determined by TEM, suggesting that water is a good quality solvent for the hybrids.
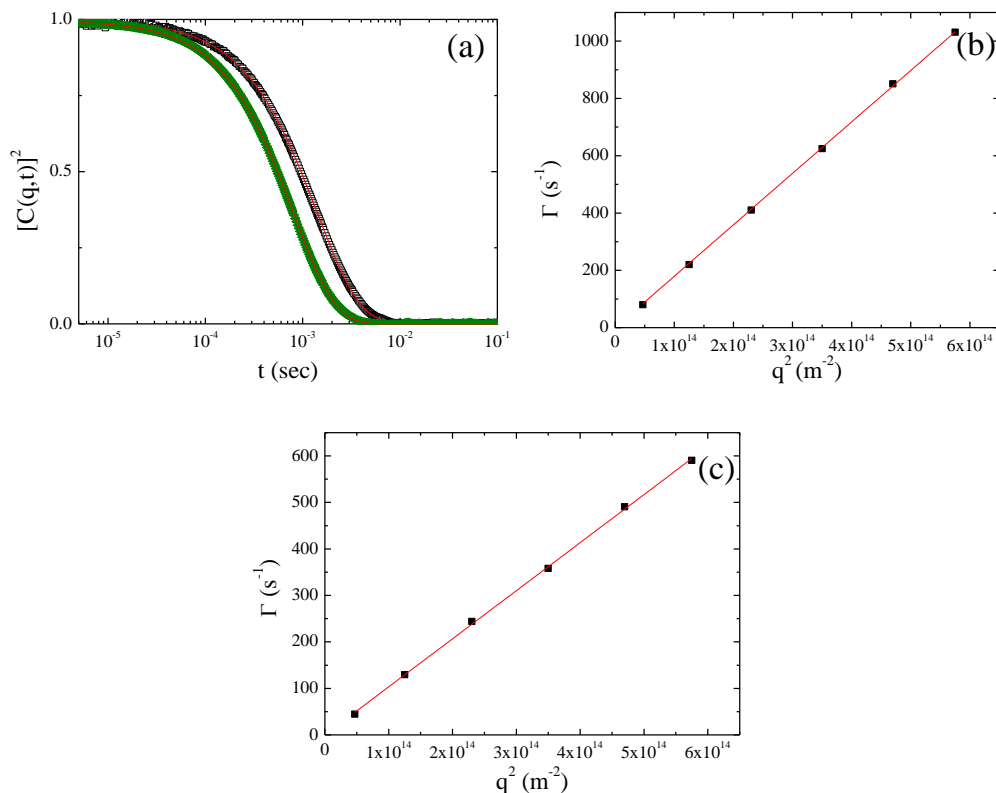
Figure 3.12. Intensity autocorrelation functions of the silica particles (◄) and the polymer modified SiO$_2$-g-(PDMAEMA-co-PSPMA)2 hybrid (□) at scattering angle θ = 90 (a). The red solid lines represent KWW fits to the data. Γ vs q^2 plots of the bare silica particles (b) and the SiO$_2$-g-(PDMAEMA-co-PSPMA)2 hybrid (c). The red solid lines represent linear fits to the data.

3.3.3.1 Photoresponsive behavior of the SiO$_2$-g-(PDMAEMA-co-PSPMA) core-shell hybrids

The photoresponsive behavior of the silica particle derivatized with the PDMAEMA-co-PSPMA polymer brushes was studied upon irradiation of the colloids with UV light in two solvent media of different polarity, water and acetonitrile (Figure 3.13a and 3.1

197

3b, respectively). When the core-shell hybrids were irradiated with UV light the non-polar colorless SP form isomerized to two dipolar isomers; the cisoid non-planar X isomer with an absorption maximum around 400 mm (blue), and the planar MC form with maximum absorption around 600 nm (red)[40-41] (see Scheme 3.5).
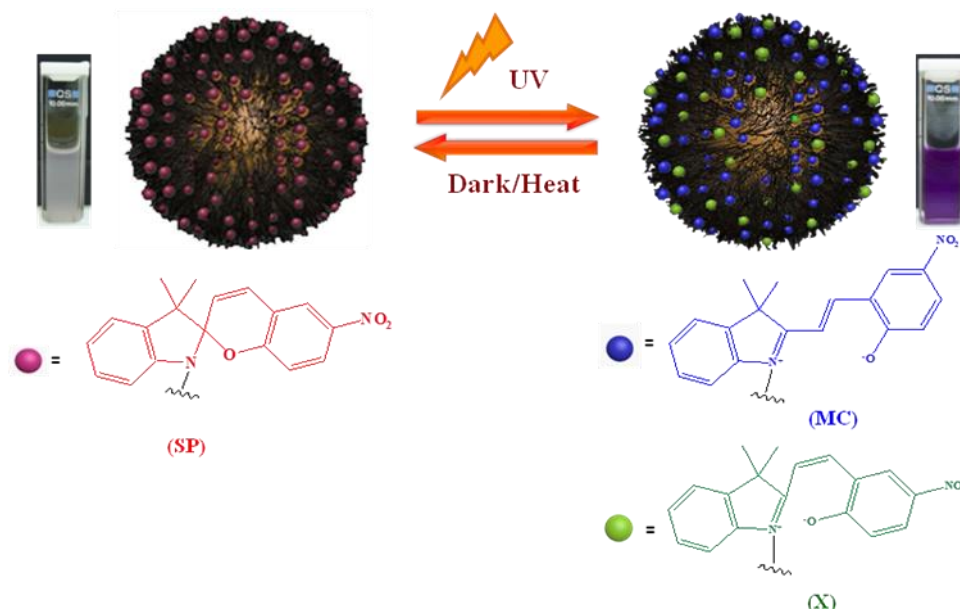
Scheme 3.5. Photo-induced ring opening process of the SP-NO$_2$ moieties in the SiO$_2$-*g*-(PDMAEMA-*co*-PSPMA) core-shell structures. SP is the parent molecule in its ground electronic state, X denotes a bipolar isomer with the two π-networks vertical to each other, and MC represents one of the several possible planar merocyanine isomers. The SP form can be retrieved either thermally or upon irradiation with visible light.

In most cases the photochromism of spiropyran occurs between the parent molecule and one of its TTC and CTC merocyanine derivatives, whereas under specific circumstances the SP molecules have been shown to isomerize to two different colored states following their photoexcitation by UV light.[40-41] The X isomer is usually observed for nitrosubstituted SPs.[42] Although the X isomer is a transient species with a short life-time and is usually detected by ultrafast studies[41] in our case it can be clearly detected in both solvent media. This is attributed to the polar microenviroment of the chromophores established by the polar DMAEMA comonomers and the solvent medium and the limited

segmental mobility of the polymer chains highly grafted onto the surface of the silica particles which favor the stabilization of the bipolar cisoid isomer.
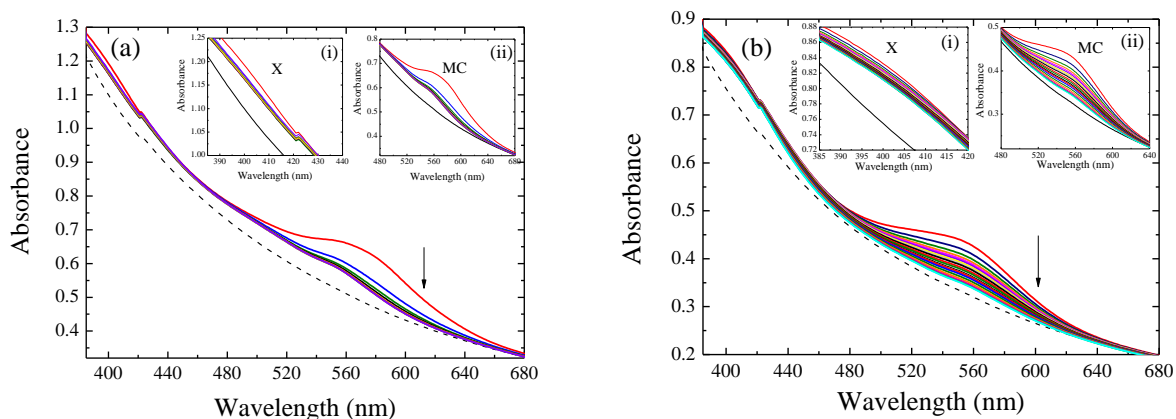

Figure 3.13. UV/vis absorption spectra of the SiO_2-*g*-(PDMAEMA-*co*-PSPMA) hybrid core-shell particles in the dark before (---) and after their irradiation with UV light in acetonitrile (a) and water (b).

Upon UV irradiation of the core-shell hybrids in aqueous media the evolution of a peak at 549 nm attributed to the switterionic MC form (Figure 3.13b, inset ii) is observed, while when the colloids are irradiated in a less polar solvent compared to water, i.e acetonitrile, the MC maximum is red shifted by 16 nm and is found at 565 nm (Figure 3.13a, inset ii). The above results suggest that the photosensitive colloids exhibit "normal photochromism", upon irradiation with UV light. The polar aqueous environment (SPP scale = 0.962)[43] stabilizes more effectively the bipolar ground state, compared to the excited MC state in contrast to acetonitrile which is a less polar solvent (SPP scale = 0.895),[43] leading to "negative solvatochromism" that is the blue shifting of the MC maximum absorbance with increasing the medium polarity.[44] On the other hand, the absorption maximum of the X isomers appears at 400 nm in both solvents (Figure 3.13a and 3.13b, inset i) suggesting that the bipolar species, whose structure is similar to that of the SP form and thus less polar compared to MC[45] do not exhibit solvatochromism.

The polarity of the microenvironment surrounding the chromophore units not only affects the position of the absorption maximum of the colored MC form but also the isomerization rates of the chromophores. It was proved in previous studies that the rate of

thermal MC-to-SP ring closure is an indicator for determining variations in the polarity, the viscosity and the free volume of the microenvironment around the chromophores. Thus, the polarity of the solvent and the DMAEMA comonomer are expected to exert an influence on the isomerization rates of the molecules which also have to overcome the confinement of the microenvironment that is the steric constraint inherent within the dense polymer brush. The X-to-SP and MC-to-SP isomerization of the hybrids in dark following their irradiation with UV light for 49 s were investigated in both water and acetonitrile by UV/vis spectroscopy by monitoring the decrease of the intensity of the X isomer at 400 nm and the MC band at 549 and 565 nm, respectively (Figure 3.13b and 3.13a, respectively). The visible absorption bands corresponding to the X and the MC species diminished slowly with time and no change in the absorption band shape was observed.

The kinetic constants for the X and MC decoloration within the polymer brush in both solvents were calculated by fitting the experimental data of the bleaching process to a superposition of two first-order rate processes expressed by eq. 2.2.1.[46] Figures 3.14a and 3.14b suggest that the thermal decoloration of the X and MC species can be described satisfactorily by to the superposition of two first-order processes. The biexponential fading process of the MC isomers has been also observed and discussed in chapter 2 for the PDMAEMA-*co*- PSPMA random copolymers carring 6 mol % nitro-substituted spiropyran derivatives and is in agreement with the literature where the non-monoexponential MC bleaching process in polymeric systems is reported. This decoloration mechanism indicates an inhomogeneity in the microenvironment surrounding the chromophores which can be related with several factors including the chain segmental mobility, the available free volume, the polymer polarity and rigidity, the volume change originated from the structure rearrangement of the molecules upon isomerisation and the distribution of the molecules within the hybrid. In the present system, the grafting of the polymers onto the surface of the particles may also have a significant contribution to the complicated fading behavior of the chromophores. It was recently shown that spherical polymer brushes are not sterically homogenous and can be practically divided into two regimes; the concentrated and the intermediate brush regime.
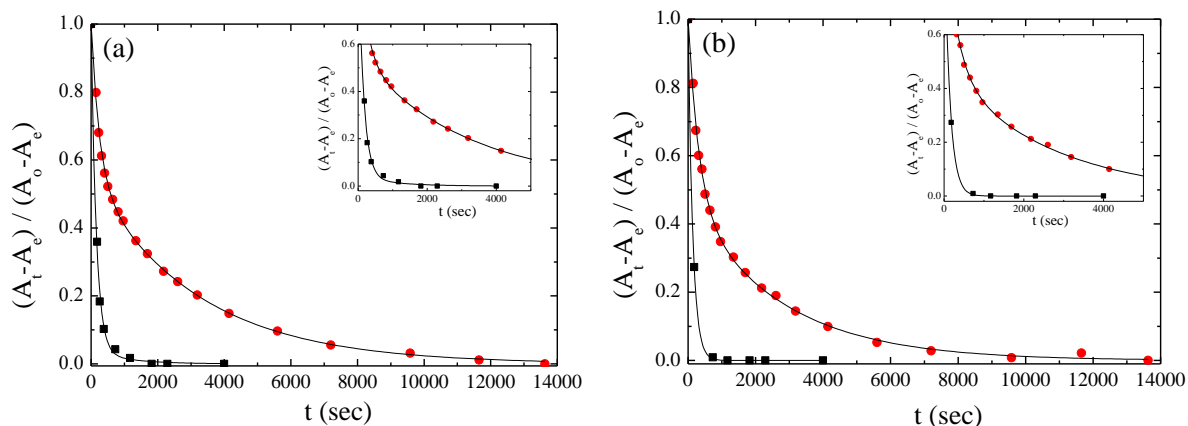
Figure 3.14. Kinetics of the MC-to-SP (a) and X-to-SP (b) thermal bleaching processes for the SiO$_2$-g-(PDMAEMA-co-PSPMA) core-shell hybrids suspended in water (●) and acetonitrile (■). The solid black lines represent fit to the data using eq. 2.2.1.The insets show a magnification at short relaxation times.

The concentrated regime, close to the particles surface, is characterized by high grafting densities and a stretched conformation of the grafted polymer chains, while as the distance from the particle surface increases and when approaching the intermediate brush regime the grafting density is reduced and the polymer chains adopt a more relaxed conformation.[48] We thus concluded that the variation in the grafting density and the steric crowding within the polymer brush can significantly affect the rate of isomerization of the chromophores. This is in contrast with what was reported earlier for the fading mechanism of the MC form in SiO$_2$-g-(PMMA-co-PSP) polymer brushes where the slower decaying of the MC species was attributed to H-type stack formation.[24] This is not the case here, since we monitored the spectral changes at the absorption maximum of the unassociated MC species, at 549 and 565 nm in water and acetonitrile, respectively for the rate constant calculation. No H-type MC-MC stacks were observed upon the short irradiation time of the colloids with UV light which would give a separate absorption maximum, blue-shifted compared to that of the free MC isomers, as we reported recently,[47] and is not observed here (Figures 3.13a and 3.13b).

The MC decoloration data plotted in Figure 3.14a as a function of time along with fits to eq. 2.2.1 showed that the MC species attain a photostationary state in acetonitrile

after 1821 s while in water 13633 s of thermal relaxation are required for the MCs to attain their photostationary state. The MC bleaching rate constants, k_1 and k_2, along with the fractions of short- and long-lived MC species, a and b, respectively, in water and in acetonitrile are summarized in Table 3.4.

Table 3.4. Rate constants and fractions of short- and long-lived MC and X species calculated for the MC-to-SP and X-to-SP isomerization in the polymer brushes at 25 °C.

Solvent	Species	λ_{max} (nm)[1]	a[2]	b[3]	Rate constants	
					k_1(s^{-1})[4]	k_2(s^{-1})[5]
Water	X	400	0.53	0.47	3.14×10^{-3}	3.68×10^{-4}
	MC	549	0.45	0.55	3.99×10^{-3}	3.13×10^{-4}
CH$_3$CN	X	400	1	-	7.16×10^{-3}	-
	MC	565	0.96	0.04	6.40×10^{-3}	9.59×10^{-4}

[1]Absorption maximum of the X and MC band. [2]Fraction of short-lived X and MC species (eq. 2.2.1). [3]Fraction of long-lived X and MC isomers (eq. 2.2.1). [4]k_1 represents the rate constant for the short-lived X and MC species. [5]k_2 represents the rate constant for the long-lived analogues.

In water, the MC species exhibited two fading rate constants $k_1 = 3.99 \times 10^{-3}$ s^{-1} and $k_2 = 3.13 \times 10^{-4}$ s^{-1} attributed to the short- and the long-lived MC moieties respectively, while in acetonitrile both processes are faster with $k_1 = 6.40 \times 10^{-3}$ s^{-1} and $k_2 = 9.59 \times 10^{-4}$ s^{-1}. The lower kinetic constants found in water compared to acetonitrile for both MC species suggest the stabilization of the switterionic MC form by the polar aqueous environment (SPP scale = 0.962) that suppress the MC-to-SP ring-closure process which has to pass through the energetically unfavored rotation around the central double bond of the molecules to form the intermediate cis-isomer and finally the close SP form.[44] Even though acetonitrile posses sufficient polarity (SPP scale = 0.895), it is less polar than water, and it cannot stabilize effectively the MC form leading to higher kinetic values. Moreover, the kinetic constants of the long-lived MC species in both solvents are an order of magnitude lower compared to those of the short-lived species, while the

short-lived MCs exhibit bleaching constants which are similar to those found for analogous PSP-*co*-PDMAEMA copolymers in solution.[47] This suggests the significant impact of the polymer brush microenvironment on the MC-to-SP isomerization rates, related with variations in polarity and the free volume inherent the brush topology. In particular, in the concentrated brush regime the restricted polymer volume obstructs the efficient rotation of the dye molecules, hinders the facile reformation of the close SP species and prolongs the lifetime of the MC species. This is in agreement with the observed retardation of the MC isomerization in PSP homopolymer brushes on SiO_2 particles upon increasing the polymer grafting density,[2] in chromophores embedded within phospholipid bilayers[49] and in resin-bound MCs[50] reported recently. On the contrary, in the intermediate brush regime the free volume available for the ring-closure reaction of the chromophores increases due to the relaxed conformation of the grafted polymer chains which promotes the faster reformation of the SP chromophores compared to the concentrated brush regime. The polarity of the surrounding microenvironment not only effects the MC-to-SP isomerization rates but also the populations of the short- and the long-lived MC species. In water the half MC isomers are long-lived while in acetonitrile the slower decaying MC isomers are only 4 % (Table 3.4). This can be attributed to the fact that water is a more polar solvent than acetonitrile and thus favors the stabilization of more bipolar species compared to acetonitrile. Thus, the polarity of the microenvironment can regulate both the isomerization rates and the contribution of species with short and long lifetimes.

The X decoloration data as a function of time are plotted in Figure 3.14b. X isomers attain a photostationary state in water after 13633 s of thermal relaxation while in acetonitrile only 1171 s are required for the X species to reach their photostationary state. The X fading rate constants, k_1 and k_2, observed in water and acetonitrile and the fractions of the short- and long-lived X species, a and b, in both solvents are summarized in Table 3.4. In water, the X species exhibit a bi-exponential bleaching behavior with $k_1 = 3.14 \times 10^{-3}$ s^{-1} and $k_2 = 3.68 \times 10^{-4}$ s^{-1} and 53 % of the molecules being short-lived and 47% long-lived. On the contrary, in acetonitrile the photoisomers exhibit a single-exponential fading behavior with $k_1 = 7.16 \times 10^{-3}$ s^{-1}. The X isomer, being less polar than

MC but still bipolar, is more effectively stabilized in water compared to acetonitrile as is indicated by the lower kinetic constants determined in the latter solvent.

The previous results indicate that the isomerization rates of the X and MC isomers are highly dependent on the microenvironment of the polymer brushes inherent variations in the polarity and the polymer free-volume. More specifically, the coexistance of long- and short-lived MC and X species within the brush can be facilitated by several factors including the polarity of the surrounding medium which regulates the isomerization rates of the species and their polulations. The grafting of the polymer chains onto the silica surface which favors the coexistence of areas with lower and higher steric confinement and thus more and less available free volume, respectively, may contribute to the establishment of an inhomogeneous environment around the chromophores that affects the half-life of the X and MC isomers.

3.3.3.2 Acidochromic properties of the SiO$_2$-g-(PDMAEMA-co-PSPMA) core-shell hybrids

The effect of the solution pH on the isomerization behavior of the SP in the PDMAEMA-co-PSPMA copolymer brush layer was studied upon the addition of acid (HCl) in an aqueous dispersion of the core-shell hybrids. The added protons catalyze the heterolytic cleavage of the C-O bond of the SP isomers which undergo a ring-opening reaction to form the open MC moieties. A further increase of the proton concentration in the medium results in the formation of [MC-OH]$^+$ isomers due to the protonation of the hydrophilic MC species. This process is fully reversible and the SP species can be retrieved upon addition of base in the system (see scheme 3.6).[51] The DMAEMA comonomer is expected to have a significant effect in the acidochromic behavior of the SP moieties since it posseses tertiary amine side groups which can also become protonated by substracting protons from the surrounding medium.
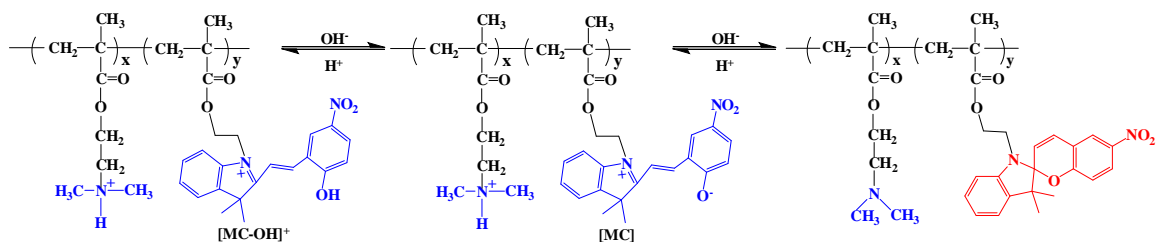
Scheme 3.6. Reversible protonation process of the PDMAEMA-*co*-PSP random copolymer brushes in acidic media.

Potentiometric titration of the SiO$_2$-*g*-(PDMAEMA-*co*-PSPMA) core-shell hybrids showed an effective pK_a for the hybrids around 5.9 (Figure 3.15a) in accordance with the literature which reports similar effective pK_a values for PDMAEMA (pK_a = 7.0)[52] and PMC (pK_a = 6-7)[53], resulting in one distinct plateau in the titration curve.
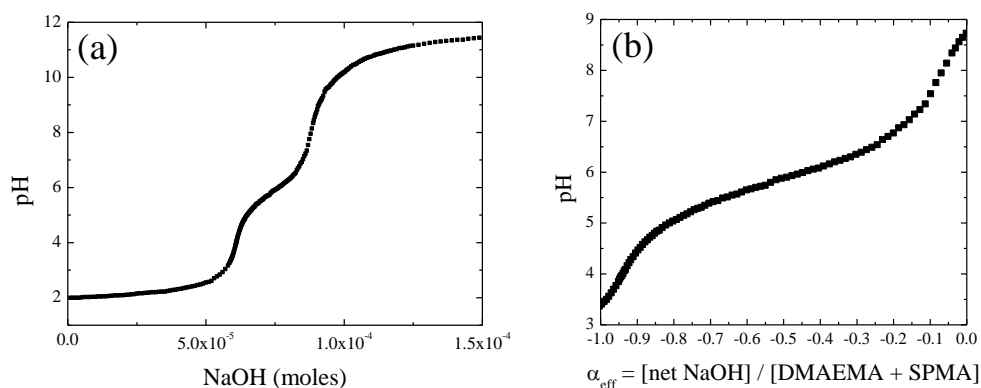
Figure 3.15. Potentiometric titration curve for a 0.21 wt % dispersion of the SiO$_2$-*g*-(PDMAEMA-*co*-PSPMA) hybrid particles (a). The data plotted as pH versus the ratio α_{eff} = [net NaOH] / [DMAEMA+SPMA monomer units] in the range -1 < aeff < 0 (b).

Figure 3.16a shows the absorption spectra for the SiO$_2$-*g*-(PDMAEMA-*co*-PSPMA) core-shell hybrids in an aqueous medium upon the gradual addition of acid. The sequential addition of 3-4 μL aliquots of 0.1 M HCl in the aqueous dispersion of the hybrids of pH 8.1, due to the low proton concentration, led to the gradual evolution of an absorption band at 528 nm attributed to the open MC isomer (Figure 3.16a, inset i). The absorption maximum of the acid-catalyzed ring-opened MC species is blue shifted by 21 nm compared to the MC moieties derived upon irradiation of the hybrids with UV light in

water (λ_{max} = 549 nm). This suggests that the presence of the protons in solution assure a microenvironment of higher polarity around the chromophores leading to "negative solvatochromism" as described above (see Figure 3.13a and 3.13b, inset ii). This observation verifies the importance of microenvironment polarity in tuning the solvatochromic properties of the dyes and the great sensing properties of the chromophores toward variations in the polarity of their microenvironment. The acid-induced appearance of the MC species within the polymer brush is accompanied with the ring-opening of the closed SP form observed as a decrease of the band at 274 nm (Figure 3.16a). Further increase of the proton concentration in the aqueous dispersion of the hybrids results progressively in a reduced intensity of the MC band at 528 nm (Figure 3.16a, inset ii) and the appearance of a new peak at 421 nm (Figure 3.16a, inset iii).[54]
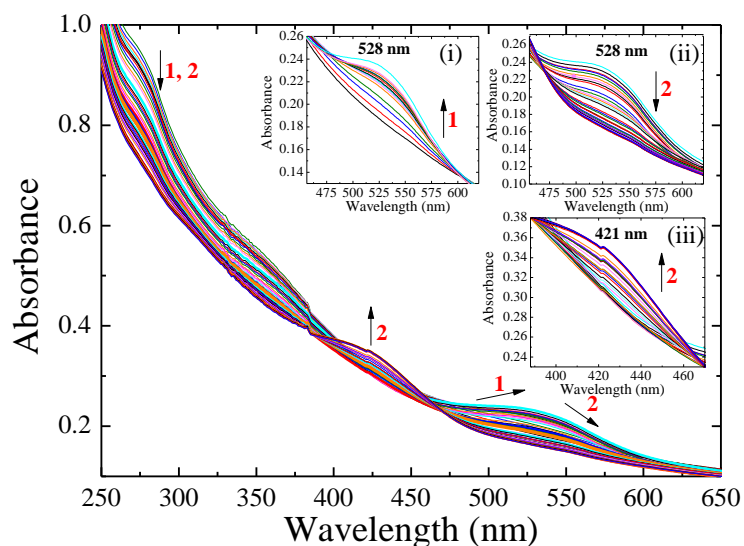
Figure 3.16a. UV/vis absorption spectra of an aqueous dispersion of the SiO$_2$-*g*-(PDMAEMA-*co*-PSPMA) core-shell hybrids upon the addition of acid (HCl). Inset (i) shows the increase of the intensity at the absorption maximum of MC (528 nm) upon the addition of 6.15×10^{-6} moles HCl. Insets (ii) and (iii) show the decrease of the absorption intensity of MC (528 nm) and the evolution of the [MC-OH]$^+$ band (421 nm), respectively, upon the further addition of 1.52×10^{-4} moles HCl.

This is consistent with the protonation of the MC isomers within the polymer brush and the formation of the *trans*-[MC-OH]$^+$ derivatives with an absorption maximum at 421

nm. Figure 3.16b(i) summarizes the absorbance intensity variations of the photochromic species as a function of the moles of acid added in the aqueous dispersion of the core-shell hybrids. The presence of protons in solution stimulates the formation of the MC species whose concentration increases gradually and reaches a maximum when 6.16×10^{-6} moles of HCl have been added in the solution (Figure 3.16b(iv)). In parallel, the opposite trend is observed for the SP moieties whose intensity decreases gradually indicating their acid-induced isomerization to the MC moieties (Figure 3.16b(ii)). Moreover, at low acid concentration ($H^+ \leq 1.18 \times 10^{-5}$ mole) a decrease in the absorption intensity is observed at 421 nm, suggesting the consumption of isomer X for the formation of the open protonated MC species (Figure 3.16b(iii)).[45]
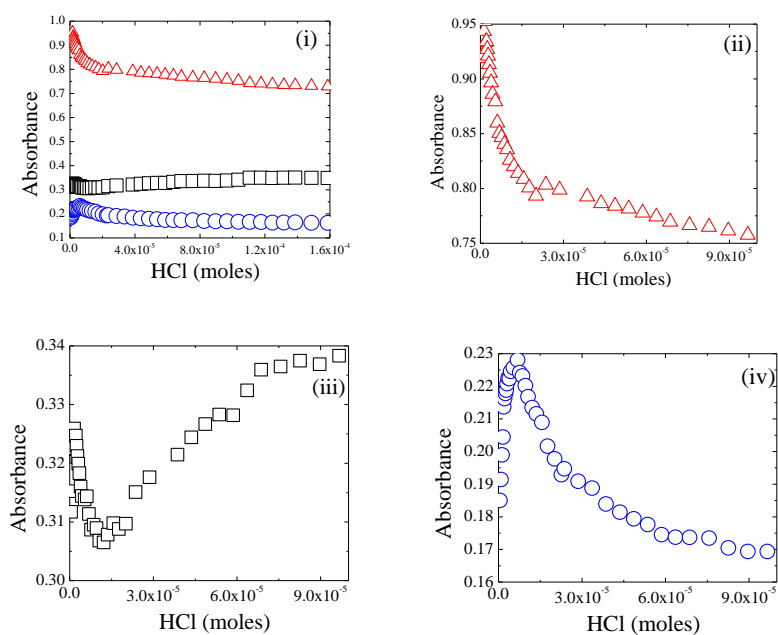
Figure 3.16b. Absorption intensities of the chromophore species in an aqueous dispesion of the SiO$_2$-g-(PDMAEMA-co-PSPMA) core-shell hybrids as a function of the added moles of HCl; SP ($\triangle$), [MC-OH]$^+$ ($\square$), MC ($\circ$) (i). Plots (ii), (iii) and (iv) show a magnification of the absorption intensities of the SP, [MC-OH]$^+$, and MC species, respectively.

Further addition of acid (6.16×10^{-6} mol $\leq H^+ \leq 2.23 \times 10^{-5}$ mol) results in the decrease of the intensity of the SP and MC species (Figure 3.16b(ii) and 3.16b(iv), respectively),

suggesting the protonation of the MC isomers and the formation of the [MC-OH]$^+$ species (Figure 3.16b(iii), which become more pronounced at higher acid concentration (2.23 × 10^{-5} mol ≤ H$^+$ ≤ 1.58 × 10^{-4} mol).

3.3.3.3 Fluorescent properties of the SiO$_2$-g-(PDMAEMA-co-PSPMA) core-shell hybrids

The fluorescent behavior of the core-shell hybrids in water was investigated. The fluorescence emission spectrum (λ_{ex}= 521 nm) of the SiO$_2$-g-(PDMAEMA-co-PSPMA) core-shell hybrids in water at pH 8 before UV irradiation (Figure 3.17, spectrum 1) exhibited two fluorescence band maxima; one at 568 attributed to the bipolar cisoid non-planar isomer X and the other at 612 nm assigned to the planar MC species. The existence of bipolar isomers within the polymer brush before irradiation is ascribed to the polar microenvironment. The bands of the two bipolar species cannot be observed in the absorption spectrum of the core-shell hybrids before UV irradiaton (Figure 3.13b) due to strong scattering effects from the SiO$_2$ colloids. However, they are clearly distinguished in the absorption spectrum of the free PSPMA-co-PDMAEMA copolymer (Figure 2.2.19) and were verified by the fluorescence spectrum of the hybrids. Both species become more pronounced upon irradiation of the copolymer with UV light as observed by UV spectroscopy (Figure 2.2.19). This is in agreement with the absorption spectrum of the hybrids showed the generation of both the X and MC species upon UV irradiation (Figure 3.13a and 3.13b).

It is interesting to note that the emission band of the isomer X, observed at 568 nm in water, overlaps well with the absorption peak of the MC species at 549 nm (Figure 3.17, inset (ii)). Thus, we thought that given the confinement in the polymer brush if the spatial distance of the two photoisomers is within the Föster radius, the X species could potentially act as donors promoting fluorescence resonance energy transfer (FRET) to the MC acceptors. This was verified by fluorescence spectroscopy. Figure 3.17 (spectrum 2) shows the fluorescence emission spectrum (λ_{ex} = 521 nm) of the SiO$_2$-g-(PDMAEMA-co-PSPMA) core-shell hybrids in water at pH 8 following their irradiation with UV light for 49 s. The photo-regulated generation of the colored MC species within the polymer brush, as indicated by the evolution of the band at 612 nm, induced a remarkable

quenching of the fluorescence intensity of the X isomers at 568 nm by 52% (Figure 3.17, inset (i)).
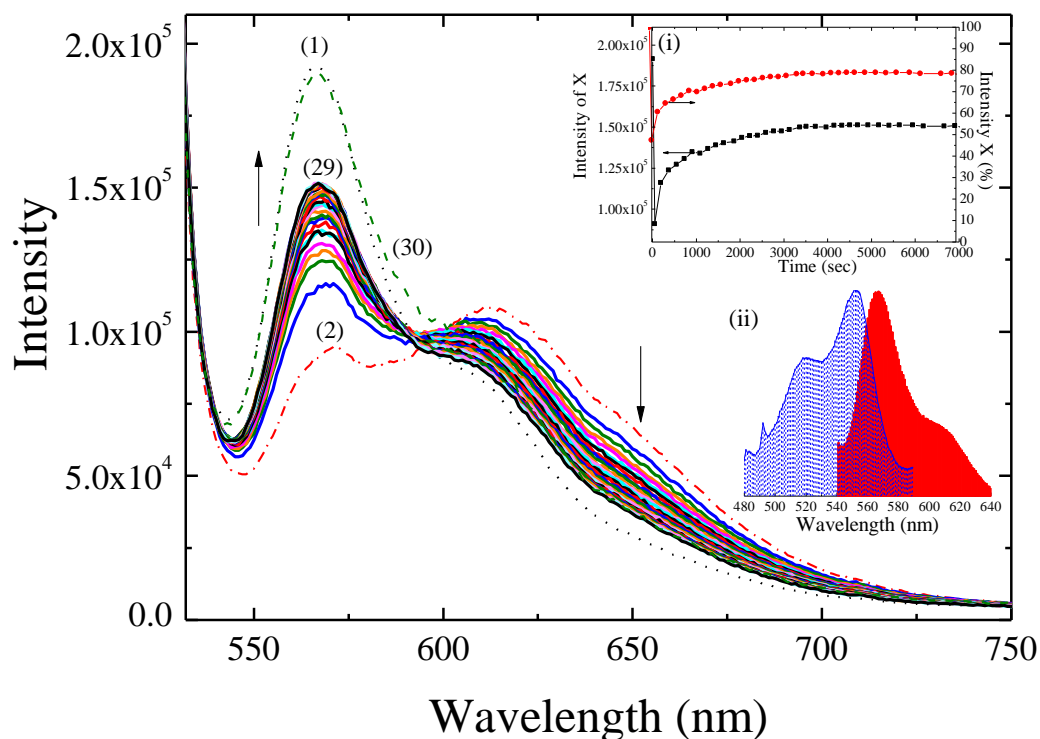
Figure 3.17. Fluorescence emission spectra (λ_{ex} = 521 nm) of the SiO$_2$-g-(PDMAEMA-co-PSPMA) core-shell hybrids in water at pH 8 before (1) and after (2) irradiation with UV light and during thermal relaxation of the chromophores at RT for several hours (3-30). Inset (i) shows the absolute (■) and % (●) variations in fluorescence emission intensity of the X species as a function of time. The minimum in the plots represents the fluorescence emission intensity of X after 49 s of irradiation with UV light. Inset (ii) shows the spectral overlap region between the donor (X) emission spectrum (red) and the acceptor (MC) absorption spectrum (blue).

At a first glance this result seems to be in contrast with the absorption measurements (Figure 3.13b) discussed above which showed the simultaneous evolution of the absorption intensity of both the X and MC isomers upon irradiation of the hybrids with UV light and did not suggest the formation of MC via the X consumption. However, when the UV/vis and fluorescent spectra are considered together they suggest that the photoinduced SP-to-MC and SP-to-X isomerization upon UV irradiation raises the

abundance of the polymer brush in X and MC moieties, constituting FRET-based donor-acceptor pairs and leads to an efficient intraparticle FRET process (Scheme 3.7).
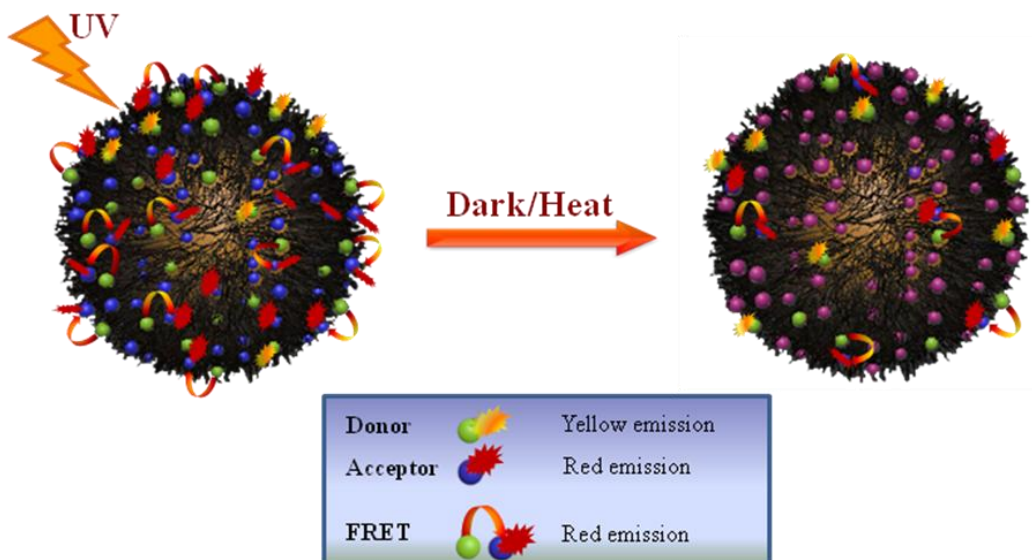
Scheme 3.7. Schematic illustration of the photo-regulated FRET process from X to MC present in the polymer brush. The FRET process can be switched "on" and "off" by UV irradiation and thermal relaxation of the MC species, respectively.

The FRET process is significantly reinforced by the fact that similar fractions of short- and long-lived X and MC species (Table 3.4) are distributed in the dense polymer brush which carries a substantial cargo of donor-acceptor FRET pairs in close proximity. Such an energy transfer process from the X to the MC species has been reported previously for 1'-octadecyl-3',3'-dimethyl-6-nitrospiro-[2H-1-benzopyran-2,2'-indoline) molecules incorporated in Langmuir-Blodgett (LB) films prepared in a mixed film with stearic acid, arachidic acid, and tripalmitine where the chromophores exhibited close proximity, for which the Föster's critical distance R_0 between donors and acceptors has been calculated to be as short as 2 nm.[55] R_0 is defined as the maximum distance between donor and acceptor species required so that 50% of the excited donors decay via energy transfer while the rest via alternative radiative or non-radiative pathways.[56] Similarly, in the present system, the entrapment of the chromophores in the spatially crowded environment of the polymer brush favors their close proximity, considering that the

distance between the grafting points is about 1.5 nm. Assuming that the R_0 for the X-MC donor-acceptor pair is 2 nm,[55] the energy transfer is calculated by the "rule of thumb" to be effective over distances in the r = $R_0 \pm 50\%$ R_0 range,[56] namely 1 nm $\leq r \leq$ 3nm, where r is the distance between the donor X and the acceptor MC. From the fluorescence data (Figure 3.17, spectrum 1), a FRET efficiency of 0.52 (eq. 2.2.3) was calculated and the distance between the donor and the acceptor was found 1.96 nm (eq. 2.2.2).[56-58] The steric confinement inherent in the polymer brush layer not only promotes the close proximity of the photoisomers and thus the FRET process but also restricts the conformation flexibility of the molecules and increases the fluorescence efficiency of X and MC isomers in water. It was previously shown that neither the SPs nor the MCs exhibit appreciable fluorescence in water whereas upon minimization of the nonradiative relaxation due to the sterically hindered internal motions of the excited molecules in the polymer brush their fluorescence efficiency enchanced in a similar way as observed upon introducing the chromophores into hydrophobic cavities.[9]

Finally, the FRET process is switched "off" slowly with time due to the thermal reversion of the MC acceptors to the closed SP form resulting in the retrieval of the fluorescent intensity of the X donors (Figure 3.17, spectrum 3-29). When the X and MC photoisomers return to the closed SP form the phenomenon ceases due to the low concentration of the donor-acceptor pairs in the polymer brush (Scheme 3.7). Figure 3.17 shows the fluorescence emission spectra of the hybrids upon excitation at 521 nm after their irradiation with UV light (spectrum 2) and during the MC thermal relaxation (spectra 3-29). The fluorescence intensity of the MC isomers is gradually attenuated with time accompanied with the simultaneous enhancement of the fluorescence intensity of the X isomers. The initial fast recovery of the X fluorescence upon switching "off" the UV stimulus which is subsequently significantly retarded can be explained by the biexponential decay profile of the MC species discussed previously (Table 3.4). The relative fluorescence intensities of the X and MC isomers during thermal fading were calculated and are plotted as a function of time (Figure 3.18). Instantly, when the hybrids were irradiated with UV light the fluorescence intensity of the X species (568 nm) was abruptly quenched by 48% while the MC moieties (612 nm) exhibited their maximum relative fluorescent intensity. After 1080 s of thermal fading the donors X gained 21 % of

their fluorescence intensity while 32 % of MC species were isomerized back to closed SP form while after 6900 s of thermal relaxation the X isomers retrieved 78 % of their fluorescence intensity and only 22% of MC moieties were present. It is worth noting that the fluorescence emission at 612 nm is a sum of the contributions from the FRET process and the isolated MC isomers while the relative contribution of the two factors is difficult to be quantified. Moreover, the fact that both the MC and X forms retrieve their initial fluorescent intensity (Figure 3.17, spectrum 30), after infinite relaxation time, indicates that the thermodynamically stable state of the system contains a small fraction of bipolar isomers, planar and non-planar, which never return to the close SP form.
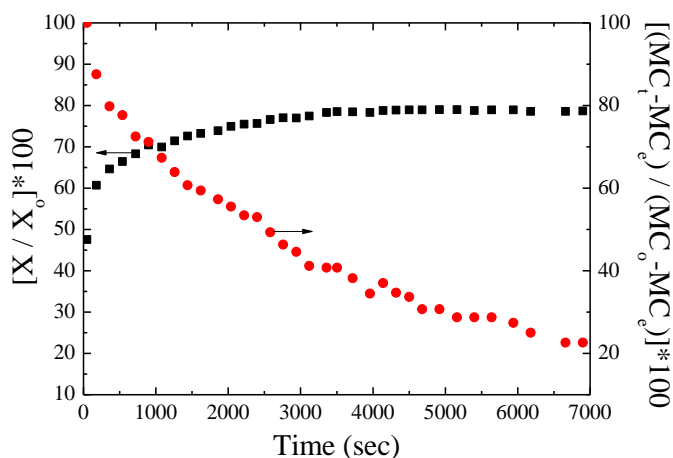
Figure 3.18. Variations in the relative fluorescence intensities of the X isomers (λ_{em} = 566 nm) and the MC species (λ_{em} = 612 nm) as a function of time following irradiation of the hybrids with UV light in water.

A series of factors including the polymer polarity and rigidity, the available free volume in the brush which exhibit significant variations due to the brush topology and the volume changes related with the structure rearrangement of the chromophores upon photoexcitation, the chain segmental mobility and the distribution of the molecules within the brush favor the stabilization of the bipolar X and MC species by the current system, prolong their life-time (Figure 3.18) and enable the read-out process. To the best of our knowledge, the FRET in polymeric materials or/and hybrids carrying X-MC donor-acceptor pairs has not reported previously while the phenomenon was observed only

when 1'-octadecyl-3',3'-dimethyl-6-nitrospiro-[2H-1-benzopyran-2,2'-indoline] was mixed with aliphatic acids or tripalmitine to form LB films, and was studied by picosecond time resolved fluorescence spectroscopy due to short lifetime of the X isomer. However, in our system the effective stabilization of both photoisomers over thermal relaxation enables the monitoring of the phenomenon. The expansion of the half-life of the MC isomers has been reported previously in the literature for chromophores substituted with a succinyl ester functionality when embedded in a gel derived from 4-*tert*-butyl-1-phenylcyclohexanol[59] or upon incorporation of the molecules within polymer matrices, enabling their use in super-resolution fluorescence imaging.[60]

The inherent photo-induced FRET process of the SiO_2-*g*-(PDMAEMA-*co*-PSPMA) core-shell hybrids in water at pH 8 and the fluorescence recovery of the X isomers related with the thermal relaxation of the MC species, was studied further in the presence of biological substances such as proteins and aminoacids. The protein of choice for these measurements was bovine serum albumin (BSA) since albumins contain specific binding sites for organic molecules and were shown to physically interact with SP isomers in aqueous media.[61-62] BSA exhibits an isoelectric point (p*I*) of 5.1[63] and a net charge of -18 at neutral pH.[64] Thus it possesses a negative net charge in the pH range at which system operates and is expected to interact electrostatically with the bipolar photoisomers. It is worth noting that PDMAEMA is not charged at this pH. Figure 3.19 shows the fluorescence emission spectra (λ_{ex} = 521 nm) of the SiO_2-*g*-(PDMAEMA-*co*-PSPMA) core-shell hybrids in water at pH 8 (α_{eff} = 0.07, Figure 3.15b) in the presence of BSA. Before UV irradiation the hybrids exhibited two fluorescence emission maxima at 568 and 612 nm, attributed to the X and MC species, respectively (Figure 3.19, spectrum 1) as discussed above. After UV irradiation for 49 s, the fluorescence intensity of the X isomer at 568 nm was significantly suppressed (by 64 %) (Figure 3.19, inset) whereas the evolution of an intense MC fluorescent band at 623 nm (Figure 3.19, spectrum 2) was observed. In the presence of BSA, a significantly larger number of photo-generated MC isomers were observed for the same irradiation time, leading to a MC/X fluorescent intensities ratio of 3.06 compared to 1.19 found in the absence of the protein (Table 3.5).
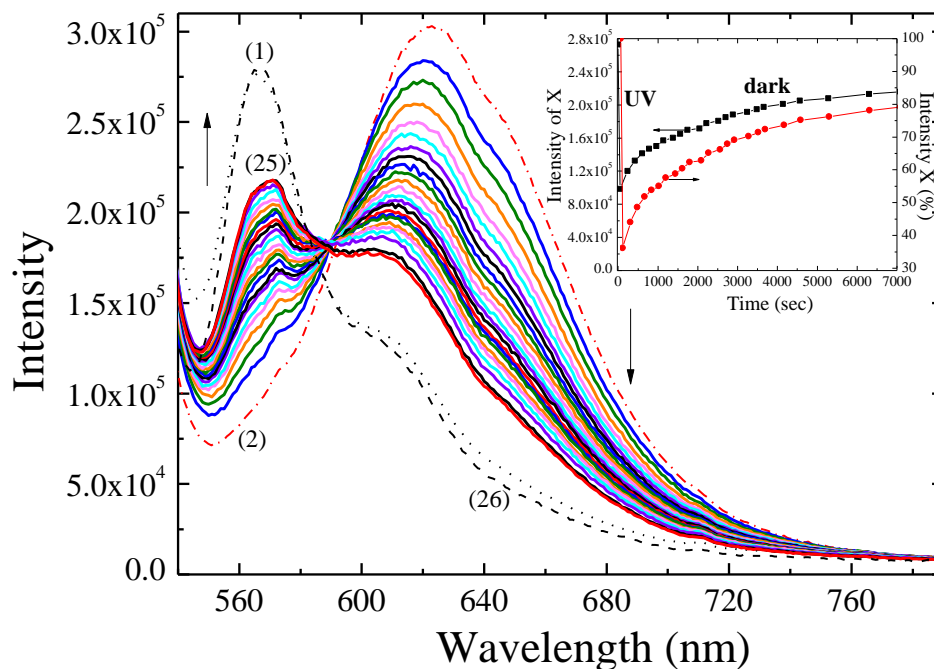
Figure 3.19. Fluorescence emission spectra (λ_{ex} = 521 nm) of the SiO$_2$-g-(PDMAEMA-co-PSPMA) core-shell hybrids in water at pH 8 in the presence of BSA before (1) and after (2) irradiation with UV light and during thermal relaxation of the chromophores at RT for several hours (3-26). The inset shows the absolute (■) and % (●) variations in fluorescence emission intensity of the X species as a function of time. The minimum in the plots represents the fluorescence emission intensity of X after 49 s of irradiation with UV light.

Table 3.5. Parameters calculated from fluorescent measurements

Sample[1]	MC/X[2]	E[3]	r[4] (nm)
Hybrids	1.19	0.52	1.96
Hybrids – BSA	3.06	0.64	1.82
Hybrids – L-histidine	0.70	0.54	1.95

[1]The measurements were carried out in water. [2]Ratio of MC to X species after 49 s of UV irradiation stimulation of the hydrids with UV light. [3]FRET efficiency as calculated by eq. 2.2.3. [4]donor-acceptor distance as calculated by eq. 2.2.2.

214

These values represent the ratio of the maximum fluorescent intensity of the MC and X species at 568 and 623 nm, respectively recorded instantly after the irradiation of the hybrids with UV light in the presence and absence of BSA, respectively. It was previously shown that the presence of albumins promotes the accelerated formation of MC species while only 30 % of MC isomers were obtained in the absence of the proteins. This phenomenon was observed only in polar buffer media at pH around 8 while in less polar solvents like dioxane or acetonitrile the MC formation was not accelerated indicating the necessity of a highly polar microenvironment for the MC-protein interaction.[65] In the present system the highly polar microenvironment required for the phenomenon is provided by the aqueous medium and the hydrophilic nature of the DMAEMA comonomer which being a weak polybase also establishes the appropriate solution pH for the accelerated MC formation and the enhancement of the FRET efficiency. The energy transfer efficiency is highly depended on the number of the available MC quenchers provided by the photo-induced SP-to-MC isomerization. Thus BSA catalyzes the enrichment of the system with MC acceptors resulting in the decrease of the donor-acceptor distance to 1.82 nm within the effective energy distance of 3 nm and the increase of the FRET efficiency by 12 % (Table 3.5). Similarly, the FRET enhancement has been achieved elsewhere upon increasing the chromophore content in polymeric nanoparticles[20] and in protein-SP complexes anchored onto QDs.[23] The X species gradually recover their fluorescent intensity due to the thermal bleaching of the MC acceptors (Figure 3.19, spectra 3-25). 1380 s of thermal relaxation enhance the fluorescent intensity of the X isomers by 22.6 % and quench the MC fluorescent intensity by 43 % (Figure 3.20). This implies the existence of excess MC species in the system which is induced by the presence of the BSA which are fading in parallel with the attenuation of the FRET. It is worth noting that after several hours of thermal relaxation both MC and X species retrieve their initial fluorescent intensity values as shown in Figure 3.19, spectrum 26.
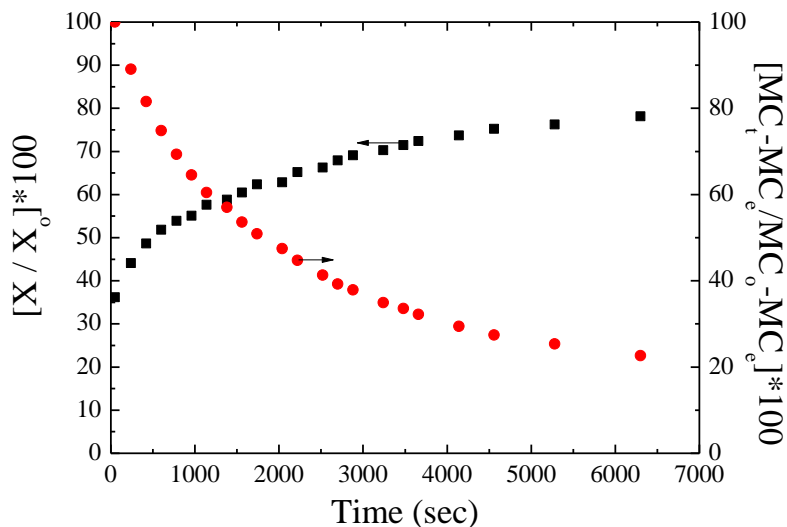
Figure 3.20. Variations in the relative fluorescence intensities of the X isomers (λ_{em} = 566 nm) and the MC species (λ_{em} = 623 nm) as a function of time in the presence of BSA after irradiation of the system with UV light in water.

The FRET efficiency of the system was studied further in the presence of an aminoacid, L-histidine. Figure 3.21 shows the fluorescence emission spectra (λ_{ex} = 521 nm) of the SiO$_2$-g-(PDMAEMA-co-PSPMA) core-shell hybrids in water at pH 8 in the presence of L-histidine (spectrum 1), upon irradiation with UV light (spectrum 2) and during thermal relaxation (Figure 3.21, spectra 3-28). The stimulation of the hybrids with UV light resulted in the decrease of the fluorescent intensity of the X isomer at 563 nm by 54 % (Figure 3.21, inset) and the increase of the fluorescent intensity of the MC species at 617 nm (Figure 3.21, spectrum 1). The FRET efficiency of the system remained unaffected by the presence of the aminoacid (Table 3.5) suggesting that the bipolar nature of the aminoacid (pI = 7.64)[66] has no effect in the donor-acceptor distance or concentration which remained stable at 1.95 nm. It should be noted that after several hours of thermal fading the initial fluorescence intensity of the X and MC species was recovered (Figure 3.21, spectrum 29).
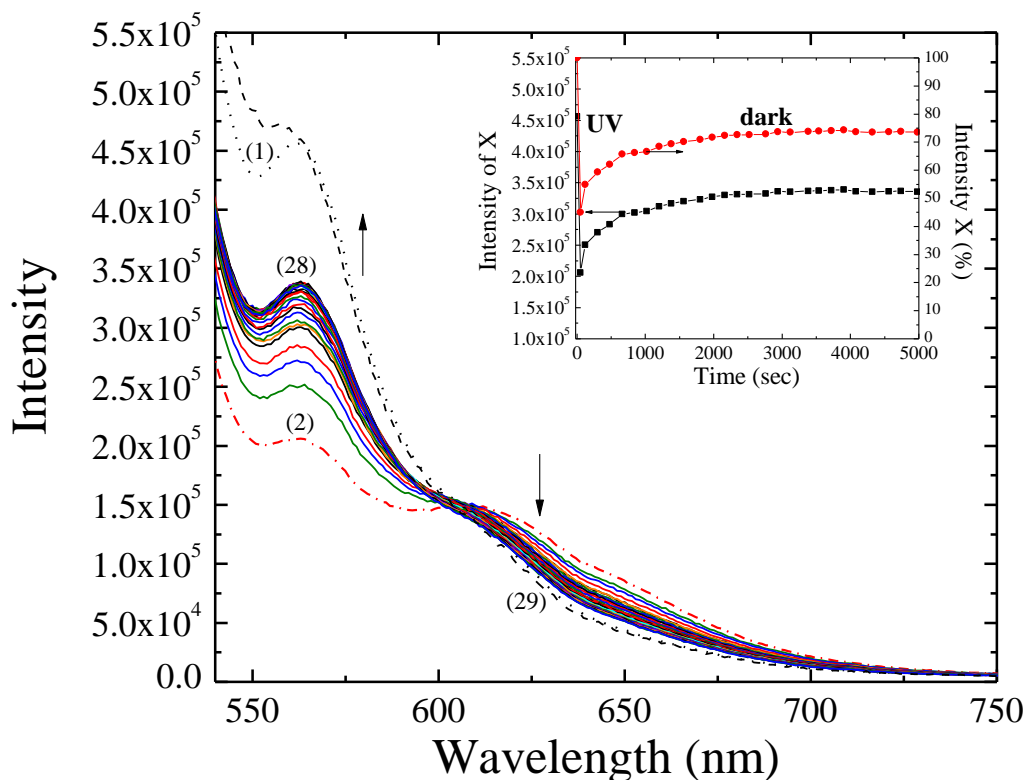
Figure 3.21. Fluorescence emission spectra (λ_{ex} = 521 nm) of the SiO$_2$-*g*-(PDMAEMA-*co*-PSPMA) core-shell hybrids in water at pH 8 in the presence of L-histidine before (1) and after (2) irradiation with UV light and during thermal relaxation of the chromophores at RT for several hours (3-29). The inset shows the absolute (■) and % (●) variations in fluorescence emission intensity of the X species as a function of time. The minimum in the plots represents the fluorescence emission intensity of X after 49 s of irradiation with UV light.

The kinetic rates of the MC thermal bleaching in the presence of BSA and L-histidine were investigated by monitoring the changes of the MC fluorescence intensity as a function of time and were compared to those found in the absence of the biological substances. The kinetic constants of the MC isomerization were calculated by fitting the experimental data to eq. 2.2.1, where A_t and A_o are the emission intensities of the isomers at time t and 0 while A_e is the emission intensity maximum of the MC species upon attaining their photostationary state in the absence of BSA and L-histidine (Figure 3.22).
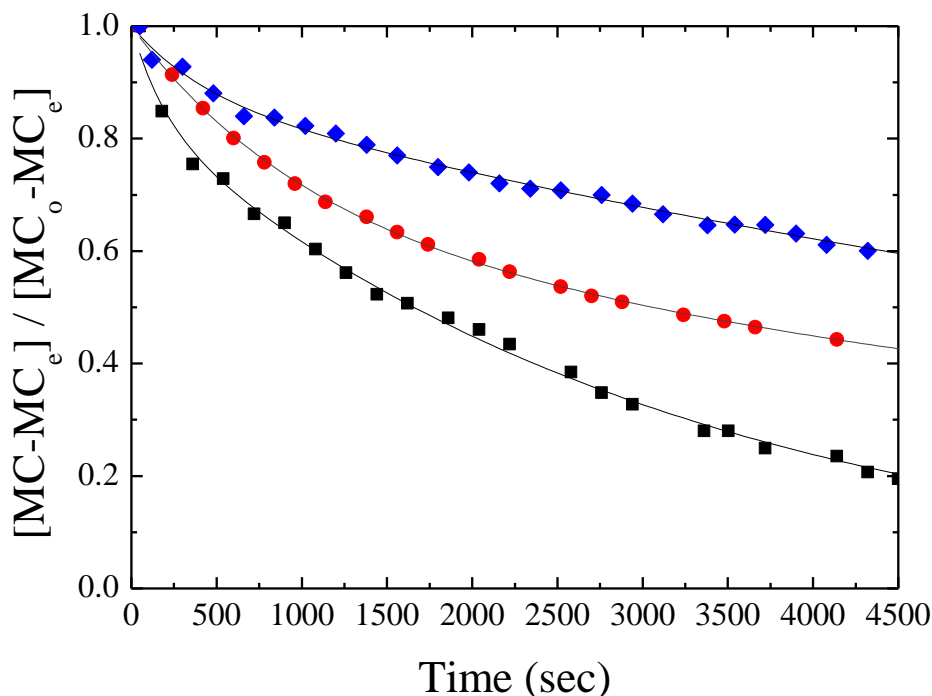
Figure 3.22. Normalized fluorescence intensities of the MC species of the SiO$_2$-g-(PDMAEMA-co-PSPMA) core-shell hybrids in the absence (■) and in the presence of BSA (●) and L-histidine (♦). The solid black lines represent fits to the data using eq. 2.2.1.

The MCs in all cases exhibited two fading rate constants attributed to the short- and the long-lived species as described above. The MC isomers in their majority were long-lived (Table 3.6), with kinetic constants 9.35×10^{-5} s^{-1} and 8.58×10^{-5} s^{-1} in the presence of BSA and L-histidine, respectively. These rate constants were an order of magnitude lower compared to 3.16×10^{-4} s^{-1} calculated for the pure hybrids indicating the electrostatic interaction of BSA and L-histidine with the photogenerated MC dipoles. BSA is negatively charged at the pH range where the system operates and can interact electrostatically with the positive charges of the MCs while the dipolar L-histidine possessing an isolectric point slightly below 8 may exhibit a two-point electrostatic interaction with the MC dipole leading to MC stabilization.

Table 3.6. Rate constants and fractions of short- and long-lived species calculated for the MC-to-SP isomerization within the polymer brush at 25 ^{o}C in the absence and in the presence of BSA and L-histidine

Sample	λ_{max} (nm)[1]	a[2]	b[3]	Rate constants	
				k_1(s^{-1})[4]	k_2(s^{-1})[5]
Hybrids	612	0.15	0.85	5.23×10^{-3}	3.16×10^{-4}
Hybrids – BSA	623	0.36	0.64	9.99×10^{-4}	9.35×10^{-5}
Hybrids – L-histidine	617	0.12	0.88	2.30×10^{-3}	8.58×10^{-5}

[1]Fluorescence maximum of the MC band. [2]Fraction of short-lived MC species (eq. 2.2.1). [3]Fraction of long-lived MC isomers (eq.2.2.1). [4]k_1 represents the rate constant for the short-lived MC species. [5]k_2 represents the rate constant for the long-lived analogues.

The interaction of MCs with L-histidine[67] has been reported previously, while similar MC-to-SP rate constants were obtained for MC-tyrosine, -tryptophan and L-DOPA complexes.[1] The high kinetic constant (2.30×10^{-3} s^{-1}) of the short-lived MCs in the presence of L-histidine which is comparable with that of the short-lived MCs in the absence of biological substances indicate that the 12 % of the molecules do not interact with L-histidine. On the contrary, the presence of BSA retards the thermal fading of both short- and long-lined MCs by an order of magnitude compared to the pure hybrids (Table 3.6). These results suggest that even though the presence of L-histidine do not enchance the FRET efficiency in a similar manner to BSA, however, the aminoacid retards the MC-to-SP isomerization and the system recovery.

3.4 Conclusions

In the present study we report the fabrication of photo-responsive spherical brushes onto SiO$_2$ particles by ATRP. Variations in the microenvironment polarity and free volume of the polymer brush layer were proved to be crucial for both the photoresponsive behavior of the hybrids and their fluorescent properties. In particular, long- and short-lived bipolar MC and X bipolar species were observed upon irradiation of the hydrids with UV light whose fading rates and populations are highly affected by the microenvironment polarity of the polymer brush layer. The grafting of the chains onto the surface of the particles

which inherent variations in the free volume of the polymer and the segmental mobility of the chains is also believe to have a contribution in the establishment of an inhomogeneous environment around the chromophores which results in chromophores fading with different rates. The chemical coloration of the hybrids due to the SP-to-MC isomerization was achieved by increasing the proton concentration in an aqueous dispersion of the hybrids, while at extreme acidic environments the MC protonation was observed. The brush topology was also a critical parameter for the occurance of energy transfer between the X and MC isomers in the nanometer distance scale since it facilitated the close proximity of the species and the donor-acceptor distance to be within the Föster radius. This effect in addition to the overlap of the emission band of the X species with the absorption band of the MC enables the FRET between the bipolar species. The FRET efficiency of the system was significantly enhanced in the presence of BSA which favors the accelerated formation of MC isomers and the increased number of acceptors surrounding the donors. Although, L-lysine did not affect the FRET efficiency of the hybrids however it interacted with the MC dipoles and retarded the MC bleaching. These results demonstrate the light-induced modulation of nanoparticles fluorescence in the presence and absence of biological substances suggesting their potential applications in biosensors, optically addressable devices and others.

3.5 References

(1)   Ipe, B. I.; Mahima, S.; Thomas, K. G. *J. Am. Chem. Soc.* **2003**, *125*, 7174- 7175.

(2)   Wu, Y.; Zhang, C.; Qu, X.; Liu, Z.; Yang, Z. *Langmuir* **2010**, *26*, 9442-9448.

(3)   Liu, D.; Chen, W.; Sun, K.; Deng, K.; Zhang, W.; Wang, Z.; Jiang, X. *Angew. Chem., Int. Ed.* **2011**, *50*, 4103-4107.

(4)   Piech, M.; George, M. C.; Bell, N. S.; Braun, P. V. *Langmuir* **2006**, *22*, 1379-1382.

(5)   George, M. C.; Mohraz, A.; Piech, M.; Bell, N. S.; Lewis, J. A.; Braun, P. V. *Adv. Mater.* **2009**, *21*, 66-70.

(6)   Einaga, Y.; Taguchi, M.; Li, G.; Akitsu, T.; Gu, Z.; Sugai, T.; Sato, O. *Chem. Mater.* **2003**, *15*, 8-10.

(7)   Osborne, E. A.; Jarrett, B. R.; Tu, C.; Louie, A. Y. *J. Am. Chem. Soc.* **2010**, *132*, 5934-5935.

(8)   Hu, D.; Tian, Z.; Wu, W.; Wan, W.; Li, A. D. Q. *J. Am. Chem. Soc.* **2008**, *130*, 15279-15281.

(9)   Zhu, M. Q.; Zhu, L.; Han, J. J.; Wu, W.; Hurst, J. K.; Li, A. D. Q. *J. Am. Chem. Soc.* **2006**, *128*, 4303-4309.

(10)   Zhu, L.; Wu, W.; Zhu, M.-Q.; Han, J. J.; Hurst, J. K.; Li, A. D. Q. *J. Am. Chem. Soc.* **2007**, *129*, 3524-3526.

(11)   Tian, Z.; Li, A. D. Q.; Hu, D. *Chem. Commun.* **2011**, *47*, 1258-1260.

(12)   Jones, C. D.; McGrath, J. G.; Lyon, L. A. *J. Phys. Chem. B* **2004**, *108*, 12652-12657.

(13)   Gan, D.; Lyon, L. A. *J. Am. Chem. Soc.* **2001**, *123*, 8203-8209.

(14)   Yin, J.; Hu, H.; Wu, Y.; Liu, S. *Polymer Chemistry* **2011**, *2*, 363-371.

(15)   Fölling, J.; Polyakova, S.; Belov, V.; Van Blaaderen, A.; Bossi, M. L.; Hell, S. W. *Small* **2008**, *4*, 134-142.

(16)   Chen, J.; Zeng, F.; Wu, S.; Zhao, J.; Chen, Q.; Tong, Z. *Chem. Commun.* **2008**, 5580-5582.

(17)   Medintz, I. L.; Uyeda, H. T.; Goldman, E. R.; Mattoussi, H. *Nat. Mater.* **2005**, *4*, 435-446.

(18)   Giepmans, B. N. G.; Adams, S. R.; Ellisman, M. H.; Tsien, R. Y. *Science* **2006**, *312*, 217-224.

(19)   Lakowicz, J. R. *Principles of Fluorescence Spectroscopy* Springer, 2006.

(20)   Chen, J.; Zhang, P.; Fang, G.; Yi, P.; Yu, X.; Li, X.; Zeng, F.; Wu, S. *J. Phys. Chem. B* **2011**, *115*, 3354-3362.

(21)   Chen, J.; Zeng, F.; Wu, S.; Su, J.; Tong, Z. *Small* **2009**, *5*, 970-978.

(22)   Zhu, L.; Zhu, M. Q.; Hurst, J. K.; Li, A. D. Q. *J. Am. Chem. Soc.* **2005**, *127*, 8968-8970.

(23)   Medintz, I. L.; Trammell, S. A.; Mattoussi, H.; Mauro, J. M. *J. Am. Chem. Soc.* **2004**, *126*, 30-31.

(24)   Piech, M.; Bell, N. S. *Macromolecules* **2006**, *39*, 915-922.

(25)   Wu, T.; Zou, G.; Hu, J.; Liu, S. *Chem. Mater.* **2009**, *21*, 3788-3798.

(26)   Ohno, K.; Morinaga, T.; Koh, K.; Tsujii, Y.; Fukuda, T. *Macromolecules* **2005**, *38*, 2137-2142.

(27)   von Werne, T.; Patten, T. E. *J. Am. Chem. Soc.* **2001**, *123*, 7497-7505.

(28)   Khan, M. A.; Idriss Ali, K. M.; Basu, S. C. *J. Appl. Polym. Sci.* **1993**, *49*, 1547-1551.

(29)   Gao, B.; Chen, Y.; Zhang, Z. *Appl. Surf. Sci.* **2010**, *257*, 254-260.

(30)   Saigal, T.; Dong, H.; Matyjaszewski, K.; Tilton, R. D. *Langmuir* **2010**, *26*, 15200-15209.

(31)   Zhang, M.; Liu, L.; Wu, C.; Fu, G.; Zhao, H.; He, B. *Polymer* **2007**, *48*, 1989-1997.

(32)   Zhang, M.; Liu, L.; Zhao, H.; Yang, Y.; Fu, G.; He, B. *J. Colloid Interface Sci.* **2006**, *301*, 85-91.

(33)   Delgado-Macuil, R.; Rojas-López, M.; Gayou, V. L.; Orduña-Díaz, A.; Díaz-Reyes, J. *Mater. Charact.* **2007**, *58*, 771-775.

(34)   Dattilo, D.; Armelao, L.; Fois, G.; Mistura, G.; Maggini, M. *Langmuir* **2007**, *23*, 12945-12950.

(35)   Del Canto, E.; Flavin, K.; Natali, M.; Perova, T.; Giordani, S. *Carbon* **2010**, *48*, 2815-2824.

(36)   Pyun, J.; Jia, S.; Kowalewski, T.; Patterson, G. D.; Matyjaszewski, K. *Macromolecules* **2003**, *36*, 5094-5104.

(37)   Edmondson, S.; Osborne, V. L.; Huck, W. T. S. *Chem. Soc. Rev.* **2004**, *33*, 14-22.

(38)   Meincken, M.; Sanderson, R. D. *Polymer* **2002**, *43*, 4947-4955.

(39)   Ohno, K.; Morinaga, T.; Takeno, S.; Tsujii, Y.; Fukuda, T. *Macromolecules* **2007**, *40*, 9143-9150.

(40)   Yoshida, T.; Morinaka, A.; Funakoshi, N. *J. Chem. Soc., Chem. Commun.* **1986**, 437-438.

(41)   Zhang, J. Z.; Schwartz, B. J.; King, J. C.; Harris, C. B. *J. Am. Chem. Soc.* **1992**, *114*, 10921-10927.

(42)   Krysanov, S. A.; Alfimov, M. V. *Chem. Phys. Lett.* **1982**, *91*, 77-80.

(43)   Catalán, J. *J. Org. Chem.* **1997**, *62*, 8231-8234.

(44) Wojtyk, J. T. C.; Wasey, A.; Kazmaier, P. M.; Hoz, S.; Buncel, E. *J. Phys. Chem. A* **2000**, *104*, 9046-9055.

(45) Zhou, J.; Li, Y.; Tang, Y.; Zhao, F.; Song, X.; Li, E. *J. Photochem. Photobiol., A* **1995**, *90*, 117-123.

(46) Ueda, M.; Kudo, K.; Ichimura, K. *J. Mater. Chem.* **1995**, *5*, 1007-1011.

(47) Achilleos, D. S.; Vamvakaki, M. *Macromolecules* **2010**, *43*, 7073-7081.

(48) Voudouris, P.; Choi, J.; Dong, H.; Bockstaller, M. R.; Matyjaszewski, K.; Fytas, G. *Macromolecules* **2009**, *42*, 2721-2728.

(49) Wohl, C. J.; Helms, M. A.; Chung, J. O.; Kuciauskas, D. *J. Phys. Chem. B* **2006**, *110*, 22796-22803.

(50) Whelan, J.; Abdallah, D.; Wojtyk, J.; Buncel, E. *J. Mater. Chem.* **2010**, *20*, 5727-5735.

(51) Wojtyk, J. T. C.; Wasey, A.; Xiao, N. N.; Kazmaier, P. M.; Hoz, S.; Yu, C.; Lemieux, R. P.; Buncel, E. *J. Phys. Chem. A* **2007**, *111*, 2511-2516.

(52) Bütün, V.; Armes, S. P.; Billingham, N. C. *Polymer* **2001**, *42*, 5993-6008.

(53) Sumaru, K.; Kameda, M.; Kanamori, T.; Shinbo, T. *Macromolecules* **2004**, *37*, 4949-4955.

(54) Raymo, F. M.; Giordani, S. *J. Am. Chem. Soc.* **2001**, *123*, 4651-4652.

(55) Minami, T.; Tamai, N.; Yamazaki, T.; Yamazaki, I. *J. Phys. Chem.* **1991**, *95*, 3988-3993.

(56) Sapsford, K. E.; Berti, L.; Medintz, I. L. *Angew. Chem., Int. Ed.* **2006**, *45*, 4562-4588.

(57) Gouanvé, F.; Schuster, T.; Allard, E.; Méallet-Renault, R.; Larpent, C. *Adv. Funct. Mater.* **2007**, *17*, 2746-2756.

(58) Chen, J.; Zeng, F.; Wu, S.; Chen, Q.; Tong, Z. *Chem. Eur. J.* **2008**, *14*, 4851-4860.

(59) Shumburo, A.; Biewer, M. C. *Chem. Mater.* **2002**, *14*, 3745-3750.

(60) Seefeldt, B.; Kasper, R.; Beining, M.; Mattay, J.; Arden-Jacob, J.; Kemnitzer, N.; Drexhage, K. H.; Heilemann, M.; Sauer, M. *Photochem. Photobiol. Sci.* **2010**, *9*, 213-220.

(61)   Rhee, K. W.; Gabriel, D. A.; Johnson Jr, C. S. *J. Phys. Chem.* **1985**, *89*, 3193-3195.

(62)   Nayak, A.; Liu, H.; Belfort, G. *Angew. Chem., Int. Ed.* **2006**, *45*, 4094-4098.

(63)   Patrickios, C. S.; Yamasaki, E. N. *Anal. Biochem.* **1995**, *231*, 82-91.

(64)   Lee, C. T.; Smith, K. A.; Hatton, T. A. *Biochemistry* **2004**, *44*, 524-536.

(65)   Pfeifer, U.; Fukumura, H.; Misawa, H.; Kitamura, N.; Masuhara, H. *J. Am. Chem. Soc.* **1992**, *114*, 4417-4418.

(66)   Liu, H. X.; Zhang, R. S.; Yao, X. J.; Liu, M. C.; Hu, Z. D.; Fan, B. T. *J. Chem. Inf. Comput. Sci.* **2004**, *44*, 161-167.

(67)   Liu, Y.; Fan, M.; Zhang, S.; Sheng, X.; Yao, J. *New J. Chem.* **2007**, *31*, 1878-1881.

CHAPTER 4

Light-regulated supramolecular engineering of polymeric nanocapsules

4.1 Introduction

Considerable scientific interest has been devoted lately to the nano-engineering of responsive polymeric spheres with hollow interiors due to their unique features in encapsulating and releasing substances or molecules upon application of a specific external stimulus. The fabrication of such hollow capsules has been tackled using different approaches among which are the block copolymer,[1] the emulsion/interfacial polymerization[2] and the colloidal templating[3] strategy. The latter has been the preferred method because it is more facile and robust involving the layer-by-layer assembly of polyelectrolytes[4] or stereocomplexes[5] onto particles or the grafting of polymers "to"[6] or "from"[7-10] the surface of spherical templates followed by the sacrifice of the latter to form the void of the capsule. The development of the controlled/"living" radical polymerization (CRPs) methods has provided synthetic flexibility towards the introduction of a variety of functionalities onto diverse substrates and has presented a new potential for the covalent grafting of dense polymer films onto the surfaces of particles which can be further degraded to provide multifunctional polymer vesicles of narrow size distribution and controlled shell thickness.[7-10] However, the fabrication of "smart" nanocapsules (NCPs) that can target and release their cargo upon stimulation is still a challenge. In typical systems, the conformational changes of the polymeric constituent of the vesicle are stimulated by classical triggers such as pH,[11-13] temperature,[14-15] and ionic strength[16] whereas recently, redox[17] and voltage[18] variations have been also reported. Nevertheless, these systems often suffer from spatial restrictions and/or inefficient disruption/swelling of the NCP wall.

A great breakthrough in this direction would be the engineering of NCPs whose properties would be reversibly altered by applying a remote stimulus such as light irradiation of specific wavelength since it involves an easily controllable photochemical process with temporal and spatial control. To fulfill this need the NCP walls were doped with either metal nanoparticles or infrared (IR) dyes, which upon NIR illumination absorbed energy and generated local heating leading to variations in the permeability[19] or rupturing[20] of the NCP wall. However, the shortcoming of this approach is related to possible light-driven local heating which can be proved hazardous for certain applications. To avoid this effect, the permeability of the NCP wall can be controlled by a local pH gradient induced by the light irradiation of a "proton-pump" molecule incorporated in the capsule shell.[21] Another approach uses

polarity changes within polymer chains, arising from the photoswitching of light-sensitive molecules such as azobenzenes, to induce reversible morphological micelle-to-"shape-persistent" vesicle transitions.[22] The incorporation of photosensitive or photolabile derivatives within self-assembled polymers has also been employed for the cross-linking and/or the disruption of the latter micellar or NCP structures.[23-30]

A well-known family of photosensitive molecules is that of the non-polar spiropyrans (SPs), which upon irradiation with UV light are isomerized to the polar merocyanines (MCs), whereas irradiation of the latter with visible light regenerates the SP form. This property has been successfully utilized to reversibly disrupt self-assembled micellar structures bearing SP moieties.[31] The tendency of the MCs to aggregate into stack-like arrangements, either of H- or J-type, under certain circumstances,[32] provides a great tool for supramolecular engineering on the basis of noncovalent π-π interactions. Recently, the light-triggered formation of nano-/micrometer size particles from SP-functionalized dendrons via intermolecular MC π-π interactions in organic media was reported.[33] π-π interactions have also been utilized successfully in the formation of highly ordered 2D assemblies[34] and the 3D patterning[35] of colloids bearing the chromophore units via interparticle association. However, light-induced intraparticle π-π interactions to cause the non-covalent cross-linking of polymer chains is unprecedented.

4.2 Experimental Section

Materials. Acetonitrile was purchased from Panreac, Spain hydrofluoric acid (HF) from Sigma,Germany and sodium hydroxide from Fluka, Germany.

4.2.1 Formation of hollow spheres

A dispersion of the polymer-coated SiO_2 particles (0.52 wt %) in an acetonitrile/water mixture (55/45, v/v) was irradiated using a Spectroline hand-held UV lamp operating at 365 nm (8 watt), for 140 min. The dispersion of the particles was diluted further with acetonitrile to yield a final particle concentration of 0.11 wt% (acetonitrile/water 91.4/8.6, v/v) and then stirred with 0.4 mL aqueous solution of 40 % hydrofluoric acid (HF) for 5h to hydrolyze the silica core. The hollow particles were isolated and dialyzed against nanopure water for 1 week to remove any traces of SiF_4 or HF. A similar purification process followed for the hollow spheres which were first

neutralized by the addition of NaOH 0.1 M to adjust the solution pH to 8 before removing the salt form by dialysis.

4.2.2 Characterization

Scanning Electron Microscopy (SEM). The morphology of the precursor core-shell particles and the NCPs was studied by field emission scanning electron microscopy (FESEM; JEOL JSM 7000F) at an accelerating voltage 10-30 kV. For this purpose, a droplet of the particles dispersion was deposited on a silicon wafer, evaporated at RT and sputter coated with 10 nm thick Au to minimize charging. To confirm the hollow nature of the NCPs the samples were dried under reduced pressure which caused the violent evaporation of the solvent and the rupturing of the NCPs wall.

Transmission electron microscopy (TEM). The TEM images were obtained on a JEOL 200-CX instrument operating at 120 kV. For this purpose a droplet of the nanoparticles dispersion was placed on a carbon-coated copper grid and dried under atmospheric pressure.
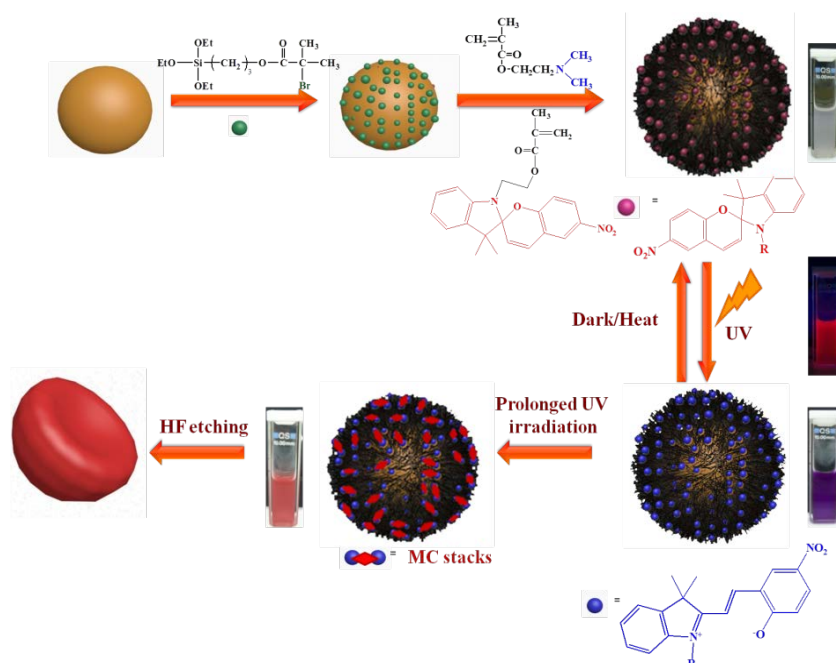
Dynamic light scattering (DLS). The hydrodynamic diameter (D_h) of the precursor silica and the core-shell hybrid particles was determined by DLS using a 3D LS Spectrometer from LS Instrument with a HeNe laser operating at 632.8 nm at fixed scattering angles of 30°, 50°, 70°, 90°, 110° and 130°. The D_h of the NCPs upon varying the solution pH was determined utilizing a Brookhaven BI-200SM light scattering system (Brookhaven Instruments Corporation) at fixed scattering angles 60°, 90° and 120° with the line of Ar^+ laser operating at 514.5 nm while the photo-induced destruction of the NCPs upon irradiation with visible light was monitored with the same set-up at 90°. The average particle sizes were obtained from the intensity autocorrelation functions by KWW analysis.

Fluorescence Measurements. The fluorescence emission and excitation spectra of the core-shell particles upon short and prolonged irradiation with UV light and after the addition of acid as well as those of the nanocapsules (NCPs) at pH 2 were recorded on a scanning spectrofluorometer with excitation provided by a Xenon arc lamp (Jobin-Yvon / Horiba Fluoromax-P). The slit widths were set at 1 nm for excitation and 5 nm for emission. The fluorescent microscopy image of an aqueous solution of the hollow particles at pH 2 was recorded on a Nikon Eclipse E800 microscope upon excitation at 516 nm.

4.3 Results and Discussion

Herein, we describe a novel concept for the supramolecular engineering of fluorescent and pH-sensitive NCPs from light-sensitive core-shell hybrid particles. The hollow capsules are constructed and disrupted upon the application of electromagnetic radiation of the appropriate wavelength. The synthetic strategy followed for the fabrication of the polymeric NCPs is illustrated in Scheme 4.1. First, a molecule capable of initiating an atom transfer radical polymerization (ATRP) process, [3-(2-bromoisobutyryl)propyl]triethoxysilane (BPTS), was immobilized onto the surfaces of silica nanoparticles. Next, the photosensitive monomer, 1´-(2-methacryloxyethyl)-3´,3´-dimethyl-6-nitrospiro-(2*H*-1-benzopyran-2,2´-indoline) (SPMA) was randomly copolymerized with 2-(dimethylamino)ethyl methacrylate (DMAEMA) via copper-mediated ATRP from the surface of the inorganic colloids to give well-defined PDMAEMA-*co*-PSPMA copolymer brushes on the surfaces of the silica particles. The PDMAEMA-*co*-PSPMA random copolymer brushes exhibited a number-average molecular weight (M_n) and polydispersity index (PDI) of 66,600 g/mol and 1.29, respectively by GPC (Table 3.2) and contained 6.1 mole % chromophore units, as determined by ^{1}H NMR (Figure 3.8). The hybrid core-shell structures had a polymer content of 36 wt % (Figure 3.9) and a polymer grafting density of 0.42 chains/nm^2.

Scheme 4.1. Synthetic procedure followed for the fabrication of the NCPs.

Characterization of the SiO$_2$ colloids and the SiO$_2$-*g*-(PDMAEMA-*co*-PSPMA) hybrids by dynamic light scattering (DLS) in neutral pH water showed that the bare

silica particles, with hydrodynamic diameter (D_h) = 267 nm, were successfully modified with the PDMAEMA-*co*-PSPMA random copolymer brushes to obtain hybrid core-shell structures with D_h = 464 nm (Figure 3.12). The morphology of the hybrids was studied by field-emission scanning electron microscopy (FESEM) and transmission electron microscopy (TEM) (Figures 4.1A and 4.1B, respectively). The polymer coated the silica surface uniformly resulting in well-defined hybrids with a diameter of 245 ± 20 nm by SEM. Similarly, TEM images showed a uniform, conformal coating on the surfaces of the particles. Isolated hybrid particles of 237 ± 12 nm diameter surrounded by a 19 ± 3 nm thick polymer layer, seen as a lighter color shell around the dark silica core, were observed (Figure 4.1B).
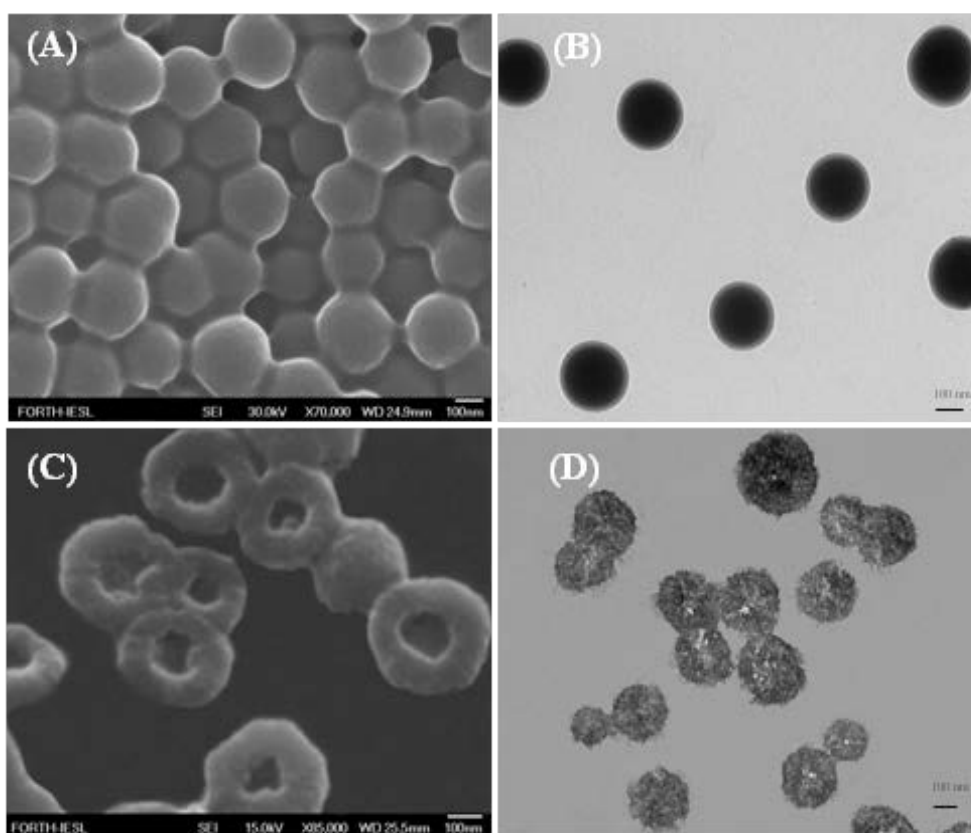

Figure 4.1. FESEM and TEM images of the SiO$_2$-*g*-(PDMAEMA-*co*-PSPMA) core-shell structures before (A and B, respectively) and after (C and D, respectively) HF etching of the inorganic core.

Next, the hybrid particles were subjected to prolonged irradiation with UV light (365 nm) to induce the SP-to-MC isomerization of the chromophore units and promote the formation of intraparticle H-type MC-MC stacks within the polymeric layer, which is favored by the hydrophilic nature of the DMAEMA comonomer and the inherent

steric crowding of the concentrated polymer brush. Upon HF etching of the silica core of the hybrids (Scheme 4.1) the H-aggregates act as non-covalent cross-link points within the dense polymer brush leading to robust NCP structures. Figure 4.1C shows the donut structures derived upon drying the water-swollen capsules, deposited on a silicon substrate, under high vacuum, which induces the rupturing of the vesicles wall. The ability of the NCPs to deform is attributed to the flexible nature of the polymer wall due to the low degree of cross-linking in the shell. The donut structures of 336 ± 31 nm diameter, observed by SEM (Figure 4.1C), indicate that despite the non-permanent character of the cross-links in the shell, the vesicles' wall is robust and retain its integrity both in solution and on the surface. The absence of interparticle association of the colloids is attributed to the low chromophore content (6.1 mole %) of the brush, which favors the observed intrasphere crosslinking. The reasons for the significantly larger size of the NCPs after the core etching compared to that of the precursor core-shell hybrids are two-fold; first the protonation of the PDMAEMA moieties at low pH induces the swelling of the polymer shell, and, second, the capsules flatten on the substrate upon the fracture of the nanocapsule walls under vacuum. TEM also verified the successful formation of the NCPs as indicated by the absence of the core-shell structure (no contrast) and the presence of nearly homogeneous spheres of 260 ± 44 nm diameter (Figure 4.1D). The size of the NCPs by TEM is close to that of the core-shell precursor particles, due to the mild conditions used for drying the NCPs on the carbon coated grid, which prevented the rupturing of the NCPs wall.

The nature of the intramolecular interactions induced within the photosensitive brush upon UV irradiation, which govern the supramolecular engineering of the NCPs, was verified by fluorescence spectroscopy. Figure 4.2A shows the emission spectra (λ_{ex} = 516 nm) of the precursor core-shell colloids upon short and prolonged irradiation with UV light, and following the addition of acid to the prolonged irradiation sample. The spectra of the hybrids after short irradiation time exhibit a band at 620 nm, assigned to the open MC residues,[36] whereas, upon prolonged irradiation the evolution of a new band at 566 nm is observed, attributed to the formation of H-stacks[37] which co-exist with the free MC species. Finally, the addition of acid (to adjust the solution pH to 2), induces the protonation of the MC isomers observed as a decrease in the intensity of the band at 606 nm, whereas the H-

aggregates remain unaffected in the extreme acidic environment as indicated by the high intensity of the peak at 566 nm (Figure 4.2A).
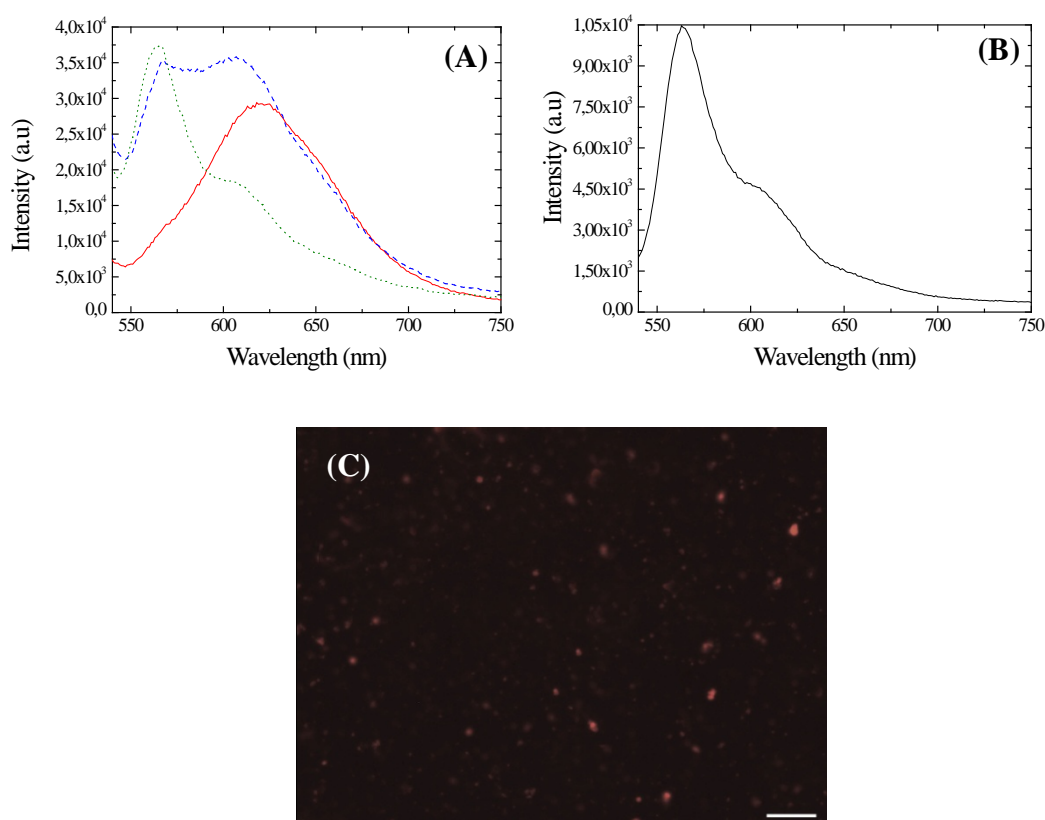

Figure 4.2. Fluorescence emission (λ_{ex} = 516 nm) spectra of the core-shell particles upon short (—) and prolonged (---) irradiation with UV light, and after the addition of acid to the prolonged irradiation sample (…) (A), fluorescence emission (λ_{ex} = 516 nm) spectrum (—) (B) and fluorescent microscopy image of an aqueous solution of the NCPs at low pH (C). The scale bar is 4 μm.

Similarly, the emission spectrum of the NCPs at pH 2, recorded upon excitation at 516 nm, exhibited two separated maxima; an intense band at 563 nm attributed to the H-aggregates and a red-shifted peak at 605 nm attributed to the MC residues of the vesicles. The above verify the formation of H-aggregates upon prolonged irradiation of the hybrid core-shell particles allowing the development of NCPs upon core etching. These aggregates serve as cross-links affording robustness to the NCP walls and rendering the vesicles stable even at low pH. Fluorescence microscopy imaging (Figure 4.2C) of an aqueous dispersion of the NCPs at low pH shows clearly that the vesicles exhibit orange-red fluorescence emission, in agreement with the

spectrum in Figure 4.2B. This inherent fluorescence of the NCPs in aqueous media is unexpected because neither the SPs nor the MCs exhibit appreciable fluorescence in water. The fluorescence efficiency of MC moieties has been reported to be enhanced under specific circumstances such as within hydrophobic cavities of polymeric particles,[38-39] which, however, is not the case for the SiO$_2$-*g*-(PDMAEMA-*co*-PSPMA) particles or the NCPs. The fluorescence of these entities in the two latter nanostructures (Figures 4.2A and 4.2B) may be attributed to the entrapment of the chromophores in the spatially crowded environment of the polymer brush and their restricted conformational flexibility which can induce minimization of the nonradiative relaxation through internal motion of the excited molecules.[38] This inherent fluorescent behavior of the NCPs render them attractive in biological fluorescent labeling applications allowing their tracking during *in vivo* experiments.

The PDMAEMA component of the NCPs is a weak polybase[40] with an effective pK_α of the tertiary amine groups of about 5.9 (Figure 3.15a). Thus at pH below 5.9, PDMAEMA behaves as a cationic polyelectrolyte while at high pH the polymer becomes uncharged. This pH-sensitive property of PDMAEMA is expected to affect the size of the NCPs which would expand due to the repulsive interactions between the charged amine groups and the osmotic pressure induced by the chloride counterions,[41] and shrink upon neutralization of the polymer at high pH (Figure 4.3B). The pH-responsive behaviour of the NCPs was studied by DLS. Figure 4.3A shows the intensity autocorrelation functions, at scattering angle $\theta = 90^o$, of the NCPs at pH 2 and 8, i.e., below and above the effective pK_α of the DMAEMA units, respectively. At low pH, a diffusion coefficient of 2.2×10^{-8} cm^2 s^{-1} corresponding to a D_h of 219 nm, assuming a hard-sphere model, is found, while upon increasing the solution pH to 8 the diffusion coefficient increases to 2.8×10^{-8} cm^2 s^{-1} indicating the decrease of the NCPs size to 172 nm.
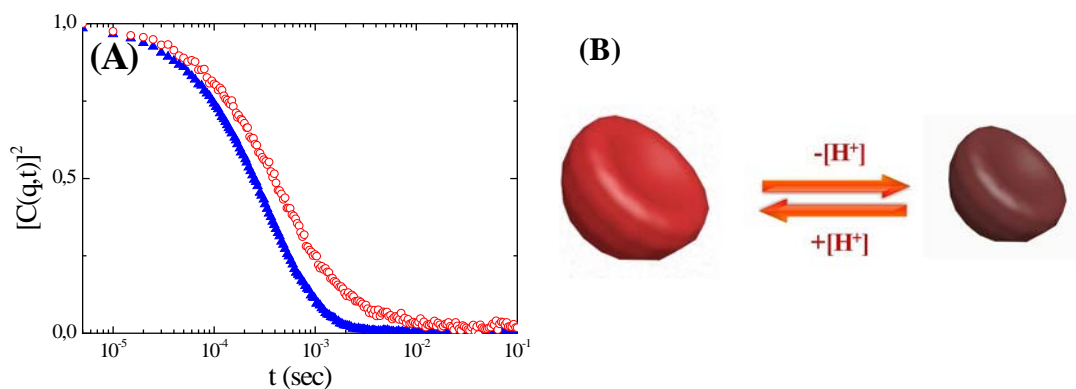
Figure 4.3. Intensity autocorrelation functions of the NCPs at pH 2 (○) and 8 (▲) (A) at scattering angle $\theta = 90^\circ$; Schematic representation of the NCPs responsive behavior to pH variations (B).

The decrease of the NCPs' diameter by 47 nm at high pH values verifies the shrinkage of the NCPs upon deprotonation of the PDMAEMA units. It should also be noted that the hydrodynamic diameter of the hollow spheres both at low and high pH was significantly smaller than that of the precursor hybrids, indicating the partial collapse of the polymer shell upon dissolution of the inorganic core (Figure 3.12). The sensitivity of the NCPs to changes of the solution pH was also confirmed by FESEM imaging at pH 2 and 8 (Figure 4.4A and 4.4B, respectively). At pH 2, when the DMAEMA units are positively charged and the repulsive forces along the macromolecular chain are dominant, the NCPs are highly hydrated and the average diameter of the ruptured nanospheres was found to be 336 ± 31 nm (Figure 4.4A).
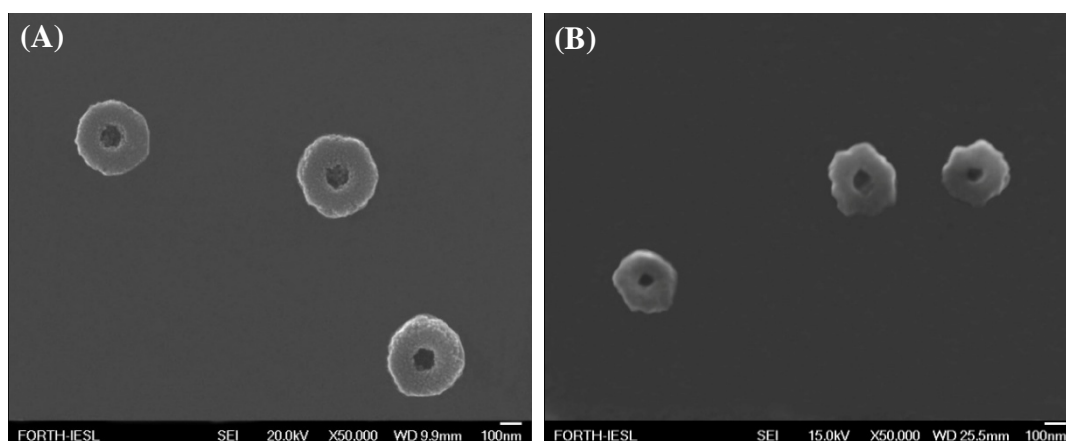
Figure 4.4. FESEM images of the NCPs at pH 2 (A) and upon increasing the solution pH to 8 (B).

234

When increasing the solution pH to 8, the average diameter of the raptured capsules decreased to 302 ± 18 nm (Figure 4.4B) suggesting the shrinkage of the vesicles, in agreement with the DLS results discussed above. It should also be noted, that the NCPs remain isolated and non- aggregated even at high pH, whereas the intraparticle stacking which provides the robustness to the vesicle wall is not affected by pH variations. This suggests that the NCPs are robust structures whose size and wall permeability can be conveniently tuned as a function of solution pH, rendering them attractive nanocarriers for stimuli responsive capture and release applications.

We have recently shown that the H-type MC-MC stacks can be dissociated upon visible light irradiation due to an MC-to-SP isomerization.[42] In this work, we report for the first time, the disruption of NCPs upon application of visible light irradiation and dissociation of the H-aggregates. An aqueous dispersion of the NCPs at low pH was exposed to visible light irradiation for various time intervals followed by DLS measurements. Figure 4.5A shows the intensity autocorrelation functions of an aqueous dispersion of the NCPs at pH 2, measured at a scattering angle $\theta = 90^\circ$, after different exposure times. The scattering intensity decreased gradually with irradiation time as shown in Figure 4.5A. Considering that the autocorrelation functions were measured at the same scattering angle ($\theta = 90^\circ$), the changes in scattering intensity upon light irradiation can be attributed to variations in the optical contrast and the volume of the scatterers according to the scattering theory of dilute solutions. The decrease of the scattering intensity at $t = 0$ as a function of irradiation time (Figure 4.5A, inset) verified the dissociation of the MC-MC H-type stacks that act as cross-link points in the NCPs wall and thus the gradual destruction of the vesicles (Figure 4.5C).[43-44] However, some residual nanoscale assemblies are evidenced even after prolonged irradiation, observed as a slow process of very low scattering intensity. These are ascribed to hydrophobic interactions between the dissociated amphiphilic polymer chains derived upon the photo-induced MC-to-SP isomerization of the chromophore units (Figure 4.5A). The disruption of the NCPs is further verified by the FESEM images of the NCPs after exposure to visible light for 18.7 hrs.
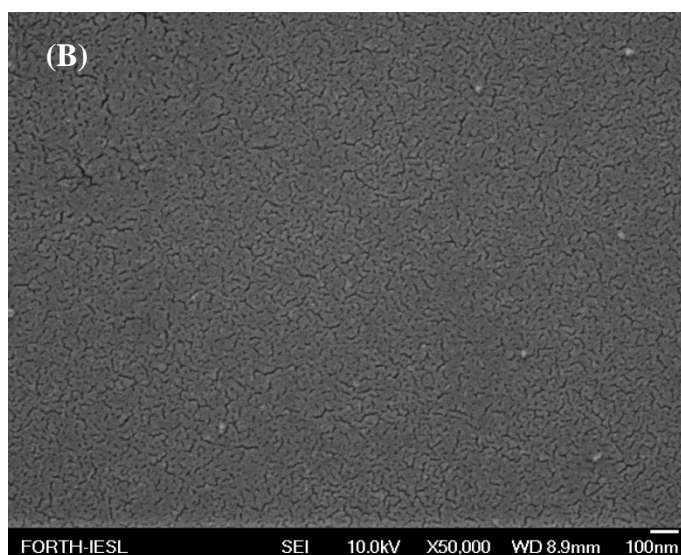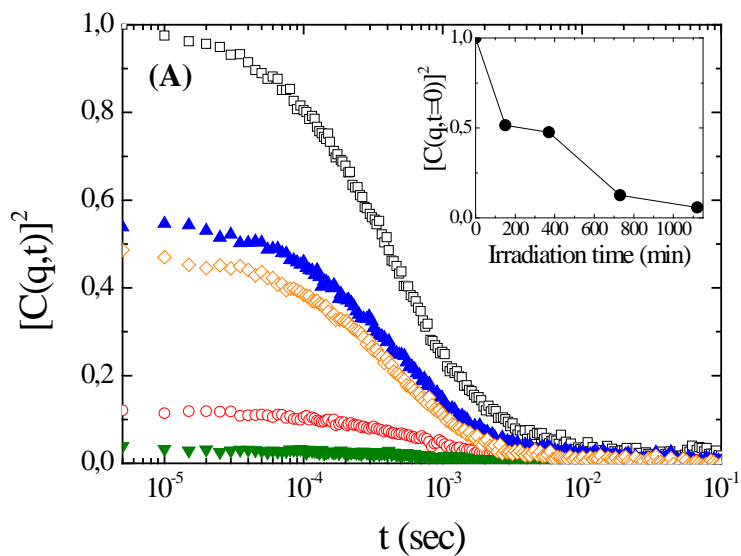
Figure 4.5. Intensity autocorrelation functions of the hollow particles after irradiation with visible light at various time intervals; 0 (□), 150 (▲), 371 (◊), 731 (○) and 1121 (▼) min at scattering angle $\theta = 90^{\circ}$ (A); FESEM image of the NCPs after irradiation with visible light for 1121 min (B) and schematic illustration of the light-induced disruption of the NCPs (C).

The absence of the polymer vesicle structures indicates that the NCPs were effectively dissociated to their constituent polymeric chains giving rise to the formation of a homogeneous polymeric film on the substrate. We anticipate that this light-induced disruption of the polymeric vesicles would be particularly advantageous for the controlled release of an encapsulated cargo by means of a harmless stimulus such as visible light and we are currently exploring this process.

4.4 Conclusions

In summary, we propose a novel approach for the supramolecular engineering of NCPs in water based on the controlled formation and dissociation of π-π H-type interactions among MC chromophore units in a polymer shell layer by application of a light-trigger of appropriate wavelength. The development of the NCPs was based on the ability of the MC isomers to form stacks, upon UV irradiation, within a sterically crowded polymer brush on silica particles. The robust NCPs derived following HF etching of the silica core of the hybrids, can be progressively disrupted in a controlled manner by applying a harmless stimulus such as visible light radiation. The pH-responsive character of the NCPs provides a facile route to alter their size by variations in the solution pH. The inherent ability of the NCPs to fluoresce in water opens new possibilities for the development of addressable nanoscale capsules that can function in environmentally benign aqueous media.

4.5 References

(1)   Liu, F.; Eisenberg, A. *J. Am. Chem. Soc.* **2003**, *125*, 15059-15064.

(2)   Lv, H.; Lin, Q.; Zhang, K.; Yu, K.; Yao, T.; Zhang, X.; Zhang, J.; Yang, B. *Langmuir* **2008**, *24*, 13736-13741.

(3)   Caruso, F.; Caruso, R. A.; Möhwald, H. *Science* **1998**, *282*, 1111-1114.

(4)   Peyratout, C. S.; Dähne, L. *Angew. Chem. Int. Ed.* **2004**, *43*, 3762-3783.

(5)   Kida, T.; Mouri, M.; Akashi, M. *Angew. Chem.* **2006**, *118*, 7696-7698.

(6)   Liu, X.; Basu, A. *J. Am. Chem. Soc.* **2009**, *131*, 5718-5719.

(7)   Morinaga, T.; Ohkura, M.; Ohno, K.; Tsujii, Y.; Fukuda, T. *Macromolecules* **2007**, *40*, 1159-1164.

(8)   Mandal, T. K.; Fleming, M. S.; Walt, D. R. *Chem. Mater.* **2000**, *12*, 3481-3487.

(9)   Fu, G. D.; Shang, Z.; Hong, L.; Kang, E. T.; Neoh, K. G. *Adv. Mater.* **2005**, *17*, 2622-2626.

(10) Kamata, K.; Lu, Y.; Xia, Y. *J. Am. Chem. Soc.* **2003**, *125*, 2384-2385.

(11) Broz, P.; Driamov, S.; Ziegler, J.; Ben-Haim, N.; Marsch, S.; Meier, W.; Hunziker, P. *Nano Lett.* **2006**, *6*, 2349-2353.

(12) Chiu, H.-C.; Lin, Y.-W.; Huang, Y.-F.; Chuang, C.-K.; Chern, C.-S. *Angew. Chem. Int. Ed.* **2008**, *47*, 1875-1878.

(13) Du, J.; Armes, S. P. *J. Am. Chem. Soc.* **2005**, *127*, 12800-12801.

(14) Pasparakis, G.; Alexander, C. *Angew. Chem. Int. Ed.* **2008**, *47*, 4847-4850.

(15) Li, Y.; Lokitz, B. S.; McCormick, C. L. *Angew. Chem. Int. Ed.* **2006**, *45*, 5792-5795.

(16) Ibarz, G.; Dähne, L.; Donath, E.; Möhwald, H. *Adv. Mater.* **2001**, *13*, 1324-1327.

(17) Power-Billard, K. N.; Spontak, R. J.; Manners, I. *Angew. Chem. Int. Ed.* **2004**, *43*, 1260-1264.

(18) Yan, Q.; Yuan, J.; Cai, Z.; Xin, Y.; Kang, Y.; Yin, Y. *J. Am. Chem. Soc.* **2010**, *132*, 9268-9270.

(19) Skirtach, A. G.; Karageorgiev, P.; Bédard, M. F.; Sukhorukov, G. B.; Möhwald, H. *J. Am. Chem. Soc.* **2008**, *130*, 11572-11573.

(20) Skirtach, A. G.; Antipov, A. A.; Shchukin, D. G.; Sukhorukov, G. B. *Langmuir* **2004**, *20*, 6988-6992.

(21) Erokhina, S.; Benassi, L.; Bianchini, P.; Diaspro, A.; Erokhin, V.; Fontana, M. P. *J. Am. Chem. Soc.* **2009**, *131*, 9800-9804.

(22) Liu, X.; Jiang, M. *Angew. Chem. Int. Ed.* **2006**, *45*, 3846-3850.

(23) Yesilyurt, V.; Ramireddy, R.; Thayumanavan, S. *Angew. Chem. Int. Ed.* **2011**, *50*, 3038-3042.

(24) Jiang, J.; Tong, X.; Zhao, Y. *J. Am. Chem. Soc.* **2005**, *127*, 8290-8291.

(25) Goodwin, A. P.; Mynar, J. L.; Ma, Y.; Fleming, G. R.; Fréchet, J. M. J. *J. Am. Chem. Soc.* **2005**, *127*, 9952-9953.

(26) Babin, J.; Pelletier, M.; Lepage, M.; Allard, J. F.; Morris, D.; Zhao, Y. *Angew. Chem. Int. Ed.* **2009**, *48*, 3329-3332.

(27) He, J.; Tong, X.; Tremblay, L.; Zhao, Y. *Macromolecules* **2009**, *42*, 7267-7270.

(28) Katz, J. S.; Zhong, S.; Ricart, B. G.; Pochan, D. J.; Hammer, D. A.; Burdick, J. A. *J. Am. Chem. Soc.* **2010**, *132*, 3654-3655.

(29) Jiang, Y.; Wang, Y.; Ma, N.; Wang, Z.; Smet, M.; Zhang, X. *Langmuir* **2007**, *23*, 4029-4034.

(30) Jiang, J.; Shu, Q.; Chen, X.; Yang, Y.; Yi, C.; Song, X.; Liu, X.; Chen, M. *Langmuir* **2010**, *26*, 14247-14254.

(31) Lee, H.-i.; Wu, W.; Oh, J. K.; Mueller, L.; Sherwood, G.; Peteanu, L.; Kowalewski, T.; Matyjaszewski, K. *Angew. Chem. Int. Ed.* **2007**, *46*, 2453-2457.

(32) Krongauz, V. A.; Goldburt, E. S. *Macromolecules* **1981**, *14*, 1382-1386.

(33) Chen, Q.; Feng, Y.; Zhang, D.; Zhang, G.; Fan, Q.; Sun, S.; Zhu, D. *Adv. Funct. Mater.* **2010**, *20*, 36-42.

(34) Piech, M.; George, M. C.; Bell, N. S.; Braun, P. V. *Langmuir* **2006**, *22*, 1379-1382.

(35) George, M. C.; Mohraz, A.; Piech, M.; Bell, N. S.; Lewis, J. A.; Braun, P. V. *Adv. Mater.* **2009**, *21*, 66-70.

(36) Wu, T.; Zou, G.; Hu, J.; Liu, S. *Chem. Mater.* **2009**, *21*, 3788-3798.

(37) Miyata, A.; Heard, D.; Unuma, Y.; Higashigaki, Y. *Thin Solid Films* **1992**, *210-211*, 175-177.

(38) Zhu, M. Q.; Zhu, L.; Han, J. J.; Wu, W.; Hurst, J. K.; Li, A. D. Q. *J. Am. Chem. Soc.* **2006**, *128*, 4303-4309.

(39) Zhu, L.; Wu, W.; Zhu, M. Q.; Han, J. J.; Hurst, J. K.; Li, A. D. Q. *J. Am. Chem. Soc.* **2007**, *129*, 3524-3526.

(40) Bütün, V.; Armes, S. P.; Billingham, N. C. *Polymer* **2001**, *42*, 5993-6008.

(41) Achilleos, D. S.; Georgiou, T. K.; Patrickios, C. S. *Biomacromolecules* **2006**, *7*, 3396-3405.

(42) Achilleos, D. S.; Vamvakaki, M. *Macromolecules* **2010**, *43*, 7073-7081.

(43) Jiang, J.; Tong, X.; Morris, D.; Zhao, Y. *Macromolecules* **2006**, *39*, 4633-4640.

(44) Han, D.; Tong, X.; Zhao, Y. *Macromolecules* **2011**, *44*, 437-439.

CHAPTER 5

Conclusions and Perspectives

5.1. Conclusions

In this work we have synthesized SP-based polymeric systems in the form of random copolymers, core-shell hybrid particles and hollow nanocapsules and we investigated the responsive solution properties of the systems. The SP-based polymeric materials were synthesized by bulk and solution ATRP from free or surface-bound initiator. The solvato-, pH-, temperature- and light-responsive behavior of the systems was investigated in detail.

Multi-responsive spiropyran-based PDMAEMA-*co*-PSP copolymers, in which the content of the photosensitive moieties was varied between 1.3 and 10 mol%, were synthesized by the random copolymerization of DMAEMA and the in-house synthesized SP monomer 1',3',3'-trimethyl-6-methacryloyloxy-spiro(2*H*-1-benzopyran-2,2'-indoline) by copper-mediated ATRP in solution. A PMMA-*co*-PSP copolymer containing 19 mol% SP was also synthesized by the same method and its absorption properties were compared to those of the PDMAEMA-*co*-PSP copolymers. The solvatochromic, pH, temperature and light responsive behavior of the PDMAEMA-*co*-PSP polymers in solution was monitored by UV/vis spectroscopy. The polarity of the comonomer was shown to selectively stabilize a certain colored form of the photosensitive moieties and thus influence the solvatochromic behavior of the polymer. In particular, DMAEMA is polar and stabilized the planar switterionic form which exhibited a hypsochromic shift upon increasing the solvent polarity, whereas, the less polar MMA comonomer stabilized a non-polar photoisomer which was not affected by the polarity of the solvent. The PDMAEMA-*co*-PSP copolymers also exhibited a reversible pH-induced SP-to-MC isomerization and protonation/deprotonation of the MC form accompanied by a color change of the polymer solution. A strong influence of the copolymer composition and the photo-induced MC-to-SP isomerization of the chromophore moieties on the phase transition behavior of the PDMAEMA-*co*-PSP copolymers was found, with an increase of the LCST with the hydrophilic MC chromophore content and a decrease of the transition temperature following the photo-induced MC-to-SP isomerization of the chromophores due to the hydrophobic character of the SP moieties. Finally, the PDMAEMA-*co*-PSP copolymers exhibited a photo-induced decoloration, upon irradiation with visible light, which was faster in acetonitrile compared to water due to the more effective stabilization of the bipolar MC isomer in polar solvent media. This

241

multi-responsive character of the synthesized copolymers and their solubility in aqueous media, present a clear advantage for their use in biomedical and environmental applications.

The property of the chromophore units of the above PDMAEMA-*co*-PSP copolymers to isomerize to the open MC form without light stimulation, created the need of synthesizing photoresponsive SP-based materials which can selectively and reversibly isomerize between the SP and MC form, upon applying electromagnetic radiation of the appropriate wavelength. For this purpose we first synthesized the photoresponsive molecule, 2-(3',3'-dimethyl-6-nitro-3'H-spiro[chromene-2,3'-indol]-1'-yl)-ethanol (SP-OH) via a three-step reaction, which was further functionalized with a methacrylate moiety to obtain the photosensitive monomer, 1´-(2-methacryloxyethyl)-3´,3´-dimethyl-6-nitrospiro-(2H-1-benzopyran-2,2´-indoline) monomer (SPMA). A photoresponsive PDMAEMA-*co*-PSPMA random copolymer carrying 6.1 mol% chromophore units was synthesized via the random copolymerization of DMAEMA and SPMA by ATRP in bulk. The polymerization conditions used, were previously optimized for homopolymerization of DMAEMA in the absence of the chromophore units and the reaction kinetics showed that the polymerization proceeded in a "controlled" and "living manner". The responsive properties of the copolymer upon application of UV irradiation and upon variation of the solution pH was studied by UV/vis spectroscopy, while the fluorescent properties of the copolymer were investigated by fluorescent spectroscopy. The stimulation of the copolymer with UV light in water generated three bipolar isomers from the same parent spiropyran (SP) molecule; namely the non-planar X isomer and two different planar merocyanine (MC) species, MC_1 and MC_2 which differ in polarity. The photo-isomers followed a biexponential thermal bleaching mechanism originated from localized barriers inherent in the polymer matrix which establish a non-homogeneous microenvironment around the chromophores. Upon addition of acid the copolymer exhibited an abundance of MC species due to the acid catalyzed SP-to-MC isomerization of the chromophore units in parallel with the formation of $[SP-NH]^+$ species, while at extreme acidic environments the $[MC-OH]^+$ form was generated. Investigation of the fluorescent properties of the copolymers showed that the macromolecular chains comprise a suitable scaffold for intra- and inter-chain FRET due to the photo-induced generation of a sufficient number of X and MC species from

242

the SP isomers, which are FRET donor-acceptor pairs. The photo-regulated energy transfer is favored by the close proximity of the bipolar isomers, promoted by the association of the random copolymers in water, and the spectral overlap of the emission and absorption bands of X and MC isomers, respectively. Finally, the FRET process was interrupted by the thermal MC-to-SP relaxation of the acceptors. However, the effective stabilization of the MC isomers in the polar microenvironment, established by the polar DMAEMA comonomer and the aqueous medium, provided adequate isomerization rates to the chromophores and enabled the read-out process. To the best of our knowledge the development of such nano-sized FRET systems based on random copolymers which associate in water and carry donor-acceptor pairs derived upon the photostimulation of a single parent molecule, is unprecedented.

In the second part of this study, well-defined photoresponsive spherical polymer brushes were synthesized by the random copolymerization of DMAEMA and SPMA from the surface of silica particles via copper-mediated ATRP in bulk. Three hybrids were prepared; two core-shell particles, SiO_2-g-(PDMAEMA-co-PSPMA) carrying 4.8 and 6.1 mol% SPMA units, and a third sample with higher SPMA content of 11.5 mol%. It was shown that well defined core-shell particles can be synthesized in the presence of a low SPMA content, while at higher SPMA fractions the polymerization control was lost. The photo- and pH-responsive behavior of the SiO_2-g-(PDMAEMA-co-PSPMA) core-shell structures carrying 6.1 mol% chromophores and their fluorescent properties were investigated in water by UV/vis and fluorescent spectroscopy, respectively. Stimulation of the hybrids with UV light resulted in the photoisomerization of the spiropyran (SP) units to two different bipolar species; the cisoid non-planar X and the planar merocyanine (MC) isomers which follow a biexponential thermal relaxation process to reform the SP isomers due to the presence of long- and short-lived bipolar species within the polymer brush. The fading rates and populations of the long- and short-lived species are highly affected by the microenvironment polarity of the polymer brush layer. The grafting of the chains onto the surface of the particles which induces inherent variations in the free volume of the polymer and the segmental mobility of the chains establishing an inhomogeneous environment around the chromophores which results in the more complicated fading mechanism of the chromophores. On the other hand, the increase in proton

243

concentration in the aqueous medium stimulates the SP-to-MC isomerization, while at extreme acidic environments the formation of [MC-OH]$^+$ species is induced similar to the results obtained above for the random PDMAEMA-co-PSPMA copolymers. Finally, the generation of two different fluorescent bipolar species, X and MC, from the same parent SP molecule upon UV irradiation of the hybrids in aqueous media provided the unique property to the system to exhibit intra-particle FRET between the X and MC residues. The occurrence of the FRET mechanism was achieved due to the spectral overlapping of the emission and the absorption bands of the X and MC isomers, respectively and the proximity of the molecules promoted by the steric crowding within the polymer brush layer. This energy transfer process was switched "off" upon the thermal fading of the MC species which exhibited appropriate kinetic rates in the polar microenvironment of the brush and enabled the monitoring of the process. To the best of our knowledge, the inherent property of a spherical polymer brush system to exhibit FRET due to the generation of X-MC donor-acceptor pairs, following the photo-stimulation of one single parent molecule, and their efficient stabilization by the surrounding microenvironment is unprecedented. This property of the nanohybrids can be successfully employed for the detection of biological substances such as proteins and aminoacids. In particular, the core-shell structures showed an excellent function in the presence of biomolecules such as proteins and aminoacids, which affected the FRET efficiency of the system; namely the presence of bovine serum albumin (BSA) in the aqueous dispersion of the hybrids was shown to enhance significantly the FRET efficiency of the system, due to the accelerated MC formation, which is catalyzed by the protein and leads to abundant MC acceptors around the X donors. On the other hand, although, L-histidine did not affect the FRET efficiency of the hybrids however it interacted with the MC dipoles and retarded the MC bleaching process. These results demonstrate the light-induced modulation of the nanoparticles' fluorescence behavior in the presence and absence of biological substances suggesting their potential applications in biosensors, optically addressable devices and others.

Finally, the photoresponsive, SiO$_2$-g-(PDMAEMA-co-PSPMA) core-shell hybrids, were used as precursors for the light-regulated supramolecular engineering of polymeric NCPs. The novelty of our approach relies on the controlled formation and dissociation of π-π H-type interactions among MC chromophore units in a polymer

shell layer by application of a light trigger of appropriate wavelength. The development of the NCPs was based on the ability of the MC isomers to form stacks, upon UV irradiation, within the sterically crowded polymer brush layer on the surface of the silica particles. More importantly, the robust NCPs derived following HF etching of the silica core of the hybrids, could be progressively disrupted in a controlled manner by applying a harmless stimulus such as visible light radiation. The pH-responsive character of the NCPs provided a facile route to alter their size by variations in the solution pH. Finally, the inherent ability of the NCPs to fluoresce in water opens new possibilities for the development of addressable nanoscale capsules that can function in environmentally benign aqueous media.

5.2   Perspectives

The novel synthesis of multiresposnive materials discussed in this work, being sensitive to various stimuli including solvent polarity, pH-, temperature and light create new perspectives for their use in various applications.

The PDMAEMA-*b*-SPMA copolymers synthesized in this study by sequential ATRP, can self-assemble in the aqueous medium forming multiresponsive micellar structures which may be disrupted upon cooperative response to more than one stimulus (pH, temperature and light). The multiresponsive self-associated structures can potentially be used as drug delivery systems by encapsulating hydrophobic drugs within the core of the micellar structures and releasing them upon application of one or more stimulus. The advantage of this system over the traditional drug release materials is its ability to respond to a remote stimulus such as light which provides spatial and temporal control. On the same basis, the SiO_2-*g*-(PDMAEMA-*co*-PSPMA) core-shell hybrids, having the ability to form oil-in-water Pickering emulsions, which can be reversibly destabilized and reformed by applying the appropriate light stimulus allow the controlled encapsulate and release of various substances.

Finally, the SiO_2-*g*-(PDMAEMA-*co*-PSPMA) core-shell hybrids can be also used as building units for the development of 3D structures via the direct laser writing of the photoresponsive colloids onto flat surfaces pre-modified with SP-containing polymer brushes, based on the formation of π-π H-type interactions among the MC chromophores in the polymer shell layer. The ability of the DMAEMA comonomer at

low pH to interact with negatively charged metal complexes can be utilized for the decoration of these 3D structures with metal nanoparticles upon reduction of the metal complex. On the basis, of the π-π H-type interactions derived upon the prolong photostimulation of the chromophore moieties of the SiO$_2$-g-(PDMAEMA-co-PSPMA) core-shell hybrids, the reversible formation of supramolecular assemblies can be studied by applying sequentially the appropriate light trigger.
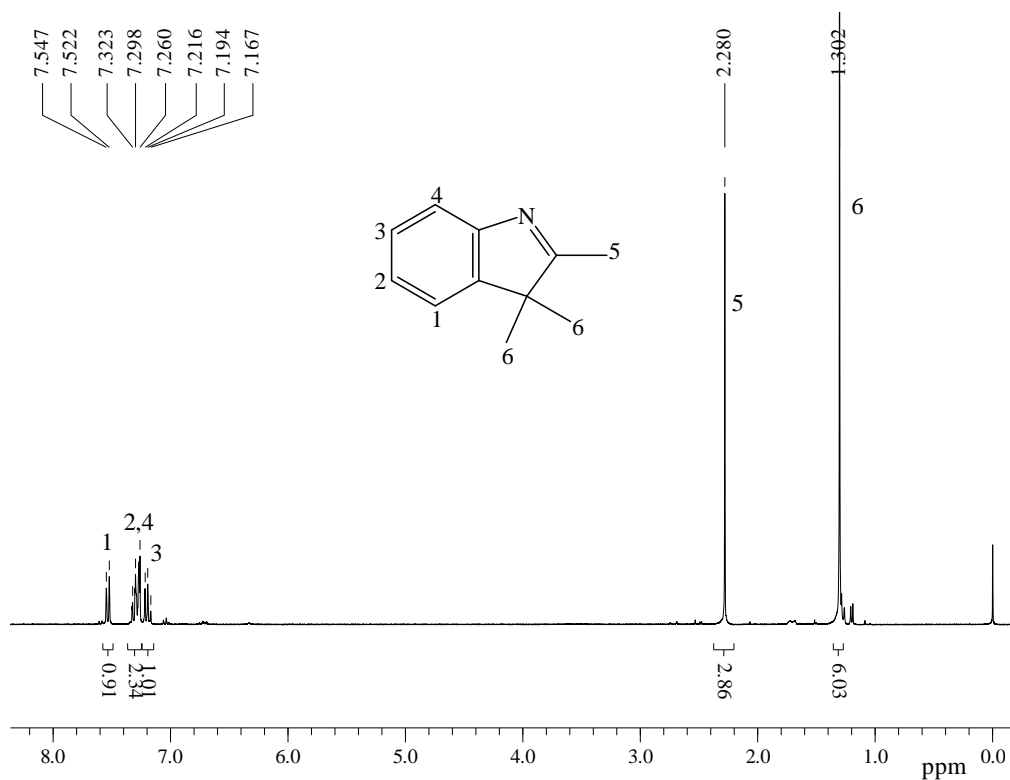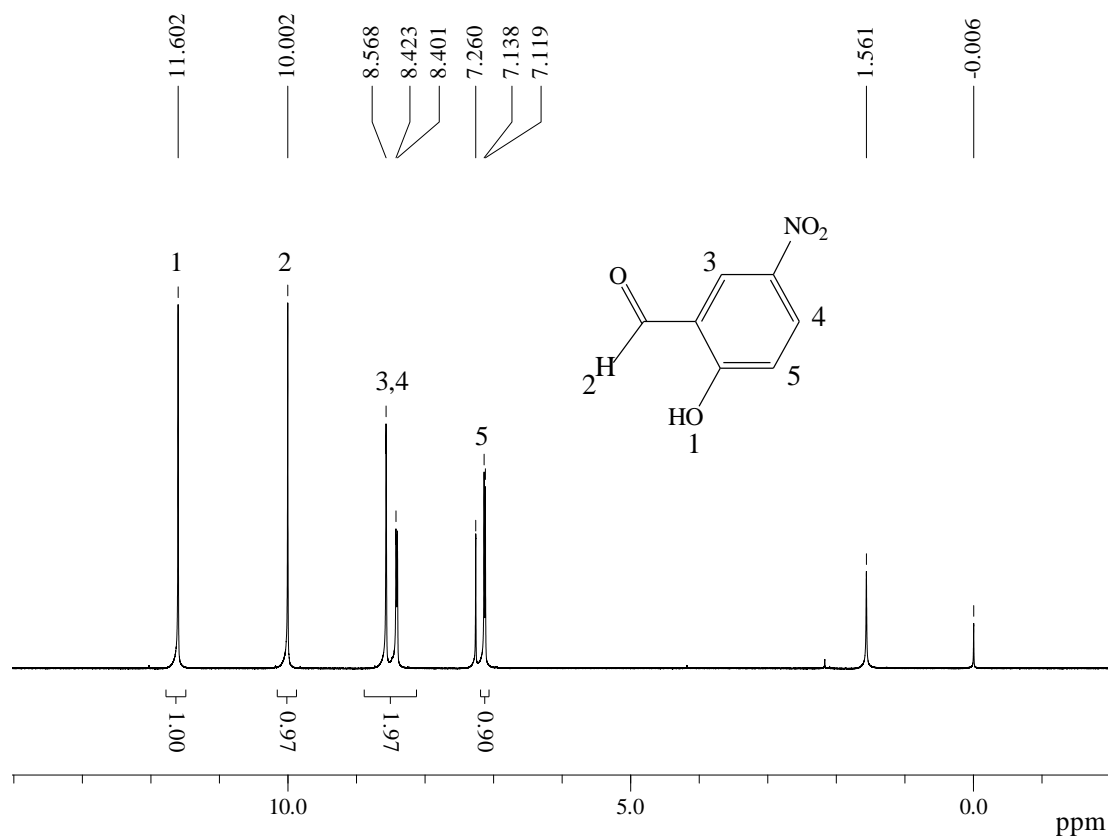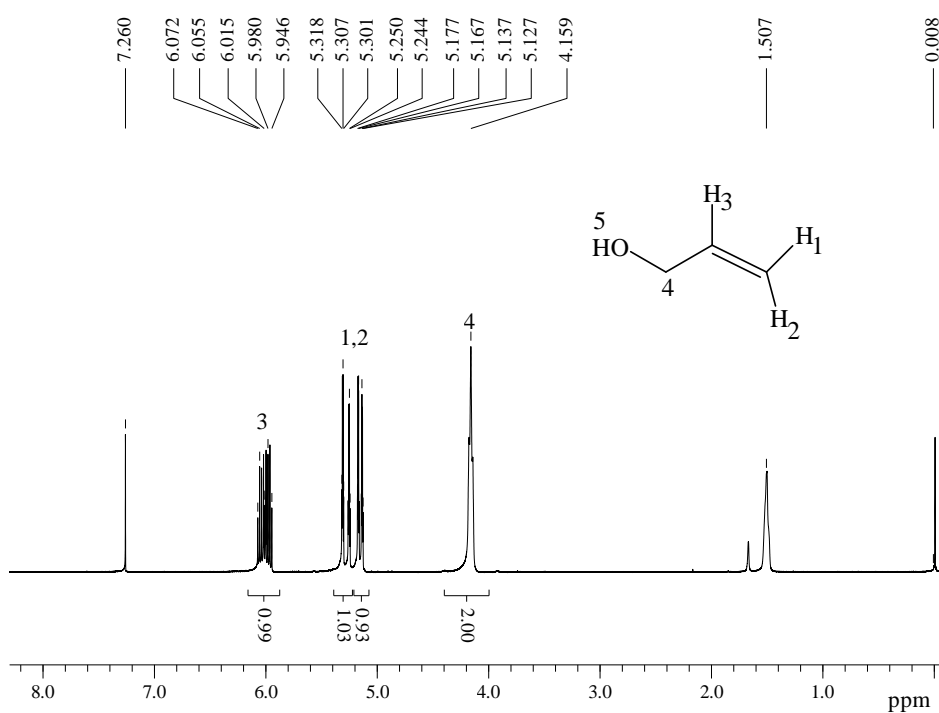
CHAPTER 6

Appendix
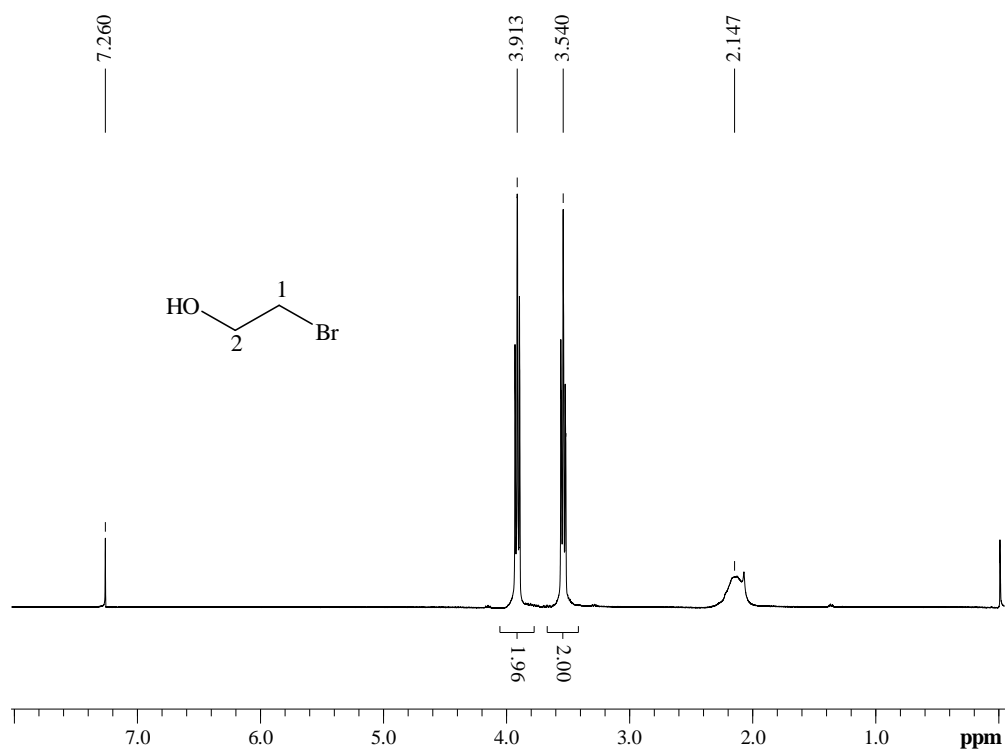
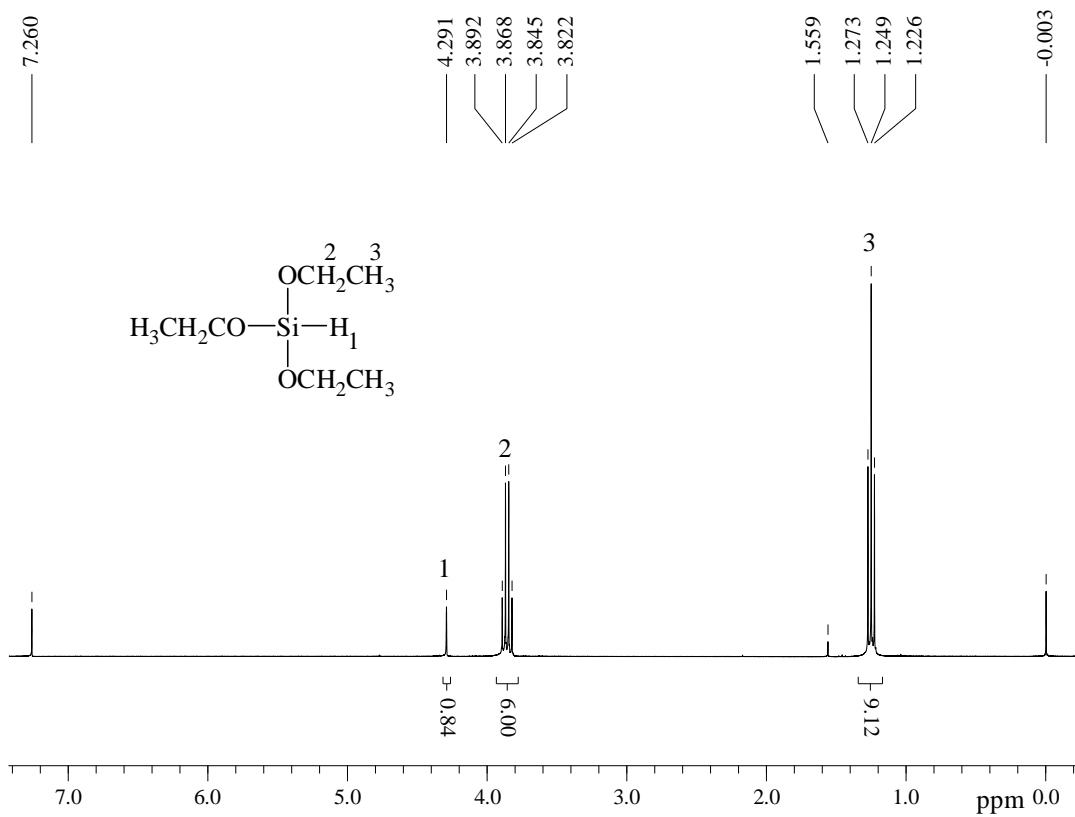**Figure 1.** ^{1}H NMR spectrum of 2-bromoethanol in CDCl3

Figure 2. ^{1}H NMR spectrum of 2,3,3-trimethyl-3*H*-indole in CDCl3

248

Figure 3. ^{1}H NMR spectrum of the precursor molecule 2-hydroxy-5-nitrobenzaldehyde in CDCl$_3$

Figure 4. ^{1}H NMR spectrum of allyl alcohol in CDCl$_3$

Figure 5. ^{1}H NMR spectrum of triethoxysilane in CDCl$_3$